Gas-phase electron diffraction studies of unstable molecules

Robert Noble-Eddy

A thesis presented for the degree of
Doctor of Philosophy
in the College of Science and Engineering
at the University of Edinburgh, 2009

Declaration

This thesis has not been previously submitted, in whole or in part, for any degree at this or any other university. The work is original and my own, carried out under the supervision of Dr. Sarah Masters; where this is not so, credit has been duly given.

(*Robert Noble-Eddy*)

Acknowledgements

I would like to thank my supervisor, Sarah Masters, and my second supervisor, David Rankin, for giving me the opportunity to do this project despite not being a chemist, and for their help and support throughout the three years, not least in reading this thesis.

Thanks must also go to the rest of the group, in particular to Derek Wann and Heather Robertson for teaching me about all aspects of GED. A big part of this thesis was conducted in collaboration with Jean-Claude Guillemin, and so thanks go to him and the rest of this group, especially for their perseverance when teaching me synthesis! The new nozzle was built by Georgiy Girichev and the rest of his group in Ivanovo, and I'd like to thank them for their continuing help. Back in Edinburgh, much of this work was only possible with the help of technical staff and I appreciate all work they did on my behalf, with particular praise going to Donald Palin in the electronics workshop and to Stuart Mains, who tried very hard to educate me in the ways of engineering!

Remaining sane during the PhD was made easier by the members of the Rankin, Morrison, Pulham, Attfield and Parsons groups, especially those involved with the creation of new lunchtime pool formats. Perhaps my biggest regret upon leaving Edinburgh is that I never managed to beat George in a best of 35 pool match!

Finally, I must thank my family for their continued support, and Laura, for putting up with me for so long and for agreeing to join me in London!

Abstract

Gas-phase electron diffraction (GED) is the only viable technique for the accurate structural study of gas-phase molecules that contain more than ∼10 atoms. Recent advances in Edinburgh have made it possible to study larger, more complex, stable molecules using the SARACEN method. This thesis is concerned with obtaining the structures of *unstable* species, using both standard GED techniques and by developing a new method in which flash vacuum pyrolysis is used to generate short-lived species *in situ*.

In the first part of this thesis nine primary phosphines (R-PH_2) with different substituents (R = methyl, vinyl, ethynyl, allenyl, allyl, propargyl, phenyl, benzyl and chloromethyl) are studied by GED. Vinylarsine and vinyldichloroarsine are also studied. Primary phosphines and arsines appear infrequently in the literature owing to their toxicity and high reactivity, especially of the unsaturated systems. The conformational behaviour in these molecules and trends throughout the series are rationalised. As appropriate, comparisons are made to analogous amines and the differences found are discussed.

Tertiary phosphines (R_3P) are routinely protected by complexation with borane (BH_3) and it has been proposed that this technique could be extended to primary phosphines. As an extension of the initial investigation, the GED study of methylphosphine-borane offers an insight into structural changes that occur upon complexation, although attempts to study larger phosphine-borane complexes by GED proved difficult. The structures and bonding trends in a series of phosphine-borane adducts are discussed, mainly using the results of *ab initio* calculations.

The second part of the thesis details the implementation of a new, very

high temperature nozzle, which allows the generation of short-lived species by pyrolysis. The workings of this nozzle are discussed and the study of the structure of ketene, generated from three different precursors, is detailed. The benzyl radical has also been studied, and a preliminary GED structure is presented. As a result of this work the molecular structures of Meldrum's acid and dibenzylsulfone are also presented, having been determined in the gas phase for the first time.

Abbreviations and acronyms

$^\circ$	An angle in degrees
*	In a basis set denotes polarisation functions on heavy atoms
**	In a basis set denotes polarisation functions on heavy and light atoms
+	In a basis set denotes diffuse functions on heavy atoms
++	In a basis set denotes diffuse functions on heavy and light atoms
$\angle$	A bond angle
ϕ	A dihedral angle
Å	Ångtröm
A_{h1}, B_{h1}, C_{h1}	Rotational constants with curvilinear corrections
A_0, B_0, C_0	Uncorrected rotational constants
B3LYP	Becke 3-parameter, Lee, Yang and Parr DFT Functional
BO	Born-Oppenheimer
BSSE	Basis Set Superposition Error
CFCs	Chlorofluorocarbons
CI	Configuration Interaction
CC	Coupled Cluster
DBS	Dibenzylsulfone
DFT	Density Functional Theory
DOSY	Diffusion Ordered Spectroscopy
e	The charge of an electron

EaStCHEM RCF	EastChem Research Computing Facility
EPR	Electron Paramagnetic Resonance
EPSRC	Engineering and Physical Sciences Research Council
FC	Frozen Core
FVP	Flash Vacuum Pyrolysis
FVP-GED	FVP coupled to the GED apparatus
G	In a basis set denotes the use of Gaussian functions
GED	Gas Electron Diffraction
GGA	Generalised Gradient Approximation
HF	Hartree-Fock
HOMO	Highest occupied molecular orbital
HT	High temperature
IR	Infrared
k	Perpendicular Vibrational Correction. Any subscript denotes the type of correction applied.
K	Kelvin
LCAO	Linear Combination of Atomic Orbitals
LDA	Local Density Approximation
LUMO	Lowest unoccupied molecular orbital
M05-2X	a DFT functional
MIC	Molecular Intensity Curve
mm	Millimetre
MO	Molecular Orbital
MOCED	Molecular Orbital Constrained Electron Diffraction
MPn	Møller-Plesset series truncated at n$^{\text{th}}$ order.
ms	Millisecond
MS	Mass Spectrometry or Mass Spectrometer
MS-GED	Mass Spectrometer Coupled GED
MT	Medium Temperature
MW	Microwave
NMR	Nuclear Magnetic Resonance

NSCCS	National Service for Computational Chemistry Software
PE	Potential Energy
PES	Potential Energy Surface
pm	Picometer
r	Interatomic Distance
r_{a}	Average Interatomic Distance (definition depends on method)
r_{e}	Equilibrium Distance
r_{h1}	Interatomic distance corrected with curvilinear distance corrections
R_{G}	R factor with off-diagonal elements
R_{D}	R factor without off-diagonal elements
RDC	Radial Distribution Curve
RINMR	Rapid injection NMR
s	Scattering angle
s	Second
SARACEN	Structure Analysis Restrained by *Ab initio* Calculations for Electron diffractioN
SCF	Self-consistent Field
STRADIVARIUS	STRuctural Analysis using DIffraction and VARIoUS other data
THF	Tetrahydrofuran
u	Amplitude of Vibration. Any subscript denotes the level of correction.
VHT	Very High Temperature
Z	The number of molecules in a unit cell
ZPE	Zero point energy

Contents

Chapter 1

Introduction

1.1 Introduction

The properties of any molecule are determined by its structure and so throughout recent history chemists have been interested in the structures of molecules.[1,2] Often it is enough to know the connectivity in a molecule but in other cases it is essential to determine precise bond lengths and angles. Numerous techniques exist which offer structural information in the gas, liquid and solid phases and the modern synthetic chemist routinely uses numerous complementary techniques.

By far the most the common technique used to determine complete structures is X-ray crystallography and it is the goal of most synthetic chemists to, where possible, grow suitable crystals of new compounds. However, there exists a number of situations in which growing a crystal is difficult or where the effects of intermolecular interactions in the crystal distort the molecular structure, and so it is in the gas phase that the molecular structure is ideally studied.

Computational chemistry is increasingly important in many areas. Whilst solid-state computational techniques are now widespread, the most sophisticated computational methods will always yield structures of isolated molecules which must be compared to gas-phase structures. It is therefore important to continue to develop new gas-phase structural determination techniques so that it is possible to benchmark computational techniques.

Gas electron diffraction (GED) is the main technique used to determine gas-phase molecular structure. Microwave (MW) spectroscopy is also available but can only offer complete structures for small molecules or if sufficient isotopic substitution can be performed. GED was traditionally limited to small or symmetric molecules but recent advances which allow the use of complementary data from other sources have allowed larger molecules to be studied. Currently GED is only routinely used to study stable molecules but the potential exists to extend the technique to study molecules that are stable on the timescale of *ms*.

This chapter details the technique of electron diffraction, the use of *ab initio* calculations and the techniques available to study short-lived molecules.

1.2 Electron Diffraction

1.2.1 Diffraction

The diffraction and interference of light was first demonstrated in Young's double slit experiment, in which coherent light passing through two adjacent slits was found to produce an interference pattern. It later became clear, for example, *via* the photoelectric effect,[3] that the classical picture of waves and particles was incorrect. The formulation of quantum mechanics in the early 20th century led to wave-particle duality - the theory that both light and matter display properties of waves and particles. Further work by de Broglie produced a relationship between the momentum of a particle (p) and its wavelength (λ),

$$p = h/\lambda, \tag{1.1}$$

where h is Planck's constant. One important consequence of this relationship is that particles can diffract and interfere in the same way as light.

The atoms in a molecule or crystal act as slits through which both light and particles can diffract and interfere, and so by measuring the interference pattern from diffraction by a molecule or crystal the interatomic spacings can be inferred. For diffraction to be observable, the wavelength of the light or particles must be comparable in size to the slit spacing, which in the case of atomic bonding is of the order of an Å. This corresponds to the wavelength of X-rays, electrons accelerated through 50 kV or to thermal neutrons.

Electrons are charged particles and therefore do not penetrate solids or liquids well, whereas X-rays are much more penetrative.[4] It is, however, much easier to produce an intense monochromatic electron beam; to do so for X-rays requires a synchrotron. This means electrons are particularly suited to the study of gases for which low penetration is not problematic, and that X-rays are better suited to the study of liquids and solids.

For both electron and X-ray diffraction the scattering intensity is dependent upon

the atomic number of the scattering atoms, and so it may be difficult or even impossible to locate lighter elements in the presence of heavier elements. This is not the case for diffraction by neutrons, but the production of neutrons is more difficult, requiring a nuclear reactor or spallation source.

1.2.2 The electron diffraction technique

A basic diagram of a typical gas electron diffraction (GED) apparatus can be seen in Figure 1.1. GED apparatus are not commercially produced and so many details vary between machines, however the underlying process is the same in each case.

The electron beam is produced by an electron gun. The electrons are emitted from a hot filament and accelerated through a potential. Accelerating voltages in the range of 30-50 kV are routinely used to produce a wavelength comparable to the interatomic spacing. The electron beam usually passes through a series of apertures and is focussed by electromagnetic lenses to produce a well collimated, narrow beam.

Figure 1.1: The layout of a typical GED apparatus.

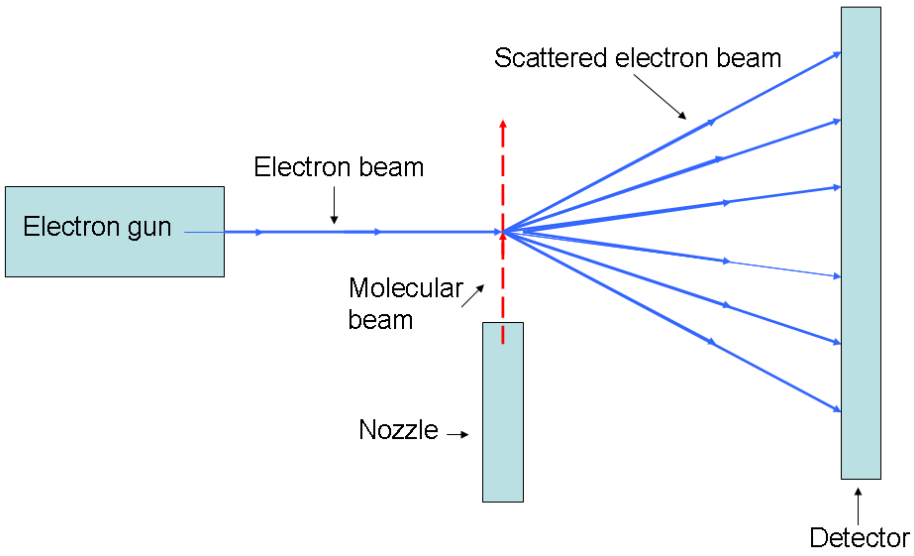

The gas sample is introduced into the path of the electron beam through a nozzle designed to produce a narrow stream of gas molecules which intersect the electron beam at right angles. The entire system must be under vacuum to minimise undesired scattering of the electron beam by background molecules. The maximum rate of flow of gas through the nozzle is limited by the vapour pressure of the sample at a given temperature; in cases where the sample is heated it is necessary to heat the nozzle to prevent the sample condensing.

The scattered electrons are recorded on a detector. Photographic film is used in Edinburgh but image plates and CCD cameras can also be used. The intensity of scattered electrons falls off as r^4, producing a range of intensities that is too large to measure on most detectors. To overcome this problem a filter is used, usually in the form of a rotating sector,[5] which is shaped in such a way to make the exposure consistent over the whole film. A beam stop is used to prevent back scattering of the undiffracted electron beam.

1.2.3 Experimental data

The recorded diffraction pattern is an average over all orientations of the gas molecules, and as such consists of a series of concentric rings. An example of a diffraction pattern produced from the Edinburgh apparatus[6] is shown in Figure 1.2. The scattering pattern is first digitised using a scanner and subsequently radially averaged to produce the total intensity scattering curve. Scattering consists of three components: the atomic scattering, the molecular scattering and the background. The molecular scattering contains the interference patterns from all pairs of atoms and is the data from which structural information can be extracted. Scattering also occurs from all combinations of three atoms, four atoms and so on, but these contributions are generally much smaller than the two-atom scattering and in most cases higher-order contributions can be ignored.[7]

The contributions from atomic scattering and the background must be separated to leave only the molecular scattering. The atomic scattering intensity arises from scattering by single atoms which do not produce an interference pattern.

Figure 1.2: An example diffraction pattern.

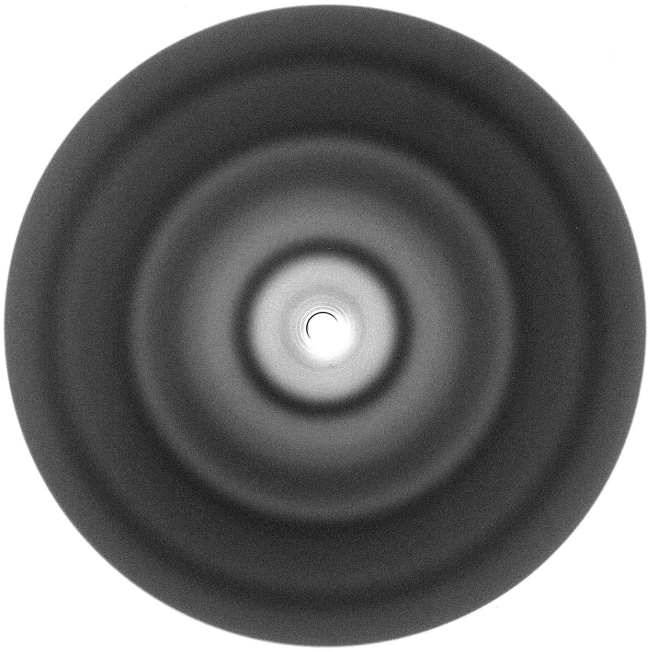

The scattering factors for individual atoms are known,[8] so this contribution is calculated and subtracted from the total scattering. The background scattering accumulates from a number of sources, including incoherent inelastic scattering and extraneous scattering, and is removed by fitting a cubic spline function to the intensity curve.

The molecular scattering is determined experimentally over a finite range. The lower limit arises because of the use of a beam stop in the rotating sector and the upper limit because of the limited radius of the detector. The range of data collected can be adjusted by altering the distance between the nozzle and the photographic plate, although recording data over a larger angle decreases the resolution of the image obtained. To obtain molecular scattering over a larger range it is common to collect data at a series of nozzle-to-camera distances.

The molecular intensity curve (MIC) is the sum of interference patterns for all pairs of atoms in the molecule, with each pair producing a damped sinusoid, the period of which gives the bond length and damping the mean amplitude of vibration. For a diatomic molecule this information is readily obtained from the

Figure 1.3: An example radial distribution curve for benzene.

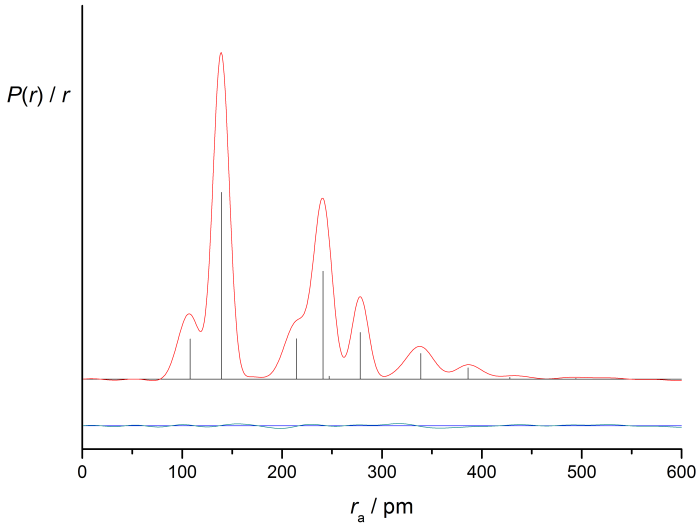

MIC but for a polyatomic molecule the MIC is more complex and cannot be interpreted easily by eye. To make appreciation of the data easier the radial distribution curve (RDC) is used, obtained by the Fourier transform of the MIC.

The RDC gives the probability $P(r)$ of finding a bond length r in the molecule and consists of an approximately Gaussian curve for each distance, centred on the average bond length of that pair of atoms (r_{ij}). The width of the Gaussian is determined by the mean vibrational amplitudes, and the area under the each peak by the masses of the two atoms (Z) and the number of times that bond occurs (n), such that

$$Area \propto n_{ij} Z_i Z_j / r_{ij}. \tag{1.2}$$

An example of a RDC for benzene can be seen in Figure 1.3. The bonded and non-bonded peaks are clearly visible, for example the C–C bonded distance at ∼140 pm and a non-bonded C...C distance at ∼240 pm. The sticks shown on the graph indicate all the distances in the molecule and the difference curve, defined as experimental – theoretical, is shown below the main curve.

1.2.4 Least squares refinement

Experimental data is analysed by a comparison of the experimental MIC to that generated from a parametrised model molecule. The model molecule is generally parametrised using a combination of bond lengths, bond angles and dihedral angles, but other parameters, such as differences between distances, can also be used when appropriate. The MIC from the model molecule is calculated using scattering equations.[9] A least-squares refinement is then used; the parameters of the model are allowed to change to minimise the difference between the model and the experimental data. The goodness of the least-squares refinement is measured by the R factor – a lower R factor denotes a better fit.

The process of least-squares refinement requires that the approximate structure of the molecule be known before the experiment. *Ab initio* calculations are usually used to search for viable structures and to provide a starting geometry for the refinement. It is important to ensure that all values remain physically reasonable during the refinement and to ensure that the numbers of parameters refined is suitable for the number of data available.

1.2.5 GED Challenges and Solutions

Analysis of GED data can be complicated by a number of factors. GED data is a 1-dimensional representation of a 3-dimensional molecule and as such there is generally a limit in the number of parameters that can be refined. When two or more distances lie close to one another in the radial distribution it is often impossible to distinguish which peak belongs to which pair of atoms. In addition scattering from lighter elements may also be difficult to resolve. As the scattering is proportional to the product of the atomic numbers of the two atoms (Equation 1.2), a distance involving two light atoms will have a much smaller area than for heavier atoms, especially if the two lighter elements are distant from one another. Data is also limited when an especially heavy atom is bonded to a lighter atom due to a phenomenon known as the phase effect.[10]

For these reasons GED has traditionally been limited to small or very symmetric

molecules which did not require a large number of parameters to describe. Often the full structure of a molecule could not be refined and some parameters were left at fixed values. This, however, led to problems estimating the uncertainty when, as was often the case, constrained parameters were correlated to refining parameters.

In order to overcome these limitations, the STRADIVARIUS method that includes data from microwave spectroscopy[11] or liquid crystal NMR[12] was developed to allow the refinement of larger or less symmetric molecules, but the amount of additional data available from these other methods is also limited. Instead attention has turned to the use of data from *ab initio* calculations in refinements of GED data, first in the MOCED technique,[13] and later in SARACEN.[14–16]

SARACEN uses the results from *ab initio* calculations to restrain GED parameters. Rather than having fixed parameters, the SARACEN method uses flexible restraints – the *ab initio* data is used as extra information in the refinement and is assigned an uncertainty reflecting the anticipated precision of the calculated values. The refinement then proceeds treating the restrained parameter and its uncertainty as if it were an experimentally derived result.

Another important consideration when analysing GED data is how intramolecular vibrations affect the bond length. The time scale for the electron-atom interaction during diffraction is 10^{-18} s, whereas the frequency of the fastest molecular process is 10^{14} Hz. Therefore as an electron diffracts from a molecule it experiences a single, fixed, vibrational position, however, each individual electron diffracts from a different vibrational state and so the observed MIC is an average over all vibrational states.

Vibrational effects can result in the shortening of distances between non-bonded atoms in linear molecules, an effect known as shrinkage. A good example of this effect is a linear triatomic molecules such as CO_2. The bending motion of such a molecule is shown in Figure 1.4. When the molecule is motionless, the distance A...C is equal to A–B + B–C. However, when the molecule is vibrating, the distance A...C is less than A–B + B–C and, according to GED, the molecule

Figure 1.4: The shrinkage effect in a linear triatomic molecule

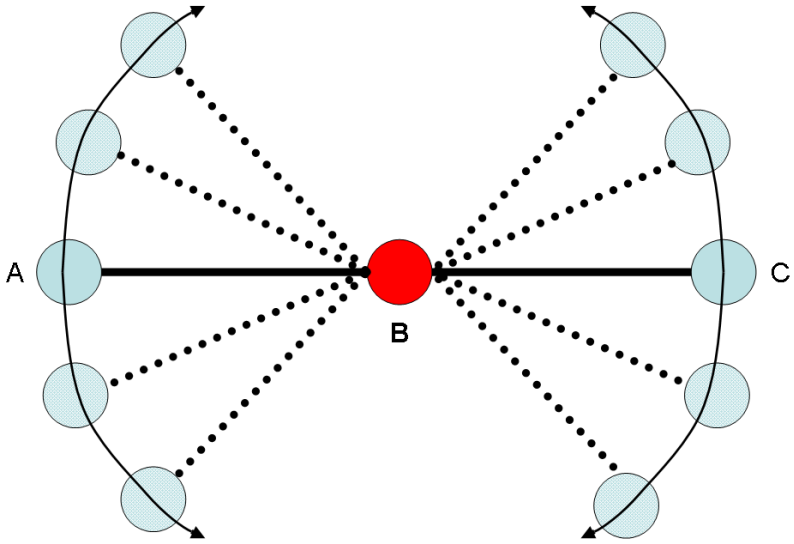

would be bent rather than linear. In order to obtain accurate structures it is necessary to correct for this effect. These corrections are routinely calculated from *ab initio* calculations using the SHRINK software[17] and a correction applied to each pair of atoms during the refinement. In certain situations where large amplitude motions are present the approximations made in SHRINK are invalid and a molecular dynamics approach is more appropriate.[18]

1.3 Computational Chemistry

Computational chemistry plays a dual role for the modern electron diffractionist, serving as both an independent method of structural study and as a source of additional information for use both with SARACEN and SHRINK. In a more general sense computational methods are invaluable tools for all chemists, allowing the study of systems in greater detail than experiment alone can afford and enabling the study of systems that would otherwise be inaccessible. The range of systems that can be studied and the accuracy of calculations continue to increase with advances in processing power. Techniques exist for calculating the properties of many systems of all sizes, from classical molecular dynamics simulations involving more than a million atoms to detailed study of the potential energy surface of a small molecule.[19,20]

1.3.1 *Ab initio* calculations

Quantum mechanical calculations are based on solving the Schrödinger equation,

$$H\Psi = E\Psi, \tag{1.3}$$

where H is the Hamiltonian operator, Ψ the wavefunction and E the energy of the system. Solution of this equation yields the energy of a particular molecular arrangement and so can be used to find the potential energy minimum for a molecule. However, the Schrödinger equation can only be solved exactly for one electron systems, with more complex systems requiring simplifications.

The first approximation made relates to the Hamiltonian operator. H consists of kinetic and potential energy terms that are functions of both the nuclear and electronic components of the system. Initially the problem is simplified by the use of the Born Oppenheimer (BO) approximation. As a nucleon is $\sim$2000 times more massive than an electron, the motion of a nucleus is slow in comparison to that of the electrons and the two can be treated independently.

Under the BO approximation the Hamiltonian is reduced to three terms; the

electron kinetic energy, the electron-nucleus interaction and the electron-electron repulsion. The first two terms are easily calculated but it is more difficult to account for the electron-electron term. In a multi-electron system each electron moves in the field generated by all of the others and so the motion of each electron is correlated with the positions of the other electrons. The electron-electron term is therefore an n-body problem and cannot be solved exactly when $n > 2$. A number of solutions to this problem have been developed, some of which are described below.

As well as simplifying the Hamiltonian it is also necessary to approximate the wavefunction. This is described in Section 1.3.2.

Model chemistries

Numerous methods exist offering various combinations of accuracy and computational expense. In general, the more accurate a method, the more computationally expensive it is. The various techniques vary in their treatment of the electron-electron interaction term, specifically with the way in which they handle electron correlation.

Hartree-Fock The Hartree-Fock (HF) method is a mean field theorem.[21] The system of n interacting electrons is replaced with an average field in which each electron moves. This simplifies the n-body problem to a series of n one electron problems but the effects of correlation are ignored. HF accounts for 99% of the energy of most systems, the difference between HF and the true energy is the correlation energy. The correlation energy is particularly important in systems with high regions of electron density, for example unsaturated systems where the lack of correlation leads HF to produce structures with shorter than expected bond distances which, as a result, have higher energy. Nevertheless HF provides a inexpensive starting point and the geometries it provides are usually a reasonable representation of the final structure.

Møller-Plesset Methods Møller-Plesset (MP) perturbation theory builds upon HF by adding electron correlation *via* a perturbation to the Hamiltonian.[22] The resultant Schrödinger equation is then expanded as a power series which is truncated at some order. It is most commonly used at second order, denoted MP2, but 3rd (MP3) and 4th (MP4) order terms are also used.

The MP2 method is the most commonly used post-HF method. Whilst computationally more expensive than HF methods, MP2 is cheaper than the other methods which include electron correlation and performs well for most systems. For this reason MP2 is the method most frequently chosen to support electron diffraction refinements. It is applicable to most systems that are studied by GED and provides easy access to the frequency calculations required for SHRINK.

Configuration Interaction and Coupled Cluster Methods The configuration interaction (CI)[23] and coupled cluster (CC)[24–27] methods are the most commonly used methods to produce very accurate structures but tend to be limited to very small systems due to their computational expense. Both methods build upon HF by mixing the ground state with excited states. If a single excitation is used, the method is labelled with an S (*e.g.* CIS), if double excitations are used then SD is added (*e.g.* CCSD). It is common to use perturbation theory, denoted by brackets, to approximate the third excitation, and so the CCSD(T) method is commonly used.

Density Functional Theory DFT is a technique that is widely used in the study of condensed systems, but can also be applied to single molecules. DFT is based on the proof by Hohenberg and Kohn that there exists a one-to-one mapping between the electron density of a system and its energy.[28] This mapping is described by a functional, but this functional is not known exactly. The exchange-correlation functional must be approximated in some way; the most common methods used include the Localised Density Approximation (LDA),[29] based on the value of the electron density at any point, and the Generalised Gradient Approximation (GGA), which also includes the first derivative of the

electron density.[30] Hybrid DFT methods mix DFT exchange-correlation with that obtained using the HF method, in which the exchange is exactly known.

DFT is generally less computationally expensive than the other methods described, and its main advantage lies in exploiting its speed to study large systems, but it is generally less accurate than the others post-HF methods described. Most of the molecules studied in this project are relatively small, so DFT methods are used infrequently.

1.3.2 Basis Sets

The wavefunction describes the spatial distribution of electrons in the system. The wavefunction, or molecular orbitals (MOs), are generally constructed from a linear combination of atomic orbitals (LCAO), the shapes of which are based on the atomic radial functions derived from the Schrödinger equation for a hydrogen atom. To describe the shape of the orbitals a finite series of simple functions, usually Gaussians, are used. This series of functions is known as basis set, and whilst a basis set with more functions will model the system more efficiently, it will also require more computational resources.

Many basis sets have been created with different properties. Minimal basis sets contain only enough functions to describe all the electrons in the system, whilst double-, triple-, *etc* zeta basis sets contain progressively more functions for each orbital. Split-valence basis sets treat the core and valence regions separately, using more functions to better describe the more important valence region. Polarisation functions give more flexibility to the shape of the orbitals, adding p-type functions to s-orbitals, d-type to p-orbitals and so on. Diffuse functions can also be added to better model space further from the nucleus, an important consideration for loosely-bound electrons, for example those in anions.

Examples of basis sets used in this work include the Pople-type split-valence basis sets[31–35] and Dunning's correlation consistent basis sets.[36–40]

1.4 Unstable and short-lived species

Whilst structure determination of stable molecules is now relatively routine there is much less work in the literature with regard to the structures of short-lived molecules. For this work the definition of short-lived molecules includes free radicals, reaction intermediates, or simply molecules that react quickly to form other species. Such species are important in many chemical and biological processes, for example, free radicals are known to play roles in combustion,[41] polymerization[42] and the depletion of the ozone layer by CFCs.[43] Knowledge of the structure of such molecules is vital to understand such processes.

Whilst short-lived molecules can be studied by a number of experimental techniques, very few of these techniques offer structural parameters, with full structures even rarer. It therefore tends to fall to computational chemistry to provide structural information on short-lived species, but as always, experimental verification is desirable to assess the precision of computed parameters.

Part of this thesis explores the potential of GED to offer complete structures of reactive species. GED has been used infrequently to study such compounds in the past but traditionally most work on short-lived molecules has been done with other techniques. Some of the various techniques available to generate and study short-lived species are discussed below.

1.4.1 Generation of short-lived species

By their very nature short-lived species are more difficult to produce than stable molecules, however a number of techniques exist which allow for the generation of, and subsequent study of, such molecules.

Flash vacuum pyrolysis

Flash vacuum pyrolysis (FVP) is routinely used as a synthetic technique in organic chemistry. A precursor is first vaporised then passed through a hotter pyrolysis oven where it decomposes to form new species, usually by a pericyclic

rearrangement or *via* a radical intermediate. The technique has been used widely to create many diverse compounds.[44,45] FVP can also be coupled with other techniques such as mass spectrometry[46] and IR spectroscopy and can be used to generate short-lived species to be trapped with matrix isolation methods.[47]

Photolysis

The dissociation of molecules by light plays an important role in atmospheric processes and the chemistry occurring in the interstellar medium. Photolysis can also be used in conventional synthesis.[48] In a structural sense photolysis can be used to create short-lived species by causing dissociation, to study excited states, or to study chemical processes such as bond dissociation. The commonly used pump–probe technique is discussed in more detail in Section 1.4.3.

Matrix isolation

One of the main difficulties in studying short-lived molecules is that, by definition, the timescale available for study is short. Whilst some techniques, such as ultrafast GED (Section 1.4.3), overcome this by adapting the analytical technique, it is also possible to increase the time for which the short-lived molecules are stable by using matrix isolation techniques. The technique usually involves trapping the target molecules on an inert solid at low temperature. It is common to mix the molecules of interest with an inert carrier gas, such as nitrogen or argon, before trapping. The resultant trapped molecules are stable and can be thought of as being analogous to gas-phase molecules with the translational and rotational motion quenched. Much work has been conducted to understand the limitations of matrix isolation and to develop the technique.[49]

Once trapped, molecules can be studied using a variety of techniques, such as IR spectroscopy or EPR spectroscopy.[50]

1.4.2 Spectroscopic techniques

NMR Spectroscopy

NMR spectroscopy can be used to study short-lived molecules in much the same way as the technique is used throughout synthetic chemistry. The number of NMR techniques available is vast and beyond the scope of this introduction, however, a few key points are worth noting. The study of reaction intermediates (and therefore short-lived molecules) is possible and tends to be performed using the rapid injection NMR (RINMR) technique.[51] The problem of signal overlap from multiple species can be overcome using diffusion ordered NMR (DOSY).[52] In general information such as connectivity is readily available from NMR, but in some cases it is also possible to derive structural parameters, albeit with a lower precision than using MW spectroscopy or diffraction techniques.[53] It must also be remembered that NMR spectroscopy is limited to nuclei with a spin of $\frac{1}{2}$ or greater.

EPR Spectroscopy

EPR spectroscopy works on a similar principle to NMR spectroscopy but it is the relaxation of the excitation of a free electron that is measured, rather than the nuclei. To be EPR active a molecule must have an unpaired electron (and therefore be paramagnetic) and so EPR is routinely applied to the study of radicals. EPR can offer a variety of information, such as the nature of lone electrons (localised or delocalised) and radical reaction rate (by measuring EPR signal during a reaction involving a radical).[54]

IR Spectroscopy

IR spectroscopy can be used to investigate short-lived molecules, often in conjunction with the flash vacuum pyrolysis technique detailed previously. One example is the study of the benzyl radical, generated by FVP, from which it was possible to draw conclusions about delocalisation and hybridisation in the

molecule.[55]

Rotational or microwave spectroscopy

Microwave (MW) spectroscopy can be used to determine accurate structures of small molecules in the gas–phase. For a diatomic molecule the rotational frequency is linked to the structure *via* the equation

$$B = \frac{\hbar^2}{2hI} \tag{1.4}$$

where B is the rotational frequency in Hz, h is Planck's constant, $\hbar$ is $h/2\pi$ and I is the moment of inertia.[56] A maximum of three rotational constants can be determined for a single species, and so to determine the structure of larger molecules it is necessary to perform isotopic substitutions to increase the number of experimental data. One example in which many isotopic substitutions were made is the study of ethylphosphine.[57] In practise the difficulties in synthesising isotopomers or the lack of isotopes for some nuclei means that MW spectroscopy is not used to determine complete structures of large molecules routinely, but is often used in combination with GED data using the STRADIVARIUS method. One advantage of MW spectroscopy is that individual species can be detected from a mixture, and so the technique is well suited for the study of short-lived molecules, where the method of generation or subsequent decay or further reaction will often lead to a mixture of species being present.

1.4.3 Diffraction techniques

Solid-state diffraction

The timescale required for crystal growth is generally longer than the lifetime of a short-lived molecule and so solid-state techniques are generally of less importance in this area. However, stable free radicals have been studied by X-ray crystallography[58] and some solid-gas reactions have been studied *in situ*.[59] Where normally short-lived molecules are studied in the solid state, they are generally

stabilised by complexation with a suitable ligand[60] and so the structure obtained may not be a good indicator for that of the isolated radical.

GED

GED has been used to study unstable molecules in the past, but no long term research programme has been established in this area. Examples of molecules studied in the past include the indenyl radical,[61] the bromoethyl radical,[62] the dibromomethylene radical[63] and the allyl radical.[64] In each case differing amounts of information were extracted from the experimental data, but such work proves that the GED study of unstable compounds is feasible. Whilst most of these experiments were conducted on standard GED apparatus in the case of the study of the allyl radical, and in the recent work by the Ivanovo group, GED is coupled with mass spectrometry. This offers independent evidence of the species present in the vapour and the amounts of each, and is likely to be much more reliable than relying on GED data alone. This technique has been used extensively by the group in Ivanovo, and has enabled the study of numerous molecules, for example TeI_2 and $TeBr_2$ generated from TeI_4 and $TeBr_4$ respectively,[65] and the structures of β-diketonates.[66]

Ultrafast GED

One of the most recent advances in the area of GED has been the development of ultrafast GED to study chemical processes on the femtosecond timescale. In 1999 Ahmed Zewail won the Nobel Prize in Chemistry for work in this area, often dubbed femtochemistry.[67] The technique used is known as a pump-probe experiment. A femtosecond laser is used both to excite the target molecules and, *via* photo emission, to create a bunch of electrons with a picosecond temporal resolution. Providing that the relative timings of the two events can be controlled the electron bunch can be made to diffract from the excited molecules at a known time after excitation, and so the processes involved with excitation can be mapped by the change in diffraction patterns. Such a technique can be applied to many

systems, with examples including the structure of the CF_3 radical[68] and the ring opening of 1,3,5–cycloheptatriene.[69]

1.5 This work

This thesis is concerned with the determination of the gas-phase structures of a series of unstable and short-lived molecules. The thesis can be divided into two sections – the first focusses on the structures of a series of unstable primary Group 15 derivatives, with the second part detailing the study of short-lived molecules generated *in situ* using FVP-GED.

The aim of the initial work undertaken was to study the structure of a series of primary phosphines and their adducts with borane. Primary phosphines are poorly represented in the literature owing to their reactivity and toxicity, whilst the more stable secondary and tertiary phosphines are used throughout modern chemistry. Whilst tertiary phosphines have greater natural resistance to oxidation, they are also routinely stabilised further by complexation with borane, and it is thought that this could also be applied to primary phosphines. It was anticipated that the study of the structures of the free phosphines and the corresponding borane adducts would offer an insight in to the changes that occur upon complexation and how they relate to the increased stability.

Chapter 2 therefore details the study of methylphosphine and methylphosphine-borane. These simple molecules presented a perfect starting point for the project, allowing the GED data to be combined with previously published rotational constants to obtain more accurate structures, and allowing the experimental structure to be compared to the results of high-level *ab initio* calculations.

The next stage of the work focussed on unsaturated systems, offering greater possibility in further synthesis, but also included a series of alkyl and aryl derivatives. In Chapter 3 the structures of eight primary phosphines are studied and bonding trends throughout the series are discussed. Chapter 4 details the attempts to study the same series of phosphine-borane adducts, however, whilst

the molecules showed better oxidative stability they appeared to be less kinetically stable than the free phosphines, and no good quality experimental structures could be determined. Chapter 4 therefore details the structures of the phosphine-borane adducts studied *ab initio*.

As the phosphine-borane work was concluded prematurely, it was decided to move attention to primary arsines, for which even fewer studies have been conducted. Chapter 5 presents the structure of vinylarsine, representing the first GED structure of a primary arsine. Primary arsines are anticipated to be less stable than the analogous free phosphine and so may prove difficult to study. It is anticipated that the dichloroarsines will be more stable and could be studied in place of unstable arsines, and so the structure of vinyldichloroarsine is also presented in Chapter 5. The structures of these two compounds are compared, and the trends down Group 15 were assessed using the calculated structures of the analogous amines.

The ability to generate short-lived molecules *in situ* would open up many new avenues for GED and offers the best chance to determine full structures of short-lived molecules. A new nozzle has been manufactured for the Edinburgh GED apparatus that allows for the generation of short-lived molecules using FVP. The workings of the nozzle, along with initial calibration and testing are given in Chapter 6. Chapter 6 also details three different routes used to generate ketene, with the future goal being the study of substituted ketenes which cannot be accessed using standard GED techniques. During the course of the work in Chapter 6 the GED structure of Meldrum's acid is determined for the first time.

Chapter 7 extents the FVP-GED work to a new area by studying the benzyl radical generated by the pyrolysis of dibenzylsulfone. Although there were problems with calibration of the nozzle-to-camera distance all indications are that the benzyl radical is formed in high yield and an initial refinement shows good agreement with calculated parameters. Again, the precursor had not been studied, and so the structure of dibenzylsulfone, existing in three conformations, is also presented.

Chapter 8 offers a conclusion on the work conducted, and contains detailed

comments on future developments to the FVP-GED technique.

1.6 References

[1] J. D. Watson and F. H. C. Crick, *Nature*, 1953, **171**, 737.

[2] H. W. Kroto, J. R. Heath, S. C. O'Brien, R. F. Curl and S. R. E., *Nature*, 1985, **318**, 162.

[3] A. Einstein, *Physik. Ges. Zurik. Mitt.*, 1916, 18.

[4] E. A. V. Ebsworth, D. W. H. Rankin and S. Cradock, *Structural Methods in Inorganic Chemistry*, CRC Press, Inc., Boca, Ranton, Florida, 1987.

[5] L. O. Brockway and L. S. Bartell, *Rev. Sci. Instrum.*, 1954, **25**, 569.

[6] C. M. Huntley, G. S. Laurenson and D. W. H. Rankin, *J. Chem. Soc., Dalton Trans.*, 1980, 954.

[7] G. Gundersen and K. Hedberg, *J. Chem. Phys.*, 1978, **68**, 3548.

[8] A. W. Ross, M. Fink and R. Hilderbrandt, *International Tables for Crystallography*, Kluwer Academic Publishers, Dordrecht, Netherlands, 1992, p. 245.

[9] I. Hargittai and M. Hargittai, *Stereochemical Applications of Gas-phase Electron Diffraction*, VCH Publishers, Inc., Verlagsgesellschaft mbH, Weinheim, 1988.

[10] H. M. Seip, *Molecular Structure by Diffraction Methods Volume 1, Specialist Periodical Reports, The Chemical Society,*, 1973, pp. 21–23.

[11] M. J. Davis, D. W. H. Rankin and H. E. Robertson, *J. Mol. Struct.*, 1990, **238**, 273.

[12] R. Blom, S. Cradock, S. L. Davidson and D. W. H. Rankin, *J. Mol. Struct.*, 1991, **245**, 369.

[13] V. J. Kimklowski, J. D. Ewbank, C. van Elsenoy and L. Schafer, *J. Am. Chem. Soc.*, 1982, **104**, 1476.

[14] A. J. Blake, P. T. Brain, H. McNab, J. Miller, C. A. Morrison, S. Parsons, D. W. H. Rankin, H. Robertson and B. A. Smart, *J. Phys. Chem. A*, 1996, **100**, 12280.

[15] P. T. Brain, C. A. Morrison, S. Parsons and D. W. H. Rankin, *J. Chem. Soc., Dalton Trans.*, 1996, 4589.

[16] N. W. Mitzel and D. W. H. Rankin, *Dalton Trans.*, 2003, 3650.

[17] V. A. Sipachev, *THEOCHEM*, 1985, **121**, 143.

[18] D. A. Wann, R. J. Less, F. Rataboul, P. D. McCaffrey, A. M. Reilly, H. E. Robertson, P. D. Lickiss and D. W. H. Rankin, *Organometallics*, 2008, **27**, 4183.

[19] D. C. Young, *Computational Chemistry: A Practical Guide for Applying Techniques to Real World Problems*, John Wiley and Sons Ltd, 2001.

[20] G. H. Grant and W. G. Richards, *Computational Chemistry*, Oxford University Press, 1995.

[21] C. C. J. Roothaan, *Rev. Mod. Phys.*, 1951, **23**, 69.

[22] C. Møller and M. S. Plesset, *Phys. Rev.*, 1934, **46**, 618.

[23] J. B. Foresman, M. Head-Gordon, J. A. Pople and M. J. Frisch, *J. Phys. Chem.*, 1992, **96**, 135.

[24] J. Cizek, *Adv. Chem. Phys.*, 1969, **14**, 35.

[25] G. D. Purvis III and R. J. Bartless, *J. Chem. Phys.*, 1982, **76**, 1910.

[26] G. E. Scuseria, C. L. Janssen and H. F. Schaefer-III, *J. Chem. Phys.*, 1988, **89**, 7382.

[27] G. E. Scuseria and H. F. Schaefer III, *J. Chem. Phys.*, 1989, **90**, 3700.

[28] P. Hohneberg and W. Kohn, *Phys. Rev.*, 1965, **136**, B864.

[29] J. P. Perdew and Y. Wang, *Phys. Rev. B*, 1992, **45**, 13244.

[30] J. P. Perdew, J. A. Chevary, S. H. Vosko, K. A. Jackson, M. R. Pederson, D. J. Singh and C. Fiolhais, *Phys. Rev. B.*, 1992, **46**, 6671.

[31] W. J. Hehre, R. Ditchfield and J. A. Pople, *J. Chem. Phys.*, 1972, **56**, 2257.

[32] P. C. Hariharan and J. A. Pople, *Theo. Chim. Acta.*, 1972, **56**, 2257.

[33] M. S. Gordon, *Chem. Phys. Lett.*, 1980, **76**, 163.

[34] A. D. McLean and G. S. Chandler, *J. Chem. Phys.*, 1980, **72**, 5639.

[35] R. Krishnan, J. S. Binkley, R. Seeger and J. A. Pople, *J. Chem. Phys.*, 1980, **72**, 650.

[36] D. E. Woon and T. H. Dunning Jr., *J. Chem. Phys.*, 1993, **98**, 1358.

[37] R. A. Kendall, T. H. Dunning Jr. and R. J. Harrison, *J. Chem. Phys.*, 1992, **96**, 6796.

[38] T. H. Dunning Jr., *J. Chem. Phys.*, 1989, **90**, 1007.

[39] K. A. Peterson, D. E. Woon and T. H. Dunning Jr., *J. Chem. Phys.*, 1994, **100**, 7410.

[40] A. Wilson, T. van Mourik and T. H. Dunning Jr., *THEOCHEM*, 1996, **388**, 339.

[41] P. L. Cramer and J. M. Campbell, *Ind. & Eng. Chem.*, 1949, **41**, 893.

[42] J. Chiefari, Y. K. Chong, F. Ercole, J. Krstina, J. Jeffery, T. P. Le, R. T. A. Mayadunne, G. F. Meijs, C. L. Moad, G. Moad, E. Rizzardo and S. H. Thang, *Macromolecules*, 1998, **31**, 5559.

[43] J. G. Anderson, D. W. Toohey and W. H. Brune, *Science*, 1991, **251**, 39.

[44] H. McNab, *Aldrichimica Acta*, 2004, **37**, 19.

[45] M. Karpf, *Angew. Chem. Int. Ed. Engl.*, 1986, **25**, 414.

[46] R. Flammang, M. Barbieux-Flammang, P. Gerbaux and C. Pedersen, *J. Chem. Soc., Perkin Trans. 2*, 1997, 1261.

[47] C. T. Pedersen, R. Flammang, P. Gerbaux and Fanghänel, *J. Chem. Soc., Perkin Trans. 2*, 1998, 1403.

[48] C. Ornelas, J. Ruiz, J. Rodrigues and D. Astruc, *Inorg. Chem.*, 2008, **47**, 4421.

[49] *See, for example, V. E. Bondybey, A. M. Smith and J. Agreiter, Chem. Rev., 1996, **96**, 2113.*

[50] D. L. Perry, P. F. Meier, R. H. Hauge and J. L. Margrave, *Inorg. Chem.*, 1978, **17**, 1364.

[51] A. C. Jones, A. W. Sanders, M. J. Bevan and H. J. Reich, *J. Am. Chem. Soc.*, 2007, **129**, 3492.

[52] S. Viela, L. Manninaa and A. Segre, *Tetrahedron Lett.*, 2002, **14**, 2515.

[53] R. T. Syvitksi and E. E. Burnell, *J. Mag. Res.*, 2000, **144**, 58.

[54] D. Griller and K. U. Ingold, *Acc. Chem. Res.*, 1980, **13**, 317.

[55] E. G. Baskir, A. K. Maltsev, V. A. Korolev, V. N. Khabashesku and O. M. Nefedov, *Russ. Chem. Bull.*, 1993, **42**, 1438.

[56] J. M. Brown, *Molecular Spectroscopy*, Oxford University Press, 1998.

[57] P. Groner, R. D. Johnson and J. R. Durig, *J. Chem. Phys.*, 1988, **88**, 3456.

[58] M. J. Plater, S. Kemp, E. Coranado, C. J. Gómez-Garcia, R. W. Harrington and W. Clegg, *Polyhedron*, 2006, **25**, 12.

[59] E. A. Gray, D. J. Cookson and T. P. Blach, *J. Appl. Cryst.*, 2006, **39**, 850.

[60] M. Kameya, T. Naito and T. Inabe, *Bull. Chem. Soc. Jap.*, 2000, **73**, 61.

[61] L. Schafer, *J. Am. Chem. Soc.*, 1968, **90**, 3919.

[62] T. L. Leggett, R. E. Kennerly and D. A. Kohl, *J. Phys. Chem.*, 1974, **60**, 3264.

[63] R. C. Ivey, P. D. Schulze, T. L. Leggett and D. A. Kohl, *J. Chem. Phys.*, 1974, **60**, 3174.

[64] E. Vajda, J. Tremmel, B. Rozsondai, A. K. Maltsev, N. D. Kagramanov and O. M. Nefedov, *J. Am. Chem. Soc.*, 1986, **108**, 4352.

[65] S. A. Shlykov, H. Oberhammer, A. V. Titov, N. I. Giricheva and G. V. Girichev, *Eur. J. Inorg. Chem.*, 2008, **33**, 5520.

[66] N. V. Tverdova, G. V. Girichev, V. V. Rybkin, S. A. Shlykov, N. P. Kuzmina and I. G. Zaitseva, *J. Struct. Chem.*, 2008, **49**, 1001.

[67] A. H. Zewail, *J. Phys. Chem.*, 1993, **97**, 12427.

[68] J. C. Williamson, M. Dantus, S. B. Kim and A. H. Zewail, *Chem. Phys. Lett.*, 1992, **196**, 529.

[69] C.-Y. Ruan, V. A. Lobastov, R. Srinivasan, B. M. Goodson, H. Ihee and A. H. Zewail, *Proc. Nat. Acad. Sci.*, 2001, **98**, 7117.

Chapter 2

Can we make primary phosphines more user friendly? The molecular structure of methylphosphine and its adduct with borane

2.1 Introduction

Relatively few studies have been conducted on the structures of the primary aliphatic phosphines, R–PH_2, and they are less widely used throughout chemistry than the aryl phosphines. This is generally attributed to their unfavourable properties; they are often pyrophoric, toxic, unstable in air and possess unpleasant odours. Primary phosphines have potential as starting materials for various applications[1] and therefore the development of more air-stable, *user-friendly* phosphines is of great interest. Increased air and moisture stability can be achieved by the addition of a bulky protecting group, for example the mesityl group in mesitylphosphine,[2] or by complexation with a suitable Lewis acid. Complexes with borane have been reported and the chemistry of the adducts explored[3] but only a few structural studies have been reported.[4] Tertiary phosphine-borane complexes are considered to be protected free phosphines, since the free phosphine can be easily recovered by reaction with excess amine. It has been shown that the same is possible for primary phosphines, albeit with a reduced yield.[3] The gas electron diffraction (GED) study of methylphosphine (CH_3PH_2, **1**) and methylphosphine-borane (CH_3PH_2–BH_3, **2**), as one of the simplest examples of a primary phosphine and its borane adduct, provides a starting point for the investigation of larger functionalised primary phosphines. The degree of increased stability imparted by formation of the adduct is of particular interest, especially with regard to the structural changes accompanying the complexation. Studying a simple system such as methylphosphine allows analysis of these phenomena without the increased complexity that would be present in larger molecules. **1** and **2** also present the opportunity to conduct high-level *ab initio* calculations, which would be prohibitively expensive for much larger phosphines. The GED study of larger phosphines will rely more heavily on the use of *ab initio* data *via* the SARACEN method,[5–7] and so it is vital to gauge the accuracy of various theoretical methods in order to identify suitable computational techniques for future work.

Lewis acid-base adducts are also interesting in a more general sense. Previous

research has found large deviations between the gas-phase and crystalline structures of some Lewis acid-base adducts; for example, in HCN–BF_3 the B–N bond length is found to be 83.5 pm shorter in the crystalline solid than in the gas phase.[8] It is therefore apparent that the bond between such a Lewis acid-base complex can be significantly shortened by the effects of crystal packing[9] and so it is vital that the structure is studied in the gas phase, free from the potential distortions present in the crystalline solid.

The structures of both systems have previously been studied to some degree, with a structure of **2** determined by microwave (MW) spectroscopy, yielding a P–B bond length of 190.6 pm,[10] close to the sum of covalent radii for the two atoms. **1** has previously been studied by both GED[11] and MW spectroscopy,[12] but both studies failed to yield complete structures. This chapter revisits both compounds utilising modern GED techniques and analysis methods to allow complete structural determination for both molecules using a combination of GED data and published rotational constants. Such analysis allows conclusions to be drawn on the effects of complexation using comparable results.

2.2 Experimental

2.2.1 Synthesis

The syntheses of methylphosphine,[3,13] diborane[14] and methylphosphine-borane[3,15] were performed by J.-C. Guillemin. Details of the methods used are given in Appendix 2.

2.2.2 Theoretical Methods

Calculations for methylphosphine were performed using a Linux cluster, whilst those for methylphosphine-borane were performed using a Silicon Graphics Altix 4700, both using the Gaussian 03 program.[16] All MP2 methods were frozen core (fc).

Geometry optimisations

An extensive search of the torsional potential of each compound was undertaken at the RHF/3-21G* level[17–19] to locate all minima. For each molecule one minimum with C_s symmetry was located. Further geometry optimisations were conducted for both molecules at the HF,[20] MP2[21] and CCSD(T)[22–25] levels of theory. At the MP2 and CCSD(T) levels optimisations were conducted using both the Pople-type basis sets (6-31G*[26–28] and 6-311G*[29,30]) and the correlation-consistent basis sets of Dunning.[31–35] The optimised structures of **1** and **2** with the atomic numbering schemes are shown in Figure 2.1.

Frequency calculations

Analytic second derivatives[36,37] of the energies with respect to nuclear coordinates calculated at the MP2/6-311++G** level for both compounds served both to confirm the nature of minima found by the optimisations and to provide vibrational information for use in the SARACEN refinements.

Figure 2.1: Lowest energy molecular structures of methylphosphine (**1**) and methylphosphine-borane (**2**).

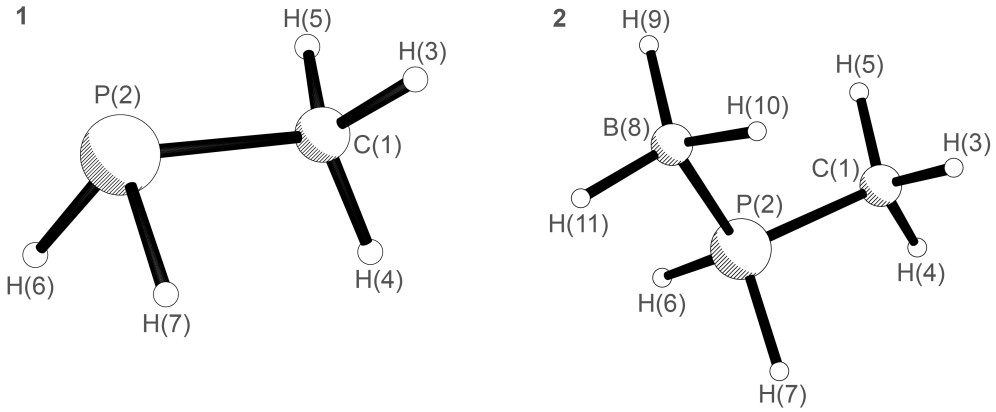

2.2.3 Gas electron diffraction measurements

Data were collected for methylphosphine and methylphosphine-borane using the Edinburgh gas diffraction apparatus.[38] For each molecule, an accelerating voltage of *ca.* 40 kV (electron wavelength *ca.* 6.0 pm) was used. Sample and nozzle temperatures were maintained at 220 and 293 K, respectively, for **1** and 300 and 320 K, respectively, for **2**. Scattering intensities were recorded on Kodak Electron Image films at nozzle-to-plate distances of 127.8 and 284.6 mm for **1** and 92.0 and 249.2 mm for **2**. The weighting points for the off-diagonal weight matrices, correlation parameters and scale factors for the two camera distances for each molecule are given in Table A2.1 in the Appendix, together with electron wavelengths, which were determined from the scattering patterns of benzene vapour, recorded immediately after the compound patterns and analysed in exactly the same way to minimise systematic errors in wavelengths and camera distances. The scattering intensities were measured using an Epson Expression 1680 Pro flatbed scanner and converted to optical densities as a function of the scattering variable, s, using an established program.[39] Data reduction and least-squares refinements were carried out using the ed@ed v2.4 program,[40] employing the scattering factors of Ross *et al.*[41]

2.3 Results

2.3.1 *Ab initio* calculations

Methylphosphine

The lowest-energy structure of methylphosphine on the potential-energy surface had a staggered conformation and possessed C_s symmetry. The effects of improving the basis set and description of electron correlation on the structural parameters were gauged by a series of calculations at the MP2 and CCSD(T) levels of theory using both Pople-type and correlation-consistent basis sets. The results of selected calculations are shown in Table 2.1 with the full results from geometry optimisations given in the Appendix in Tables A2.2 and A2.3.

Table 2.1: Molecular geometries of the lowest-energy structures of methylphosphine (**1**) at the MP2 and CCSD(T) levels of theory using the 6-311++G** (A) and aug-cc-pVQZ (B) basis sets.[a]

	MP2		CCSD(T)	
	A	B	A	B[b]
rC(1)–H(3)	109.2	108.7	109.6	109.1
rC(1)–H(4)	109.1	108.5	109.4	108.9
rP(2)–C(1)	185.6	185.1	186.7	185.9
rP(2)–H(6)	141.0	141.1	141.7	141.7
∠P(2)–C(1)–H(3)	109.0	108.6	109.0	108.9
∠P(2)–C(1)–H(4)	113.8	113.4	113.6	113.2
∠H(3)–C(1)–H(4)	108.7	109.2	108.7	109.2
∠H(3)–C(1)–H(5)	107.5	107.7	107.6	107.8
∠C(1)–P(2)–H(6)	97.6	97.8	97.2	97.6
∠H(6)–P(2)–H(7)	94.6	93.5	94.4	93.3
Energy[c]	–381.8117	–381.9166	–381.8599	–381.9685

[a] All distances in pm and angles in °. See Figure 2.1 for atom numbering.
[b] Extrapolated using CCSD(T)/aug-cc-pVQZ = CCSD(T)/aug-cc-pVTZ + [MP2/aug-cc-pVQZ - MP2/aug-cc-pVTZ].
[c] Energy in Hartrees.

The structure of **1** was found to be largely independent of the level of theory used, with two main exceptions. In the MP2 optimisations using Pople-type basis sets

the P–H distance shortens by 0.7 pm when polarisation functions are added to the H atoms, indicating the need for such functions to describe this bond accurately. The P–C bond length is also sensitive to the level of theory, varying by 1.6 pm across the calculations shown in Table 2.1.

Methylphosphine-borane

The lowest-energy structure of methylphosphine-borane on the potential-energy surface was an all-staggered conformation with C_s symmetry, and the same series of calculations was performed as for **1**.

Table 2.2: Molecular geometries of the lowest-energy structure of methylphosphine-borane (**2**) at the MP2 and CCSD(T) levels of theory using the 6-311++G** (A) and aug-cc-pVQZ (B) basis sets.[a]

	MP2		CCSD(T)	
	A	B	A	B[b]
rC(1)–H(3)	109.2	108.7	109.5	109.0
rC(1)–H(4)	109.1	108.5	109.4	108.9
rP(2)–C(1)	182.1	181.3	182.9	182.2
rP(2)–H(6)	140.1	140.0	140.5	140.5
rP(2)–B(8)	192.8	191.4	193.9	192.5
rB(8)–H(9)	120.9	120.6	121.3	121.1
rB(8)–H(11)	120.6	120.2	121.0	120.6
∠P(2)–C(1)–H(3)	108.6	108.1	108.6	108.3
∠P(2)–C(1)–H(4)	112.3	112.4	112.2	112.0
∠H(3)–C(1)–H(4)	109.5	109.9	109.5	109.9
∠H(3)–C(1)–H(5)	108.2	108.3	108.4	108.4
∠C(1)–P(2)–H(6)	103.2	103.5	103.1	103.4
∠H(6)–P(2)–H(7)	100.3	99.8	100.3	99.7
∠C(1)–P(2)–B(8)	115.0	114.5	115.2	114.7
∠P(2)–B(8)–H(9)	103.3	102.8	103.4	102.9
∠P(2)–B(6)–H(11)	106.1	106.3	106.0	106.4
∠H(9)–B(8)–H(10)	113.7	113.8	113.8	113.7
∠H(9)–B(8)–H(11)	114.3	114.7	114.3	114.7
Energy[c]	–408.3568	–408.4922	–408.4268	–408.5644

[a] All distances in pm and angles in °. See Figure 2.1 for atom numbering.
[b] Extrapolated using CCSD(T)/aug-cc-pVQZ = CCSD(T)/aug-cc-pVTZ + [MP2/aug-cc-pVQZ - MP2/aug-cc-pVTZ].
[c] Energy in Hartrees.

A selection of the structural parameters and energies from these calculations is given in Table 2.2, with the full results from the series of optimisations given in Tables A2.4 and A2.5 in the Appendix. The absolute values of most structural parameters were found to be independent of the level of theory and basis set used. However, the P–C and P–B bond lengths were found to vary significantly across the range of calculations performed. In calculations with the largest basis sets the P–C bond length varied from 181.3 pm to 182.9 pm and the P–B bond varied from 191.4 pm to 193.9 pm. In both cases the CCSD(T) calculations produced longer bond lengths than MP2, and the Pople-type basis sets longer bond lengths than the correlation-consistent basis sets.

2.3.2 Gas electron diffraction refinements

Methylphosphine

On the basis of the *ab initio* calculations described above, electron-diffraction refinements were carried out using a model with appropriate C_s symmetry. The calculations show that the CH_3 group does not possess local C_3 symmetry, with the C–H bond lengths differing by 0.2 pm and the H(3)–C–H(4) and H(3)–C–H(5) angles by around 1°. The difference in C–H bond lengths of 0.2 pm is too small to be differentiated by the diffraction experiment, so the C–H bond length in the CH_3 group was modelled by a single parameter. The deviation in angle is more pronounced and was therefore included in the model.

The structure of **1** was defined in terms of eight independent geometric parameters, comprising three bond lengths and five bond angles (Table 2.3; atom numbering shown in Figure 2.1). The C, P and H(4) atoms lie on the mirror plane of the molecule. The C–H bond lengths were modelled by a single parameter (p_1) and the P–C (p_2) and P–H (p_3) bond lengths were also included. The two P–C–H angles were defined by the average (p_4) and difference (p_5), given by [∠P(2)–C(1)–H(4) + ∠P(2)–C(1)–H(3)]/2 and [∠P(2)–C(1)–H(4) – ∠P(2)–C(3)–H(3)]/2, respectively. The remaining bond angles were ∠H(3)–C(1)–H(5)

(p_6), ∠C(1)–P(2)–H(6) (p_7) and ∠H(6)–P(2)–H(7) (p_8). To allow for deviations from perfect C_s symmetry the H(3)–C(1)–P(2)–X dihedral angle was included as a parameter, where X is defined as the H(6)–P(2)–H(7) bisector. However, no significant deviations were found from C_s symmetry and so this parameter was not included in the final refinement.

The starting parameters for the r_{h1} refinement[42] were taken from the theoretical geometry optimised at the MP2/6-311++G** level. A theoretical Cartesian force field was obtained at this level and converted into a force field described by a set of symmetry coordinates using the SHRINK program,[42] which generated both the amplitudes of vibration (u_{h1}) and the curvilinear corrections (k_{h1}).

Three rotation constants for **1** were combined with the GED data.[12] The rotational constants A_0, B_0 and C_0 were corrected to A_{h1}, B_{h1} and C_{h1} for the structural refinements using values calculated by SHRINK,[42] based on the MP2/6-311++G** force field. To minimise the applied uncertainties the three corrected rotational constants were included in the refinements as the absolute value of B_{h1}, and the differences B_{h1} – A_{h1} and B_{h1} – C_{h1}. These constants are given in Table 2.3. The vibrational corrections to the rotational constants, which transform, for example, A_0 into A_{h1}, are summations of the corrections for each of the normal modes of **1**. For the rotational constant A this correction was 1141.3 MHz and for B and C it was 2.5 and 4.4 MHz, respectively. The uncertainties of the vibrational corrections to the rotational constants were taken as 10% of the value of the vibrational correction for B and 10% of the difference between the corrections for the two differences. The 10% figure is standard for vibrational corrections to rotational constants, based on our experience of how these quantities vary with the computational method used. The weights applied to all data depended on the uncertainties of the observations, in accordance with the SARACEN method.[5–7]

When the refinement was conducted with only the GED data it was possible to refine rP–H and rC–P but rC–H was poorly determined. The P–C–H and C–P–H bond angles refined to reasonable values but had large e.s.d.s of around 4°. It was not possible to refine any bond angles which include two H atoms. Including the

rotation constants reduced the e.s.d.s on all refining parameters, in particular rP–H and the average P–C–H bond angle. However, it was still not possible to refine ∠H(6)–P(2)–H(7) or the difference between the two P–C–H angles. The final refinement combined the GED data, rotational constants and restraints based on the results of *ab initio* calculations using the SARACEN method[5–7] which allowed all eight geometric parameters and four groups of vibrational amplitudes to be refined. Altogether, four geometric restraints (Table 2.3) and one amplitude restraint (Table A2.6) were employed.

The success of the final refinement, for which $R_G = 0.081$ ($R_D = 0.055$), can be assessed on the basis of the radial-distribution curve (Figure 2.2) and the molecular-scattering intensity curves (Figure A2.1). The sticks shown in Figure 2.2 indicate all the interatomic distances in the molecule. Final refined parameters are listed in Table 2.3. Appendix 2 contains the interatomic distances and the corresponding amplitudes of vibration (Table A2.6), with the least-squares correlation matrix (Table A2.7) and the experimental coordinates from the GED analysis (Table A2.8).

Figure 2.2: Experimental and difference (experimental – theoretical) radial-distribution curves, $P(r)/r$, for methylphosphine (**1**). Before Fourier inversion the data were multiplied by $s.\exp(-0.00002s^2)/(Z_C - f_C)(Z_P - f_P)$.

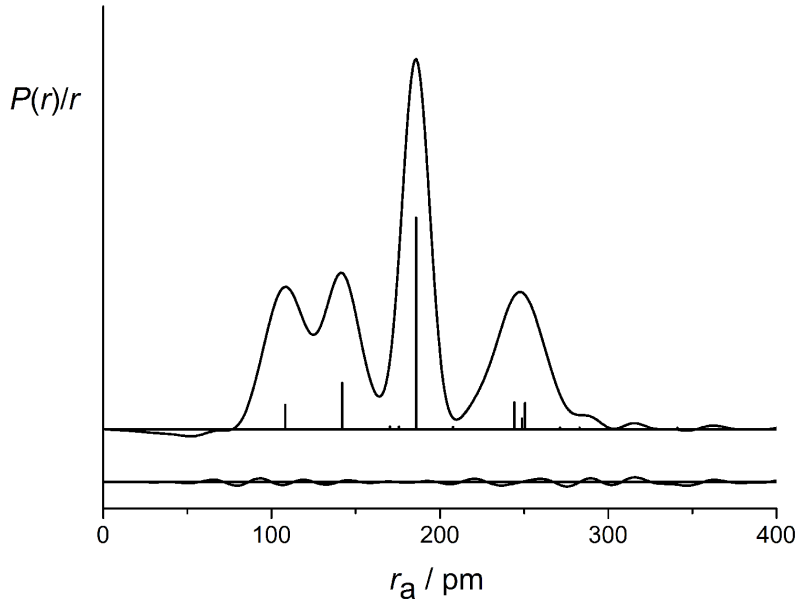

Table 2.3: Refined and calculated geometric parameters for methylphosphine (**1**) (distances in pm and angles in °) from the GED study and rotational constants, in MHz, used in the GED refinements.[a,b]

	Parameter	MP2/ 6-311++G**	SARACEN (r_{h1})	Restraint
Independent parameters				
p_1	rC(1)–H(3)	109.2	108.0(1)	109.1(10)
p_2	rP(2)–C(1)	185.6	185.72(6)	—
p_3	rP(2)–H(6)	141.0	142.1(1)	—
p_4	∠P(2)–C(1)–H_{av}	111.4	111.7(4)	—
p_5	∠P(2)–C(1)–H_{dif}	2.4	2.4(4)	2.4(4)
p_6	∠H(3)–C(1)–H(4)	108.7	109.0(9)	—
p_7	∠C(1)–P(2)–H(6)	97.6	97.4(8)	97.6(10)
p_8	∠H(6)–P(2)–H(7)	94.6	94.2(8)	94.6(10)
Dependent parameters				
dp_1	∠P(2)–C(1)–H(3)	109.0	109.4(4)	—
dp_2	∠P(2)–C(1)–H(4)	113.8	114.1(6)	—
Rotational constants				
Constant	Exp.	GED	Exp. – GED	Uncertainty
B_{h1}	11795.10	11795.08	0.02	0.25
$B_{h1} - A_{h1}$	–61129.20	–61082.05	–47.15	114.00
$B_{h1} - C_{h1}$	113.00	113.01	–0.01	0.20

[a] Figures in parentheses are the estimated standard deviation of the last digits.
[b] See text for parameter definitions.

Methylphosphine-borane

The refinement of the structure of methylphosphine-borane was conducted using a model of C_s symmetry. Again it was found that the CH_3 group did not possess local C_3 symmetry, and neither did the BH_3 group. As before, the deviation in angles was modelled but the deviation in bond lengths was not, because calculated differences were very small. All C–H and all B–H bond lengths were thus assumed to be the equal. Fourteen independent geometric parameters were used to model the molecule, comprising five bond lengths and nine bond angles. The CH_3PH_2 fragment of **2** was described in the same way as **1**, with the exception that an average and difference were used to describe rP–C and rP–B bond lengths. The unique parameters for **2** were rB–H (p_5), ∠C(1)–P(2)–B(8) (p_{12}), ∠H(9)–B(8)–

H(10) (p_{13}) and the two ∠P(2)–B(8)–H, for which an average and difference were used (p_8, p_9) such that ∠P(2)–B(8)–H(11) = p_8 + p_9 and ∠P(2)–B(8)–H(9) = p_8 – p_9. As for **1** additional parameters were available to allow for deviation from C_s symmetry in the form of ϕH(4)–C(1)–P(2)–B(8) and ϕC(1)–P(2)–B(8)–H(11), but again neither of these parameters refined to a value that indicated a meaningful deviation from C_s symmetry, and so they were not included in the final refinement. The starting parameters, amplitudes of vibration and curvilinear corrections were obtained in the same way as for **1**.

A total of nine rotational constants for **2** were combined with the GED data.[10] These corresponded to the parent compound (labelled I) and the ^{13}C (II) and ^{10}B (III) isotopomers. Although microwave data were available for the deuterated species, these were not included in the refinement because C-D bond lengths and angles may differ from their C-H analogues and so the data are likely to introduce unknown errors in the structure. The rotational constants were corrected in the same way as for **1**. To minimise the applied uncertainties the corrected rotation constants were included in the refinements as the absolute value of C_{h1} for the parent compound, the differences between C_{h1} for the parent and isotopomers *i.e.* C_{h1}(I) – C_{h1}(II), C_{h1}(I) – C_{h1}(III) and as differences between C_{h1} and $A_{\mathrm{h1}}/B_{\mathrm{h1}}$ for each isotopomer, *i.e.* C_{h1}(I) – B_{h1}(I), C_{h1}(I) – C_{h1}(I), C_{h1}(II) – B_{h1}(II) *etc.* These constants are given in Table 2.4.

As for **1** an initial refinement was conducted using only the GED data. In this case it was possible to refine the bond distances and ∠C–P–B, although the e.s.d. for ∠C–P–B was over 1°. No other parameters refined to reasonable values. When the rotational constants were included the e.s.d.s on the bond distances reduced slightly and the e.s.d. on ∠C–P–B reduced dramatically to 0.1°. With the MW data it was possible to refine 2–3 additional bond angles such as P–B–H and P–C–H, but when additional parameters were refined the precision and accuracy reduced, presumably due to correlation. In **2** there are lots of similar distances and eight of the eleven atoms are H, so it is unsurprising that so few parameters can be refined. This refinement benefits greatly from the use of calculated restraints.

Figure 2.3: Experimental and difference (experimental – theoretical) radial-distribution curve, $P(r)/r$, for methylphosphine-borane (**2**). Before Fourier inversion the data were multiplied by $s.\exp(-0.00002s^2)/(Z_C - f_C)(Z_P - f_P)$.

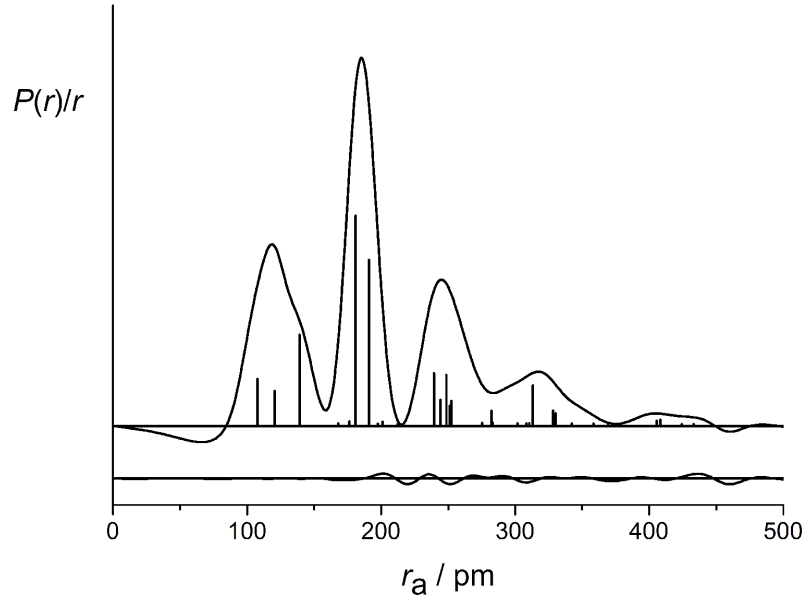

In the final refinement all fourteen geometric parameters and eight groups of vibrational amplitudes were refined. Eleven geometric restraints (Table 2.4) and six amplitude restraints (Appendix Table A2.9) were employed using the SARACEN method.[5–7] The success of the final refinement, for which $R_G = 0.100$ ($R_D = 0.080$), can be assessed on the basis of the radial-distribution curve (Figure 2.3) and the molecular scattering intensity curves (Appendix Figure A2.2). Final refined parameters are listed in Table 2.4. The Appendix contains the interatomic distances and the corresponding amplitudes of vibration (Table A2.9), with the least-squares correlation matrix (Table A2.10) and the experimental coordinates from the GED analysis (Table A2.11).

Table 2.4: Refined and calculated geometric parameters for methylphosphine-borane (**2**) (distances in pm and angles in °) from the GED study and microwave rotation constants, in MHz, used in the GED refinements.[a,b]

	Parameter	MP2/ 6-311++G**	SARACEN (r_{h1})	Restraint
Independent parameters				
p_1	rP–C/rP-B_{av}	187.5	186.1(1)	—
p_2	rP–C/rP–B_{dif}	5.4	5.0(2)	—
p_3	rC–H	109.2	108.7(5)	109.2(8)
p_4	rP–H	140.1	139.3(5)	140.1(8)
p_5	rB–H	120.8	119.9(5)	120.8(10)
p_6	∠P–C–H_{av}	110.4	111.1(6)	110.5(10)
p_7	∠P–C–H_{dif}	1.9	1.8(4)	1.9(4)
p_8	∠P–B–H_{av}	104.7	106.2(5)	104.7(7)
p_9	∠P–B–H_{dif}	1.4	1.3(5)	1.4(5)
p_{10}	∠H(3)–C(1)–H(4)	109.5	110.2(8)	109.5(10)
p_{11}	∠C–P–H	103.2	102.6(8)	103.2(10)
p_{12}	∠C–P–B	115.0	115.0(1)	—
p_{13}	∠H(9)–B(8)–H(10)	114.3	114.4(6)	114.3(7)
p_{14}	∠H(7)–P(2)–H(6)	100.3	99.8(9)	100.3(10)
Dependent parameters				
dp_1	rP(2)–C(1)	182.1	181.1(2)	—
dp_2	rP(2)–B(8)	192.8	191.1(2)	—
dp_3	∠P(2)–C(1)–H(3)	108.6	109.3(6)	—
dp_4	∠P(2)–C(1)–H(4)	112.3	112.9(7)	—
dp_5	∠P(2)–B(8)–H(11)	106.1	107.5(7)	—
dp_6	∠P(2)–B(8)–H(10)	103.3	104.9(6)	—

Rotational constants

Constant	Exp.	GED	Exp. – GED	Uncertainty
C_{h1}(I)-A_{h1}(I)	–12739.5	–12731.1	–8.4	12.8
C_{h1}(I)-B_{h1}(I)	–1011.7	–1011.3	–0.4	1.6
C_{h1}(I)	4985.8	4985.4	0.4	0.8
C_{h1}(II)-A_{h1}(II)	–12758.3	–12767.9	9.6	13.0
C_{h1}(II)-B_{h1}(II)	–1056.8	–1057.6	0.9	1.5
C_{h1}(II)-C_{h1}(II)	–151.9	–152.0	0.1	0.1
C_{h1}(III)-A_{h1}(III)	–12687.2	–12679.6	–7.6	12.5
C_{h1}(III)-B_{h1}(II)	–977.7	–976.9	–0.7	1.5
C_{h1}(III)-C_{h1}(III)	121.0	121.0	0.0	0.1

[a] Figures in parentheses are the estimated standard deviation of the last digits.

[b] See text for parameter definitions.

2.4 Discussion

The molecular structures of methylphosphine and methylphosphine-borane have been investigated in the gas phase by GED supplemented by rotational constants and *ab initio* calculations *via* the SARACEN method. An theoretical investigation of the structures was also undertaken.

The experimental structure of **1** is found to be generally in good agreement with both the theoretical structures and previous experimental results. For comparison, a selection of parameters from previous GED and MW studies are given in Table 2.5. It should be noted that neither the previous MW nor the earlier GED structure is complete, with each offering only a partial structure or requiring the use of fixed parameters.

Table 2.5: A selection of structural parameters (distances in pm and angles in °) from previous GED[11] and MW[12] studies of methylphosphine (**1**) and a MW[10] study of methylphosphine-borane (**2**).[a,b]

Parameter	Previous GED[11]	MW[10,12]	This study
Methylphosphine			
rP–C	185.8(3)	186.3[e]	185.72(6)
rC–H[c]	109.4(8)	109.3[e]	108.0(1)
rP–H	142.3(7)	141.4[e]	142.1(1)
∠H–P–H	—	93.2[e]	94.2(8)
∠C–P–H	96.5[d]	—	97.4(8)
Methylphosphine-borane			
rP–C	—	180.9(6)	181.1(2)
rP–B	—	190.6(6)	191.1(2)
rP–H	—	140.4(6)	139.3(5)
∠H–P–H	—	99.4(9)	99.8(9)
∠C–P–H	—	103.2(6)	102.6(8)
∠C–P–B	—	115.7(4)	115.0(1)

[a] Figures in parentheses are the estimated standard deviation of the last digits.
[b] See text for parameter definitions.
[c] In both studies the methyl group was assumed to possess local C_3 symmetry.
[d] The parameter was fixed at this value and not allowed to refine.
[e] No estimated standard deviations were reported for this parameter.

The calculated structure was found to be generally independent of the level of theory and basis set used, with parameters generally varying by less than 1 pm in the case of bond lengths or 1° for angles, despite the wide range of calculations conducted. The largest deviations were observed for the P–C distance, which varied by 1.5 pm. Therefore it can be stated that the molecule is adequately described by the MP2/6-311++G** level of theory.

Comparing our experimental structure to the theoretical results, the P–C distance of 185.72(6) pm is in the middle of the range of calculated values, closest to the MP2/6-311++G** calculations. The relatively small uncertainty on the experimental distance brings in to question the precision of the calculated distances, and no clear convergence is found as the level of theory and basis set is improved. The experimental distance is also comparable to the previous GED structure.

The P–H distance [142.1(1) pm] is in agreement with the largest calculated values, and is consistent with the value obtained from the previous GED study. The longest calculated bond lengths were obtained using correlation-consistent basis sets, with the P–H distance being 141.7 pm at CCSD(T)/aug-cc-pVQZ, and longer still when double- or triple-zeta basis sets are used. In contrast, the experimental C–H bond distances were found to agree with the shortest experimental bond lengths, corresponding to the MP2/aug-cc-pVQZ level of theory.

The remaining parameters, all bond angles, are found to be in good agreement with theoretical structures, although it must be noted that they all refer to angles involving hydrogen atoms and theoretical restraints were used for some parameters. The H–P–H angle is found to be 94.2(8)°, slightly larger than the 93.6(3)° angle found in PH_3 [43] and significantly smaller than the >100° angle that is generally found in tertiary phosphines. The reduction in cone angle corresponds to an increase in *s* character in the phosphorus lone pair and a decrease in basicity, and is expected to lead to different properties when such molecules are used as ligands. [1]

The previous GED experiment assumed a fixed C–P–H angle of 96.5°, whilst the current study found the angle to be 97.4(8)°. The calculated angle was consistently around 97.5°. It is therefore likely that the previous study underestimated the C–P–H angle, which may have influenced the experimentally determined parameters.

For **2**, a selection of structural parameters from a previous MW study is shown in Table 2.5. As was the case with **1**, the structure of **2** was found to be largely independent of the level of theory used. The only major exception to this is the P–B bond length, which varies by >2.5 pm across the range of calculations performed. This bond length is likely to be sensitive to the nature of the charge transfer from the phosphorus lone pair to the empty *p*-orbital of the boron atom, so it is understandable that the parameter is dependent on both the description of electron correlation employed, and the basis set used.

The experimental and computed structures show a good level of agreement. The P–B bond length is found by experiment to be 191.1(2) pm, a value which is consistent with the shortest of the calculated bond lengths, lying just below the MP2/6-311++G** value. As both bond lengths calculated at the CCSD(T) level of theory deviated from the experimental value by a large amount, this result seems to suggest that the MP2 level of theory is better at predicting this bond length. The experimental P–C bond length is 181.1(2) pm, again at the shorter end of the theoretical values, closer to the values calculated at the MP2 level of theory. For **1** the experimental P–H bond length was found to be closest to the longer theoretical distances, whereas in the complex the reverse is true. The distance from this study, 139.3(5) pm, is shorter than all the theoretical values and the value from the MW study, although this is only 1-2σ smaller than the calculated values at the MP2/6-311++G** and MP2/aug-cc-pVQZ levels. The experimental B–H distance is again consistent with the shortest of the calculated values, being around 1σ from the computed value at the MP2/aug-cc-pVQZ level of theory [119.9(5) pm compared to 120.4 pm].

The remaining experimental bond angles and torsion angles are all reasonably close to the calculated parameters, with the exception of the P–B–H bond angles,

Table 2.6: The changes in structural parameters (bond lengths in pm and angles in °), defined as methylphosphine-borane – methylphosphine, from this study and *ab initio* calculations at the MP2 and CCSD(T) levels of theory using the 6-311++G** (A) and aug-cc-pVQZ (B) basis sets.[a,b]

		MP2		CCSD(T)		Theoretical
	This study[c]	A	B	A	B	average
rC–H	0.7(5)	0.0	0.0	–0.1	–0.1	–0.05(5)
rC(1)–H(3)	0.7(5)	0.0	0.0	0.0	0.0	0.0(0)
rP(2)–C(1)	–4.6(2)	–3.5	–3.8	–3.8	–3.8	–3.7(2)
rP(2)–H(6)	–2.8(5)	–0.9	–1.1	–1.2	–1.3	–1.1(2)
∠P(2)–C(1)–H(3)	–0.1(7)	–0.4	–0.5	–0.4	–0.4	–0.42(3)
∠P(2)–C(1)–H(4)	–1.2(9)	–1.5	–1.1	–1.4	–1.0	–1.3(3)
∠C(1)–P(2)–H(6)	5.2(11)	5.6	5.7	5.9	5.8	5.7(1)
∠H(6)–P(2)–H(7)	5.6(12)	5.8	6.3	6.0	6.5	6.1(3)

[a] Figures in parentheses are the estimated standard deviation of the last digits. For the theoretical average the standard deviation was calculated from the four sets of calculations shown.
[b] See text for parameter definitions.
[c] For the SARACEN refinement no distinction was made between the two rC–H.

which are slightly larger than the calculations suggest.

To investigate the structural changes in **1** upon complexation to form **2**, the differences between comparable parameters were calculated. The changes in parameters from the SARACEN refinements and a selection of theoretical calculations are shown in Table 2.6.

Significant differences between the geometry of **1** and **2** are found, particularly around the phosphorus atom. The P–C bond is found to shorten by around 4 pm by both experiment and theory, whilst both the H–P–H and C–P–H angles increase by approximately 6°. This represents a move towards a more regular tetrahedral geometry, with the cone angles now found around phosphorus being close to those found in the more stable secondary and tertiary phosphines. [For example, the C–P–C angle in trimethylphosphine is 98.9(2)°.][44]

The borane group, previously having D_{3h} symmetry, becomes pyramidal upon complexation and does not possess local C_{3v} symmetry as the complex has overall C_s symmetry. The B–H bond length is about 1.5 pm shorter in the adduct

Table 2.7: The changes in Mulliken charge of the P atom in units of e, defined as methylphosphine-borane – methylphosphine, from *ab initio* calculations at the MP2 and CCSD(T) levels of theory using the 6-311++G** (A) and aug-cc-pVQZ (B) basis sets.

MP2		CCSD(T)	
A	B	A	B
0.34	0.60	0.33	0.47

(based on the calculated B–H bond length in BH_3), and the H–B–H angles reduce from 120° to around 114°. The newly formed P–B–H angles are 107.5(7)° and 104.9(6)°.

The shortening of the P–H bond upon complexation, estimated by calculation to be 1.1 pm, is found to be 2.8 pm by this study. The experimentally determined P–H bond length was found to be at the longer end of the calculated bond lengths for **1** and at the shorter end for **2**; these results combine to produce the larger change in bond length by experiment than theory suggests.

The P–C bond is found to shorten dramatically (-4.6 pm by experiment, -3.7 pm by theory) upon complexation. Such a shortening can be rationalised by considering charge transfer. The relative electronegativities of P and C (Pauling scale; C = 2.55, P = 2.19)[45] suggest the P–C bond is polarised such that the C atom has a negative charge. When the P atom donates electron density to boron in **2** it must become more positive, and therefore more strongly bound to the negatively charged C, shortening the P–C bond. This is backed up by the calculated Mulliken charges, which suggest P becomes more positive by around $0.4e$. The change in charge of the P atom upon complexation shown in Table 2.7.

The gas-phase dissociation energy of methylphosphine-borane, defined as $MePH_2{\cdot}BH_3 \rightarrow BH_3 + MePH_2$, has been assessed at the MP2/6-311++G** level of theory and was found to 95 kJ mol^{-1}. The counterpoise method was used to account for BSSE and ZPE corrections were included.[46,47] For comparison, the same quantity in the nitrogen analogue, $MeNH_2{\cdot}BH_3$, was previously estimated to be 146 kJ mol-1.[48] The enthalpy of formation, defined as $\frac{1}{2}B_2H_6 + MePH_2 \rightarrow MePH_2{\cdot}BH_3$, was calculated in the same way and found to be -27.8 kJ mol^{-1},

whilst for $MeNH_2.BH_3$ the value is -73 kJ mol^{-1}.[49] The weaker bonding in the phosphine is expected due to its lower basicity.[50]

2.5 Conclusion

Primary phosphines have received relatively little attention in the literature and are not widely used by chemists. However, complexation with borane results in a protected, less volatile compound which can be used in further synthesis more easily than the free phosphine. The complete gas-phase structures of methylphosphine and methylphosphine-borane have been determined for the first time and the structural changes that occur on complexation have been assessed. Large changes in geometry around the phosphorus atom are found, including a widening of the H–P–H angle and a shortening of the P–C bond upon complexation. The P–B distance is found to be 191.1(2) pm.

2.6 References

[1] M. Brynda, *Coord. Chem. Rev.*, 2005, **249**, 2013.

[2] G. Becker, O. Mundt, M. Roessler and E. Schneider, *Z. Anorg. Allg. Chem.*, 1978, **443**, 42.

[3] K. Bourumeau, A.-C. Gaumont and J.-M. Denis, *J. Organomet. Chem.*, 1997, **529**, 205.

[4] H. Dorn, R. A. Singh, J. A. Massey, J. M. Nelson, C. A. Jaska, A. J. Lough and I. Manners, *J. Am. Chem. Soc.*, 2000, **122**, 6699.

[5] A. J. Blake, P. T. Brain, H. M. Nab, J. Miller, C. A. Morrison, S. Parsons, D. W. H. Rankin, H. Robertson and B. A. Smart, *J. Phys. Chem. A*, 1996, **100**, 12280.

[6] P. T. Brain, C. A. Morrison, S. Parsons and D. W. H. Rankin, *J. Chem. Soc., Dalton Trans.*, 1996, 4589.

[7] N. W. Mitzel and D. W. H. Rankin, *J. Chem. Soc., Dalton Trans.*, 2003, 3650.

[8] S. Reeve, W. A. Burns, F. J. Lovas, R. D. Suenram and K. R. Leopold, *J. Phys. Chem.*, 1993, **97**, 10630.

[9] K. R. Leopold, M. Canagaratna and J. A. Phillips, *Acc. Chem. Res.*, 1997, **30**, 57.

[10] P. S. Bryan and R. L. Kuckowski, *Inorg. Chem.*, 1972, **11**, 553.

[11] L. S. Bartell, *J. Chem. Phys.*, 1960, **32**, 832.

[12] T. Kojima, E. L. Breig and C. C. Lin, *J. Chem. Phys.*, 1961, **35**, 2139.

[13] W. L. Jolly, *Inorg. Synth.*, 1968, **11**, 124.

[14] W. L. Jolly, *Inorg. Synth.*, 1968, **11**, 15.

[15] A. B. Burg and R. I. Wagner, *J. Am. Chem. Soc.*, 1953, **75**, 3872.

[16] M. J. Frisch, G. W. Trucks, H. B. Schlegel, G. E. Scuseria, M. A. Robb, J. R. Cheeseman, J. A. Montgomery, Jr., T. Vreven, K. N. Kudin, J. C. Burant, J. M. Millam, S. S. Iyengar, J. Tomasi, V. Barone, B. Mennucci, M. Cossi, G. Scalmani, N. Rega, G. A. Petersson, H. Nakatsuji, M. Hada, M. Ehara, K. Toyota, R. Fukuda, J. Hasegawa, M. Ishida, T. Nakajima, Y. Honda, O. Kitao, H. Nakai, M. Klene, X. Li, J. E. Knox, H. P. Hratchian, J. B. Cross, V. Bakken, C. Adamo, J. Jaramillo, R. Gomperts, R. E. Stratmann, O. Yazyev, A. J. Austin, R. Cammi, C. Pomelli, J. W. Ochterski, P. Y. Ayala, K. Morokuma, G. A. Voth, P. Salvador, J. J. Dannenberg, V. G. Zakrzewski, S. Dapprich, A. D. Daniels, M. C. Strain, O. Farkas, D. K. Malick, A. D. Rabuck, K. Raghavachari, J. B. Foresman, J. V. Ortiz, Q. Cui, A. G. Baboul, S. Clifford, J. Cioslowski, B. B. Stefanov, G. Liu, A. Liashenko, P. Piskorz, I. Komaromi, R. L. Martin, D. J. Fox, T. Keith, M. A. Al-Laham, C. Y. Peng, A. Nanayakkara, M. Challacombe, P. M. W. Gill, B. Johnson, W. Chen, M. W. Wong, C. Gonzalez and J. A. Pople, *Gaussian 03, Revision C.02*, Gaussian, Inc., Wallingford, CT, 2004.

[17] J. S. Binkley, J. A. Pople and W. J. Hehre, *J. Am. Chem. Soc.*, 1980, **102**, 939.

[18] M. S. Gordon, J. S. Binkley, J. A. Pople, W. J. Pietro and W. J. Hehre, *J. Am. Chem. Soc.*, 1982, **104**, 2797.

[19] W. J. Pietro, M. M. Francl, W. J. Hehre, D. J. DeFrees, J. A. Pople and J. S. Binkley, *J. Am. Chem. Soc.*, 1982, **104**, 5039.

[20] C. C. J. Roothaan, *Rev. Mod. Phys.*, 1951, **23**, 69.

[21] C. Møller and M. S. Plesset, *Phys. Rev.*, 1934, **46**, 618.

[22] J. Cizek, *Adv. Chem. Phys.*, 1969, **14**, 35.

[23] G. D. Purvis III and R. J. Bartless, *J. Chem. Phys.*, 1982, **76**, 1910.

[24] G. E. Scuseria, C. L. Janssen and H. F. Schaefer-III, *J. Chem. Phys.*, 1988, **89**, 7382.

[25] G. E. Scuseria and H. F. Schaefer III, *J. Chem. Phys.*, 1989, **90**, 3700.

[26] W. J. Hehre, R. Ditchfield and J. A. Pople, *J. Chem. Phys.*, 1972, **56**, 2257.

[27] P. C. Hariharan and J. A. Pople, *Theo. Chim. Acta.*, 1972, **56**, 2257.

[28] M. S. Gordon, *Chem. Phys. Lett.*, 1980, **76**, 163.

[29] A. D. McLean and G. S. Chandler, *J. Chem. Phys.*, 1980, **72**, 5639.

[30] R. Krishnan, J. S. Binkley, R. Seeger and J. A. Pople, *J. Chem. Phys.*, 1980, **72**, 650.

[31] D. E. Woon and T. H. Dunning Jr., *J. Chem. Phys.*, 1993, **98**, 1358.

[32] R. A. Kendall, T. H. Dunning Jr. and R. J. Harrison, *J. Chem. Phys.*, 1992, **96**, 6796.

[33] T. H. Dunning Jr., *J. Chem. Phys.*, 1989, **90**, 1007.

[34] K. A. Peterson, D. E. Woon and T. H. Dunning Jr., *J. Chem. Phys.*, 1994, **100**, 7410.

[35] A. Wilson, T. van Mourik and T. H. Dunning Jr., *THEOCHEM*, 1996, **388**, 339.

[36] M. J. Frisch, M. Head-Gordon and J. A. Pople, *Chem. Phys. Lett.*, 1990, **166**, 275.

[37] M. J. Frisch, M. Head-Gordon and J. A. Pople, *Chem. Phys. Lett.*, 1990, **166**, 281.

[38] C. M. Huntley, G. S. Laurenson and D. W. H. Rankin, *J. Chem. Soc., Dalton Trans.*, 1980, 954.

[39] H. Fleischer, D. A. Wann, S. L. Hinchley, K. B. Borisenko, J. R. Lewis, R. J. Mawhorter, H. E. Robertson and D. W. H. Rankin, *Dalton Trans.*, 2005, 2469.

[40] S. L. Hinchley, H. E. Robertson, K. B. Borisenko, A. R. Turner, B. F. Johnston, D. W. H. Rankin, M. Ahmadian, J. N. Jones and A. H. Cowley, *Dalton Trans.*, 2004, 2469.

[41] A. W. Ross, M. Fink and R. Hilderbrandt, *International Tables for Crystallography*, Kluwer Academic Publishers, Dordrecht, Netherlands, 1992, p. 245.

[42] V. A. Sipachev, *THEOCHEM*, 1985, **121**, 143.

[43] O. N. Ulenikov, E. S. Bekhtereva, G. A. Onopenko and E. A. Sinistin, *J. Mol. Spec.*, 2002, **216**, 252.

[44] P. S. Bryan and R. L. Kuczkowski, *J. Chem. Phys.*, 1971, **55**, 3049.

[45] J. Emsley, *The Elements*, Oxford University Press, Oxford, 1989.

[46] S. Simon, M. Duran and J. J. Dannenberg, *J. Chem. Phys.*, 1996, **105**, 11024.

[47] S. F. Boys and F. Bernardi, *Mol. Phys.*, 1970, **19**, 553.

[48] A. Haaland, *Angew. Chem., Int. Ed. Engl.*, 1989, **78**, 2061.

[49] R. E. McCoy and S. H. Bauer, *J. Am. Chem. Soc.*, 1956, **78**, 2061.

[50] S. Ikuta and P. Kebarle, *Can. J. Chem.*, 1983, **61**, 97.

Chapter 3

Structures of primary phosphines. Are they different from amines?

3.1 Introduction

Following the study of methylphosphine and methylphosphine–borane detailed in Chapter 2, it was decided to study a series of substituted primary phosphines and their adducts with borane. The study is split into two parts, with the structures of the primary phosphines detailed in this chapter and the phosphine–borane adducts presented in Chapter 4.

Primary phosphines have many potential applications[1] and are interesting from a structural perspective. Previous microwave (MW) spectroscopic studies of alkylphosphines have shown the P–C bond length to vary greatly,[2] with values including 183.4 pm in cyclopropylphosphine[3] and 189.6 pm in $(CH_3)_3CPH_2$,[4] although no e.s.d.s were quoted. A similar range of bond lengths is found when strongly electronegative fluorine atoms are substituted for either the methyl or phosphino hydrogen atoms in methylphosphine, with a P–C length of 182.0 pm for CH_3PF_2[5] (no e.s.d. reported) and 190.0(6) pm for CF_3PH_2,[6] both using MW spectroscopy. Primary phosphines also display interesting conformational behaviour that is often quite different to that of their nitrogen analogues. For example, whilst propargylamine ($HCCCH_2NH_2$) has a C_s conformation that is lower in energy than C_1 by around 6 kJ mol^{-1}, propargylphosphine ($HCCCH_2PH_2$) consists of roughly equal amounts of C_s and C_1 conformers.[7,8] Such differences are attributed to the more diffuse P lone pair and the longer, less polar, P–H bonds. For primary phosphines with more than one conformation, significant structural differences have previously been noted between the various conformers. For example, in chloromethylphosphine ∠Cl-C-P was found to be 115.7(1)° in the *anti* conformer and 107.8(5)° in the *gauche*, when determined using gas-phase electron diffraction.[9] This difference was rationalised by considering the nature of the overlap between non-bonding and antibonding molecular orbitals for each conformer. A similar difference in bond angles between different conformations was also observed in a MW spectroscopic study of ethylphosphine.[2]

A number of primary phosphines have been studied by MW spectroscopy but

very few complete experimental structures have ever been determined. The GED structures of eight primary phosphines (allyl, allenyl, propargyl, vinyl, ethynyl, chloromethyl, phenyl and benzylphosphine) are presented in this chapter. Allylphosphine,[10] allenylphosphine,[11] propargylphosphine,[8] vinylphosphine[12] and ethynylphosphine[13] have been studied using MW spectroscopy before but full structures were not determined. Chloromethylphosphine[9] and phenylphosphine[14] have been studied previously by GED but are now studied using modern refinement techniques. The structure of benzylphosphine is studied for the first time. The structures of methylphosphine,[15] ethylphosphine[2] and cyclopropylphosphine[3] have been determined in previous studies and will be used for comparison. The systematic study of α-β and β-γ unsaturated alkenyl– and alkynyl–phosphines and arylphosphines offers an excellent opportunity to assess the structural effects and bonding trends in primary phosphines as a function of the substitutent. As a result of the structural information obtained, trends in key parameters such as the P–C bond length and the C–C–P bond angles are identified, and are compared with rules devised for similar systems.[16]

3.2 Experimental

3.2.1 Syntheses

The syntheses of all compounds were performed by J.-C. Guillemin and B. Khater (Rennes, France).

The starting materials lithium aluminium hydride, aluminium trichloride, diethyl vinylphosphonate, dichlorophenylphosphine, diethyl benzylphosphonate and tetraethyleneglycol dimethyl ether (tetraglyme) were all purchased from Aldrich. All the experiments at atmospheric pressure were performed under nitrogen.

The preparations of allylphosphine (**1**),[17] propargylphosphine (**2**),[18] allenylphosphine (propadienylphosphine) (**3**),[19] vinylphosphine (**4**),[20] benzylphosphine (**5**),[21] chloromethylphosphine (**6**),[22,23] ethynylphosphine[24] (**7**) and phenylphosphine[21] (**8**) have already been reported. In several cases the published syntheses have been partially modified in this work. The exact experimental procedures used to synthesise compounds **1**–**8** are given in Appendix 3.1.

3.2.2 Computational methods

Calculations were performed for all compounds studied using the resources of the NSCCS[25] and the EaStCHEM RCF[26] using the Gaussian 03 program.[27] All MP2 methods were frozen core (fc).

Geometry optimisations

An extensive search of the torsional potential of each compound was undertaken at the RHF/3-21G* level[28–30] to locate all minima. Geometry optimisations were conducted at the RHF[31] and MP2[32] levels of theory using both the Pople-type basis sets (6-31G*[33–35] and 6-311G*[36,37]) and the correlation-consistent basis sets of Dunning.[38–42] The optimised structures of the compounds studied, along with the atomic numbering schemes, are shown in Figures 3.1 and 3.2.

Frequency calculations

Analytic second derivatives[43,44] of the energies with respect to nuclear coordinates were calculated at the MP2/6-311++G** level for each compound both to confirm the nature of the minima found by the optimisation and for use with the SHRINK program.[45]

Figure 3.1: Molecular structures of the relevant conformations of allylphosphine (**1a**–**c**), propargylphosphine (**2a**,**b**), allenylphosphine (**3a**,**b**) and vinylphosphine (**4a**,**b**).

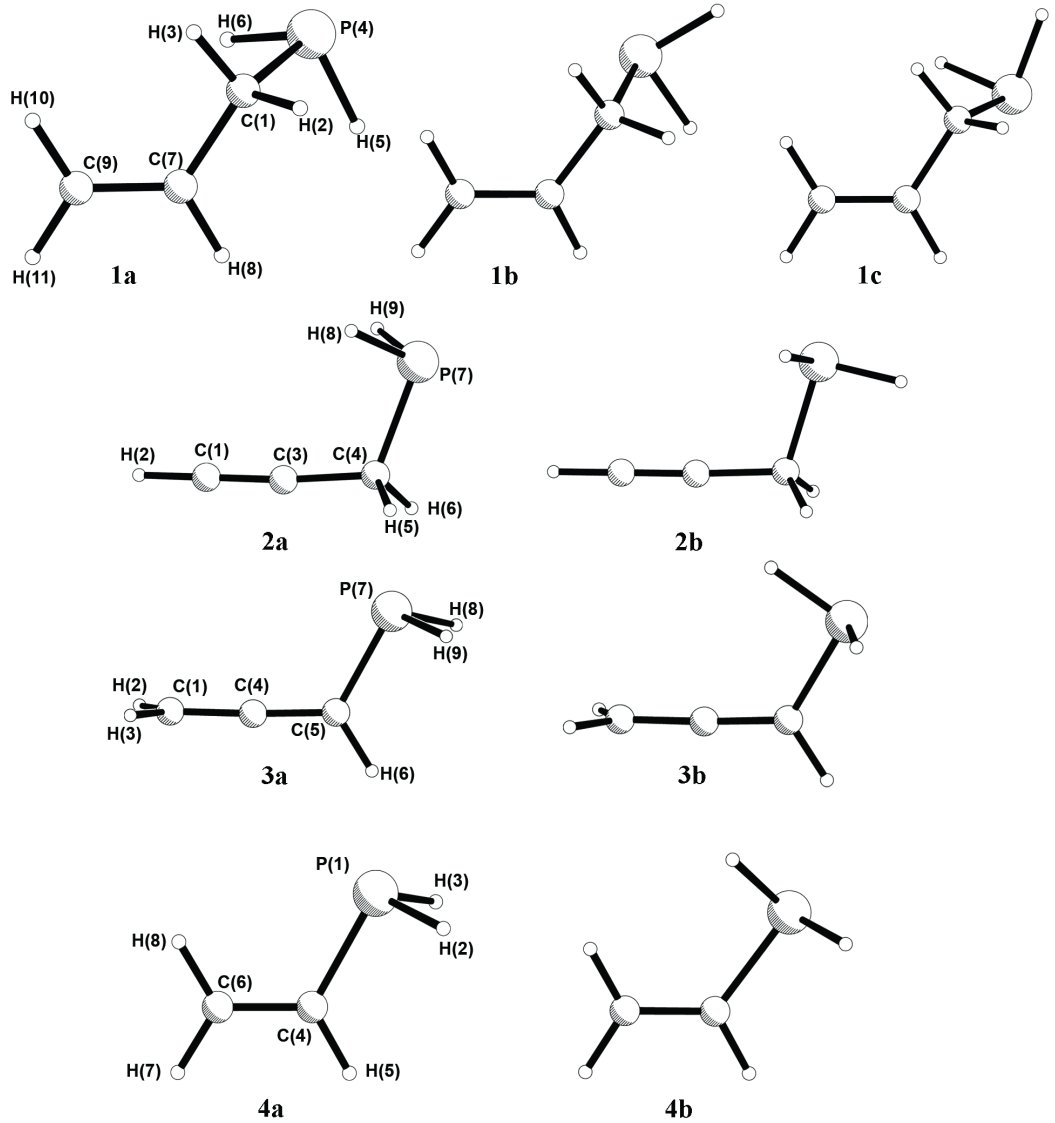

Figure 3.2: Molecular structures of the relevant conformations of benzylphosphine (**5a**,**b**), chloromethylphosphine (**6a**,**b**), ethynylphosphine (**7**) and phenylphosphine (**8**).

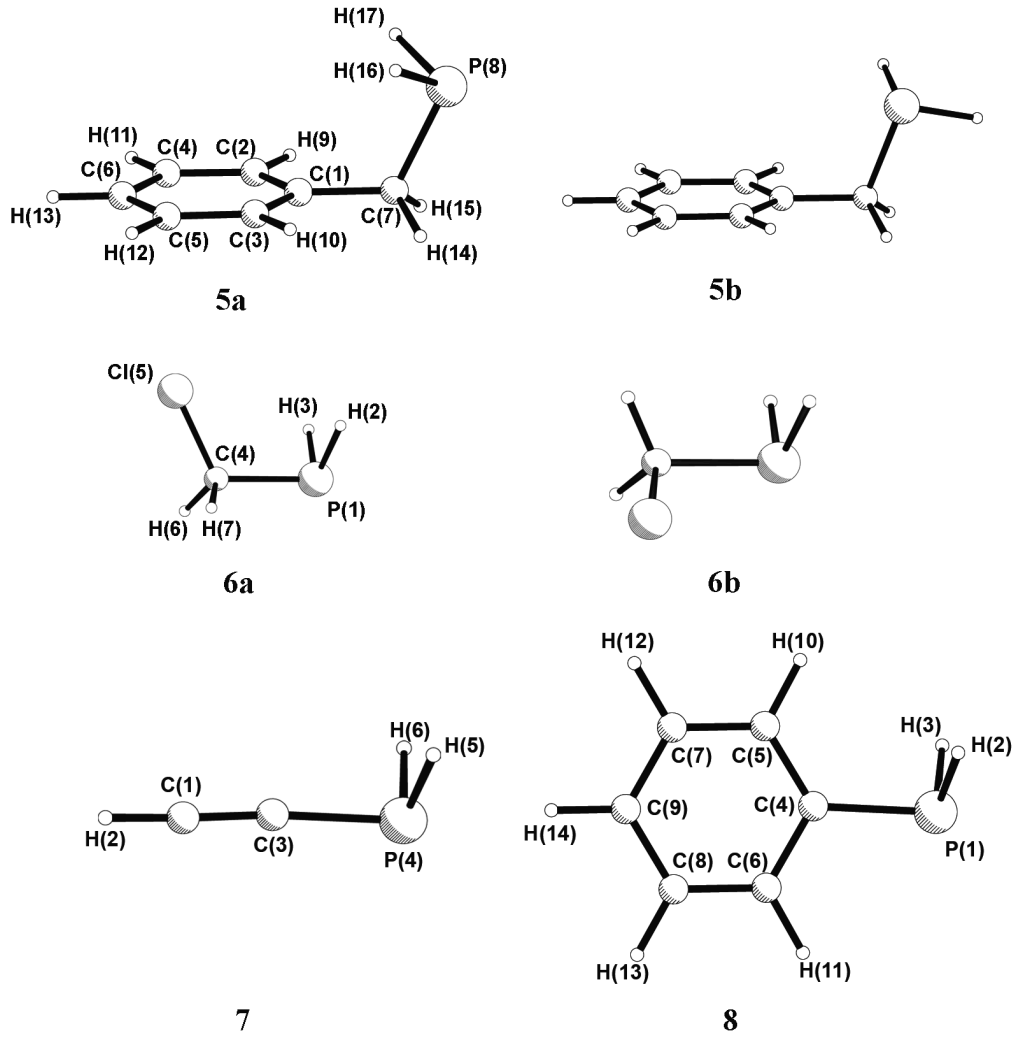

3.2.3 GED measurements

Data were collected for all the compounds studied using the Edinburgh gas electron diffraction apparatus.[46] For each molecule, an accelerating voltage of *ca.* 40 kV (electron wavelength *ca.* 6.0 pm) was used. Scattering intensities were recorded on Kodak Electron Image films. Sample and nozzle temperatures

and nozzle-to-plate distances for each compound can be found in Appendix 3, along with the weighting points for the off-diagonal weight matrices, correlation parameters, scale factors and electron wavelengths. The electron wavelengths were determined from the scattering patterns of benzene vapour, recorded immediately before or after the compound patterns and analysed in exactly the same way to minimise systematic errors in wavelengths and camera distances. The scattering intensities were measured using an Epson Expression 1680 Pro flatbed scanner and converted to optical densities as a function of the scattering variable, s, using an established program.[47] Data reduction and least-squares refinements were carried out using the ed@ed v3.0 program,[48] employing the scattering factors of Ross *et al.*[49]

3.3 Results

3.3.1 *Ab initio* calculations

Selected parameters for the optimised geometries of all compounds studied at the MP2/6-311++G** and MP2/aug-cc-pVTZ levels of theory are given in Table 3.1. A complete set of structural parameters for each compound is given in Appendix 3. Where frequency calculations were available the relative abundance of each conformer was calculated using ΔG, but where frequency calculations were prohibitively expensive, ΔE was used.

3.3.2 GED refinements

The starting parameters for the r_{h1} refinements[45] were taken from the theoretical geometries optimised at the MP2/6-311++G** level for each molecule. A theoretical Cartesian force field was obtained at this level and converted into a force field described by a set of symmetry coordinates using the SHRINK program,[45] which generated both the amplitudes of vibration (u_{h1}) and the curvilinear corrections (k_{h1}). All relevant geometric parameters and vibrational amplitudes were then refined. Flexible restraints were employed during the refinements using the SARACEN method.[50–52] The success of the final refinements can be assessed on the basis of the radial-distribution curves and the molecular-scattering intensity curves, which are shown in Appendix 3, along with full lists of refined parameters. With the exception of allenylphosphine, for which $R_G = 12.7\%$, R_G for the refinements ranged from 6.9% to 9.7%. A summary of the most important parameters is given in Table 3.1. Appendix 3 also contains the interatomic distances and the corresponding amplitudes of vibrations, least-squares correlation matrices and experimental coordinates from the GED analyses.

Table 3.1: Selected geometrical parameters of the studied compounds, including experimental values and those obtained at the MP2/6-311++G** (A) and MP2/aug-cc-pVTZ (B) levels of theory.[a]

Allylphosphine									
	1a			**1b**			**1c**		
Parameter	GED	A	B	GED	A	B	GED	A	B
rP–C	187.5(1)	186.9	187.0	188.0(2)	187.4	187.5	187.7(1)	187.1	187.2
rP–H[b]	142.2(15)	141.2	141.5	142.2(15)	141.3	141.6	142.2(15)	141.2	141.4
∠H–P–H	94.2(10)	94.1	93.4	94.2(10)	94.1	93.4	94.9(10)	94.8	94.1
∠C–P–H[b]	96.9(10)	96.4	96.7	96.7(10)	96.7	97.1	96.9(10)	96.9	97.1
rC$_\alpha$–C$_\beta$	152.1(4)	149.6	148.9	152.4(4)	149.9	149.3	152.4(4)	149.9	149.3
rC$_\beta$–C$_\gamma$	135.7(7)	134.3	133.7	135.7(7)	134.2	133.6	135.7(7)	134.2	133.6
∠P–C–C	114.0(2)	114.5	114.2	109.3(10)	109.9	109.3	108.9(5)	109.5	109.1
∠C–C–C	122.9(8)	124.3	124.4	122.9(8)	124.5	124.5	122.9(8)	124.0	124.1
%[c]	79.0(40)	66.3	69.9[d]	—	11.9	8.6	—	21.8	21.5
Propargylphosphine									
	2a			**2b**					
Parameter	GED	A	B	GED	A	B			
rP–C	187.1(2)	187.3	187.4	187.5(2)	187.7	187.8			
rP–H[b]	141.6(6)	141.0	141.3	141.6(6)	141.2	141.5			
∠H–P–H	94.2(10)	94.8	93.5	94.2(10)	94.3	93.7			
∠C–P–H[b]	96.6(10)	96.2	96.3	96.2(10)	96.0	96.3			
rC$_\alpha$–C$_\beta$	145.4(3)	145.6	145.1	145.7(3)	145.9	145.3			
rC$_\beta$–C$_\gamma$	120.6(4)	122.0	121.7	120.7(3)	122.0	121.6			
∠P–C–C	113.6(2)	114.9	114.4	108.5(5)	110.2	109.3			
∠C–C–C	176.0(7)	179.2	179.5	176.0(11)	179.2	177.4			
%[c]	68.0(50)	64.4[d]	58.7	32.0(50)	35.6[d]	41.3			

Allenylphosphine						
		3a			**3b**	
Parameter	GED	A	B	GED	A	B
rP–C	183.6(2)	183.6	183.5	–	183.5	183.5
rP–H^b	142.9(6)	141.3	141.6	–	141.2	141.4
∠H–P–H	92.4(10)	93.2	92.7	–	95.0	94.2
∠C–P–H^b	97.7(9)	96.6	97.0	–	97.0	97.1
rC$_\alpha$–C$_\beta$	131.6(2)	131.5	130.9	–	131.6	131.1
rC$_\beta$–C$_\gamma$	131.6(2)	131.5	131.1	–	131.4	130.9
∠P–C–C	120.0(4)	120.4	119.4	–	124.2	123.5
∠C–C–C	177.6(7)	179.4	178.6	–	179.1	178.4
%^{c}	100.0	66.8^d	58.6	0.0	33.2^d	41.4
Vinylphosphine						
		4a			**4b**	
Parameter	GED	A	B	GED	A	B
rP–C	182.9(1)	183.1	183.0	182.4(2)	182.5	182.5
rP–H^b	141.2(7)	141.2	141.5	141.2(7)	141.2	141.4
∠H–P–H	94.2(10)	93.7	92.8	95.0(10)	95.3	94.5
∠C–P–H^b	97.1(9)	97.1	97.5	97.2(9)	97.3	97.1
rC$_\alpha$–C$_\beta$	134.3(3)	134.3	133.8	134.3(3)	134.4	133.8
rC$_\beta$–C$_\gamma$	–	–	–	–	–	–
∠P–C–C	119.1(4)	120.6	120.1	126.8(3)	125.5	125.3
∠C–C–C	–	–	–	–	–	–
%^{c}	65.0(50)	58.0	64.5	35.0(5)	42.0	35.5

Benzylphosphine						
	5a			**5b**		
Parameter	GED	A	B	GED	A	B
rP–C	188.1(2)	187.3	187.2	188.3(2)	187.4	187.3
rP–H^{b}	143.0(8)	141.2	141.5	143.0(8)	141.4	141.6
∠H–P–H	94.0(10)	94.0	93.2	94.0(10)	94.3	93.9
∠C–P–H^{b}	96.0(10)	96.2	96.2	96.0(10)	96.8	97.1
rC$_{\alpha}$–C$_{\beta}$	150.8(4)	150.2	149.6	151.2(4)	150.6	150.0
rC$_{\beta}$–C$_{\gamma}$	138.7(6)	140.4	139.8	138.6(6)	140.4	139.8
∠P–C–C	116.8(6)	115.0	114.4	111.8(5)	109.8	108.6
∠C–C–C	119.7(2)	120.8	120.7	119.7(2)	120.7	120.7
%^{c}	33.0(110)	41.2	51.3	67.0(110)	58.8	48.7
Chloromethylphosphine						
	6a			**6b**		
Parameter	GED	A	B	GED	A	B
rP–C	186.8(6)	185.2	185.2	187.9(6)	186.4	186.3
rP–H^{b}	142.7(5)	140.8	141.2	142.7(5)	141.2	141.5
∠H–P–H	94.7(10)	95.0	94.2	94.7(10)	94.8	93.7
∠C–P–H^{b}	97.0(9)	96.8	96.5	97.0(9)	95.5	95.7
rC$_{\alpha}$–C$_{\beta}$	–	–	–	–	–	–
rC$_{\beta}$–C$_{\gamma}$	–	–	–	–	–	–
∠P–C–C	–	–	–	–	–	–
∠C–C–C	–	–	–	–	–	–
%^{c}	84.0(30)	74.6	64.2	16.0(30)	25.4	35.8

Ethynylphosphine			
		7	
Parameter	GED	A	B
rP–C	178.5(1)	177.8	177.5
rP–H[b]	142.4(4)	141.0	141.3
∠H–P–H	94.0(10)	95.2	94.0
∠C–P–H[b]	96.4(6)	96.8	96.8
rC$_\alpha$–C$_\beta$	121.9(2)	122.5	122.0
rC$_\beta$–C$_\gamma$	–	–	–
∠P–C–C	175.5(23)	169.7	173.4
∠C–C–C	–	–	–
Phenylphosphine			
		8	
Parameter	GED	A	B
rP–C	183.8(3)	184.4	184.3
rP–H[b]	141.5(3)	141.2	141.5
∠H–P–H	94.6(10)	94.1	93.2
∠C–P–H[b]	96.8(9)	97.3	97.4
rC$_\alpha$–C$_\beta$	139.9(4)	140.7	140.1
rC$_\beta$–C$_\gamma$	139.2(3)	139.9	139.3
∠P–C–C	124.2(7)	123.6	123.3
∠C–C–C	120.7(3)	120.7	120.7

[a] All distances in pm and angles in °. See Figures 3.1 and 3.2 for atom numbering.
[b] An average value was used when a molecule had no symmetry and the H atoms bonded to the P were non-equivalent.
[c] Unless otherwise stated the abundances were calculated using ΔG for A and ΔE for B.
[d] ΔE was used.

Allylphosphine (1). A potential-energy surface (PES) scan around ϕC–C–C–P and ϕC–C–P–H revealed five stable conformations, two of which were discarded as they were calculated to be much higher in energy. This result is consistent with the conformations previously identified.[10] In the three lowest energy conformers ϕC–C–C–P is *anticlinal*, whereas it is *synperiplanar* in the two higher energy conformers. It is likely that the *synperiplanar* configuration is higher in energy due to increased steric repulsion between the phosphino group and the vinyl group. The remaining three conformers (**1a**–**c**) all possess C_1 symmetry and differ in the orientation of the PH_2 group. In **1a** the two CCPH dihedral angles are $\pm$*synclinal*, in **1b** they are approximately –*synclinal* and *antiperiplanar*, and in **1c** are approximately +*synclinal* and *antiperiplanar*. All three conformers have the same statistical weight. On the basis of the *ab initio* calculations, electron-diffraction refinements were carried out using a model containing the three lowest energy conformers. The model was described using relevant bond lengths, bond angles and dihedral angles and where two or more distances were close together the average and differences were used. A more detailed description of the model used, along with parameter descriptions for allylphosphine and all other compounds studied, is given in Appendix 3. Initial refinements using the three-conformer model showed that the ratio of **1b** to **1c** was poorly defined, and so it was decided to fix the ratio of the abundances **1b**/**1c** at the *ab initio* value of **1b**/**1c** = 0.50. This behaviour can be explained by considering the differences between the three conformers. At first glance the three lower energy conformations of allylphosphine appear to differ mainly in the orientation of the phosphino group. However, as the positions of these hydrogen atoms only influence the H...C and H...H distances, they are unlikely to be well resolved. Of greater importance is that for **1a** $\angle$C–C–P is around 115° whilst for **1b** and **1c** it is around 110°, and therefore it is likely that the majority of the information about conformational ratios will come from the P(4)...C(7) distance and, to a lesser extent, the P(4)...C(9) distance. In the MP2/6–311++G** calculations for **1a** rP(4)...C(7) is 283.7 pm and rP(4)...C(9) is 383.5 pm, for **1b** these distances are 277.0 and 372.1 pm, respectively, and for **1c** are 276.1 and 375.3 pm, respectively. As the distances for **1b** and **1c** are similar, whilst the distances

for **1a** are distinct, it would be expected that the GED refinement would predict the ratio of **1a** to the total of **1b** + **1c** well, but that the abundances of **1b** and **1c** themselves would be poorly determined.

Propargylphosphine (2). Propargylphosphine exists in two conformations,[8] one with C_s symmetry (**2a**), with the two C–C–P–H dihedral angles ±*synclinal*, and a C_1 conformer (**2b**), with one ϕC–C–P–H approximately *antiperiplanar* and the other approximately *synclinal*. **2b** has a statistical weight twice that of **2a**. The GED refinement was carried out using a model containing both conformers.

Allenylphosphine (3). Allenylphosphine has previously been shown by MW spectroscopy to have two conformations.[11] The first conformer (**3a**) possesses C_s symmetry, with the two C–C–P–H dihedral angles being ±*anticlinal*. The second conformer (**3b**) has C_1 symmetry with one ϕC–C–P–H close to *synperiplanar* and the second approximately *anticlinal*. Again, **3b** has a statistical weight twice that of **3a**. When the data for allenylphosphine was refined using a model containing both conformers, the amount of **3b** in the refinement fell to 0%. The R factor for this refinement is higher than for all the others, suggesting the presence of an impurity in the sample. The results of the refinement and the structure of **3a** are presented here, although it should be noted that the results are not expected to be precise or intended to offer any information on the relative energies of **3a** and **3b**.

Vinylphosphine (4). Vinylphosphine displays the same conformational behaviour as allenylphosphine.[12] Both **4a** and **4b** were included in the refinement.

Benzylphosphine (5). A two-dimensional PES scan around ϕC–C–C–P and ϕC–C–P–H was conducted to locate all PES minima. A contour plot of the scan is shown in the Appendix (Figure A3.6.1). The scan revealed two minima differing mainly in the orientation of the phosphino group. It also shows that there is no significant rotation of the benzene ring and so it is not necessary to construct a dynamic model. Conformer **5a** has C_s symmetry, with a mirror plane through the P(8), C(7), C(6) and C(1) atoms, and the two ϕC–C–P–H ±*synclinal*. In **5b** the symmetry is broken, although the phosphine does not move far from the mirror plane present in **5a** and the ring is still very close to having C_s symmetry. The main difference in **5b** is the rotation of the phosphino groups such that one ϕC–

C–P–H is approximately *antiperiplanar* and the other approximately *synclinal*.

Chloromethylphosphine (6). Chloromethylphosphine has two conformations with different Cl–C–P–H dihedral angles.[9] **6a** has C_s symmetry with the Cl–C–P–H dihedrals $\pm$*synclinal*, whereas the second conformer, **6b** has C_1 symmetry, with one of the two dihedral angles being close to *antiperiplanar* and the other close to *synclinal*.

Ethynylphosphine (7). PES scans revealed that ethynylphosphine (**7**) exists as a single conformer of C_s symmetry, consistent with the previous study.[13] The data were refined using a model containing eight parameters.

Phenylphosphine (8). Previous studies of phenylphosphine (**8**) suggested that the phosphino hydrogens were staggered either side of the phenyl ring.[14] Scans about ϕC–C–P–H were conducted at various levels of theory and are shown in Appendix 3 (Figure A3.9.1). Although the lowest energy structure was always found to have a C–C–P–H dihedral angle of approximately 50°, the PES curve in each case was quite flat and the barrier to rotation was low, suggesting that the molecule is close to free rotation at the experimental temperature. When the PH_2 group rotates the structure differs mainly in the positions of the hydrogen atoms, with changes in $\angle$C–C–P of, at most, a couple of degrees. A dynamic model was created using a sine-wave-like barrier parameterised with a single parameter (barrier height), but this model did not offer an improved fit over a model using a single C_s conformer, and the barrier height could not be refined. This is to be expected as, assuming $\angle$C–C–P does not change dramatically, the P–H and C(4)...H distances will vary little as the group rotates. Only non-bonded distances between the phosphino hydrogen atoms and the ring atoms change significantly, and such distances are very weakly scattering. It was therefore decided to ignore the rotation and use a model containing a single C_s conformer.

3.4 Discussion

The molecular structures of a number of primary phosphines have been investigated in the gas phase by GED supplemented by *ab initio* calculations *via* the SARACEN method.[50–52] An independent theoretical investigation of the structures was also undertaken.

Allylphosphine (1). The experimental structure of allylphosphine is generally in good agreement with the theoretical structures. The P–C bond length is 187.5(1) pm for the most abundant conformer (**1a)** and is slightly longer than those calculated at the highest levels of theory (186.9 pm and 187.0 pm by MP2/6–311++G** and MP2/aug–cc–pVTZ respectively). The C–C and C=C bond lengths are also slightly longer than those calculated, at 152.1(4) and 135.7(7) pm for **1a** compared to calculated values in the range 148.9–150.8 and 131.6–135.2 pm. As found in previous studies of similar molecules,[16] a large difference in ∠C–C–P is found between different conformers, with that in **1a** consistently larger than in **1b** and **1c** by $\sim 5°$. The P–C bond length is also slightly shorter in **1a** than in **1b** and **1c**. The experimental abundance of **1a** of 79(5)% lies slightly above the calculated values, which range from 51% to 70%. The abundance of **1b** and **1c** combined was therefore 21(5)% but it was not possible to refine the abundance of **1b** relative to **1c**. The conformational behaviour of allylphosphine is quite different to that of allylamine, for which four conformers have been identified.[53–56]

Propargylphosphine (2). Again good agreement is found between the experimental structure and the theoretical structures. The experimental rP–C for **2a** of 187.1(2) pm compares well to the calculated values of 187.3 pm and 187.4 pm at the MP2/6–311++G** and MP2/aug–cc–pVTZ levels, respectively. This bond length is very close to that found in allylphosphine, in which phosphorus is also bonded to an sp^3-hybridised carbon. The experimental rC–C for **2a** is also in good agreement with calculations, whilst rC≡C is a little shorter by experiment [120.6(4) pm] than the high-level theory predicts (122.0 and 121.7 pm by MP2/6–311++G** and MP2/aug–cc–pVTZ, respectively), although it is consistent with the range of calculated distances, which vary from 118.7–123.6 pm. For **2a** the

calculated ∠C–C–C varies from 178.1 to 179.9°. The experimental value is a little narrower at 176.0(7)°. To try to understand why this angle deviated from 180° the molecular orbitals were plotted from the theoretical calculations. The HOMO is shown in Figure 3.3. It can be seen that the HOMO consists of contributions from C≡C, the P lone pair, the C–P bond and the P–H bond. Whilst the HOMO picture does not offer conclusive proof as to why C–C–C is not 180°, it does suggest that there is some interaction between C≡C and C–C, but that this interaction only places electron density on the side of the C–C bond pointing away from the P atom. It is likely that the asymmetry of HOMO in this area causes the C–C–C angle to be nonlinear. As with the other systems exhibiting multiple conformers, a large difference was found in ∠C–C–P with **2b** having a value around 5° narrower than **2a**. The values of ∠C–C–P for both **2a** and **2b** were slightly smaller by experiment than theory predicted. The experimental value is 113.6(2)° for **2a**, whilst the smallest angle predicted by theory is 114.4° at the MP2/aug–cc–pVTZ level. For **2b** the experimental and smallest *ab initio* values are 108.5(5) and 109.3°, respectively. Small differences between **2a** and **2b** were also found for rP–C, which is 0.4(1) pm longer in **2b**, and for rC–C, which is 0.3(1) pm longer in **2b**. The experimental abundance of **2a** is 68(5)%, which is slightly larger than values predicted by calculation, which vary from 45 to 64%. The same two conformations are found in the amine analogue,[7] but the analogous conformer to **2a** is significantly lower in energy than the conformer that resembles **2b**. This is probably because of increased repulsion between the nitrogen lone pair and C≡C, which destabilises the amine **2b** conformation, and also because of an increased attraction between the amino hydrogen atoms and the triple bond due to the higher electronegativity of N, which stabilises **2a**.

Allenylphosphine (3). Despite the worse-than-usual R factor and the inability to refine the structure of the second conformer, the refined structure of **3a** matches the theoretical structures very well, with the refinement using a comparable number of restraints to the other structures. It must be noted, however, that both the *ab initio* results and a previous MW study[11] suggest that **3a** and **3b** should be present in a ratio of roughly 2:1 and so modelling a single conformer is not realistic.

Figure 3.3: The HOMO for the lowest energy conformations of propargylphosphine and allenylphosphine taken from the calculations at the MP2/6-311++G** level.

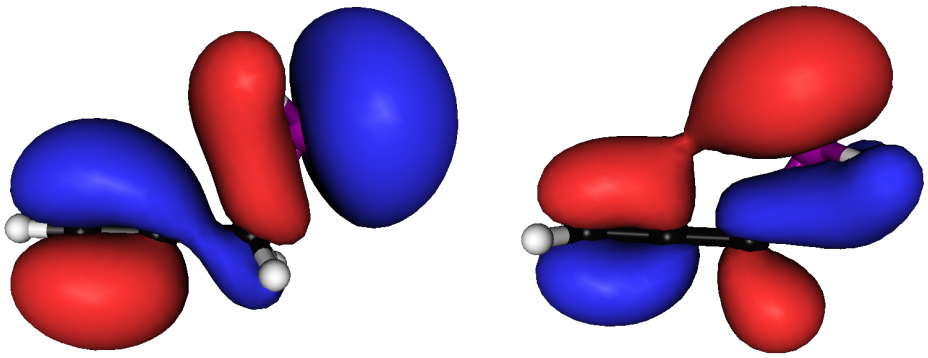

For the refinement with **3a** only, the P–C bond length is found to be 183.6(2) pm by experiment with the theoretical values varying from 182.8 to 185.4 pm and the highest level calculations predicting 183.6 and 183.5 pm. Calculations suggested that any difference between the two C=C bond lengths was small, and less than the anticipated experimental error. This was reflected in the refined values with both C=C distances refining to 131.6(2) pm. This compares well to calculated values, which are 131.5 and 131.0 pm at the MP2/6-311++G** and MP2/aug–cc–pVTZ levels. As with propargylphosphine, the refined C–C–C angle of 177.6(7)° was a little narrower than calculations suggested. As for propargylphosphine, to attempt to understand this deviation from linearity molecular orbitals were plotted using the results of the calculations, with the HOMO shown in Figure 3.3. It can be clearly seen that the HOMO consists mainly of the P lone pair and one of the C=C bonds. There is a clear interaction between the lone pair and the π-bond and it is likely that this accounts for the slight deviation from linearity of the C–C–C bond. Again, calculations predicted that ∠C–C–P varied between the two conformers, with the value in **3b** around 4° larger than in **3a**. The refined value of ∠C–C–P for **3a** was 120.0(4)°, which is consistent with the calculated values. The amine analogue, allenylamine, has been synthesised using flash vacuum pyrolysis[57] but has never been structurally characterised.

Vinylphosphine (4). The structure and conformational behaviour of

vinylphosphine is very similar to that of allenylphosphine. The experimental P–C bond length of 182.9(1) pm for **4a** is close to that found in allenylphosphine and is consistent with the values obtained from theoretical calculations. The experimental rC–C [134.3(3) pm] is also consistent with the calculated values and is, as expected, significantly longer than rC=C in allenylphosphine. The calculated ∠C–C–P for **4a** ranges from 120.1 to 121.6°, whilst for **4b** the angles range from 125.3 to 126.2°. The experimental values lie a little outside of these ranges, being 119.1(4) and 126.3(8)° for **4a** and **4b**, respectively, corresponding to a slightly larger than calculated difference between ∠C–C–P in the two conformers. The experimental abundance of **4a**, 65(5)%, is in good agreement with the theoretical abundances. The nitrogen analogue, vinylamine, is found entirely in a conformation resembling **4b**.[58–60]

Benzylphosphine (5). A search of the available literature revealed little previous work concerning this compound, and none relating to its structure. The conformational behaviour of benzylphosphine (**5a** and **5b**, see Figure 3.2) is analogous to that of propargylphosphine (**2a** and **2b**, see Figure 3.1), so that the two systems are virtually identical apart from the $-C_6H_5$ and –C≡C–H fragments. The most stable conformation, **5a**, has ϕC–C–P–H ±*synclinal*. This conformation is most likely to be stabilised either because of a favourable interaction between the phosphino hydrogen atoms and the ring system (a weak intramolecular hydrogen bond), or because this conformation minimises repulsion between the lone pair of electrons and the ring. The P–C bond lengths in this molecule are the longest encountered in this study, with the value for **5a** being 188.1(2) pm. This is around 4σ away from the highest level *ab initio* calculations (187.2 and 187.3 pm calculated using MP2/6–311++G** and MP2/aug–cc–pVTZ, respectively), and no obvious reason for this discrepancy can be found; in similar systems in this study the agreement between the theoretical and experimental values of P–C is much better. The P–C bond length in **5b** was found to be 188.3(2) pm. As with the other systems with multiple conformations, a difference of around 5° in ∠C–C–P was found between **5a** and **5b**. ∠C–C–P was found to be 117.0(6)° for **5a** and 111.8(5)° for **5b**, both of which are larger ($\sim$3-4σ) than the highest level calculations suggest. **5a** and **5b** are calculated to be very

close in energy, with **5a** slightly lower in energy in all but two of the calculations that use ΔG. The experimental abundance of **5a** is 33(11)% which, because of the large uncertainty, is consistent with most of the calculations. Benzylamine is also found to exist in two conformers.[61] The lower energy conformer in benzylamine is analogous to **5a** with the second conformer being similar to **5b**, but with the C–C–C–N dihedral angle rotated by around 50°.

Chloromethylphosphine (6). The GED structure of chloromethylphosphine has previously been published and will not be discussed here in detail.[9] The previous study used an r_g refinement with some parameters fixed. The new refinement, using the SARACEN method,[50–52] gives an r_{h1} structure with all relevant parameters refining. The results of the new refinement are generally comparable to the old refinement within experimental error. The major differences in the new refinement are that the ∠Cl–C–P angles in **6a** and **6b** are 0.5 and 0.9° narrower, respectively, with the e.s.d.s being 0.1 and 0.7°, respectively. The previously determined abundance of **6b** was 22(5)% and in the new refinement it is 16(3)%. Both values are consistent with the abundances calculated *ab initio*, which vary widely, from 16 to 46%. Comparison with the nitrogen derivative cannot be performed since only the more stable isomeric form of chloromethylamine, the iminium salt, has been characterized.[62]

Ethynylphosphine (7). The P–C bond length in ethynylphosphine is the shortest encountered in this study, with an experimental value of 178.5(1) pm. This is significantly larger than that found for the highest level calculations (177.8 and 177.0 pm by MP2/6–311++G** and MP2/aug–cc–pVQZ, respectively) but is consistent with the range of bond lengths found at lower levels of theory. An earlier experimental study found the distance to be 177.4(5) pm, although some parameters were fixed.[13] Of particular interest is any deviation from linearity of ∠C–C–P. Analogous compounds have been found to have Y–C=X angles that are well away from 180°. For example, ∠P–C=N in F_2PCN is 171.2(8)°.[63] Such large distortions are difficult to explain in a consistent manner, although it appears that the effect is caused by the interaction of the lone pair with the triple bond, as similarly large deviations from linearity are found when Y = N or P and X = C or N.[13] The uncertain nature of this angle in the present case is reflected in the

calculated values, with the lowest value being 169.1° at the MP2/6–31G* level and the highest 177.0° at the HF/3–21G* level. The experimental value of 175.5(23)° compares with the larger calculated values, but the large uncertainty makes it difficult to draw firm conclusions. The previous study of this compound found the angle to be 173(2)°.[13] The HOMO and LUMO for ethynylphosphine are plotted in Figure 3.4, but do not offer an obvious reason for the nonlinearity. The HOMO consist mainly of a C≡C π-bond and the P lone pair, and does not seem to indicate a strong interaction between them. All other experimental parameters, including rC≡C of 121.9(2) pm, were close to both the calculated values and to those found in the previous study. Ethynylamine has never been characterized by GED or MW spectroscopy but has been studied using photoelectron spectroscopy.[64]

Figure 3.4: The HOMO and LUMO for ethynylphosphine taken from the calculations at the MP2/6-311++G** level.

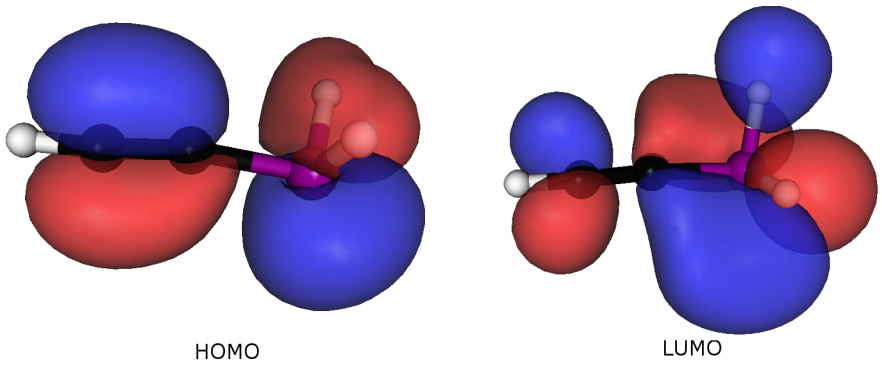

Phenylphosphine (8). Phenylphosphine has been studied previously,[14] and so the results will not be discussed in detail. The structural parameters obtained are consistent with the previous work, but the parameters from this study generally have smaller e.s.d.s. Our approach, an r_{h1} refinement using the SARACEN method to refine all relevant parameters, is expected to provide more reliable parameters than the previous r_a refinement with fixed parameters. With the exception of rC–H, all parameters in the current study are close to those given by the highest level calculations. The distance rP–C is found to be 183.8(3) pm, compared to 184.3 pm at the MP2/aug–cc–pVTZ level, and the larger of the two C–C–P angles is 124.2(7)°, which is consistent with the larger calculated angles.

Table 3.2: P–C bond lengths in primary phosphines from this study and calculated at the MP2/6-311++G** level of theory.

	C_α	rP–C / pm	
	hybridisation	Experimental	MP2/6–311++G**
Propargylphosphine	sp^3	187.1(2)	187.3
Benzylphosphine	sp^3	188.1(2)	187.3
Allylphosphine	sp^3	187.4(1)	186.9
Ethylphosphine[a]	sp^3	186.2[b]	185.8
Methylphosphine[c]	sp^3	185.72(6)	185.6
Chloromethylphosphine	sp^3	186.8(6)	185.2
Phenylphosphine	$\sim sp^2$	183.8(3)	184.4
Allenylphosphine	sp^2	183.6(2)	183.6
Cyclopropylphosphine[d]	sp^2[e]	183.4[b]	182.9
Vinylphosphine	sp^2	182.9(1)	183.1
Ethynylphosphine	sp	178.5(1)	177.8

[a] Ref 2.
[b] No e.s.d.'s were reported.
[c] Ref 11.
[d] Ref. 3.
[e] According to the Walsh orbital description.

In the previous refinement these (r_a) values were 183.3(6) pm and 120.2(30)°. Aniline has been studied previously and found to adopt a C_s configuration with both amino hydrogen atoms on the same side of the ring.[65]

P–C bond lengths

The structures of methylphosphine,[15] ethylphosphine[2] and cyclopropylphosphine[3] have been studied previously. For comparison the key structural parameters for these systems are listed in Table 3.2, along with the parameters from this study. The range of bond lengths spans ∼10 pm, with propargylphosphine, benzylphosphine and allylphosphine being the longest and ethynylphosphine the shortest. The general trend is that, as expected, the bond is longest when the alpha carbon (C_α) is sp^3 hybridised and gets progressively shorter for sp^2 and sp hybridisation. This shortening is consistent with that found for a C–C bond in analogous environments and can be explained either by hyperconjugation[66] or by the interaction between the lone pair on P and the C–C π-system leading to the formation of resonance structures. For example, in vinylphosphine (and similarly for other sp^2-hybridised systems)

the resonance structure H_2C^-–CH=P^+H_2 is possible, and for ethynylphosphine, HC^-=C=P^+H_2. Such a resonance structure is not possible if carbon is sp^3 hybridised. The more subtle changes in bond lengths for molecules with the same C_α-hybridisation appear to be related to an interaction between P and C_β. The results suggest that the P–C bond length is longer when a π–system exists at the β position, and that the bond length is longer if there is a more extensive π-system, for example rP–C is longer in propargylphosphine than in allylphosphine. It has previously been shown that the P lone pair interacts strongly with a π–system at the β position,[17] and so this trend in bonding appears to be indicative of repulsion between the phosphorus lone pair and any π-system at the β position.

Structural changes

The structural changes between systems with two or more conformations are shown in Table 3.3.

A previous study suggested a rule for systems which contain a X–C–Y fragment and exist as multiple conformers. The rule sugest that the most stable conformer should have the shortest bond and the smallest bond angles.[16] In general the higher-energy conformer will be more sterically crowded, leading to longer bonds and wider angles. Six of the seven molecules have a shorter bond length in the more stable conformer, thereby in most cases supporting this hypothesis. The exception is vinylphosphine, in which the lower-energy conformer has a longer bond [182.9(1) pm] than the higher-energy conformer [182.4(1) pm]. It is somewhat surprising that this behaviour in vinylphosphine is different to that of allenylphosphine, despite the molecules being so similar. Five of the seven systems, including all those with an sp^3 hybridized C_α, show a larger bond angle in the more stable conformation, contrary to what the general rule suggests. The two exceptions are the two systems in which C_α is sp^2 hybridized, for which the lower-energy conformation has a narrower C–C–P angle. In the two sp^2 hybridized systems the P–H bonds point away from the C=C bond whilst most of the sp^3 systems have the P–H bonds pointing towards the C–C bond. It is likely that in the sp^3 systems the lower-energy conformation is favoured because this minimises repulsion from the phosphorus lone pair but that this conformation

Table 3.3: Conformational differences in P–C bond length (ΔrP–C) and differences in C–C–P angle ($\Delta\angle$C–C–P) for various phosphines at the MP2/6–311++G** level of theory.[a]

	ΔrP–C / pm	$\Delta\angle$C–C–P / °
Allylphosphine[b]	–0.5	4.6
Propargylphosphine	–0.4	4.7
Allenylphosphine	–0.1	–3.8
Vinylphosphine	0.6	–4.9
Benzylphosphine[b]	–0.1	5.2
Chloromethylphosphine	–1.2	6.0[c]
Ethylphosphine[d]	–0.4	5.1

[a] Differences defined as the more stable conformer minus the less stable conformer.
[b] For allylphosphine with 3 conformers the difference was defined as **1a-1b** and for benzylphosphine, in which the energy of the two conformers is ambiguous, it was defined as **5a-5b**.
[c] Angle is $\Delta\angle$Cl–C–P.
[d] Ref. 2.

necessitates a larger C–C–P angle to accommodate the P–H bonds. In the higher-energy conformations of the sp^3 systems the PH_2 group is rotated and so the C–C–P angle relaxes. The general rule appears to work well in predicting bond length changes but performs poorly when predicting bond angle changes.

3.5 Conclusion

The gas-phase structures of a series of primary phosphines have been determined using gas–phase electron diffraction and compared to the structure predicted using quantum chemical calculations. The C–P bond length was found to vary by around 10 pm across the systems studied with the general trend being that the longest bond is found when C_α is sp^3 hybridized and the shortest when *sp* hybridized. For compounds with multiple conformers differences were found between the conformations, with changes in rC–P of 0.5 pm and in ∠C–C–P of ∼5 ° being common. Many of the phosphines studied display different conformational behaviour when compared to analogous amines. The amines most similar to their phosphine analogues are propargylamine, which exists in the same conformations as propargylphosphine albeit in a different ratio, and vinylamine, which exists solely as one of the two conformers of vinylphosphine. The other systems show greater variations. Benzylphosphine shares one conformation with benzylamine but both molecules have a unique second conformer, and whilst in phenylphosphine both H atoms are staggered with respect to the ring in aniline they both lie to the same side of the ring. Allylamine, with four conformers, displays even more complex conformational behaviour than that found in allylphosphine. Unfortunately for the remaining three compounds a direct comparison is not possible: allenylamine and ethynylamine have not been structurally characterised and chloromethylamine is found as the more stable isomeric iminium salt. It can be concluded that phosphines tend to behave differently to their amine analogues.

3.6 References

[1] M. Brynda, *Coord. Chem. Rev.*, 2005, **249**, 2013.

[2] P. Groner, R. D. Johnson and J. R. Durig, *J. Chem. Phys.*, 1988, **88**, 3456.

[3] L. A. Dinsmore, C. O. Britt and J. E. Boggs, *J. Chem. Phys.*, 1971, **54**, 915.

[4] Y. S. Li, A. W. Cox and J. R. Durig, *J. Mol. Spect.*, 1978, **70**, 34.

[5] E. G. Codding, R. A. Creswell and R. H. Schwendeman, *Inorg. Chem.*, 1974, **13**, 856.

[6] I. Y. M. Wang, C. O. Brott, A. H. Cowley and J. E. Boggs, *J. Chem. Phys.*, 1968, **48**, 812.

[7] R. Cervellati, W. Caminati, C. D. Esposti and A. M. Mirri, *J. Mol. Spect.*, 1977, **66**, 389.

[8] J. Demaison, J.-C. Guillemin and H. Møllendal, *Inorg. Chem.*, 2001, **40**, 3719.

[9] P. T. Brain, D. W. H. Rankin, H. E. Robertson, A. J. Downs, T. M. Greene, M. Hoffman and P. V. R. Schleyer, *J. Mol. Struct.*, 1995, **352**, 135.

[10] H. Møllendal, J. Demaison and J.-C. Guillemin, *J. Phys. Chem. A.*, 2002, **106**, 11481.

[11] H. Møllendal, J. Demaison, D. Petiprez, G. Wlodarczak and J.-C. Guillemin, *J. Phys. Chem. A*, 2005, **109**, 115.

[12] P. Dean, M. Le Guennec, J. C. Lopez, J. L. Alonso, J.-M. Denis, M. Kreglewski and J. Demaison, *J. Mol. Spect.*, 1994, **166**, 210.

[13] E. Cohen, G. A. McRae, H. Goldwhite, S. D. Stefano and R. A. Beaudet, *Inorg. Chem.*, 1987, **26**, 4000.

[14] V. Naumov, M. A. Tafipol'skii and S. Samdal, *Rus. J. Gen. Chem.*, 2003, **73**, 896.

[15] R. Noble-Eddy, S. L. Masters, D. W. H. Rankin, D. A. Wann, B. Khater and J.-C. Guillemin, *Dalton Trans.*, 2008, 5041.

[16] V. S. Mastryukov, J. E. Boggs and J. R. Durig, *J. Mol. Struct.*, 2001, **567**, 101.

[17] S. L. Serre, J.-C. Guillemin, T. Kápáti, L. Soos, L. Nyulászi and T. J. Veszprémi, *Org. Chem.*, 1998, **63**, 59.

[18] J.-C. Guillemin and K. Malagu, *Organomet.*, 1999, **18**, 5259.

[19] J.-C. Guillemin, P. Savignac and J.-M. Denis, *Phosp. Sulf. & Sil. & Rel. Elem.*, 1989, **44**, 27.

[20] J.-L. Cabioch and J.-M. Denis, *J. Organomet. Chem.*, 1989, **377**, 227.

[21] L. Horner, H. Hoffman and P. Beck, *Chem. Ber.*, 1958, **91**, 1583.

[22] J.-L. Cabioch, B. Pellerin and J.-M. Denis, *Phosp. & Sulfur, Silicon Rel. Elem.*, 1989, **44**, 27.

[23] L. Margules, J. Demaison, P. B. Sreeja and J.-C. Guillemin, *J. Mol. Spect.*, 2006, **238**, 234.

[24] J. P. Albrand, S. P. Anderson, H. Goldwhite and L. Huff, *Inorg. Chem.*, 1975, **14**, 570.

[25] *EPSRC National Service for Computation Chemistry Software. URL: http://www.nsccs.ac.uk.*

[26] *EaStCHEM Research Computing Facility (http://www.eastchem.ac.uk/rcf). This facility is partially supported by the eDIKT initiative (tttp://www.edikt.org).*

[27] M. J. Frisch, G. W. Trucks, H. B. Schlegel, G. E. Scuseria, M. A. Robb, J. R. Cheeseman, J. A. Montgomery, Jr., T. Vreven, K. N. Kudin, J. C. Burant, J. M. Millam, S. S. Iyengar, J. Tomasi, V. Barone, B. Mennucci, M. Cossi, G. Scalmani, N. Rega, G. A. Petersson, H. Nakatsuji, M. Hada, M. Ehara,

K. Toyota, R. Fukuda, J. Hasegawa, M. Ishida, T. Nakajima, Y. Honda, O. Kitao, H. Nakai, M. Klene, X. Li, J. E. Knox, H. P. Hratchian, J. B. Cross, V. Bakken, C. Adamo, J. Jaramillo, R. Gomperts, R. E. Stratmann, O. Yazyev, A. J. Austin, R. Cammi, C. Pomelli, J. W. Ochterski, P. Y. Ayala, K. Morokuma, G. A. Voth, P. Salvador, J. J. Dannenberg, V. G. Zakrzewski, S. Dapprich, A. D. Daniels, M. C. Strain, O. Farkas, D. K. Malick, A. D. Rabuck, K. Raghavachari, J. B. Foresman, J. V. Ortiz, Q. Cui, A. G. Baboul, S. Clifford, J. Cioslowski, B. B. Stefanov, G. Liu, A. Liashenko, P. Piskorz, I. Komaromi, R. L. Martin, D. J. Fox, T. Keith, M. A. Al-Laham, C. Y. Peng, A. Nanayakkara, M. Challacombe, P. M. W. Gill, B. Johnson, W. Chen, M. W. Wong, C. Gonzalez and J. A. Pople, *Gaussian 03, Revision C.02*, Gaussian, Inc., Wallingford, CT, 2004.

[28] J. S. Binkley, J. A. Pople and W. J. Hehre, *J. Am. Chem. Soc.*, 1980, **102**, 939.

[29] M. S. Gordon, J. S. Binkley, J. A. Pople, W. J. Pietro and W. J. Hehre, *J. Am. Chem. Soc.*, 1982, **104**, 2797.

[30] W. J. Pietro, M. M. Francl, W. J. Hehre, D. J. DeFrees, J. A. Pople and J. S. Binkley, *J. Am. Chem. Soc.*, 1982, **104**, 5039.

[31] C. C. J. Roothaan, *Rev. Mod. Phys.*, 1951, **23**, 69.

[32] C. Møller and M. S. Plesset, *Phys. Rev.*, 1934, **46**, 618.

[33] W. J. Hehre, R. Ditchfield and J. A. Pople, *J. Chem. Phys.*, 1972, **56**, 2257.

[34] P. C. Hariharan and J. A. Pople, *Theo. Chim. Acta.*, 1972, **56**, 2257.

[35] M. S. Gordon, *Chem. Phys. Lett.*, 1980, **76**, 163.

[36] A. D. McLean and G. S. Chandler, *J. Chem. Phys.*, 1980, **72**, 5639.

[37] R. Krishnan, J. S. Binkley, R. Seeger and J. A. Pople, *J. Chem. Phys.*, 1980, **72**, 650.

[38] D. E. Woon and T. H. Dunning Jr., *J. Chem. Phys.*, 1993, **98**, 1358.

[39] R. A. Kendall, T. H. Dunning Jr. and R. J. Harrison, *J. Chem. Phys.*, 1992, **96**, 6796.

[40] T. H. Dunning Jr., *J. Chem. Phys.*, 1989, **90**, 1007.

[41] K. A. Peterson, D. E. Woon and T. H. Dunning Jr., *J. Chem. Phys.*, 1994, **100**, 7410.

[42] A. Wilson, T. van Mourik and T. H. Dunning Jr., *THEOCHEM*, 1996, **388**, 339.

[43] M. J. Frisch, M. Head-Gordon and J. A. Pople, *Chem. Phys. Lett.*, 1990, **166**, 275.

[44] M. J. Frisch, M. Head-Gordon and J. A. Pople, *Chem. Phys. Lett.*, 1990, **166**, 281.

[45] V. A. Sipachev, *THEOCHEM*, 1985, **121**, 143.

[46] C. M. Huntley, G. S. Laurenson and D. W. H. Rankin, *J. Chem. Soc., Dalton Trans.*, 1980, 954.

[47] H. Fleischer, D. A. Wann, S. L. Hinchley, K. B. Borisenko, J. R. Lewis, R. J. Mawhorter, H. E. Robertson and D. W. H. Rankin, *Dalton Trans.*, 2005, 2469.

[48] S. L. Hinchley, H. E. Robertson, K. B. Borisenko, A. R. Turner, B. F. Johnston, D. W. H. Rankin, M. Ahmadian, J. N. Jones and A. H. Cowley, *Dalton Trans.*, 2004, 2469.

[49] A. W. Ross, M. Fink and R. Hilderbrandt, *International Tables for Crystallography*, Kluwer Academic Publishers, Dordrecht, Netherlands, 1992, p. 245.

[50] A. J. Blake, P. T. Brain, H. Mc Nab, J. Miller, C. A. Morrison, S. Parsons, D. W. H. Rankin, H. Robertson and B. A. Smart, *J. Phys. Chem. A*, 1996, **100**, 12280.

[51] P. T. Brain, C. A. Morrison, S. Parsons and D. W. H. Rankin, *J. Chem. Soc., Dalton Trans.*, 1996, 4589.

[52] N. W. Mitzel and D. W. H. Rankin, *J. Chem. Soc., Dalton Trans.*, 2003, 3650.

[53] G. J. Roussy, J. Demaison, J. Barriol and H. D. Rudolph, *J. Mol. Spect.*, 1971, **38**, 535.

[54] I. Botskor, H. D. Rudolph and G. J. Roussy, *J. Mol. Spect.*, 1974, **52**, 457.

[55] I. Botskor, H. D. Rudolph and G. J. Roussy, *J. Mol. Spect.*, 1974, **53**, 15.

[56] I. Botskor and H. D. Rudolph, *J. Mol. Spect.*, 1978, **71**, 430.

[57] A. Hakiki, J.-L. Ripoll and A. Thuillier, *Tetrahedron Lett.*, 1984, **25**, 3459.

[58] Y. Hamada, K. Hashiguchi, M. Tsuboi, Y. Koga and S. Konda, *J. Mol. Spect.*, 1984, **105**, 93.

[59] Y. Hamada, N. Sato and M. Tsuboi, *J. Mol. Spect.*, 1987, **124**, 172.

[60] D. McNaughton and E. G. Robertson, *J. Mol. Spect.*, 1994, **163**, 80.

[61] S. Melandri, A. Maris, P. G. Favero and W. Caminati, *Chem. Phys. Chem.*, 2001, **2**, 172.

[62] M. Bohme and H. G. Viehe, *Iminium Salts in Organic Chemistry*, John Wiley and Sons, 1979.

[63] P. L. Lee, K. Cohn and R. H. Schwendeman, *Inorg. Chem.*, 1972, **11**, 1917.

[64] C. Wentrup, H. Briehl, P. Lorencak, U. J. Vogelbacher, H. W. Winter, A. Maquestiau and R. J. Flammang, *J. Am. Chem. Soc.*, 1988, **110**, 1337.

[65] G. Schultz, G. Portalone, F. Romando, A. Domenicano and I. Hargittai, *Struct. Chem.*, 1996, **7**, 59.

[66] K.-T. Chou, G.-D. Zhou and W. Chen, *Fundamentals of Structural Chemistry*, World Scientific, River Edge, NJ, 1993.

Chapter 4

The study of phosphine-borane adducts

4.1 Introduction

Following the successful study of the series of primary phosphines and of methylphosphine-borane, the next goal was to extend the work to a series of primary phosphine-borane adducts. As detailed in the previous two chapters primary phosphines have many potential applications but are generally too reactive and unstable to be widely used.[1] Borane (BH_3) is commonly used as a protecting group for tertiary phosphines and it is thought that the same technique could be applicable to primary phosphines.[2]

Recently there has been renewed interest in the borane adducts of primary phosphines, with examples including the measurement of the gas-phase acidity of a series of P-B adducts,[3] along with photoelectron[4] and IR spectra.[5] By studying the gas-phase structures of the phosphine-borane adducts it was hoped to understand the stabilisation offered by the BH_3 group better and to gain further insight into the nature of bonding in these Lewis acid-base complexes.

In the wider context there has been been much research into the properties of ammonia-borane (NH_3BH_3). Ammonia-borane is very hydrogen-dense and so along with related compounds has attracted attention as a hydrogen storage material.[6] For example the structure and aggregation of methylamine-borane ($CH_3NH_2BH_3$)has recently been studied using a range of techniques, including GED.[7] Whilst it is unlikely that phosphorus analogues would be of any commercial value, being less hydrogenous and likely more toxic, their study can only increase the understanding of such systems.

The initial aim was to study the borane adducts of the same series of compounds as in Chapter 3, focussing first on the unsaturated derivatives. The first compounds synthesised for study were vinylphosphine-borane ($CH_2CHPH_2BH_3$), allylphosphine-borane ($CH_2CHCH_2PH_2BH_3$) and propargylphosphine-borane ($CHCCH_2PH_2BH_3$). The previous studies show that syntheses were successful on small scales (< 50 mg) but around 0.5 g is required for a GED experiment. It proved impossible for our synthetic collaborators to scale synthesis to this quantity. An unidentified white solid tended to form on distillation of the

phosphine-borane, presumably due to polymerisation. The samples of these compounds available for GED study were therefore small, typically less than 100 mg. The small amount of sample available, coupled with the same polymerisation occurring upon vaporisation meant that the GED data obtained were generally of poor quality. Where data were collected it was often clear that the sample was not pure. Despite attempts to refine the synthetic technique it was not possible to obtain significantly improved samples, and therefore it proved impossible to collect high quality data for these compounds. The only refinable data collected were for vinylphosphine-borane and so the experimental study of the other unsaturated compounds was abandoned.

At this stage it was decided to focus on a series of more stable phosphine-boranes, thus eliminating the difficulties with synthesis and quantity of sample. The compounds studied were phenylphosphine-borane ($C_6H_5PH_2BH_3$), benzylphosphine-borane ($C_6H_5CH_2PH_2BH_3$), chloromethylphosphine-borane ($CH_2ClPH_2BH_3$) and cyclopropylmethylphosphine-borane ($C_3H_5CH_2PH_2BH_3$). Other than for the cyclopropylmethyl derivative, the corresponding free phosphines have been studied, as described in Chapter 3, and the corresponding paper.[8]

However, whilst these compounds were easier to synthesise and study than the unsaturated systems the GED data revealed that there was significant decomposition of the adduct back to the free phosphine and, presumably, BH_3 leading to B_2H_6.

GED refinements of the vinyl and phenyl derivatives are presented, which show significant levels of decomposition. The benzyl, chloromethyl and cyclopropylmethyl derivatives showed similar decomposition and so are not presented. Little useful information with regard to the structure of the adducts can be obtained from these refinements and so the experimental information presented is kept brief. Instead an independent theoretical investigation has been undertaken. The differences in structures between the various phosphine-boranes and the bonding trends in the series are discussed, and the changes that occur between the free phosphines and the phosphine-boranes are analysed.

4.2 Experimental

4.2.1 Synthesis

The syntheses of all compounds used in this chapter were conducted by B. Khater and J.-C. Guillemin (Rennes, France). The methods used were analogous to those used to synthesise previous P–B adducts and are detailed in Appendix 4.[3–5]

4.2.2 Theoretical Methods

Calculations were performed for allyl (**1**), propargyl (**2**), allenyl (**3**), vinyl (**4**), benzyl (**5**), chloromethyl (**6**), ethynyl (**7**) and phenyl (**8**) phosphine-borane. The resources of the NSCCS[9] and the EaStCHEM RCF[10] were used employing the Gaussian 03 program.[11] All MP2 methods were frozen core (fc).

Geometry optimisations

An extensive search of the torsional potential of each compound was undertaken at the RHF/3-21G* level[12–14] to locate all minima. Geometry optimisations were conducted at the RHF[15] and MP2[16] levels of theory using the Pople-type basis sets (6-31G*[17–19] and 6-311G*[20,21]). It was decided not to conduct calculations using other basis sets – as this study is mainly computational it is bonding trends that are of greater importance than absolute values. It is already known from Chapter 2 that certain parameters are sensitive to the basis set used, but without accurate experimental data for comparison such deviations are of less interest. The bonding trends depend on the differences between computed parameters which are expected to be largely independent of the level of theory used. The optimised structures of the compounds studied, along with the atomic numbering schemes, are shown in Figures 4.1 and 4.2.

Figure 4.1: Molecular structures of the relevant conformations of allylphosphine-borane (**1a**, **1b**, **1c**), propargylphosphine-borane (**2a**, **2b**) and allenylphosphine-borane (**3a**, **3b**).

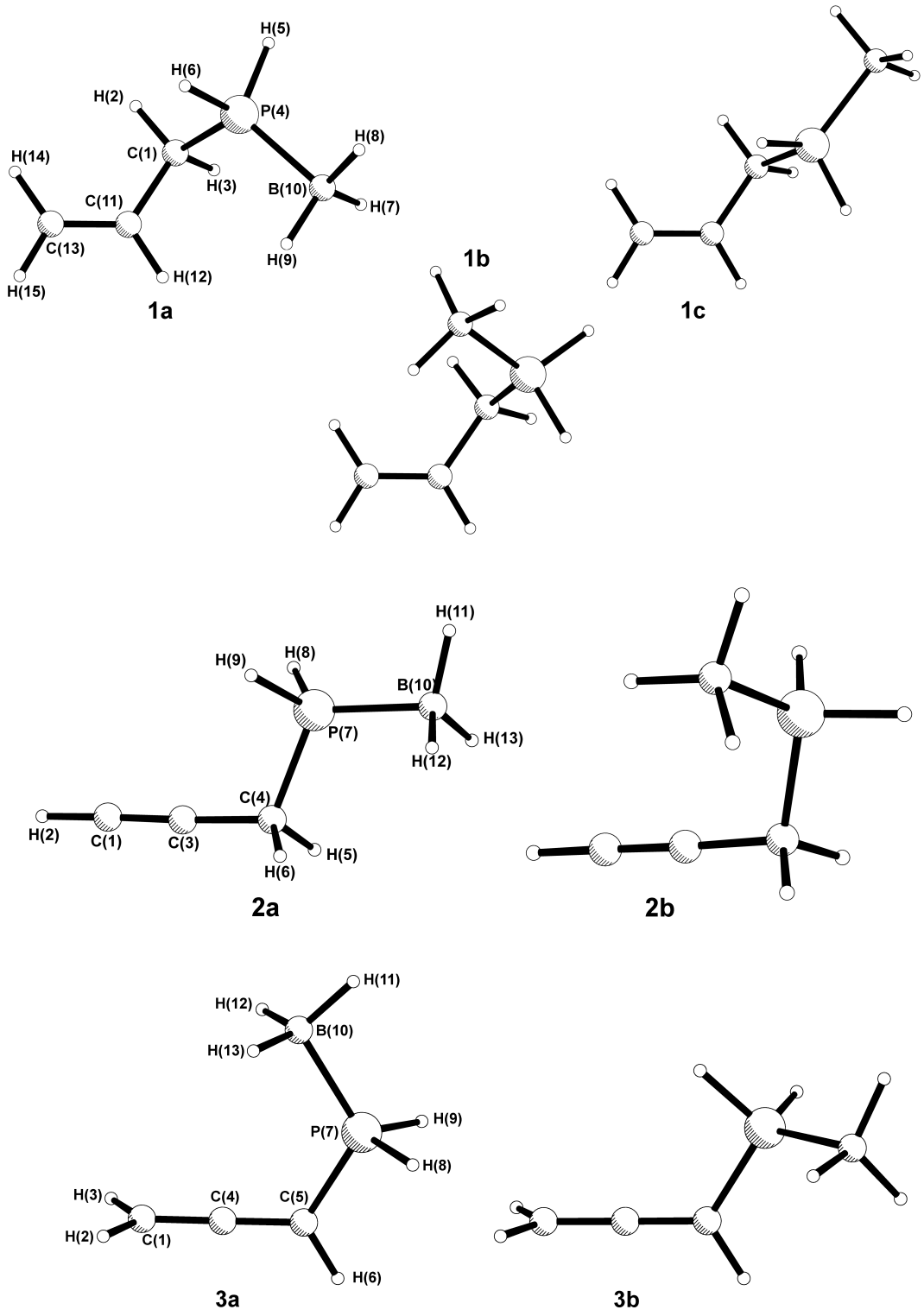

Figure 4.2: Molecular structures of the relevant conformations of vinylphosphine-borane (**4a**, **4b**) benzylphosphine-borane (**5a**, **5b**), chloromethylphosphine-borane (**6a**, **6b**), ethynylphosphine-borane (**7**) and phenylphosphine-borane (**8**).

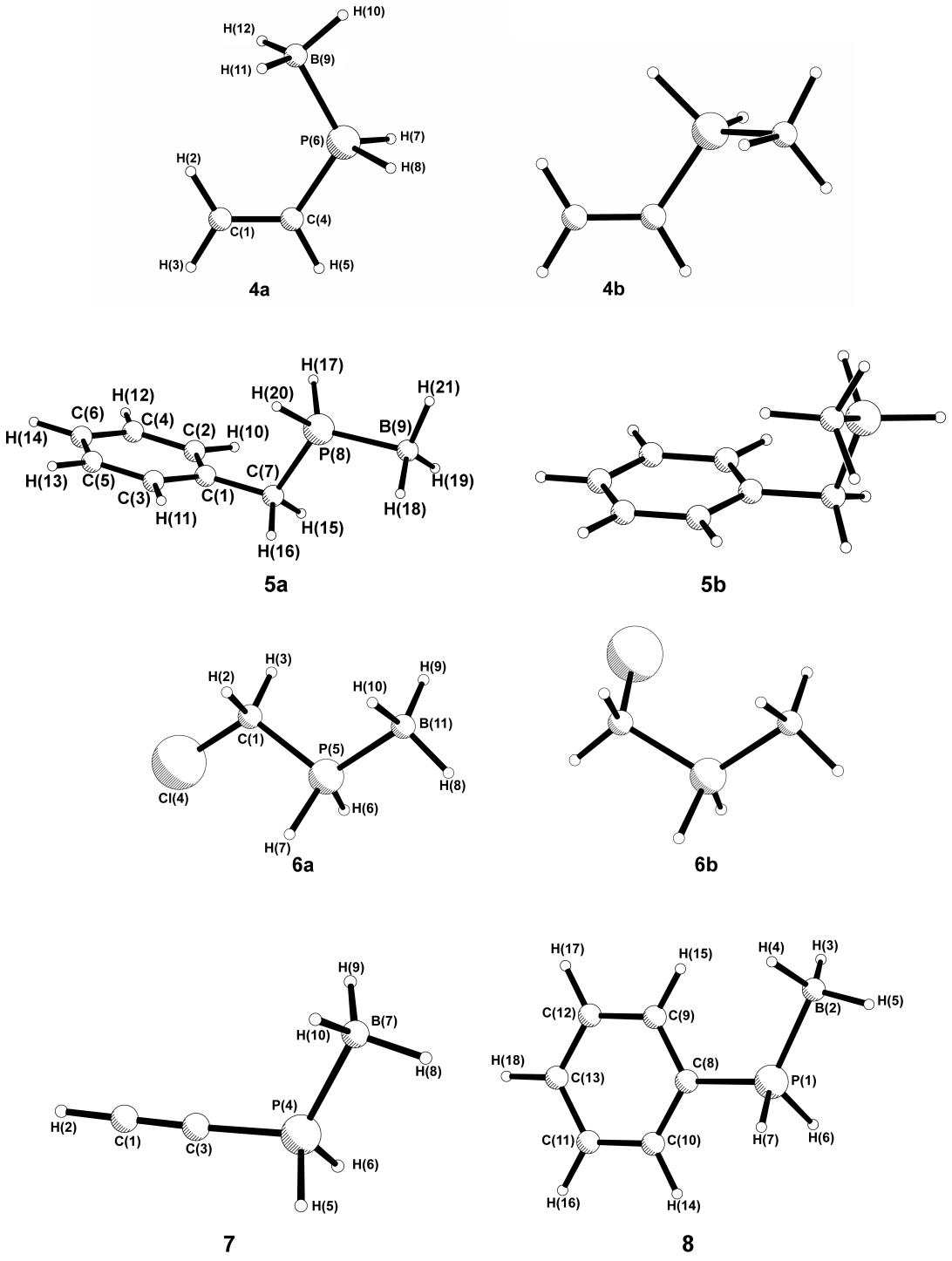

Frequency calculations

Analytic second derivatives[22,23] of the energies with respect to nuclear coordinates were calculated for each compound both to confirm the nature of the minima found by the optimisation and for use with the SHRINK program.[24]

4.2.3 GED measurements

Data collection was performed in the same way as described in the previous chapter. As none of the refinements were of sufficient quality to be considered reliable experimental structures detailed information is not presented. However, it was felt worthwhile to document the attempts that were made.

4.3 Results

4.3.1 Theoretical calculations

Selected parameters for the optimised geometries of all compounds studied are given in Table 4.1, calculated at the MP2/6-311++G** level. A complete set of structural parameters for each compound at other levels of theory used is given in Appendix 4 as follows; allyl (Table A4.1), propargyl (Table A4.2), allenyl (Table A4.3), vinyl (Table A4.4), benzyl (Table A4.5), chloromethyl (Table A4.6), ethynyl (Table A4.7) and phenyl (Table A4.8).

For each of the P–B adducts PES scans were conducted to determine the conformational behaviour. All the P–B adducts show the same conformational behaviour as the corresponding free phosphines, with the BH_3 hydrogen atoms adopting a staggered position with respect to the phosphino H atoms. For multiple conformer systems the energy differences between conformers was found to be roughly similar to the energy differences found in the analogous phosphine studied in Chapter 3.

4.3.2 Gas electron diffraction refinements

None of the refinements were of high enough quality to give reliable experimental structures, but some information could be extracted. Heavy-atom parameters for vinylphosphine-borane were obtained and, in general, the analysis of these data allowed the fact that these compounds dissociate to be discovered. It was therefore felt to be worthwhile to describe the process that was followed and to present the analysis of the data obtained.

Vinylphosphine-borane

It was anticipated that vinylphosphine-borane would be the most stable unsaturated system and so data collection was attempted on several occasions. The refinements of two datasets are presented here, for samples synthesised on

Table 4.1: Selected structural parameters for the phosphine-borane adducts calculated at the MP2/6-311++G** level of theory.[a,b]

	Allylphosphine-borane			Propargylphosphine–borane	
Parameter	**1a**	**1b**	**1c**	**2a**	**2b**
rP–B	193.1	193.1	193.0	192.8	192.8
rP–C	183.7	183.5	184.0	184.0	184.3
rP–H	140.2	140.2	140.2	140.0	140.2
rB–H	120.8	120.7	120.7	120.7	120.7
rC$_\alpha$–C$_\beta$	150.2	150.0	150.3	145.7	145.8
rC$_\beta$–C$_\gamma$	134.2	134.2	134.1	121.9	121.9
∠C–P–B	115.2	115.6	115.7	114.4	116.0
∠P–C–C	110.3	113.4	110.7	113.1	110.5
∠C–C–C	123.2	123.7	123.7	178.1	178.1
∠H–P–H	100.8	100.3	100.5	100.7	100.8
% (293 K)[c]	40.6	49.4	10.0	84.3	15.7

	Allenylphosphine-borane		Vinylphosphine–borane	
Parameter	**3a**	**3b**	**4a**	**4b**
rP–B	193.1	193.1	193.3	193.3
rP–C	180.8	180.8	180.7	180.4
rP–H	140.2	140.2	140.2	140.2
rB–H	120.7	120.7	120.7	120.6
rC$_\alpha$–C$_\beta$	131.6	131.5	134.3	134.3
rC$_\beta$–C$_\gamma$	131.1	131.4	–	–
∠C–P–B	117.1	115.5	116.9	116.1
∠P–C–C	119.6	122.1	120.3	123.6
∠C–C–C	179.0	178.9	–	–
∠H–P–H	99.9	100.8	99.9	100.9
% (293 K)[c]	35.9	64.1	75.8	24.2

	Benzylphosphine-borane		Chloromethylphosphine–borane	
Parameter	**5a**	**5b**	**6a**	**6b**
rP–B	192.7	193.2	192.9	192.7
rP–C	183.6	183.9	183.1	183.9
rP–H	140.8	140.3	139.9	140.2
rB–H	121.1	120.8	120.7	120.6
rC$_\alpha$–C$_\beta$	150.5	150.8	177.7	177.5
rC$_\beta$–C$_\gamma$	140.4	140.4	–	–
∠C–P–B	115.7	116.1	113.4	116.6
∠P–C–C	113.0	110.5	114.0	111.0
∠C–C–C	120.5	120.4	–	–
∠H–P–H	100.3	100.8	101.0	100.9
% (293 K)[c]	49.4	50.6	94.1	5.9

Parameter	Ethynylphosphine-borane **7**	Phenylphosphine–borane **8**
rP–B	193.5	193.4
rP–C	175.8	181.7
rP–H	140.0	140.2
rB–H	120.6	120.7
rC$_\alpha$–C$_\beta$	122.3	140.5
rC$_\beta$–C$_\gamma$	–	139.9
∠C–P–B	117.7	116.8
∠P–C–C	173.0	121.8
∠H–P–H	100.8	100.1

[a] Bond distances in pm and angles in °.
[b] Where two distances, such as rP–H, were not symmetry-related the average is given.
[b] Calculated from the Bolztmann equation using the calculated ΔE assuming a temperature of 293 K.

separate visits by our synthetic collaborator (J.-C. Guillemin, Rennes, France). Once it was realised that dissociation was occurring the possibility of this was included in the models used. The first refinement offers the best fit when a model containing only vinylphosphine-borane is used whilst the second dataset fits to a mixture of the free phosphine and the borane adduct.

The model of **4** was constructed by modifying the model created for vinylphosphine as detailed in Chapter 3. The BH_3 fragment was added using relevant bond angles and the B–H distance, with the only other major change being that rP–C and rP–B were described using an average and a difference. Local C_{3v} symmetry was assumed for the BH_3 group.

The RDC for the first refinement is shown in Figure 4.3. The R factor (R_G = 0.185, R_D = 0.143) is higher than expected for a good fit. Whilst the quality of data obtained was low due to small amounts of sample and long collection times this is not the cause of the problems. The poor fit in the non-bonded region clearly points to the presence of an impurity or some decomposition occurring on vaporisation. In addition the best R factor is obtained when the percentage of **4a** is set to 100%, which again indicates the poor quality of the refinement, as all other indications suggest that a mixture of **4a** and **4b** should be found.

The fit in the bonded region is better, with both the P–C and P–B bond lengths

Figure 4.3: Experimental and difference (experimental – theoretical) radial-distribution curves, $P(r)/r$, for vinylphosphine-borane (**4**) from the first data set. Before Fourier inversion the data were multiplied by $s.\exp(-0.00002s^2)/(Z_C - f_C)(Z_P - f_P)$.

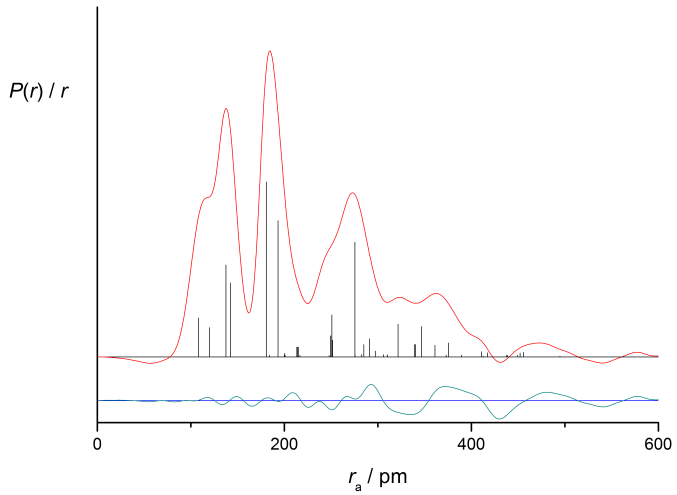

being refined without need to restrain the difference between them. However, the C–C bond length is unrealistically long and only the P–C–C angle is refined without a restraint.

This refinement clearly shows that the sample contained a significant impurity and the results obtained are not expected to be of high quality. However, this refinement offers the best experimental estimate of structure that has been possible, and it is expected that the parameters relating to the heavy atoms will still be reasonably accurate.

The data collected for the second refinement were of better quality, with the sample of **4** being dissolved and vaporised out of the involatile solvent tetraglyme. Initially these data were fitted to the same model as that used for the previous dataset but during the course of the refinement the P–B distance refined to an unreasonably short value (less than 190.0 pm) whilst the shortest value predicted by theoretical calculations is 193.0 pm. Once it became apparent that other phosphine–borane adducts were dissociating it became clear that partial dissociation of **4** could be responsible for the apparent shortening of the P–B

Figure 4.4: Experimental and difference (experimental – theoretical) radial-distribution curves, $P(r)/r$, for a model containing vinylphosphine-borane (**4**), vinylphosphine and diborane. Before Fourier inversion the data were multiplied by $s.\exp(-0.00002s^2)/(Z_C - f_C)(Z_P - f_P)$.

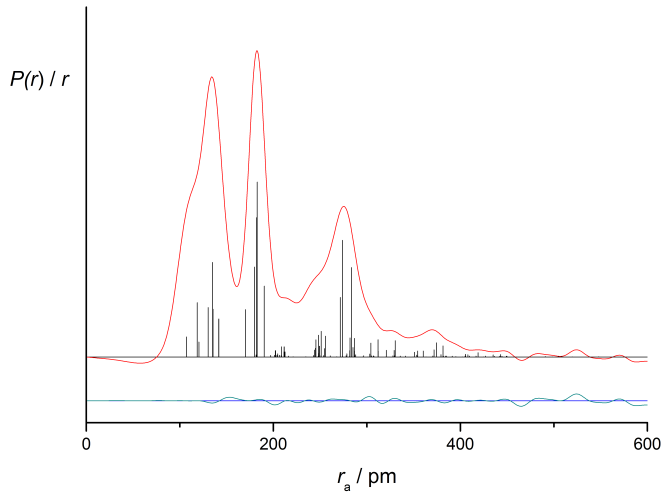

distance, which appears under the same peak as the P–C distance. A number of trial models were then created containing combinations of vinylphosphine, vinylphosphine–borane, borane and diborane.

In the final refinement both conformers of vinylphospine and vinylphosphine-borane were included in the model along with B_2H_6. The structure of vinylphosphine obtained in Chapter 3 was used as additional data during this refinement, applied as restraints using the SARACEN method.[25–27] The amounts of the two conformers of vinylphosphine determined in Chapter 3 [65(5)% C_s at 215 K] was converted to an energy difference and, at the temperature of this experiment (293 K), gave an abundance of 56% of the C_s conformer. The ratio of the conformers **4a** and **4b** were fixed at the MP2/6-311++G** values of 75% of **4a** and 25% of **4b**. The amount of decomposition was then varied until the minimum R factor was obtained.

The resultant fit for this second refinement, shown in Figure 4.4, is much better, with $R_G = 0.067$ ($R_D = 0.062$), but the refinement suggests 80% decomposition of **4**. With such a small fraction of **4** present in the vapour it is inevitable that the

parameters will be poorly determined and in this case the rP–C/rP–B distance difference required a restraint.

The refined parameters for both refinements are given in Table 4.2.

Phenylphosphine-borane

The GED data collected for phenylphosphine-borane (**8**) did not fit well to a model containing just the P–B adduct. When a model that included the presence of phenylphosphine was used a much better fit was obtained, with the resultant refinement showing that only a small amount of the borane adduct was present. It was obvious from the boiling point of the sample used in the GED experiment that the sample was initially **8** and that decomposition occurred as the sample was vaporised. This was confirmed by our synthetic collaborators, who found that when the stable phosphine-borane adducts were vaporised quickly and subsequently trapped there was little decomposition, but when the distillation was slow, as is the case during a GED experiment, decomposition to the free phosphine and B_2H_6 occurred.

The final refinement indicated only around 18% of **8**, which is too small an amount to allow accurate structural parameters to be determined from GED, with the entire structure of **8** being subjected to restraints. rP–B was found to be 191.4(18) pm. The RDC is shown in Figure 4.5.

Table 4.2: Selected refined and calculated geometric parameters for vinylphosphine-borane (**4**) (distances in pm and angles in °) .

Parameter	MP2/6-311++G**	Refinement 1	Refinement 2
rP–B	193.3	193.3(4)	190.2(8)
rP–C	180.7	180.8(3)	180.0(4)
rC–C	134.3	137.7(5)	135.6(3)
∠C–P–B	116.9	118.9(9)	115.3(8)
∠P–C–C	120.3	119.6(6)	118.4(4)

Figure 4.5: Experimental and difference (experimental – theoretical) radial-distribution curves, $P(r)/r$, for phenylphosphine-borane (**8**). Before Fourier inversion the data were multiplied by $s.\exp(-0.00002s^2)/(Z_C - f_C)(Z_P - f_P)$.

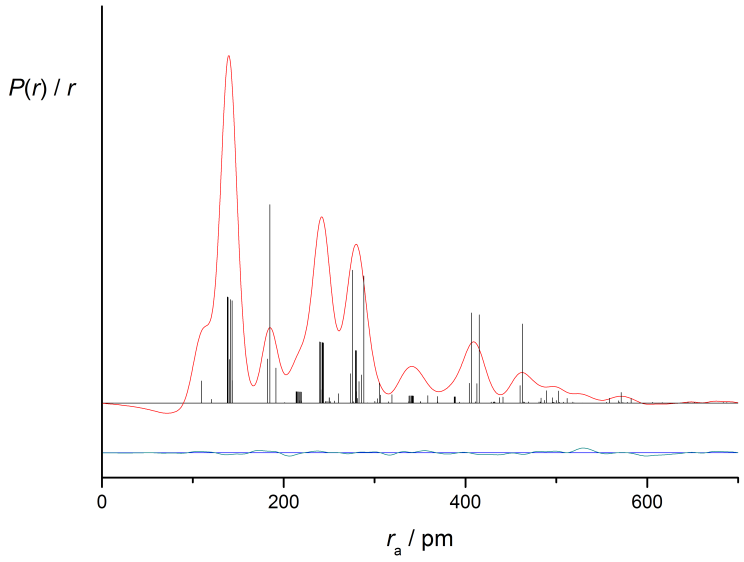

Benzyl, chloromethyl and cyclopropylmethyl derivatives

Preliminary refinements of the data collected for benzylphosphine-borane, chloromethylphosphine-borane and cyclopropylmethylphosphine-borane all showed evidence of significant decomposition back to the corresponding free phosphine. As little information would be obtained with regard to the structures of the borane adducts these data were not fully analysed.

4.4 Discussion

4.4.1 Experimental efforts

The experimental study of this series of compounds proved unsuccessful and, with the exception of unreliable estimates of some heavy-atom parameters for **4** and **8**, no useful experimental data could be obtained. Two separate datasets were analysed for **4**. The first offered a poor quality fit but did not appear to show decomposition back to the free phosphine, whereas the second dataset showed a better fit and lower R factor, but had undergone around 80% decomposition back to the free phosphine. The two sets of structural parameters for **4** from these two refinements were not consistent, and, with both refinements having problems, it is difficult to ascertain which is more reliable.

For the study of **8** the high level of decomposition meant that the structure obtained was likely to be imprecise and/or heavily restrained. The P–B distance reflects this, being 191.4(18) pm, compared to 192.4(4) pm from a previous crystal structure.[28]

Data were also collected for **5**, **6** and cyclopropylmethylphosphine-borane, but the refinements were abandoned when it became clear that significant dissociation had occurred.

The difficulty encountered in studying these compounds calls into question the usefulness of the extra stability that is inferred upon complexation to form the borane adduct. This observation is consistent with previous measurements that suggested that the allyl and propargyl derivatives possess less kinetic stability than the free phosphines themselves.[29] However, it is important to remember that complexation also greatly changes the nature of the reactivity around the P atom making different reactions viable, such that the phosphine-borane may be incorporated into a structure that could not be achieved using the free phosphine. It must also be remembered that the temperatures required for GED study of the phosphine-borane adducts are higher than those required for the free phosphines, whilst if such compounds were to be used in reactions the free phosphines and

phosphine-borane adducts would probably both be used at the same temperature.

The GED study of these compounds was unsuccessful. The low kinetic stability of the unsaturated compounds is obviously an issue. For the more stable systems the dissociation can probably be explained using Le Chatelier's principle, but no detailed investigation of the relationship between pressure and dissociation was undertaken.

4.4.2 Calculated structures

Despite the disappointing experimental results it was felt worthwhile to investigate the structures of these molecules using *ab initio* calculations as other than for the GED study of methylphosphine-borane[30] and the crystal structure of **8**,[28] no other structures of primary phosphine-boranes were found prior to this work commencing. In the intervening period a few other studies have been published by our collaborator J.-C. Guillemin.[3–5]

The results of Chapter 2 showed that rP–B is poorly estimated by theory, and so it is not the absolute values of structural parameters that are of interest from a computational study, but rather the trends within the series, and how the structures of the phosphine fragment change upon complexation. Unless otherwise stated, all structural parameters given herein relate to those calculated at the MP2/6-311++G** level of theory.

The first interesting point is to note that the P–B adducts display the same conformational behaviour as the free phosphines. The relative stability of the conformers is similar in each case, with the slight variations in stabilities of the conformers of the P–B adducts compared to free phosphine seeming to have no trend. For example, the C_s conformer of **3** is less stable than for the corresponding free phosphine, whilst the C_s conformer of **6** is more stable.

The values of rP–C, rP–B and ∠C–P–B are given in Table 4.3. To study the changes in the geometry of the phosphine fragment upon complexation the changes in comparable parameters between the phosphine-borane and the free phosphine are given in Table 4.5. Where multiple conformers existed the changes

Table 4.3: rP–C, rP–B and ∠C–P–B in the phosphines-borane adducts studied, at the MP2/6-311++G** level.[a]

	C_α hybridisation	rC–P	rP–B	∠C–P–B
Propargylphosphine	sp^3	184.0	192.8	114.4
Benzylphosphine	sp^3	183.6	192.7	115.7
Allylphosphine	sp^3	183.5	193.1	115.6
Chloromethylphosphine	sp^3	183.1	192.9	113.4
Methylphosphine[b]	sp^3	182.1	192.8	115.0
Phenylphosphine	$\sim sp^2$	181.7	193.4	116.8
Allenylphosphine	sp^2	180.8	193.1	117.1
Vinylphosphine	sp^2	180.7	193.3	116.9
Ethynylphosphine	sp	175.8	193.5	117.7

[a] Bond distances in pm and angles in °.
[b] See Chapter 2 or corresponding paper.[30]

were assessed only between the lowest energy free phosphine and the lowest energy phosphine-borane.

The P–B bond length is surprisingly consistent, varying by only 0.8 pm between the longest (193.5 pm in **7**) and shortest (192.7 pm in **5a** and **6b**) bond lengths. These distances appears to be consistent with other secondary and tertiary P–B complexes, with [2-(1H-inden-3-yl)ethyl]diphenylphosphine-borane having a P–B distance of 192.3(3) pm[31] and an average P–B distance of 191.7 pm in triphenylphosphine-borane.[32] It therefore seems that the P–B bond is not strongly affected by the environment of the P atom and is certainly less variable than, for example, the P–C bond in primary phosphines.

In the same series of primary phosphines, studied in Chapter 3, rP–C was found to vary from 177.8 pm to 187.7 pm, with propargylphosphine and benzylphosphine offering the longest rP–C and ethynylphosphine the shortest. In the P–B adducts the range is reduced slightly, but the order is similar, with propargylphosphine-borane being the longest at 184.0 pm and ethynylphosphine-borane the shortest at 175.8 pm. In general it can be seen from Table 4.5 that rP–C tends to shorten by around 3 pm on adduct formation.

These small differences in the length of the P–B bond and the change in the P–C length can only be influenced by the nature of the substituent and especially the

Table 4.4: Calculated Mulliken charges for three free phosphines and the corresponding phosphine-borane adducts, calculated at the MP2/6-311++G** level of theory. All values are in units of *e*.

Compound	Charge P	Charge C	Difference (P - C)
Allylphosphine	0.37	-0.08	0.45
Allylphosphine-borane	0.53	-0.66	1.19
Vinylphosphine	-0.01	-0.05	0.04
Vinylphosphine-borane	0.30	-0.03	0.33
Ethynylphosphine	-0.12	-0.73	0.61
Ethynylphosphine-borane	-0.02	-0.81	0.79

environment of the α-C atom, as otherwise the complexes are the same. It can be seen from Table 4.3 that this is the case, with the P–B bond length longest when the α-C is *sp*-hybridised and shortest in the sp^3-hybridised cases, with the sp^2 cases lying in-between.

Whilst the absolute range of the P–B bond length was much less than is observed for the P–C bond, it is interesting to try to understand the reason for the differing lengths. The shortening of the P–C length upon complexation is dependant upon charge transfer from P to B; P becomes more positive and therefore more strongly attracted to the more electronegative C. This is backed up by the calculated Mulliken charges on the P atom in the complex and the free phosphine, a selection of which are listed in Table 4.4. In each case the P atom becomes more positive in the adduct and the difference in charge between P and C atoms is larger in the adduct.

It also seems likely that the more charge transfer from P to B there is, the shorter the bond length. If this is true then the contraction of the P–C bond length should be correlated to P–B bond length. The data is plotted in Figure 4.6, with a list of the C–P and B–P lengths also given in Table 4.3.

The graph shows that, with the exception of chloromethylphosphine-borane (**6**), the two parameters are indeed correlated such that the more rP–C shortens, the shorter rP–B is found to be. This is consistent with the concept of electron density moving from P to B upon complexation. The HOMOs of **3** and **6** were calculated and are shown in Figure 4.7. The movement of electron density from

Figure 4.6: Graph showing the relationship between the contraction of rP–C and rP–B.

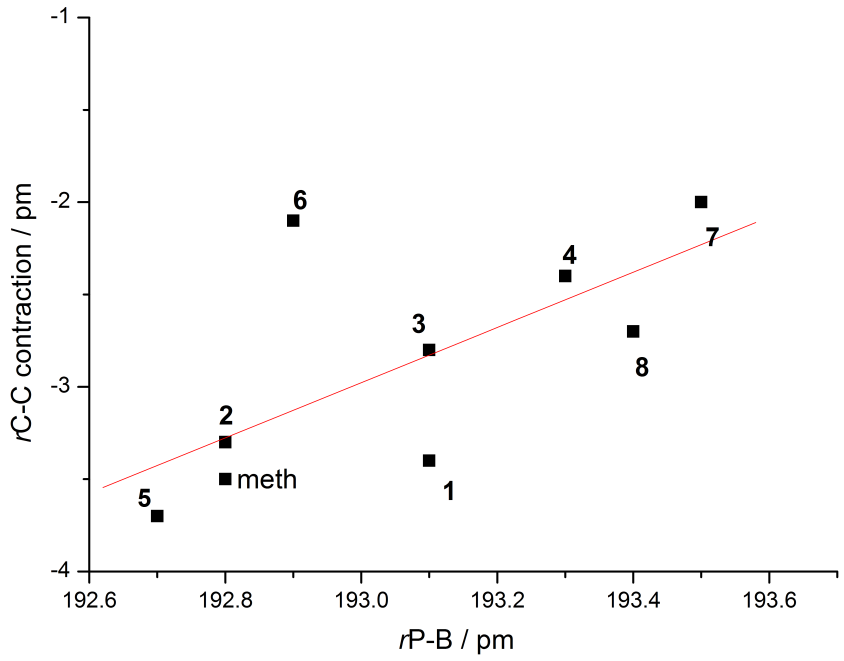

the P lone pair towards the B atom is clearly visible, especially when compared to the HOMOs for the free phosphines shown in Chapter 3. It is less clear why **6** behaves differently to the other molecules but, with the HOMO including lone pairs on the chlorine atom, it is clear that the bonding in **6** is likely to be distinct from the other molecules studied.

The shortening of the C–P bond is generally greatest when the α-C is sp^3-hybridised, shorter when sp^2-hybridised and shortest in the single sp-hybridised case. The most likely explanation for this is that in the sp case more of the P electron density is in the C–P bond so less charge is transferred upon complexation.

The angle $\angle$C–P–B varies considerably, with values ranging from 117.7° in **7** to 113.4° in **6a**. Again the bond angle tends to be related to the α-C atom hybridisation, with narrower bond angles generally found in the sp^3 cases. In this case the effect appears to be steric, however, as the molecules that have an

Figure 4.7: Figure showing the HOMO for allenylphosphine-borane and chloromethylphosphine-borane from calculations at the MP2/6-311++G** level of theory.

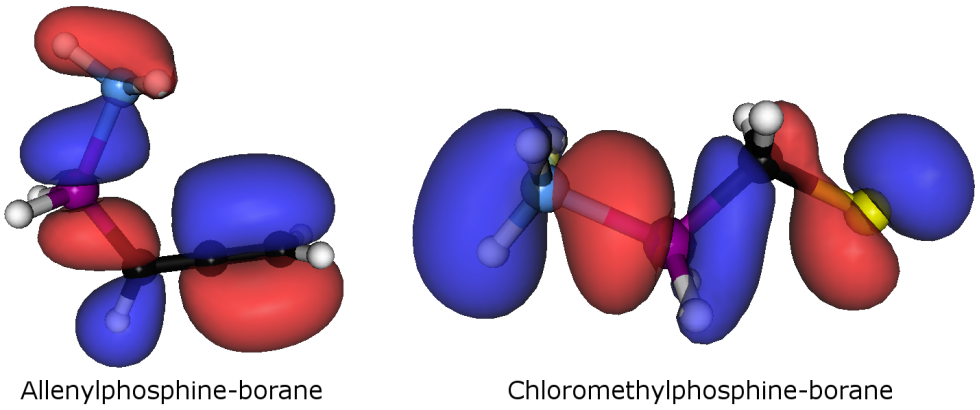

sp^2 or *sp* α-C tend to have the boron atom pointing towards the substituent. Examination of Figures 4.1 and 4.2 shows that **3a, 4a, 7** and **8** have the BH_3 group pointing back towards the rest of the molecule, an orientation which must lead to maximum repulsion between the heavy atoms and necessitate a wider bond angle. The argument for sterics affecting ∠C–P–B is made stronger when it is noted that the angle is narrower in **3b** and **4b**, where the boron atom is rotated away from the carbon atoms and the repulsion is therefore reduced.

One of the most distinctive features of the primary phosphines studied in Chapter 3 was the large changes found in ∠C–C–P in different conformers of the same molecule. Examples include differences of 4.7° in propargylphosphine and 4.9° in vinylphosphine. In the corresponding P–B adducts these changes are reduced, with a difference of 2.6° in propargylphosphine-borane and 3.3° in vinylphosphine-borane. These changes are difficult to rationalise as a group, but in most cases can be understood by looking at the changes found for an individual molecule.

Table 4.5: Changes in structural parameters upon complexation of the free phosphine to form a phosphine-borane adduct, calculated at the MP2/6-311++G** level of theory. A negative number indicates a shorter bond length or narrower bond angle.[a]

Compound	ΔrC–P	ΔrP–H	ΔrC–C	$\Delta\angle$H–P–H	$\Delta\angle$C–P–H	$\Delta\angle$C–C–P
Allyl **1**	-3.4	-1.0	0.4	6.2	5.9	-0.6
Allenyl **2**	-3.3	-0.8	0.2	5.9	5.7	-1.8
Allenyl **3**	-2.8	-1.1	0.1	6.7	5.6	-0.8
Vinyl **4**	-2.4	-1.0	0.0	6.2	5.9	-0.3
Benzyl **5**	-3.7	-0.4	0.3	6.3	5.8	-2.0
Chloromethyl **6**	-2.1	-0.9	-0.9[b]	6.0	5.2	2.6[b]
Ethynyl **7**	-2.0	-1.0	-0.2	5.6	4.9	3.3
Phenyl **8**	-2.7	-1.0	-0.2	6.0	6.3	1.8
Methyl	-3.5	-0.9	–	5.7	5.6	–

[a] Bond distances in pm and angles in °.
[b] Distance is rCl–C and angle is $\angle$Cl–C–P.

For example in propargylphosphine the C_s conformer has ∠C–C–P of 114.9° whilst the C_1 conformer has ∠C–C–P equal to 110.2°. In propargylphosphine-borane ∠C–C–P decreases in the C_s conformer to 113.1° whilst the bond angle in the C_1 conformer remains approximately constant at 110.5°. The bond angle in the C_s conformer of propargylphosphine is probably wider due to the P lone pair pointing towards the propargyl fragment causing repulsion. In this conformation of propargylphosphine-borane the lone pair is no longer present, being involved with the P–B bond, and so the electron density no longer causes repulsion with the propargyl fragment. On the contrary, in the C_1 conformer of propargylphosphine, where the P lone pair is rotated out of the plane of the other heavy atoms, the bond angle cannot be widened by repulsion, and so little change is found when the complex with borane is formed.

As was found for methylphosphine-borane (Chapter 2), ∠C–P–H and ∠H–P–H widen dramatically upon complexation as the bond angles around P relax towards tetrahedral values.

4.5 Conclusion

The GED of a series of phosphine-borane adducts was attempted but the experiments were not successful and very little information could be extracted. The unsaturated systems generally showed less kinetic stability than the analogous free phosphine and the more stable alkyl and aryl systems were found to dissociate under the conditions required for GED.

An independent theoretical investigation was therefore undertaken to study the structures of these molecules. The P–B distance was found to be consistently around 193.0 pm at the MP2/6-311++G** level of theory, with the small variations in rP–B appearing to be correlated to the shortening of the C–P bond.

4.6 References

[1] M. Brynda, *Coord. Chem. Rev.*, 2005, **249**, 2013.

[2] K. Bourumeau, A.-C. Gaumont and J.-M. Denis, *J. Organomet. Chem.*, 1997, **529**, 205.

[3] M. Hurtado, M. Yánez, R. Herrero, A. Guerrero, J. Dávalos, M. A. José-Luis, B. Khater and J.-C. Guillemin, *Chem.-Eur. J.*, 2009, **15**, 4622.

[4] B. Németh, B. Khater, T. Veszprémi and J.-C. Guillemin, *Dalton Trans.*, 2009, **18**, 3526.

[5] B. Khater, J.-C. Guillemin, A. Benidar, D. Bégué and C. Pouchan, *J. Chem. Phys.*, 2008, **129**, 224308.

[6] F. H. Stephens, V. Pons and R. T. Baker, *Dalton Trans.*, 2007, 2613.

[7] S. Aldridge, A. J. Downs, C. Y. Tang, S. Parsons, M. C. Clarke, R. D. L. Johnstone, H. E. Robertson, D. W. H. Rankin and D. A. Wann, *J. Am. Chem. Soc.*, 2009, **131**, 2231.

[8] R. Noble-Eddy, S. L. Masters, D. W. H. Rankin, D. A. Wann, H. E. Robertson, B. Khater and J.-C. Guillemin, *Inorg. Chem.*, 2009, **48**, 8603.

[9] *EPSRC National Service for Computation Chemistry Software. URL: http://www.nsccs.ac.uk.*

[10] *EaStCHEM Research Computing Facility (http://www.eastchem.ac.uk/rcf). This facility is partially supported by the eDIKT initiative (tttp://www.edikt.org).*

[11] M. J. Frisch, G. W. Trucks, H. B. Schlegel, G. E. Scuseria, M. A. Robb, J. R. Cheeseman, J. A. Montgomery, Jr., T. Vreven, K. N. Kudin, J. C. Burant, J. M. Millam, S. S. Iyengar, J. Tomasi, V. Barone, B. Mennucci, M. Cossi, G. Scalmani, N. Rega, G. A. Petersson, H. Nakatsuji, M. Hada, M. Ehara, K. Toyota, R. Fukuda, J. Hasegawa, M. Ishida, T. Nakajima, Y. Honda,

O. Kitao, H. Nakai, M. Klene, X. Li, J. E. Knox, H. P. Hratchian, J. B. Cross, V. Bakken, C. Adamo, J. Jaramillo, R. Gomperts, R. E. Stratmann, O. Yazyev, A. J. Austin, R. Cammi, C. Pomelli, J. W. Ochterski, P. Y. Ayala, K. Morokuma, G. A. Voth, P. Salvador, J. J. Dannenberg, V. G. Zakrzewski, S. Dapprich, A. D. Daniels, M. C. Strain, O. Farkas, D. K. Malick, A. D. Rabuck, K. Raghavachari, J. B. Foresman, J. V. Ortiz, Q. Cui, A. G. Baboul, S. Clifford, J. Cioslowski, B. B. Stefanov, G. Liu, A. Liashenko, P. Piskorz, I. Komaromi, R. L. Martin, D. J. Fox, T. Keith, M. A. Al-Laham, C. Y. Peng, A. Nanayakkara, M. Challacombe, P. M. W. Gill, B. Johnson, W. Chen, M. W. Wong, C. Gonzalez and J. A. Pople, *Gaussian 03, Revision C.02*, Gaussian, Inc., Wallingford, CT, 2004.

[12] J. S. Binkley, J. A. Pople and W. J. Hehre, *J. Am. Chem. Soc.*, 1980, **102**, 939.

[13] M. S. Gordon, J. S. Binkley, J. A. Pople, W. J. Pietro and W. J. Hehre, *J. Am. Chem. Soc.*, 1982, **104**, 2797.

[14] W. J. Pietro, M. M. Francl, W. J. Hehre, D. J. DeFrees, J. A. Pople and J. S. Binkley, *J. Am. Chem. Soc.*, 1982, **104**, 5039.

[15] C. C. J. Roothaan, *Rev. Mod. Phys.*, 1951, **23**, 69.

[16] C. Møller and M. S. Plesset, *Phys. Rev.*, 1934, **46**, 618.

[17] W. J. Hehre, R. Ditchfield and J. A. Pople, *J. Chem. Phys.*, 1972, **56**, 2257.

[18] P. C. Hariharan and J. A. Pople, *Theo. Chim. Acta.*, 1972, **56**, 2257.

[19] M. S. Gordon, *Chem. Phys. Lett.*, 1980, **76**, 163.

[20] A. D. McLean and G. S. Chandler, *J. Chem. Phys.*, 1980, **72**, 5639.

[21] R. Krishnan, J. S. Binkley, R. Seeger and J. A. Pople, *J. Chem. Phys.*, 1980, **72**, 650.

[22] M. J. Frisch, M. Head-Gordon and J. A. Pople, *Chem. Phys. Lett.*, 1990, **166**, 275.

[23] M. J. Frisch, M. Head-Gordon and J. A. Pople, *Chem. Phys. Lett.*, 1990, **166**, 281.

[24] V. A. Sipachev, *THEOCHEM*, 1985, **121**, 143.

[25] A. J. Blake, P. T. Brain, H. Mc Nab, J. Miller, C. A. Morrison, S. Parsons, D. W. H. Rankin, H. Robertson and B. A. Smart, *J. Phys. Chem. A*, 1996, **100**, 12280.

[26] P. T. Brain, C. A. Morrison, S. Parsons and D. W. H. Rankin, *J. Chem. Soc., Dalton Trans.*, 1996, 4589.

[27] N. W. Mitzel and D. W. H. Rankin, *Dalton Trans.*, 2003, 3650.

[28] H. Dorn, R. A. Singh, J. A. Massey, J. M. Nelson, C. A. Jaska, A. J. Lough and I. Manners, *J. Am. Chem. Soc.*, 2000, **122**, 6699.

[29] R. H. Shay, B. N. Diel, D. M. Schubert and A. D. Norman, *Inorg. Chem.*, 1988, **27**, 2378.

[30] R. Noble-Eddy, S. L. Masters, D. W. H. Rankin, D. A. Wann, B. Khater and J.-C. Guillemin, *Dalton Trans.*, 2008, 5041.

[31] L. F. Groux and D. Zargarian, *Cryst. Struct. Comm.*, 2000, **C56**, e366–e367.

[32] J. C. Huffman, W. A. Skupinski and K. G. Caulton, *Cryst. Struct. Comm.*, 1982, **11**, 1435.

Chapter 5

The structures of vinylarsine, vinyldichloroarsine and arsine

5.1 Introduction

Very few structural studies of the primary derivatives of arsine, R–AsH_2, have been reported. Following the determination of the structures of a series of primary phosphines, including vinylphosphine (see Chapter 3 or the corresponding paper[1]), it was decided to continue the study of unsaturated group 15 compounds with vinylarsine (CH_2CHAsH_2, **1**) and vinyldichloroarsine ($CH_2CHAsCl_2$, **2**). The structure of arsine (AsH_3, **3**) is also reported.

The enamine functional group (R_2NCRCR_2) is of particular interest due to its ambident nature; it can react at both the β–C site or at the heteroatom.[2–4] For this reason it is thought that vinylphosphine and vinylarsine could form the basis of bidentate ligands in organometallic chemistry.[5] However, unsaturated arsines are less stable than the phosphorus analogues, and so it is unclear how stable such compounds would be under the conditions required by gas electron diffraction (GED). Vinylarsine is expected to be one of the more stable unsaturated primary arsines[6] and so for this reason, along with the interest in the vinyl substituent, vinylarsine was chosen as the first primary arsine for study.

At the same time as vinylarsine was studied a preliminary attempt was made to obtain the structure of allylarsine. Unfortunately, at the temperature required for the GED experiment, allylarsine was found to decompose with subsequent analysis of the diffraction pattern revealing that the only volatile decomposition product was arsine (AsH_3). Whilst it is hoped that that the vapour pressure requirements could be lowered in order to study allylarsine, it was also felt to be worthwhile to investigate the dichloroarsines (R–$AsCl_2$) as more stable analogues of the primary arsines. If future attempts to conduct GED on the less stable primary arsines prove difficult then it will be possible to compare the structures of the dichloroarsine derivatives instead. It was therefore decided that the structure of vinyldichloroarsine would also be studied. However, the study of dichloroarsine derivatives is itself complicated by the difficulty in obtaining pure samples free from $AsCl_3$. Thus the study of vinyldichloroarsine will also be of interest with regard to the amount of structural information that can be gathered from a

mixed sample. As for the primary arsines, very little work has been conducted on dichloroarsines, with the closest work in the literature relating to the chemical weapon Lewisite ($HClCCHAsCl_2$).[7]

As well as offering the first complete gas-phase structure of a primary arsine this work also facilitates the comparison of bonding trends in the primary vinyl derivatives of Group 15 elements. A previous microwave (MW) spectroscopic investigation of vinylamine found a single conformation, and the GED study of vinylphosphine in Chapter 3 found two conformers.[1] Vinylarsine has previously been studied by MW spectroscopy.[8] Two conformers, similar to those found in vinylphosphine, were identified but no experimental estimate of the energy difference was possible. In order to obtain the most accurate structure possible in this work the published rotational constants have been combined with the GED data using the SARACEN method.[9–11] A further comparison between the structures of the vinylarsine and vinyldichloroarsine has also been made in order to assess the effect of replacing the arsino H atoms with Cl.

5.2 Experimental

5.2.1 Synthesis

The syntheses of vinyldichloroarsine and vinylarsine were performed by J.-C. Guillemin (Rennes, France). The syntheses have already been reported[6] with details of minor changes made to the published experimental procedure given in Appendix 5. Photoelectron,[12] infrared[5] and microwave spectra[8] of vinylarsine have been recorded previously along with its gas-phase acidity.[13]

5.2.2 Theoretical Methods

Calculations were performed using a Linux cluster and a Silicon Graphics Altix 4700, both using the Gaussian 03 program.[14] All MP2 methods were frozen core (fc).

Geometry optimisations

An extensive search of the torsional potential of every compound was undertaken at the RHF/3-21G* level[15–17] to locate all minima. For both **1** and **2**, two unique minima were found corresponding to *syn* and *gauche* conformations. Further geometry optimisations were conducted for both molecules at the HF[18] and MP2[19] levels of theory using Pople-type basis sets (6-31G*[20–22] and 6-311G*[23,24]). To investigate the shape of the barrier to rotation around the C–As bond for **1** and **2** potential-energy surface (PES) scans were conducted using MP2/6-311++G** in which this dihedral angle was varied from 0° to 360° in 10° steps. The optimised structures of **1** and **2** with the atomic numbering schemes are shown in Figure 5.1.

Frequency calculations

Analytic second derivatives[25,26] of the energies with respect to nuclear coordinates calculated at the MP2/6-31+G* level served both to confirm the nature of the

Figure 5.1: Molecular structures of vinylarsine (**1a**, **1b**) and vinyldichloroarsine (**2a**, **2b**).

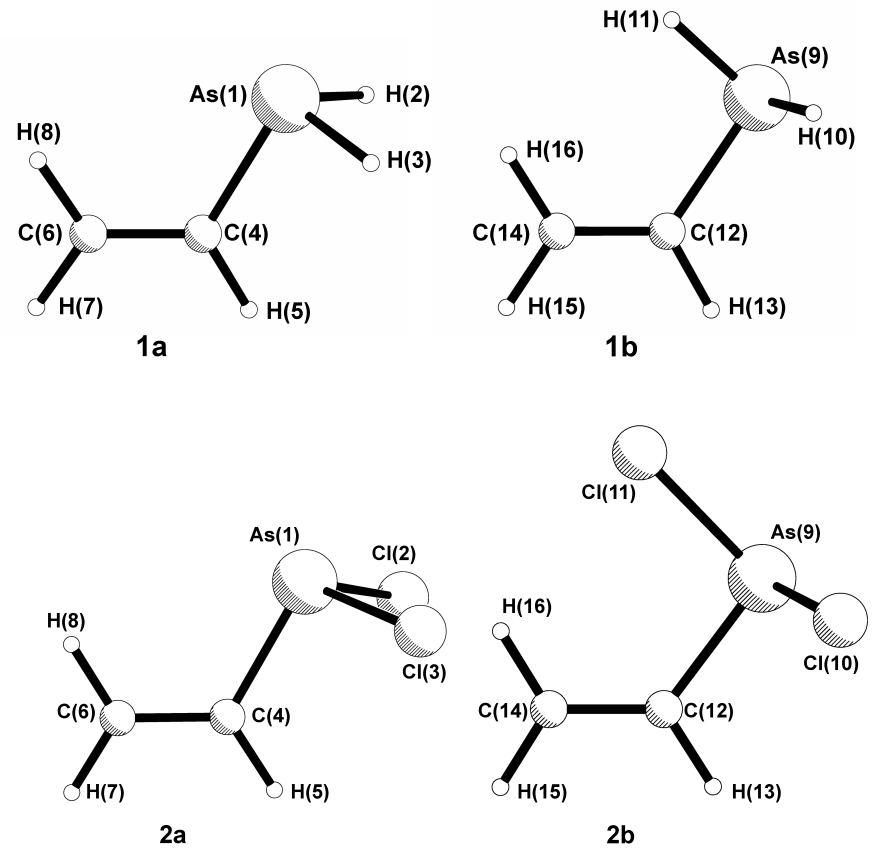

minima found by the optimisations and to provide vibrational information for use in the SARACEN refinement.

5.2.3 Gas electron diffraction measurements

Data were collected for **1**, **2** and **3** using the Edinburgh gas diffraction apparatus.[27] For each molecule, an accelerating voltage of ca. 40 kV (electron wavelength ca. 6.0 pm) was used. Sample temperatures were maintained at 215 K for **1**, 288 K for **2** and 205 K for **3**. The nozzle temperature was 293 K for each compound. Scattering intensities were recorded on Kodak Electron Image films at nozzle-to-plate distances of 126.8 and 283.2 mm for **1**, 127.0 and 284.6 mm for **2** and 283.6 mm for **3**. The refinement for arsine was conducted using only the data from the long camera distance as there were very few rings

on the short plates, presumably because the large difference between the phase of the scattering factors of As and H leads the scattering to beat out quickly. The weighting points for the off-diagonal weight matrices, correlation parameters and scale factors for each camera distance used for each molecule are given in Appendix 5 (in Tables A5.4, A5.8 and A5.12), together with electron wavelengths, which were determined from the scattering patterns of benzene vapour, recorded immediately after the compound patterns and analysed in exactly the same way to minimise systematic errors in wavelengths and camera distances. The scattering intensities were measured using an Epson Expression 1680 Pro flatbed scanner and converted to optical densities as a function of the scattering variable, s, using an established program.[28] Data reduction and least-squares refinements were carried out using the ed@ed v3.0 program,[29] employing the scattering factors of Ross *et al.*[30]

5.3 Results

5.3.1 *Ab initio* calculations

Vinylarsine

A PES scan around the CC–AsH bond revealed the presence of two conformers, in agreement with the previous MW spectroscopic study.[8] The first conformer (**1a**) has C_s symmetry with the two ϕC–C–As–H $\pm$*synclinal*. The second conformer (**1b**) has the point group C_1, with one ϕC–C–As–H *synperiplanar* and the second *anticlinal*. **1b** has a statistical weight twice that of **1a**.

The effects of improving the basis set and description of electron correlation on the structural parameters were gauged by a series of calculations at the HF and MP2 levels of theory using Pople-type basis sets. Selected parameters are shown in Table 5.1, with the full list of parameters given in Table A5.1 in Appendix 5. The theoretical structure appears to converge as the size of the basis set is increased, with the main exceptions being rAs–H, which shortens by 1.6 pm

Figure 5.2: Barrier to rotation around the C-C-XH_2 bisector, where X = N, P, As, calculated at the MP2/6-311++G** level of theory. The energy is relative to the lowest energy conformation for each molecule.

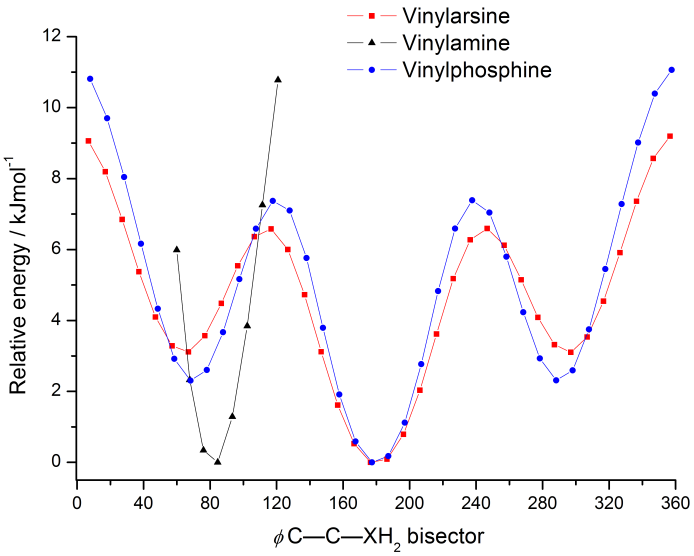

Table 5.1: Selected parameters for the lowest-energy structures of **1a**, **1b**, **2a** and **2b** calculated at the MP2 level of theory using the 6-311++G** (**A**) and 6-311++G(3*df*,3*pd*) (**B**) basis sets.[a,b]

Basis set	**A**	**B**	**A**	**B**
		1a		**1b**
rAs–H	151.4	151.8	151.4	151.6
rAs–C	195.3	194.5	195.1	194.3
rC–C	134.3	133.7	134.4	133.6
∠H–As–H	92.3	91.8	93.5	93.3
∠H–As–C	95.9	95.9	95.6	95.6
∠As–C–C	120.2	120.4	124.8	125.1
Energy[c]	-2313.1894	-2313.2737	-2313.1882	-2313.2727
		2a		**2b**
rAs–Cl	219.7	217.9	219.7	217.8
rAs–C	192.6	192.3	193.6	193.2
rC–C	134.4	133.7	134.4	133.5
∠Cl–As–Cl	98.6	98.7	100.3	100.3
∠Cl–As–C	96.2	96.3	96.9	96.8
∠As–C–C	118.7	118.6	125.4	125.7
Energy[c]	-3231.3670	-3231.5660	-3231.3650	-3231.5647

[a] Bond distances in pm and angles in °.
[b] See Figure 5.1 for atom numbering.
[c] Energy in Hartrees.

when diffuse and polarisation functions are included on the H atoms, and rAs–C and rC–C, which both shorten by 0.5 pm when the larger 6-311++G(3*df*,3*pd*) basis set is used. To investigate the nature of the barrier to rotation around ϕC–C–As–H a PES scan was conducted at the MP2/6-311++G** level. To enable comparison the same scan was conducted for vinylamine and vinylphosphine. The vinylphosphine curve is shown alongside the vinylarsine curve in Figure 5.2, but for vinylamine the curve is more complex and only a section has been included. The complication arises for the amine because of the ability of the second H atom, for which the dihedral angle is not fixed, to invert its position during the scan, starting the optimisation at one side of the N atom and ending on the other. For example, if the optimisation was started with the two ϕC-C-N-H at 70° (fixed) and -170°, the resultant optimised structure has ϕC–C–N–H as 70° and -35°. Attempts to fix both dihedral angles failed because the resultant structure could not be optimised. This effect does not occur for vinylphosphine or vinylamine

because rP–H and rAs–H are much longer. Vinylamine is predicted to exist in a single conformation, a result which is consistent with previous experimental studies.[31]

Vinyldichloroarsine

A PES scan around ϕC–C–As–Cl was conducted with the results shown in Figure 5.1. It can be seen that vinyldichloroarsine displays the same conformational behaviour as vinylarsine. The same series of calculations was performed with selected results given in Table 5.1. A full list of structural parameters is given in the Appendix 5, Table A5.2. Using the 6-311++G(3*df*,3*pd*) basis set shortened the As–Cl bond length by 1.7 pm over the 6-311++G** basis set. No other parameters changed as dramatically when this basis set was used and, as for vinylarsine, the rest of the calculated parameters appear to converge as the size of the basis set is increased. A more in depth discussion of these results are shown in the discussion in Section 5.4.6.

Figure 5.3: Barrier to rotation around the C-C-XCl_2 bisector, where X = N, P, As, calculated at the MP2/6-311++G** level of theory. The energy is relative to the lowest energy conformation for each molecule.

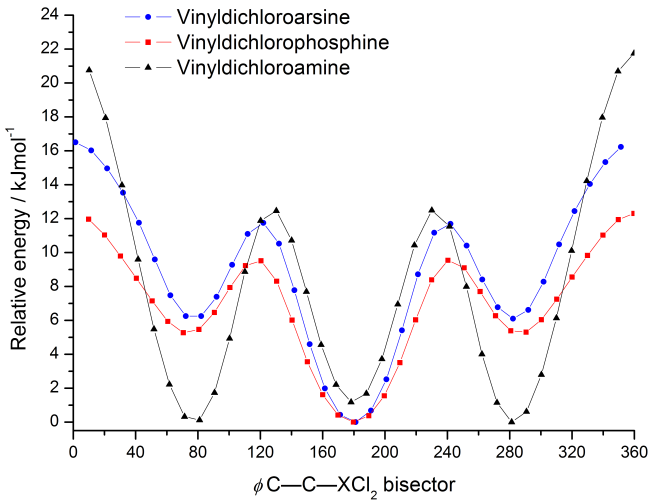

Arsine and arsenic trichloride

Calculations for AsH_3 and $AsCl_3$ were carried out at the same levels of theory as for **1** and **2**, with the results given in Table A5.3 in Appendix 5.

5.3.2 Gas electron diffraction refinements

Vinylarsine

The refinement of the structure of vinylarsine was conducted using an appropriate model containing two conformers. In order to reduce the number of parameters a number of simplifications were made. Calculations showed that in both conformers the variation in the various rC–H were too small to be detected experimentally and so all rC–H distances were modelled using a single parameter (p_1). Similarly the differences in the two ∠C(4)=C(6)–H and the two ∠C(12)=C(14)–H angles were small when compared to the anticipated experimental precision and so a single angle (p_5) was used in both conformers. Similarly ∠C(6)=C(4)–H(5) and ∠C(14)=C(12)–H(13) were also included in the refinement as a single parameter (p_6). The difference between rC(4)–As(1) and rAs(9)–C(12) was significant enough to warrant inclusion, and so rC(4)–As(1) was included (p_3) along with a difference (p_{10}) to rAs(9)–C(12) given by p_{10} = [rC(4)–As(1) - rAs(9)–C(12)].

rC=C and rAs–H in **1a** were included as an average (p_2) and a difference (p_4), given by [rC=C + rAs–H]/2 and [rAs–H - rC=C]/2 respectively. The same rC=C distance was used in **1b**. However, rAs–H(9) and rAs–H(10) are not identical, with calculations suggesting that rAs–H(10) is consistently close to rAs–H in **1a** and that rAs–H(11) is consistently ∼0.2 pm shorter. An extra parameter (p_{16}) was therefore included to allow rAs–H(10) to be shorter than rAs–H(11), such that p_{16} = rAs–H(10) - rAs–H(11).

∠C=C–As was also found to differ significantly between the conformers and was modelled as an average (p_7) and difference (p_{11}) given by p_7 = [∠C(6)=C(4)–As(1) + ∠C(14)=C(12)–As(9)] / 2 and p_{11} = [∠C(6)=C(4)–As(1)

- ∠C(14)=C(12)–As(9)] / 2. In **1a** one ∠C–As–H (p_8) was used due to symmetry whilst in **1b** ∠C(12)–As(9)–H(10) and ∠C(12)–As(9)–H(11) are distinct and thus were modelled using two parameters (p_{13} and p_{12} respectively). ∠H(2)–As(1)–H(3) (p_9) and ∠H(10)–As(9)–H(11) (p_{15}) were also included as distinct parameters.

The rotation of the AsH_2 group in **1b**, which is the most obvious difference between **1a** and **1b**, was modelled using the dihedral to the bisector of the two As–H bonds (p_{14}). A dihedral angle, ϕH(16)–C(14)=C(12)–As(9) (p_{17}), was included to allow for the slight out-of-plane displacement of As with respect the vinyl fragment. A final parameter was included to vary the ratio of the two conformers (p_{18}).

The starting parameters for the r_{h1} refinement[32] were taken from the theoretical geometry optimised at the MP2/6-31+G* level. A theoretical Cartesian force field was obtained at this level and converted into a force field described by a set of symmetry coordinates using the SHRINK program,[32] which generated both the amplitudes of vibration (u_{h1}) and the curvilinear corrections (k_{h1}).

Six rotation constants for **1** were combined with the GED data.[33] The rotation constants A_0, B_0 and C_0 for each conformer were corrected for the structural refinements using values calculated by SHRINK,[32] based on the MP2/6-31+G* force field. The resultant corrected constants, labelled A_{h1}, B_{h1} and C_{h1}, are given in Table 5.2. The vibrational corrections to the rotational constants, which transform, for example, A_0 into A_{h1}, are summations of the corrections for each of the normal modes of **1a** and **1b**. For **1a** the corrections for A, B and C were 489.8 MHz, 10.6 MHz and 11.3 MHz respectively, and for **1b** they were 571.0 MHz, 7.7 MHz and 9.9 MHz. The uncertainties of the vibrational corrections to the rotational constants were taken as 10% of the value of the vibrational correction for each constant listed above. The 10% figure is standard for vibrational corrections to rotational constants, based on our experience of how these quantities vary with the computational method used. The weights applied to all data depended on the uncertainties of the observations, in accordance with the SARACEN method.[9–11]

Table 5.2: Refined and calculated geometric parameters for vinylarsine (**1**) (distances in pm and angles in °) from the GED study and microwave rotation constants, in MHz, used in the GED refinements.[a,b]

	Parameter	MP2/ 6-311++G**	SARACEN (r_{h1})	Restraint
Independent parameters				
p_1	rC–H	108.8	110.0(4)	109.0(10)
p_2	rAs–H/rC=C_{av}	142.9	142.4(2)	—
p_3	rC(4)–As(1)	195.3	195.1(1)	—
p_4	rAs–H/rC=C_{dif}	8.6	8.0(2)	—
p_5	∠C(4)=C(6)–H	121.5	123.3(7)	121.5(10)
p_6	∠C(6)=C(4)–H(5)	119.9	119.9(8)	119.9(10)
p_7	∠C=C–As_{av}	122.5	122.7(1)	—
p_8	∠C(4)–As(1)–H	95.9	95.5(8)	95.9(10)
p_9	∠H(2)–As(1)–H(3)	92.3	93.3(6)	92.3(10)
p_{10}	ΔrC(12)–As(9)	0.2	0.2(1)	0.2(1)
p_{11}	∠C=C–As_{dif}	2.3	2.4(1)	—
p_{12}	∠C(12)–As(9)–H(10)	96.2	96.4(9)	96.2(10)
p_{13}	∠C(12)–As(9)–H(11)	95.0	95.2(9)	95.0(10)
p_{14}	ϕC(14)=C(12)–As(9)-H	64.5	65.3(18)	64.5(20)
p_{15}	∠H(10)–As(9)–H(11)	93.5	91.1(8)	93.5(10)
p_{16}	ΔrAs(9)–H(11)	0.2	0.3(1)	0.2(1)
p_{17}	ϕH(16)–C(14)=C(12)–As(9)	6.0	5.8(10)	6.0(10)
p_{18}	Proportion **1a**	0.64	0.37(6)	—
Dependent parameters				
dp_1	rAs–H	151.4	150.5(4)	—
dp_2	rC=C	134.3	134.4(2)	—
dp_3	rAs(9)–H(11)	151.3	150.1(4)	—
dp_4	rAs(9)–C(12)	195.1	194.9(1)	—
dp_5	∠C(6)=C(4)–As(1)	120.2	119.4(2)	—
dp_6	∠C(14)=C(12)–As(9)	124.8	124.1(2)	—

Rotational constants

Constant	Exp.	GED	Exp. – GED	Uncertainty
A_{h1}(**1a**)	35833.17	35853.62	–20.44	48.90
B_{h1}(**1a**)	3930.73	3931.20	-0.47	1.06
C_{h1}(**1a**)	3667.20	3666.73	0.49	1.13
A_{h1}(**1b**)	36870.41	36836.24	34.17	57.00
B_{h1}(**1b**)	3848.80	3848.45	0.35	0.77
C_{h1}(**1b**)	3587.91	3588.54	-0.63	0.99

[a] Figures in parentheses are the estimated standard deviation of the last digits.

[b] See text for parameter definitions.

Figure 5.4: Experimental and difference (experimental – theoretical) radial-distribution curve, $P(r)/r$, for vinylarsine (**1**). Before Fourier inversion the data were multiplied by $s.\exp(-0.00002s^2)/(Z_C - f_C)(Z_{As} - f_{As})$.

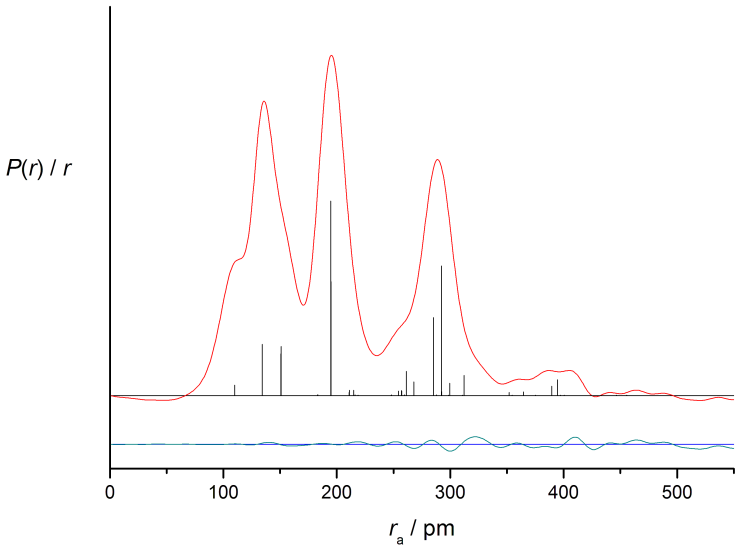

The refinement was initially conducted using the GED data alone, with which it was possible to refine rAs–C, an average for rC=C and rAs–H, and rC–H. The difference between rC=C and rAs–H could be refined but had a large e.s.d., as did the two ∠C=C–As angles when refined simultaneously. Other than for the corresponding amplitudes of vibration, no other parameters could be refined with reasonable e.s.d's. In the second refinement the six rotational constants were included. The MW data helps to distinguish between the two conformers, allowing refinement of both C–C–As angles without need to restrain the difference and vastly improving the e.s.d's on rAs–H and rC–H. The MW data also enables the refinement of the two H–As–H angles and two of the three C–As–H angles. However, the C–C–H angles and the dihedral angles could still not be refined, and it must be noted that the MW data offer no more information as to the relative stability of the two conformers. The final refinement was undertaken with GED data, rotational constants and restraints derived from *ab initio* calculations using the SARACEN method.[9–11] This allowed all seventeen geometric parameters and nine groups of vibrational amplitudes to be refined. Altogether, twelve geometric restraints (Table 5.2) and four amplitude restraints (Table A5.5) were employed.

The success of the final refinement, for which $R_G = 0.099$ ($R_D = 0.078$), can be assessed on the basis of the radial-distribution curve (Figure 5.4) and the molecular-scattering intensity curves (Figure A5.1). Final refined parameters are listed in Table 5.2. Appendix 5 includes the interatomic distances and the corresponding amplitudes of vibration (Table A5.5), with the least-squares correlation matrix (Table A5.6) and the experimental coordinates from the GED analysis (Table A5.7).

Vinyldichloroarsine

An initial refinement of the structure of vinyldichloroarsine (**2**) was conducted using an appropriate model containing two conformers. As it was anticipated that some $AsCl_3$ would remain in the sample its presence was also modelled. An initial refinement indicated the presence of $AsCl_3$, whilst the fraction of **2b** refined to 0. Given that the *ab initio* calculations suggest that **2b** is up to 10 kJ mol^{-1} higher in energy, and therefore present in a very small fraction at the experimental temperature (3% when $\Delta E = 10$ kJ mol^{-1}, calculated using the Boltzmann equation), such a result is not unexpected. **2b** was therefore not included in the final refinement, which was conducted using a model of **2a** and $AsCl_3$. **2a** was described in the same way as for **1a** with the exception that the similar As–Cl and As–C distances were modelled using an average and a difference, such that $p_3 = [r\text{As–Cl} + r\text{As–C}] / 2$ and $p_4 = [r\text{As–Cl} - r\text{As–C}] / 2$, and that rC=C was described by a single parameter (p_2). $AsCl_3$ was modelled with fixed C_{3v} symmetry using two parameters, the shortening of the As–Cl bond length from **2a** (p_{11}) and the Cl–As–Cl angle (p_{12}). All twelve geometric parameters and six groups of vibrational amplitudes were then refined. Flexible restraints were employed during the refinement using the SARACEN method.[9–11] Altogether, five geometric restraints (Table 5.3) and five amplitude restraints (Table A5.8) were employed. The success of the final refinement, for which $R_G = 0.056$ ($R_D = 0.039$), can be assessed on the basis of the radial-distribution curve (Figure 5.5) and the molecular scattering intensity curves (Figure A5.3). Final refined parameters are listed in Table 5.3.

Figure 5.5: Experimental and difference (experimental – theoretical) radial-distribution curve, $P(r)/r$, for vinyldichloroarsine (**2**). Before Fourier inversion the data were multiplied by $s.\exp(-0.00002s^2)/(Z_{\mathrm{Cl}} - f_{\mathrm{Cl}})(Z_{\mathrm{As}} - f_{\mathrm{As}})$.

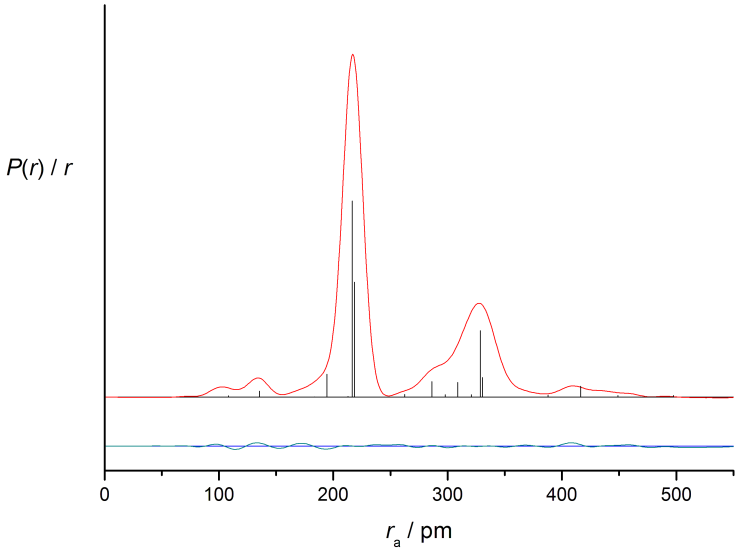

Arsine

Arsine was modelled with $C_{3\mathrm{v}}$ symmetry using two parameters. The first (p_1) describes rAs–H and second (p_2) ∠H–As–H. Both parameters and their related amplitudes of vibration were refined. Flexible restraints were employed during the refinement using the SARACEN method.[9–11] One geometric restraint (Table 5.4) and one amplitude restraint (Table A5.13) were employed. The success of the final refinement, for which $R_{\mathrm{G}} = 0.101$ ($R_{\mathrm{D}} = 0.068$), can be assessed on the basis of the radial-distribution curve (Figure A5.4) and the molecular scattering intensity curves (Figure A5.5). Final refined parameters are listed in Table 5.4.

Table 5.3: Refined and calculated geometric parameters for vinyldichloroarsine (**2**) (distances in pm and angles in °) from the GED refinement.[a,b]

	Parameter	MP2/ 6-311++G**	SARACEN (r_{h1})	Restraint
Independent parameters				
p_1	rC–H	108.7	108.5(9)	108.7(10)
p_2	rC=C	134.4	135.5(15)	—
p_3	rAs–C/rAs–Cl_{av}	206.2	206.5(6)	—
p_4	rAs–C/rAs–Cl_{dif}	13.6	11.9(6)	—
p_5	∠C(4)=C(6)–H	121.6	121.7(9)	121.6(10)
p_6	∠C(6)=C(4)–H(5)	122.4	122.6(9)	122.4(10)
p_7	∠C=C–As_{av}	118.7	119.7(12)	—
p_8	∠C–As–Cl	96.2	97.1(6)	—
p_9	∠Cl–As–Cl	98.6	98.6(9)	98.6(10)
p_{10}	$AsCl_3$ ΔrAs–Cl	-1.7	-1.8(9)	-1.7(10)
p_{11}	$AsCl_3$ ∠Cl–As–Cl	98.6	98.9(3)	—
p_{12}	Fraction $AsCl_3$	—	0.48(3)	—
Dependent parameters				
dp_1	rAs–C	192.6	194.4(10)	—
dp_2	rAs–Cl in **2**	219.7	218.4(6)	—
dp_3	rAs–Cl	218.0	216.6(4)	—

[a] Figures in parentheses are the estimated standard deviation of the last digits.
[b] See text for parameter definitions.

Table 5.4: Refined and calculated geometric parameters for arsine (distances in pm and angles in °) from the GED refinement.[a,b]

	Parameter	MP2/ 6-311++G**	SARACEN (r_{h1})	Restraint
Independent parameters				
p_1	rAs–H	151.1	150.3(2)	—
p_2	∠H–As–H	93.0	93.2(9)	93.0(10)

[a] Figures in parentheses are the estimated standard deviation of the last digits.
[b] See text for parameter definitions.

5.4 Discussion

The molecular structures of vinylarsine and vinyldichloroarsine have been investigated in the gas phase using GED supplemented by *ab initio* calculations *via* the SARACEN method. For vinylarsine, published rotational constants were also included in the refinement to supplement the GED data. An theoretical investigation of the structures was also undertaken.

5.4.1 Vinylarsine

The experimental structure of vinylarsine (**1**) is generally in good agreement with that calculated *ab initio*. The experimental rC(4)–As(1) of 195.1(1) pm falls between those calculated at the higher levels of theory, being 0.2 pm shorter than the value calculated at the MP2/6-311++G** level and 0.6 pm larger than at the MP2/6-311++G(3*df*,3*pd*) level. The bond length rAs(1)–H(2) is also found to be slightly shorter by experiment [150.5(4) pm] than theory suggests [151.4 / 151.8 pm using MP2/6-311++G** / MP2/6-311++G(3*df*,3*pd*)]. The experimental rC(1)=C(4) is found to be consistent with those found in the MP2 calculations with the larger basis sets.

The angles ∠C(6)=C(4)–As(1) and ∠C(14)=C(12)–As(9), being 119.4(2)° and 124.1(2)°, are slightly narrower than those calculated – the MP2/6-311++G(3*df*,3*pd*) values are 120.4° and 125.1°. However, the experimental difference between these two angles, 4.7(2)°, is in agreement with the theoretical value, which is consistently around 4.7°. This large difference in angle between the two conformers is consistent with that found for the two conformers of vinylphosphine and other similar phosphines.[1] The MW constants used in the refinement lead to smaller e.s.d's for these angles than would be achieved by GED alone and so it is likely that the slight difference in the experimental and theoretical angles is due to deficiencies in the *ab initio* calculations. A few of the other bond angles involving H atoms, such as ∠C(4)–C(6)–H and ∠H(10)–As(9)–H(11), lie around 2σ away from the *ab initio* values, but in general the bond angles and dihedral angles are consistent with the calculations.

The experimental fraction of **1a** is 0.37(6), which corresponds to an energy difference of 0.4(6) kJ mol^{-1}. This experimental energy difference is in favour of the same conformer as predicted by *ab initio* calculations, but by a lesser amount. At the MP2 level these differences range from 2.5 to 3.6 kJ mol^{-1}, but calculations at this level are not particularly accurate at predicting conformational abundances and a discrepancy of this size is not uncommon.[34]

5.4.2 Vinyldichloroarsine

When the experiment was started it was anticipated that around 10-20% of the vapour would consist of $AsCl_3$. Unfortunately the refinement suggests that 48(3)% of $AsCl_3$ is present. Such a large impurity, even though known, is likely to have an effect on the quality of structural data obtained. This is reflected in the e.s.d's obtained, which are generally larger than found for **1**, although larger e.s.d's on some parameters, such as rC–C, are to be expected even for a pure sample of **2** due to scattering from the heavy As and Cl atoms dominating the recorded pattern. For example, the two rAs–Cl produce scattering approximately 20 times more intense than the single rC–C in **2**, whilst in **1** the two rAs–H produce scattering only around twice as intense as rC–C.

The experimental structure of **2** is generally in agreement with that calculated *ab initio* but some of the experimental parameters have large e.s.d's. The experimental rAs–C of 194.4(10) pm lies 2σ from both the MP2/6-311++G** value of 192.6 pm and the MP2/6-311++G(3*df*,3*pd*) value of 192.3 pm. The rAs–Cl of 218.4(6) pm is also around 2σ from the MP2/6-311++G** value of 219.7 pm but is consistent with the value of 217.8 pm obtained at the MP2/6-311++G(3*df*,3*pd*) level. It therefore seems apparent that additional diffuse functions are required to describe the As–Cl bond correctly. The experimental rC–C of 135.5(15) pm, whilst imprecise, is consistent with the computed values. The bond angles tend to agree reasonably closely; the experimental ∠C=C–As of 119.7(12)° compares with 118.6° at the MP2/6-311++G(3*df*,3*pd*) level, and ∠C–As–Cl is 97.1(6)° by experiment, slightly wider than the 96.3° predicted by

theory. ∠Cl–As–Cl, dependant on the Cl...Cl peak that overlaps with that for $AsCl_3$ but is only one third as intense, required a restraint, and therefore the experimental value of 98.6(9)° matches the theoretical value.

5.4.3 Arsenic trichloride

One advantage of having a large proportion of $AsCl_3$ in the vapour is that its structure can also be determined. For $AsCl_3$ the experimental rAs–Cl is found to be 216.6(4) pm, which, as in the case of **2**, is shorter than that found at the MP2/6-311++G** level of theory (218.0 pm) but is consistent with the value of 216.3 pm found at the MP2/6-311++G(3*df*,3*pd*) level. The experimental ∠Cl–As–Cl of 98.9(3)° lies very close to the MP2/6-311++G(3*df*,3*pd*) value of 98.8°. The r_g structure of $AsCl_3$ has been determined by GED previously,[35] with rAs–Cl found to be 216.21(33) pm and ∠Cl–As–Cl 98.34(34)°, both of which are 1-2σ from the values found in this study.

5.4.4 Arsine

rAs–H is found to be 150.3(2) pm by experiment, 4σ from the MP2/6-311++G** value of 151.1 pm. ∠H–As–H required a restraint; the experimental value of 93.2(9)° is therefore close to the computed one.

5.4.5 Comparison of 1 and 2

A comparison of relevant structural parameters for **1** and **2** is shown in Table 5.5. It can be seen that the geometries around the As atoms in the two molecules are quite different, with rAs–C being 2.7 pm shorter in the case of **2**, ∠Cl–As–Cl being 6.3° wider than ∠H–As–H and ∠C=C–As being 1.5° narrower in **2**. The vinyl fragment itself appears to be unaffected, with rC=C being comparable in both molecules. The shorter rAs–C can be attributed to the greater electronegativity of the Cl atoms – the As atom has a more positive partial charge in **2** and is therefore more strongly bound to the negatively charged C

atom. This is backed up by the Mulliken charges obtained from the calculations; at the MP2/6-311++G** level the partial charge on As in **1a** is 0.28e whilst in **2a** it is 0.33e. The wider ∠Cl–As–Cl in **2** compared to ∠H–As–H in **1** is probably due to increased steric repulsion between the two bulky Cl atoms.

5.4.6 Comparison of N and P analogues

The structures of the nitrogen and phosphorus analogues of **1** and **2** have been calculated and the barrier to rotation about the CC–XY bond (X = N, P or As and Y = H or Cl) has been assessed. A comparison of key structural parameters is shown in Table 5.5, with the shapes of the barrier to rotations for the H derivatives shown in Figure 5.2 and for the Cl derivatives in Figure 5.3.

It is clear from these results that, whilst the phosphorus and arsenic compounds display similar behaviour, the analogous amines behave very differently. Vinylamine exists as a single conformer similar to **1b** with no stable analogue of **1a**. Although it has been studied by MW spectroscopy[36–38] it has never been studied by GED. Vinyldichloroamine has, to the best knowledge of the author, never been synthesised.

The PES scan shown in Figure 5.2 for vinyldichloroamine does show both conformations found in the phosphorus and arsine equivalents, but the conformer resembling **2b** is found to be slightly more stable than that resembling **2a**, whereas for vinyldichlorophosphine and vinyldichloroarsine the **2a** conformer is significantly more stable than the **2b**. Vinyldichlorophosphine has previously been studied by GED but the investigation was not supported by *ab initio* calculations and the results were ambiguous with regard to the conformational makeup.[39]

In both the arsine and the dichloroarsine the barriers to rotation for the P and As species are very similar. The trends in bond angle around the group 15 element are the same as those found in the Group 15 trihalides,[40] with the widest bonds in the N case and the narrowest in the As case.

The difference in behaviour between the N-containing systems and the P- and

Table 5.5: Comparison of structural parameters (distances in pm and angles in °) calculated at the MP2/6-311++G** level of theory for the lowest energy conformations of vinylamine, vinylphosphine, vinylarsine, vinyldichloroamine, vinyldichlorophosphine and vinyldichloroarsine.[a]

Parameter	-amine (X = N)	-phosphine (X = P)	-arsine (X = As)
vinyl-XH_2			
rX–C	139.9	183.0	195.4
rX–H	101.1	141.8	151.4
rC–C	134.5	134.3	134.3
∠H–X–H	111.2	93.7	92.3
∠H–X–C	114.2	97.1	95.9
∠X–C–C	125.8	120.6	120.2
vinyl-XCl_2			
rX–Cl	176.6	207.6	219.7
rX–C	142.4	180.3	192.6
rC–C	134.0	134.4	134.4
∠H–X–H	109.8	101.0	98.6
∠H–X–C	111.1	97.7	96.2
∠X–C–C	127.2	118.9	118.7

[a] Where parameters, such as rX–H, are not symmetry-related the average is given.

Figure 5.6: p orbitals in N, P and As indicating an increase in the number of radial nodes down the group.

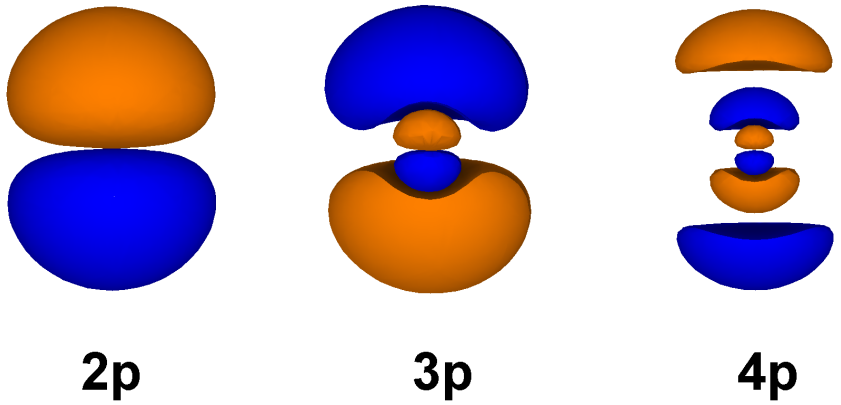

As-containing systems can be explained by considering the nature of the valence orbitals. N and C possess $2p$ orbitals and so the most favourable overlap between these orbitals occurs when the two $2p$ orbitals perpendicular to the N–C bond are

aligned. However, P has $3p$ orbitals, which possess a single radial node, and As has $4p$ orbitals, which possess two radial nodes (shown in Figure 5.6). Therefore in the P and As cases the nature of the overlap between the $3p$ or $4p$ orbitals and the $2p$ orbital on the C is more complex and rotation about C–P or C–As will not cause as large a change in the overlap between orbitals. It is this difference in the nature of the valence orbitals in N, P and As that is responsible for differences observed, both in terms of conformational make-up and the geometry around the heteroatom. It is interesting to note that despite the differences in bonding orbitals used by the α-C atom, the vinylic C=C bond length varies little between the amine, phosphine and arsine.

5.5 Conclusion

The structures of vinylarsine, vinyldichloroarsine, arsenic trichloride and arsine have been determined from GED data using the SARACEN method. This study provides the first complete structure of a primary arsine. The conformational and structural behaviour of the arsenic systems has been compared to that of the analogous amines and phosphines with the general trend being that the phosphorus and arsenic systems behave similarly but that the amines are very different, both in terms of structure and conformational behaviour. It is hoped that this study can be extended to other primary arsines. However, a preliminary attempt found allylarsine to be unstable under the current conditions required for GED, so such work is likely to require modifications to reduce the vapour pressure requirements.

5.6 References

[1] R. Noble-Eddy, S. L. Masters, D. W. H. Rankin, D. A. Wann, H. E. Robertson, B. Khater and J.-C. Guillemin, *Inorg. Chem.*, 2009, **48**, 8603.

[2] S. F. Dyke, *The Chemistry of the Enamines*, Cambridge University Press, 1973.

[3] M. R. Ellenberger, D. A. Dixon and W. E. Farneth, *J. Am. Chem. Soc.*, 1981, **103**, 5377.

[4] B. J. Smith and L. Radom, *J. Am. Chem. Soc.*, 1992, **114**, 36.

[5] A. Benidar, R. L. Doucen, J.-C. Guillemin, O. Mó and M. Yánez, *J. Phys. Chem. A.*, 2002, **106**, 6262.

[6] J.-C. Guillemin and L. Lassalle, *Organomet.*, 1994, **13**, 1525.

[7] P. M. El'kin, O. V. Pulin and V. F. Pulin, *J. App. Spect.*, 2004, **71**, 588.

[8] P. Dréan, D. Petitprez, J. Demaison, J. C. López, J. L. Alonso, J.-C. Guillemin and J. E. Boggs, *J. Mol. Spectrosc.*, 1998, **190**, 365.

[9] A. J. Blake, P. T. Brain, H. Mc Nab, J. Miller, C. A. Morrison, S. Parsons, D. W. H. Rankin, H. Robertson and B. A. Smart, *J. Phys. Chem. A*, 1996, **100**, 12280.

[10] P. T. Brain, C. A. Morrison, S. Parsons and D. W. H. Rankin, *J. Chem. Soc., Dalton Trans.*, 1996, 4589.

[11] N. W. Mitzel and D. W. H. Rankin, *J. Chem. Soc., Dalton Trans.*, 2003, 3650.

[12] V. Métail, A. Senio, L. Lassalle, J.-C. Guillemin and G. Pfister-Guillouzo, *Organomet.*, 1995, **14**, 4732.

[13] J.-C. Guillemin, M. Decouzon, J.-F. Gal, P.-C. Maria, O. Otilia and M. Yánez, *J. Phys. Chem. A.*, 1997, **101**, 9525.

[14] M. J. Frisch, G. W. Trucks, H. B. Schlegel, G. E. Scuseria, M. A. Robb, J. R. Cheeseman, J. A. Montgomery, Jr., T. Vreven, K. N. Kudin, J. C. Burant, J. M. Millam, S. S. Iyengar, J. Tomasi, V. Barone, B. Mennucci, M. Cossi, G. Scalmani, N. Rega, G. A. Petersson, H. Nakatsuji, M. Hada, M. Ehara, K. Toyota, R. Fukuda, J. Hasegawa, M. Ishida, T. Nakajima, Y. Honda, O. Kitao, H. Nakai, M. Klene, X. Li, J. E. Knox, H. P. Hratchian, J. B. Cross, V. Bakken, C. Adamo, J. Jaramillo, R. Gomperts, R. E. Stratmann, O. Yazyev, A. J. Austin, R. Cammi, C. Pomelli, J. W. Ochterski, P. Y. Ayala, K. Morokuma, G. A. Voth, P. Salvador, J. J. Dannenberg, V. G. Zakrzewski, S. Dapprich, A. D. Daniels, M. C. Strain, O. Farkas, D. K. Malick, A. D. Rabuck, K. Raghavachari, J. B. Foresman, J. V. Ortiz, Q. Cui, A. G. Baboul, S. Clifford, J. Cioslowski, B. B. Stefanov, G. Liu, A. Liashenko, P. Piskorz, I. Komaromi, R. L. Martin, D. J. Fox, T. Keith, M. A. Al-Laham, C. Y. Peng, A. Nanayakkara, M. Challacombe, P. M. W. Gill, B. Johnson, W. Chen, M. W. Wong, C. Gonzalez and J. A. Pople, *Gaussian 03, Revision C.02*, Gaussian, Inc., Wallingford, CT, 2004.

[15] J. S. Binkley, J. A. Pople and W. J. Hehre, *J. Am. Chem. Soc.*, 1980, **102**, 939.

[16] M. S. Gordon, J. S. Binkley, J. A. Pople, W. J. Pietro and W. J. Hehre, *J. Am. Chem. Soc.*, 1982, **104**, 2797.

[17] W. J. Pietro, M. M. Francl, W. J. Hehre, D. J. DeFrees, J. A. Pople and J. S. Binkley, *J. Am. Chem. Soc.*, 1982, **104**, 5039.

[18] C. C. J. Roothaan, *Rev. Mod. Phys.*, 1951, **23**, 69.

[19] C. Møller and M. S. Plesset, *Phys. Rev.*, 1934, **46**, 618.

[20] W. J. Hehre, R. Ditchfield and J. A. Pople, *J. Chem. Phys.*, 1972, **56**, 2257.

[21] P. C. Hariharan and J. A. Pople, *Theo. Chim. Acta.*, 1972, **56**, 2257.

[22] M. S. Gordon, *Chem. Phys. Lett.*, 1980, **76**, 163.

[23] A. D. McLean and G. S. Chandler, *J. Chem. Phys.*, 1980, **72**, 5639.

[24] R. Krishnan, J. S. Binkley, R. Seeger and J. A. Pople, *J. Chem. Phys.*, 1980, **72**, 650.

[25] M. J. Frisch, M. Head-Gordon and J. A. Pople, *Chem. Phys. Lett.*, 1990, **166**, 275.

[26] M. J. Frisch, M. Head-Gordon and J. A. Pople, *Chem. Phys. Lett.*, 1990, **166**, 281.

[27] C. M. Huntley, G. S. Laurenson and D. W. H. Rankin, *J. Chem. Soc., Dalton Trans.*, 1980, 954.

[28] H. Fleischer, D. A. Wann, S. L. Hinchley, K. B. Borisenko, J. R. Lewis, R. J. Mawhorter, H. E. Robertson and D. W. H. Rankin, *Dalton Trans.*, 2005, 2469.

[29] S. L. Hinchley, H. E. Robertson, K. B. Borisenko, A. R. Turner, B. F. Johnston, D. W. H. Rankin, M. Ahmadian, J. N. Jones and A. H. Cowley, *Dalton Trans.*, 2004, 2469.

[30] A. W. Ross, M. Fink and R. Hilderbrandt, *International Tables for Crystallography*, Kluwer Academic Publishers, Dordrecht, Netherlands, 1992, p. 245.

[31] R. D. Brown, P. D. Godfrey and B. Kleibómer, *J. Mol. Spect.*, 1987, **124**, 21.

[32] V. A. Sipachev, *THEOCHEM*, 1985, **121**, 143.

[33] T. Kojima, E. L. Breig and C. C. Lin, *J. Chem. Phys.*, 1961, **35**, 2139.

[34] T. van Mourik, P. G. Karamertzanis and S. L. Price, *J. Phys. Chem. A.*, 2005, **110**, 8.

[35] S. Konaka and M. Kimura, *Bull. Chem. Soc. Jap.*, 1970, **43**, 1693.

[36] Y. Hamada, K. Hashiguchi, M. Tsuboi, Y. Koga and S. Konda, *J. Mol. Spect.*, 1984, **105**, 93.

[37] Y. Hamada, N. Sato and M. Tsuboi, *J. Mol. Spect.*, 1987, **124**, 172.

[38] D. McNaughton and E. G. Robertson, *J. Mol. Spect.*, 1994, **163**, 80.

[39] V. A. Naumov, V. Y. Nesterov and I. A. Aleksandrova, *Zh. Strukt. Khim.*, 1984, **24**, 137.

[40] M. Brynda, *Coord. Chem. Rev.*, 2005, **249**, 2013.

Chapter 6

The very high temperature nozzle and the generation of ketene

6.1 Introduction

As outlined in Chapter 1, little work has been conducted in the area of GED studies of short-lived species and, where work is reported, it has generally been as a result of a fortuitous accident rather than part of targeted research. Whilst the study of such species with GED is likely to be challenging, GED offers a unique opportunity for full structure determination, something which is not routinely possible with other techniques.

The work of Zewail has demonstrated that femtosecond GED can offer a window on chemical processes and the structures of short-lived species.[1–3] However, the pump-probe experimental set-up is still rare, with the expensive equipment putting such research beyond the means of most electron diffraction groups. Instead, work in Edinburgh has focussed on the millisecond to second timescale with molecules generated using pyrolysis. Such an experimental set-up would enable the study of a wide range of unstable molecules, including radicals, for which little structural information is currently available.

The first half of this chapter outlines the new very high temperature (VHT) nozzle in use in Edinburgh and gives details of calibration and testing that was required. The second half of this chapter details the attempts to study the structure of ketene - a test system for the new nozzle.

6.2 The VHT nozzle

To enable the generation of short-lived species and their study by GED it was necessary to construct a new very high temperature (VHT) nozzle. The basic concept was to combine the techniques of flash vacuum pyrolysis (FVP, see Chapter 1) with GED. The FVP equipment can be broken down in to three main sections; an oven to vaporise the precursor, a hotter pyrolysis zone, and a trap to collect the product. In the case of an FVP-GED system the GED apparatus itself takes the place of the trap - the apparatus must therefore consist of a way to initially vaporise a sample and a pyrolysis oven.

To achieve this goal a number of differing approaches are possible. At one extreme a standard FVP apparatus can be used outside the GED apparatus, with the two linked by a hot nozzle allowing transport of the pyrolysed gas from the FVP apparatus to the scattering zone within the GED machine. This method would offer maximal control of the parameters of the FVP apparatus and different FVP systems could be used for different experiments. However, it is anticipated that the construction of a hot nozzle, extending from the outside of the machine to the scattering zone and able to maintain a temperature of 1000 K, would be difficult. It should be noted that it may often be possible for the pyrolysis products to be transported at a lower temperature than is required for pyrolysis. The other extreme of design involves the construction of a FVP system fully self-contained within the GED apparatus such that no external FVP equipment is needed. This method allows the use of a much smaller pyrolysis oven within the nozzle, although in this case adjustment of the pyrolysis conditions would limited. A number of intermediate designs can also be envisioned, for example, the oven used to vaporise the precursor could be external to the GED machine with the pyrolysis zone within the nozzle.

The mechanical workshop in Edinburgh has little previous experience with such high temperature systems and the materials used in their construction and so this was undertaken by the group of Prof. Georgiy Girichev (Ivanovo State University of Chemistry and Technology, Russia), who have previous experience of VHT

GED experiments.[4]

The nozzle was designed prior to the start of this PhD and was constructed as a self-enclosed unit with both the very high temperature pyrolysis oven and the medium temperature (MT) vaporising oven being part of the nozzle, internal to the GED apparatus. The facility also exists for gas to be passed into the nozzle from the outside at room temperature. The general workings of the nozzle, the process of testing the nozzle and some of the problems encountered are briefly detailed in this chapter. Discussion of potential improvements to the design of the nozzle and ideas for the future will be discussed in the final chapter.

A number of modifications were necessary to make the nozzle work with the Edinburgh GED apparatus. The gas inlet was adapted to be compatible with our fittings and new O-rings were fitted to the gas pass-through. The space available for the thermocouple vacuum pass-through was limited and commercial feedthroughs were too large to fit in the space available, so these were moved to a spare port utilising user-friendly push-on connectors.

6.2.1 Possible configurations

A schematic of the four possible configurations for the VHT nozzle is shown in Figure 6.1. Scheme A allows the study of involatile samples, extending the range of temperatures accessible using the Edinburgh GED apparatus. Scheme B allows the pyrolysis of gases with vapour pressures sufficient for study at room temperature, and benzene calibration can be obtained by simply switching samples. Schemes C and D allow the pyrolysis of samples that require heating to achieve sufficient vapour pressure, and are likely to be the most widely-used configurations.

Initially only scheme C was available, and this was used for the study of the benzyl radical in Chapter 7, but to offer the chance to perform benzene calibrations scheme D was made possible by the design of a new cell for the MT oven. In scheme D the pyrolysis experiment must be conducted first, ensuring that all the sample in the MT oven is vaporised, before benzene is passed through from

Figure 6.1: The four possible configurations of the Edinburgh VHT nozzle.

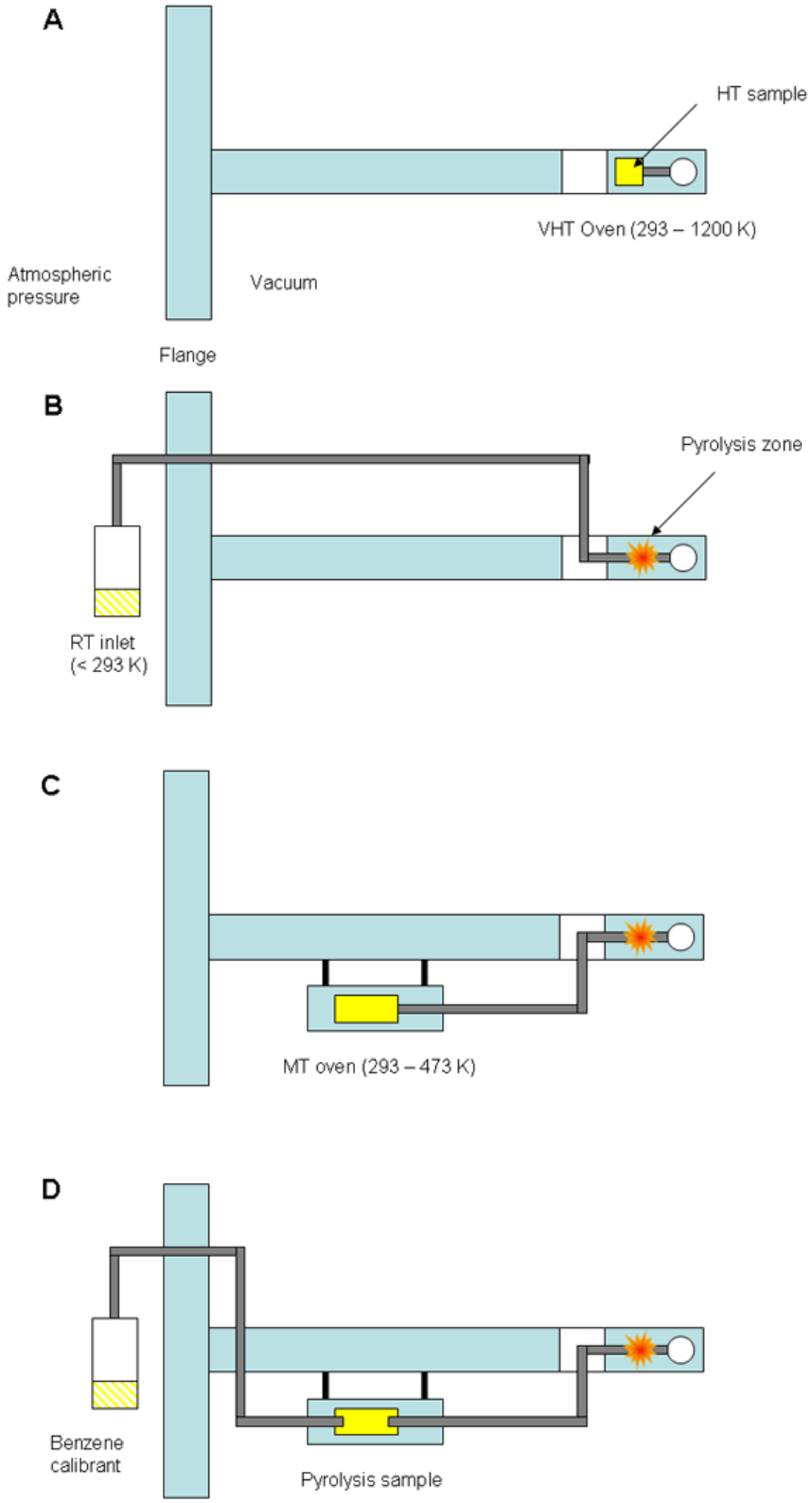

the external gas inlet. Shortly after the construction of the new cell for the MT oven a problem developed with the VHT oven that could not be repaired quickly, meaning that data could not be collected using scheme D in the timescale available.

The difficulty calibrating the nozzle-to-camera distance arises because it is difficult, given the space limitations, to have multiple routes for gas within the VHT nozzle. The group in Ivanovo use a fine mesh, coated with a crystalline compound such as ZnO, to calibrate the nozzle-to-camera distance. The mesh is mounted on a rotating arm and swung into place as required. However, the lack of a viewing port on the Edinburgh apparatus to facilitate positioning of the mesh meant that this method was not feasible. It was initially hoped that the nozzle would be rigid enough to make calibration on each run unnecessary, but whilst it was found that the nozzle-to-camera distance was constant over a heating and cooling cycle, it varied greatly once the nozzle was removed from the machine and prepared for a new experiment. It was therefore necessary to rely on calibration using benzene. This is not ideal, as there is no guarantee that benzene itself will be stable at the temperatures used. However, during the course of these studies no sign of benzene decomposition was noted.

6.2.2 Distance calibration

The standard high temperature nozzle (up to 500 K) used in Edinburgh can be used in one of two ports on the GED apparatus, in a total of three positions, termed the long, medium and short nozzle-to-camera distances. The VHT nozzle is bulky and only fits in the larger of these two ports, in which it can be used in two positions, roughly comparable to the long and medium positions. However, due to its large size the VHT nozzle is close to being central on the flange used to connect it to the GED apparatus, meaning the two positions are relatively close together. The first task was to investigate how different the nozzle-to-camera distances were in these two positions and to devise a strategy for data collection. Using benzene as a calibrant the nozzle-to-camera distance at the long position

was found to be ∼243 mm whilst at the medium position it was ∼213 mm. The long position offered data from $s = 2$ nm^{-1} whilst the medium position offered data from around 2.6 nm^{-1}. The extra data range of the medium distance, up to around $s = 19$ nm^{-1}, would always be required, so the long position effectively offers data only in the additional range 2 - 2.6 nm^{-1}. It was therefore decided that data would only be routinely collected in the medium position. The data range, approximately 2.6 - 19 nm^{-1}, is roughly comparable to that obtained when long and medium plates are obtained using the standard HT nozzle, for which the range is routinely 2 - 21nm^{-1}.

6.2.3 Oven glowing

During initial attempts to collect data using the VHT nozzle, after the benzene calibrations had been completed, it was noticed that the developed films often showed marks, probably due to exposure to light. In most cases this rendered the data unusable. This was initially difficult to understand as the benzene calibration films had appeared to be satisfactory. After further investigation two individual issues were discovered. The first related to the use of the MT oven and the second to the VHT oven.

It was found that the MT oven emitted light during heating. This problem only occurred when power was flowing to the oven, and was attributed to a faulty segment of filament wire where a protective coating had chipped off. As the rate of cooling of the MT oven was very slow (around 1 K per minute at 575 K) the oven temperature and therefore vapour pressure was constant for long enough to complete a data collection, and so this problem was easily overcome by simply ensuring no power was flowing to the MT oven when a film was in the camera.

However, further tests revealed that the MT oven was not responsible for all of the problems, as issues with the films were found when the MT oven was not in use. It later became clear that, at very high temperatures, the VHT oven was glowing sufficiently to fog the photographic film. This was not a problem for the benzene calibrations because the high vapour pressure of benzene meant that film

exposure lasted for around 10 seconds, but exposure times for other samples are frequently around 90 seconds.

The VHT oven is fitted with a number of features to reduce light pollution inside the GED apparatus and so, in order to discover the cause of the light, the camera was partially removed from the GED apparatus so that the nozzle was clearly visible. A photograph was taken and is shown in Figure 6.2 alongside the same area of the nozzle when cool. In the left-hand photo the outer cover and inner foil shield are visible, as is the tapered section leading out of the scattering zone. It can be seen on the right-hand picture that these two shields are blocking light, but that light is visible from the VHT oven close to the scattering zone. The heat shields are in place and working correctly, but it is inevitable that in order for a direct path to exist from the scattering zone to the detector some of the oven must be visible.

It was always realised that light could be a problem and the nozzle was designed to shield as much light as possible. Discussion with our collaborators revealed that they do not suffer this problem but the Ivanovo apparatus use a nozzle-to-camera distance roughly double that of the Edinburgh set-up, and so applying the inverse square law, the photographic film will receive one quarter as much light.

The problem with light was difficult to anticipate, and other than the use of image plates it is difficult to solve. Previous researchers have coated photographic plates with indian ink to overcome this problem, but this is not possible with the film used in Edinburgh. As no solution could be found it effectively lowers the temperature available for the VHT oven. A maximum temperature of 900 K is suitable for exposures of around 60 seconds.

6.2.4 Image plates

A possible solution for the glowing VHT oven is to use image plates rather than photographic film. Image plates are sensitive to electrons but are much less sensitive to light and so would not be affected strongly by the light from the

VHT oven. Image plates have been used by other electron diffraction groups and offer data of at least as high quality as obtained from photographic film, but have a larger dynamic range and have even been used without a rotating sector.[5]

Image plates have not been used in Edinburgh prior to this work and so an initial test was conducted using benzene as the scattering gas. A test image plate was obtained from the group of Prof. David Rice (Reading, UK) and adapted for use with the camera on the Edinburgh apparatus. The image plate was exposed for roughly the same amount of time as for a photographic film and once exposed was scanned using the Fuji scanner in Reading. The resulting scanned images were extracted using a modified version of Z2IDP (written and modified by Dr. Alexander V. Zakharov, Ivanovo State University of Chemistry and Technology, Russia) and refined in the usual way using the ed@ed program.[6] The resultant fit was comparable to that expected using standard photographic films.

At this stage the feasibility of using image plates with the Edinburgh apparatus had been proven, but it would not be possible to rely on the Reading group to scan the plates, nor would it be sensible to purchase a full set of image plates without a permanent scanning solution. An image plate scanner was located within the University of Edinburgh and so the test plate was re-exposed and scanned using this scanner. The scanner, manufactured by the now defunct Molecular Dynamics, is no longer supported and little information could be found with regard to its usage. A metal plate was made to allow the image plate from the diffraction machine to be scanned using this machine but whilst it was possible to obtain an image from this scanner, data processing proved to be impossible. The conversion function from image intensity to the number of incident electrons was not known and there was no way to understand the myriad of options available in the software. It is clear from the images that the two scanners produce different images, with the Edinburgh scanner producing an inverted image. It was decided that there were too many variables to contend with and so this project was halted. However, the use of image plates remains strongly desirable when using equipment at very high temperatures.

The images obtained from the Reading Fuji scanner (left) and the scanner in

Figure 6.2: VHT oven glow (right) alongside the same area of the nozzle when cool (left).

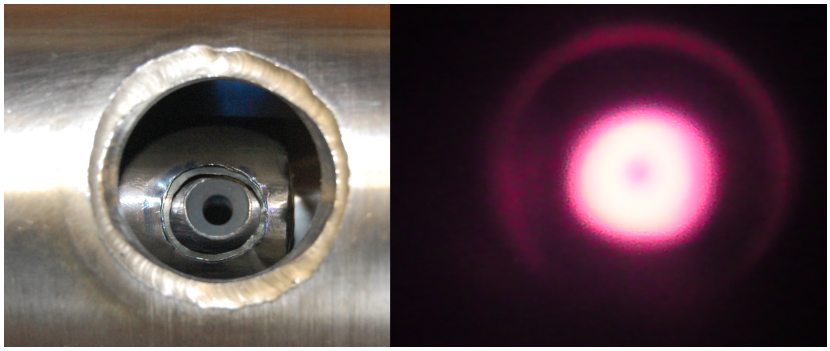

Edinburgh (right) are shown in Figure 6.3.

6.2.5 High-temperature pressure drop

During the study of acetic anhydride, discussed later in this chapter, the sample showed sufficient vapour pressure when the VHT oven was at room temperature, but greatly reduced scattering was observed when the VHT oven was around 825 K. Upon discussion with the Ivanovo group it transpired that they observed the same phenomenon and had termed it "thermodynamic jam". A rough explanation can be offered by considering the equation of state and assuming that, because the hole in the effusion cell that allows the gas to flow in to the path of the beam is very small, the system consisting of the gas sample, tubing and hot effusion cell can effectively be considered to be at equilibrium. Therefore the pressure, given by $P = \rho RT$ (where ρ is the density, R the gas constant and T the temperature), will be approximately the same at each point in this system. However, the temperature in the effusion cell is higher than that in the sample reservoir and so for the pressure to be constant the density of gas in the hot effusion cell must be lower. The equation suggests the relationship is linear, such that if the temperature in the effusion cell is double that of the sample reservoir the density of gas will be half, and this was roughly what was observed in the study of acetic anhydride.

Figure 6.3: Image plates of benzene scanned using the Reading scanner (left) and Edinburgh scanner (right).

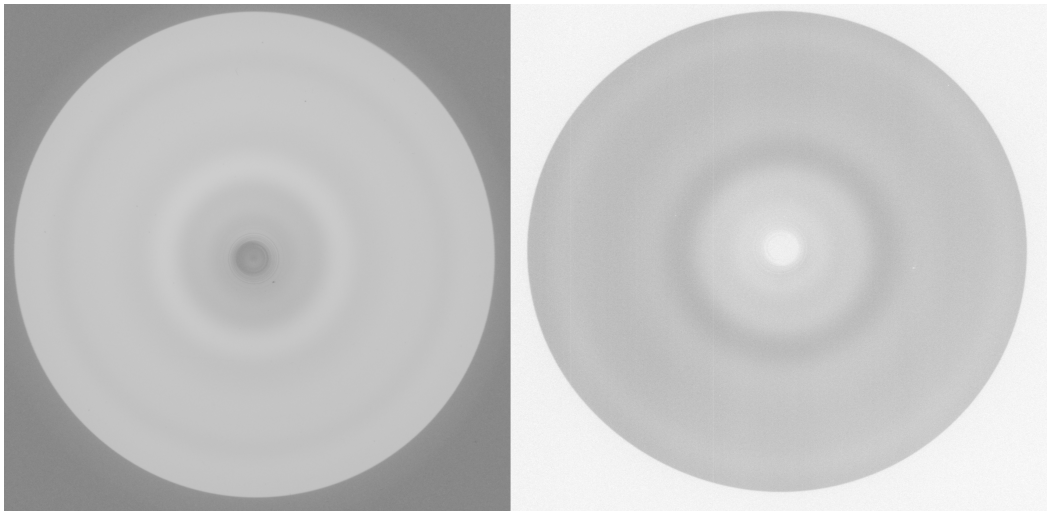

6.3 Generation of ketene

Once the nozzle had been fitted to the Edinburgh apparatus and tested the first goal was to study the generation of ketene. Ketene (CH_2CO, Figure 6.4) was chosen as the test case for a number of reasons. Ketene is an unstable molecule which dimerises rapidly to form diketene ($OCCH_2OCCH_2$, Figure 6.4) at room temperature.[7] Ketene itself has been studied before by GED by carefully storing a cold sample,[8,9] and so the aim of this work was to test a number of *in situ* generation methods to assess whether the FVP-GED method is viable. Ketene is a strong test case because the structure is known, and because a total of four different methods of generation were identified.

The simplest route is the pyrolysis of diketene to form pure ketene. The second route identified uses Meldrum's acid [$(CH_3)_2CO_2COCOCH_2$] as a precursor, which has been shown to pyrolyse to form ketene, CO_2 and acetone [$OC(CH_3)_2$]. The third uses acetic anhydride [$(CH_3O)_2O$] to produce acetic acid and ketene, whilst the final route uses acetone to produce ketene and methane (CH_4). Unfortunately diketene is no longer commercially available in the UK, presumably due to its volatile and flammable nature, and so no sample was available to test this route. The other three routes were explored and are detailed in the remainder of this chapter.

If ketene can be studied successfully it allows the study of new, more interesting substituted ketenes, including asymmetrically substituted ketenes. A number of other ketenes have been studied by GED, including diketene and methyldiketene,[10] bis(trimethylgermyl)ketene,[11] bis(trifluoromethylthio)ketene[12] and perhaps most interestingly, dichloroketene,[13] generated from the precusor trichloroacetyl chloride using a gas-solid reaction.

As it is likely that some unreacted starting material will remain after pyrolysis it was necessary to investigate the structure of the precursor prior to attempting pyrolysis. Of the three starting materials only Meldrum's acid has not been studied by GED before and so its structure is presented for the first time. Acetic anhydride has been studied previously, but the analysis used a dynamic model

Figure 6.4: Molecular structures of ketene and diketene.

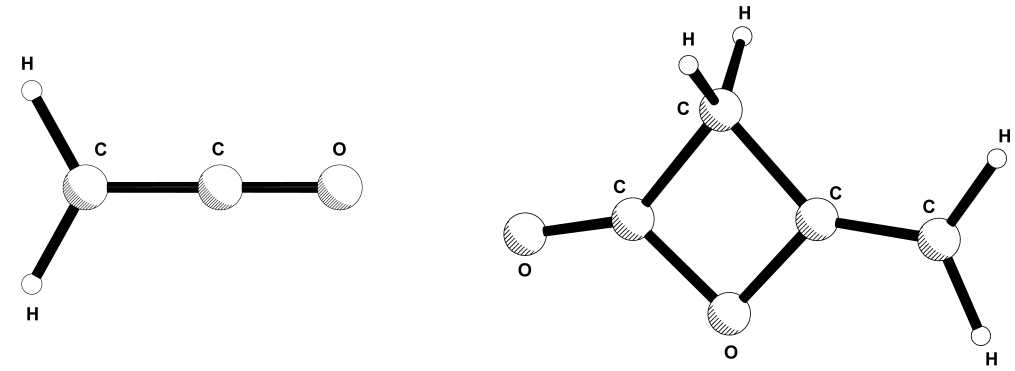

which is too complex to incorporate into a model that also includes decomposition products. A simpler model was created for acetic anhydride, and so in order to test its validity the data obtained in the previous study were re-analysed using the simpler model and the parameters obtained are compared to those obtained previously. Acetone is much simpler and has been studied before, so was not reinvestigated.

Before presenting the results of the pyrolysis experiments the structure of Meldrum's acid is reported as well as the results of the analysis of the data previously collected for acetic anyhydride.

6.3.1 Meldrum's Acid

Meldrum's acid, also known as 2,2-dimethyl-1,3-dioxane-4,6-dione, was first discovered by Andrew Norman Meldrum in 1908, and was initially misidentified as a β-lactone.[14] This initial misidentification was made due to Meldrum's acid's high pK_a, but the correct structure was later reached.[15] Meldrum's acid has since been the subject of structural studies using theoretical methods[16] and X-ray crystallography,[17] and is used in organic chemistry,[18,19] but has never been studied by GED before this work.

Experimental

Purified Meldrum's acid was obtained from Prof. Hamish McNab (Edinburgh, UK) and used directly in the experiment.

Theoretical Methods Calculations were performed at the MP2 level with the Pople-type basis sets (6-31G*[20–22] and 6-311G*[23,24]) and the correlation-consistent basis sets of Dunning.[25–29] The details of the geometry optimisations and frequency calculations are the same as given in previous chapters. The optimised structure of Meldrum's acid is shown in Figure 6.5.

Gas-phase electron diffraction (GED) measurements Data were collected for Meldrum's acid using the Edinburgh gas electron diffraction apparatus.[30] The data used in the refinement were collected at the long and medium nozzle-to-camera positions using the standard HT nozzle. At the temperatures required for data collection in the short position Meldrum's acid was found to decompose. Sample and nozzle temperatures were maintained at 363 and 373 K for the long and medium distances respectively. The nozzle-to-plate distances were 259.3 and 189.4 mm. All other details, including the programs[6,31] and scattering factors,[32] are the same as given in previous chapters, with all relevant experimental information given in Appendix 6 (Table A6.2).

Figure 6.5: Molecular structure of Meldrum's acid with atom numbering.

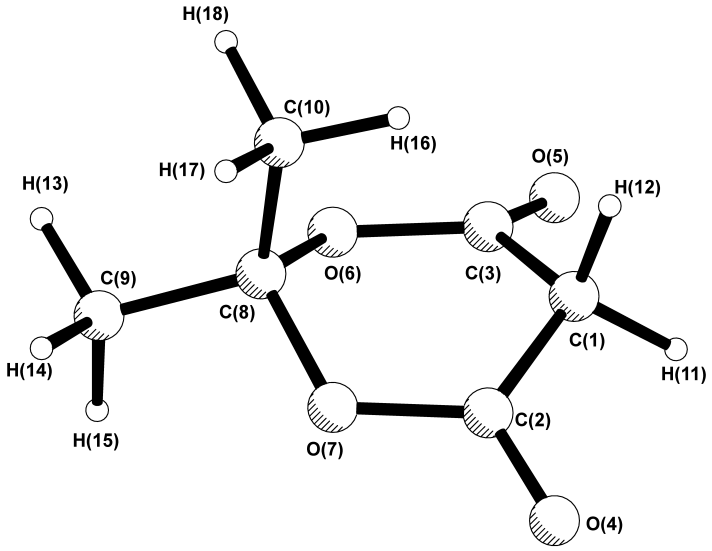

Results

***Ab initio* calculations** Both the previous X-ray[17] and theoretical studies[16] found Meldrum's acid to adopt a boat conformation. This behaviour was confirmed in this work, with a single PES minimum found corresponding to a boat conformation with C_s symmetry. Attempts to optimise a chair structure proved unsuccessful. The two CH_3 groups each have one H atom lying in the mirror plane [H(15) and H(16)] as shown in Figure 6.5.

The key structural parameters obtained for Meldrum's acid obtained at various levels of theory are given in Table 6.2 in the Discussion with full results in the Appendix (Table A6.1).

Gas electron diffraction refinement On the basis of the *ab initio* calculations described above, electron-diffraction refinements were carried out using a model with appropriate C_s symmetry.

The ring was modelled using C_s symmetry and the decision was taken to define the ring using two angles and all three unique distances. As the three unique C–C distances and the two unique C–O distances were all close to one another, and

likely to lie under the same peak in the RDC, the average and four differences were used. The average (p_1) was given by r_{av} = [rC(1)–C(2) + rC(8)–C(9) + rC(8)–C(10) + rC(2)–O(7) + rC(8)–O(7)] / 5 whilst the differences used were defined as r_{dif1} = rC(8)–C(10) - rC(8)–C(9) (p_2), r_{dif2} = rC(8)–C(10) - rC(1)–C(2) (p_3), r_{dif3} = rC(8)–C(10) - rC(8)–O(7) (p_6) and r_{dif4} = rC(8)–C(10) - rC(2)–O(7) (p_7). The other bond distances used were a single value for all rC–H (p_4), and rC(2)=O(4) (p_5).

The geometry of the ring was defined using ∠C(2)–C(1)–C(3) (p_8) and ∠O(6)–C(8)–O(7) (p_9) by creating one triangle consisting of C(1), C(2) and C(3) and a second containing O(6), O(7) and C(8) before moving them apart the required distance, calculated using the bond distances. These triangles were then bent out of planarity, to create the boat-like conformation, using one angle to tilt the C(1) atom (p_{10}) and another to tilt C(8) (p_{11}).

O(4) and O(5) were placed using ∠O(7)–C(2)=O(4) and ϕC(8)–O(7)–C(2)=O(4). H(11) and H(12) were placed using the H(11)-C(1)-H(12) angle (p_{12}).

The two methyl groups on C(8) were placed using the C(9)–C(8)–C(10) angle (p_{15}) and another angle to define the tilt out of the triangular plane defined by the O(6), O(7) and C(8) atoms (p_{18}). The C–C–H angles were generally close to one another with the exception of C–C–H(16), which deviated by around 2°, and so the other five positions were described by one parameter (p_{16}), and the unique nature of C–C–H(16) was included using a difference (p_{17}) between it and p_{16}.

The starting parameters for the $r_{a3,1}$ refinement[33] were taken from the theoretical geometry optimised at the MP2/6-311++G** level. A theoretical Cartesian cubic force field was obtained at the RHF/6-31G* level and converted into a force field described by a set of symmetry coordinates using the SHRINK program,[33] which generated both the amplitudes of vibration (u_{h1}) and the anharmonic corrections ($k_{a3,1}$). A discussion of the nomenclature used to describe the $r_{a3,1}$ structure has been previously published.[34] All eighteen geometric parameters and twelve groups of vibrational amplitudes were then refined. Flexible restraints were employed during the refinement using the SARACEN method.[35–37] Altogether, thirteen geometric restraints (Table 6.1) and nine amplitude restraints (Table A2.6) were

Table 6.1: Refined and calculated geometric parameters for Meldrum's acid (distances in pm and angles in °) from the GED refinement.[a,b]

	Parameter	MP2/ 6-311++G**	SARACEN ($r_{a3,1}$)	Restraint
Independent parameters				
p_1	rC–O/C–C_{av}	146.9	147.1(2)	—
p_2	rC–O/C–C_{dif1}	1.0	1.1(2)	1.0(2)
p_3	rC–O/C–C_{dif2}	0.6	0.6(2)	0.7(2)
p_4	rC–H	109.3	108.1(10)	—
p_5	rC=O	120.4	119.7(8)	—
p_6	rC–O/C–C_{dif3}	8.7	6.9(8)	8.7(10)
p_7	rC–O/C–C_{dif4}	15.9	14.5(8)	15.9(10)
p_8	∠C(2)–C(1)–C(3)	115.2	116.1(5)	115.2(5)
p_9	∠O(6)–C(8)–O(7)	111.4	112.2(5)	111.4(5)
p_{10}	O(6)–C(8)–$O(7)_{tilt}$	22.4	19.0(17)	22.4(20)
p_{11}	C(2)–C(1)–$C(3)_{tilt}$	46.5	41.7(20)	—
p_{12}	∠H–C(1)–H	106.8	106.7(11)	106.8(10)
p_{13}	∠O(7)–C(2)=O(4)	120.4	121.7(7)	120.4(10)
p_{14}	ϕC(8)–O(7)–C(2)=O(4)	169.9	175.4(11)	169.9(20)
p_{15}	∠C(9)–C(8)–C(10)	112.9	112.5(9)	112.9(10)
p_{16}	∠C–C–H_{av}	109.4	109.5(9)	109.4(10)
p_{17}	∠C–C–$H(16)_{dif}$	2.7	2.5(11)	2.7(10)
p_{18}	$(CH_3)_{2\ tilt}$	5.0	1.3(11)	5.0(15)
Dependent parameters				
dp_1	rC(8)–C(10)	151.9	151.7(4)	—
dp_2	rC(8)–O(7)	143.6	144.8(5)	—
dp_3	rC(2)–O(7)	136.1	137.3(7)	—
dp_4	rC(8)–C(9)	151.0	150.7(5)	—
dp_5	rC(1)–C(2)	151.4	151.1(5)	—
dp_6	∠C(1)–C(2)–O(7)	115.8	116.8(5)	—
dp_7	∠C(2)–O(7)–C(8)	118.8	117.6(9)	—
dp_8	ϕC(8)–O(7)–C(2)–C(1)	11.8	13.7(16)	—
dp_9	∠C–C–H(16)–C(1)	112.1	112.0(14)	—

[a] Figures in parentheses are the estimated standard deviation of the last digits.

[b] See text for parameter definitions.

employed. The success of the final refinement, for which $R_G = 0.088$ ($R_D = 0.072$), can be assessed on the basis of the radial-distribution curve (Figure 6.6) and the molecular-scattering intensity curves (Figure A6.1). Final refined parameters are listed in Table 6.1. Appendix 6 contains the interatomic distances and the corresponding amplitudes of vibration (Table A6.3), with the least-squares

Figure 6.6: Experimental and difference (experimental – theoretical) radial-distribution curves, $P(r)/r$, for Meldrum's acid. Before Fourier inversion the data were multiplied by $s.\exp(-0.00002s^2)/(Z_C - f_C)(Z_O - f_O)$.

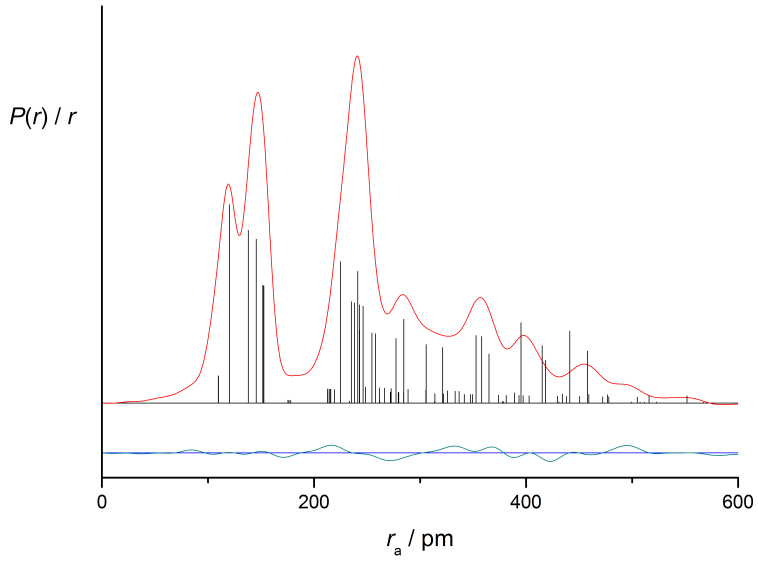

correlation matrix (Table A6.4) and the experimental coordinates from the GED analysis (Table A6.5).

Discussion

The key parameters for Meldrum's acid obtained from *ab initio* calculations at the MP2/6-311++G** level, the MP2/aug-cc-pvTZ level, this GED study and a previous X-ray crystallographic study[17] are given in Table 6.2. The X-ray study, for which $Z = 8$, did not produce a molecule with C_s symmetry, presumably due to the packing effects, and so averages are given where required.

Throughout the range of calculations conducted no large deviations in the theoretical structure were found and, with the exception of the calculations using the smallest basis sets, bond lengths tend to range over no more than 1 pm, and bond angles by no more than 1°.

The structure of Meldrum's acid was refined using data collected at the long and medium camera positions. Data collected at the short position required

Table 6.2: Selected structural parameters for lowest energy structure of Meldrum's acid.[a]

Parameter	MP2/ 6-311++G**	MP2/ aug-cc-pVTZ	This study	X-ray[b]
rC(10)–C(8)	152.1	151.6	151.7(4)	150.4(6)
rC(8)–C(9)	151.1	150.7	150.7(5)	150.4(6)
rC(8)–O(6)	143.4	143.3	144.8(5)	144.4(4)
rO(6)–C(3)	136.2	135.9	137.3(7)	135.2(4)
rC(3)=O(5)	120.4	120.3	119.7(8)	119.3(4)
rC(3)–C(1)	151.5	150.8	151.1(4)	149.4(5)
∠C(9)–C(8)–C(10)	112.9	112.7	112.5(9)	113.7(3)[c]
∠O(6)-C(8)-O(7)	111.4	111.5	112.2(5)	110.2(3)[c]
∠O(6)-C(3)-C(1)	115.8	115.8	116.8(5)	116.3(3)[c]
∠C(8)-O(6)-C(3)	118.8	119.1	117.6(9)	120.2(3)[c]
∠C(3)-C(1)-C(2)	115.2	115.0	116.1(5)	114.8(3)[c]
∠O(5)=C(3)-O(6)	120.4	120.3	121.7(7)	118.9(3)[c]
ϕC(8)-O(6)-C(3)-C(1)	-11.8	-10.2	-13.7(16)	—[d]
ϕC(8)-O(6)-C(3)=O(5)	169.9	171.4	175.4(11)	—[d]

[a] Bond distances in pm and angles in °.
[b] For details see original paper.[17] The crystal structure did not possess C_s symmetry so average parameters are given.
[c] The error on the bond angle was estimated.
[d] This parameter was not reported.

heating by an additional 20 K and, at this increased temperature, the compound decomposed to form an unidentified gas and a brown residue. Data collected at the short position presumably contained a mixture of Meldrum's acid and decomposition products, and did not fit the model of Meldrum's acid. Whilst the difference curve in Figure 6.6 is not as flat as those for some refinements presented in this thesis, it is consistent with what is expected for a complex molecule containing lots of similar distances, and the data collected at the medium and long positions show no obvious sign of decomposition.

As would be expected for such a ring system the RDC shows the presence of a large number of similar bonded and non-bonded distances and as such the refinement relied heavily on restraints applied using the SARACEN method.[35–37] The experimental bonded distances are generally close to those calculated *ab initio*, with most lying within 1–2σ of the values calculated at the MP2/6-311++G** level. The three C–C distances show good agreement; for example,

the experimental rC(3)–C(1) of 151.1(4) pm lies between the 6-311++G** and aug-cc-pVTZ values of 151.5 pm and 150.8 pm respectively. The worst agreement is for rC(8)–O(6) which, being 144.8(5) pm by experiment, is a little longer than the MP2/6-311++G** value of 143.4 pm suggests.

The geometry of the ring was described using two angles and three bond lengths. Ideally only the difference between the two bond angles would have been restrained, but when this technique was attempted the two bond angles refined to unreasonably large angles, and so each angle required a restraint. This is probably caused by the fact that there are so many heavy-atom non-bonded distances in the molecule; in addition to the ring system there are two more C atoms and two more O atoms that give rise to similar non-bonded distances. The final ring bond angles all lie without about 2σ of the theoretical values.

Of the non-ring bond angles the experimental and theoretical values for $\angle$C(9)–C(8)–C(10) agree closely but the positions of O(4) and O(5) seem to be less well determined, with the experimental values for $\angle$O(5)=C(3)–O(6) and ϕC(8)–O(6)–C(3)=O(5) both showing deviation from those calculated *ab initio*. The experimental $\angle$O(5)=C(3)–O(6) of 121.7(7)° is 2σ larger than the calculation with the 6-311++G** basis set suggests, whilst ϕC(8)–O(6)–C(3)=O(5) of 175.4(11) ° is around 4σ from the calculated values despite being restrained.

The boat structure of Meldrum's acid is similar in both the experimental structure and the calculations, with one of the two *tilt* parameters being refined without restraint, offering good experimental evidence for this conformation.

The gas-phase structure is only roughly comparable to the X-ray structure. The bond distances tend to agree within the quoted e.s.d.s, with the main exceptions being rO(6)–C(3), which is 5σ shorter in the crystal, and rC(3)–C(1), which was 3σ shorter in the crystal. A few of the bond angles also show significant deviations, but the estimated error of 0.3° on all the crystallographic bond angles is probably excessively optimistic. Given that the crystal structure has no molecular symmetry it seems likely that the intermolecular interactions between molecules in the crystal are important, and therefore, makes comparison of the gas phase and solid-state structures impossible.

Conclusion

The structure of Meldrum's acid has been studied by GED for the first time. Meldrum's acid was found to adopt a boat structure in agreement with previous studies. The experimental structural parameters are generally comparable to those calculated *ab initio* with some key experimental parameters being rC(3)=O(5) = 119.7(8) pm, rO(6)–C(3) = 144.8(5) pm, rC(10)–C(8) = 151.7(4) pm and rC(8)–C(9) = 150.7(5) pm.

6.3.2 Acetic anhydride

Acetic anhydride [$(CH_3CO)_2O$] is widely used in organic synthesis, and has previously been the subject of an intensive study combining GED and IR spectroscopy.[38] Due to the relatively low barrier to rotation around the central C–O–C=O dihedral angles, the previous GED study used a dynamic model consisting of a number of pseudoconformers at different points on the PES. Such a model, whilst a good way to model large amplitude motions, is complex, and is not suitable for use in a multi-fragment model that will be required to model the decomposition products of pyrolysis. Therefore it was decided that a simpler model was required, and to ensure that such a model was suitable, the original data would be refined using the new model and the impact on the structural parameters assessed. As this structure has already been studied the results presented here are kept brief.

There are two PES minima of acetic anhydride. Both are non-planar and, as is standard in the literature, are labelled (*sp*, *sp*) and (*sp*, *ac*). The two conformers, with atom numbering, are shown in Figure 6.7.

In place of the previous dynamic model, a two-conformer model was constructed in the usual way using a total of 23 parameters. Although this is more parameters than used in the original study, the previous study did not use the SARACEN method[35–37] and as such the methodology used is quite different. The RDC for

Figure 6.7: Molecular structures of the two PES minima of acetic anhydride.

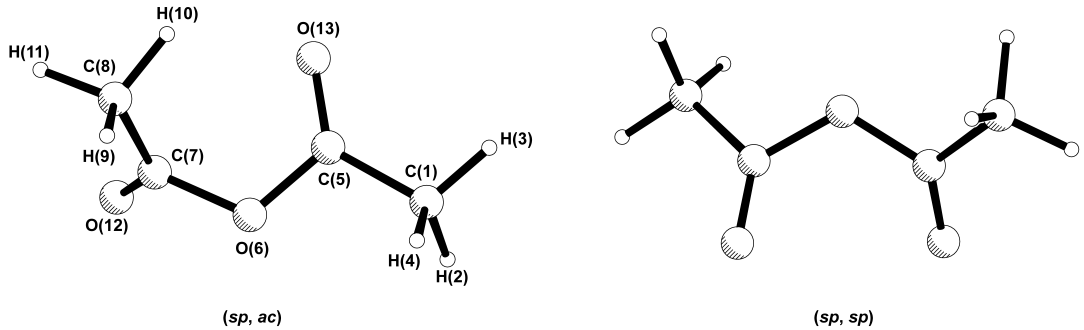

Figure 6.8: Experimental and difference (experimental – theoretical) radial-distribution curves, $P(r)/r$, for acetic anhydride. Before Fourier inversion the data were multiplied by $s.\exp(-0.00002s^2)/(Z_C - f_C)(Z_O - f_O)$.

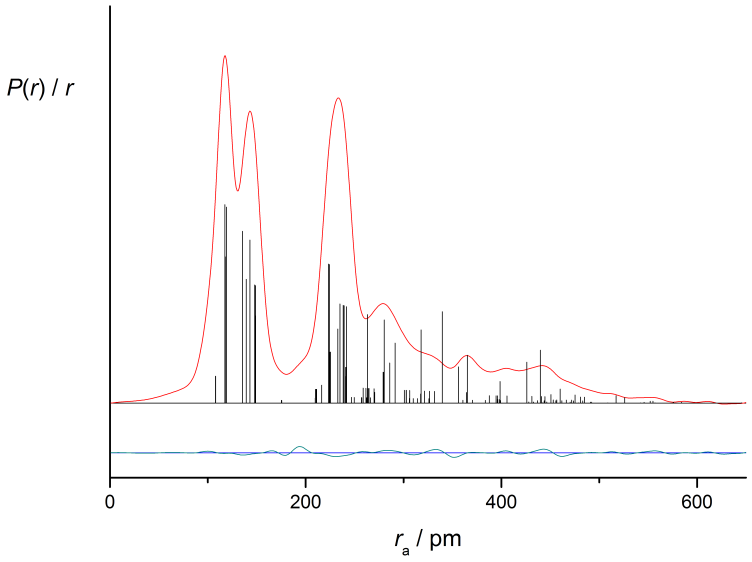

this refinement is shown in Figure 6.8. Structural parameters for the (*sp*, *ac*) conformer obtained from this new refinement are shown alongside those from the previous refinement in Table 6.3, as are those obtained at the MP2/6-311++G** level. Full details of all the calculations performed and information about this refinement are given in Appendix 6 as follows: *ab initio* parameters (Table A6.6), nozzle-to-plate distances, weighting functions, *etc.* (Table A6.7), refined parameters (Table A6.8), interatomic distances and amplitudes of vibration (Table A6.9), correlation matrix (Table A6.10), experimental coordinates (Table A6.11), molecular intensity curves (Figure A6.2), ratio of (*sp*, *ac*) vs. *R*-factor (Figure A6.3).

It can be seen that the new refinement produces parameters that are, in most cases, comparable to those obtained in the previous study. Some of the new bond lengths are a little shorter than those from the previous study. For example, rC(7)=O(12) is now 117.5(2) pm compared with 118.2(3) pm in the previous refinement, but the new refinement is more detailed, for example treating all the C–C distances uniquely whilst the previous study did not. Where structural

Table 6.3: Selected structural parameters for the (*sp*, *ac*) conformation of acetic anhydride.[a]

Parameter	MP2/ 6-311++G**	Previous study[38]	This study
rC(1)–C(5)	150.3	148.9(2)	148.9(14)
rC(5)=O(13)	120.9	119.4(3)	118.9(2)
rC(5)–O(6)	136.8	137.0(13)	135.7(5)
rO(6)–C(7)	143.0	140.6(6)	143.1(7)
rC(7)=O(12)	119.4	118.2(3)	117.5(2)
rC(7)–C(8)	149.8	148.9(2)	147.9(9)
∠O(6)–C(5)=O(13)	122.8	117.1(10)	123.0(7)
∠O(6)–C(7)=O(12)	119.2	124.2(18)	118.4(8)
∠C(5)–O(6)–C(7)	115.1	121.0(15)	115.6(8)
∠O(6)–C(5)–C(1)	110.4	110.9(17)	111.4(9)
∠O(6)–C(7)–C(8)	112.5	111.1(22)	112.6(9)
ϕO(12)=C(7)–O(6)–C(5)	104.2	122.0(39)	118.5(30)
ϕO(13)=C(5)–O(6)–C(7)	-0.3	-27.4(53)	0.0[b]
% (*sp*, *sp*)	58.0	37.0(150)	27.0(30)

[a] Bond distances in pm and angles in °.
[b] Fixed.

parameters deviate by a larger amount it is generally the case that the current refinement is closer to the *ab initio* value, reflecting of the fact that the new refinement uses the SARACEN method. Examples of this include ∠C(5)–O(6)–C(7) which in the previous study was around 6°, or 4σ, larger than the *ab initio* calculations suggest. The angles ∠O(6)–C(5)=O(13) and ∠O(6)–C(7)=O(12) also show a similarly poor agreement. Of course, it must be remembered that a GED experiment does not need to agree with theory, but for such a simple molecule these large differences are unlikely. Whilst the previous study is probably the best that can be achieved without the SARACEN method, the differences highlight the benefits that modern refinement techniques offer.

The optimal model for acetic anhydride would combine the previous dynamic model with the SARACEN method. However these results show that the simpler model is suited for the study of acetic anhydride in the multi-component vapour expected from pyrolysis.

6.3.3 Pyrolysis of Meldrum's Acid

The pyrolysis of Meldrum's acid and its derivatives to form CO_2, acetone and ketene derivatives has been studied extensively.[39] Much work in this area has been conducted by Prof. Hamish McNab (University of Edinburgh) and so it was after discussion with Prof. McNab that Meldrum's acid was used as a precursor to study ketene.[39–41] This precursor is the most interesting because substituted Meldrum's acid derivatives can be used to produce substituted ketenes.

The proposed mechanism for the decomposition of Meldrum's acid is shown in Figure 6.9.[39,41]

Figure 6.9: The mechanism of the thermal decomposition of Meldrum's acid.

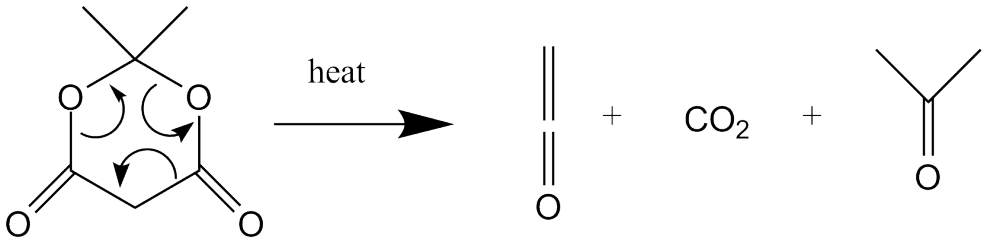

Experimental

In order to assess the temperature dependence of pyrolysis, two different pyrolysis temperatures were attempted. The lower temperature used the standard high-temperature nozzle to overheat the sample to 500 K at the nozzle tip whilst the higher temperature, 770 K, was obtained using the VHT nozzle and Scheme C described in Figure 6.1.

However, difficulties were experienced during the higher temperature experiments. During the normal GED study of Meldrum's acid it was found that the sample decomposed if heated much above 373 K and it was clear from the brown residue remaining that this decomposition was not producing the same products as would be obtained *via* pyrolysis (as neither acetone, ketene or CO_2 are brown or solid under these conditions). The standard high-temperature nozzle

and inlet system afford fine control over the temperatures used, whereas a much more coarse level of control is available when vaporising a sample in the MT oven in the VHT nozzle. As the VHT nozzle lacks any form of valves, the sample was slowly heated until the background pressure and measured scattering intensity was at the desired level. Due to the construction of the oven and the positioning of the thermocouples it is anticipated that the recorded temperature in the MT oven is accurate to around 20 K. Whilst the recorded temperature in the MT oven was at all times lower than the temperature that Meldrum's acid was found to decompose, after the experiment had finished a brown residue was found in the MT oven, suggesting decomposition had occurred. For a successful experiment it was important that it is Meldrum's acid, and not some unknown decomposition products, which reaches the pyrolysis zone.

Despite these problems a dataset was collected and data analysis attempted.

Results

The refinement of the data collected with an overheated nozzle tip temperature of 500 K did not show any significant deviation from the standard structure obtained in the previous section. The refinements detailed therefore relate to the dataset obtained at 770 K.

The refinement was carried out using a model containing Meldrum's acid, acetone, carbon dioxide and ketene. It was obvious from a trial refinement that decomposition had occurred - the fit with 100% of Meldrum's acid was terrible, with a distinct lack of longer bonded distances (C–C and C–O as opposed to C=C and C=O). This is to be expected if Meldrum's acid had decomposed, as it contains eight C–C or C–O distances whereas the expected decomposition products contain only two.

Initially the ratio of decomposition was altered, varying the amounts of Meldrum's acid compared to the anticipated decomposition products, with the minimum R factor found at around 82% decomposition. However, at this level of decomposition the quality of fit was still worse than would be anticipated and the

average distances in the molecule refined to unreasonable values. This suggested that the model contained the wrong species, but as no nozzle-to-camera distance calibration was possible, the problem could be even more complex.

At this point a series of refinements were undertaken. The first ignored potential nozzle-to-camera distance problems and restrained the structure of Meldrum's acid to the values obtained in the previous section and then refined the parameters relating to ketene, carbon dioxide and acetone. The resultant RDC, shown in Figure 6.10, with a resultant $R_G = 28\%$ and 82% decomposition shows clear disagreement in the bonded region, suggesting that the model contains different species to the experimental data.

However, in order to rule out the possibility that it was an incorrect nozzle-to-camera distance that was at fault a second refinement was carried out, where the two average distances for the two main bonded peaks were refined freely. If the nozzle-to-camera distance were causing problems it would be expected that both distances would scale to be longer or shorter by a similar percentage. However, the longer peak refined from 146.3 pm to 141.9 pm, a shrinkage of 3%, whilst the shorter peak increased in length from 118.6 pm to 118.9 pm. These inconsistencies do not rule out the nozzle-to-camera distance being incorrect, but it is unlikely that it is the major cause of error in this experiment.

In a final attempt to make sense of the data a refinement was carried out whereby the ratios of the amounts of each of the four decomposition products were varied separately. This has some physical basis, as it is plausible that if some acetone is produced by pyrolysis, it is itself pyrolysed to ketene and methane, as described later in this chapter. However, refining these ratios separately did not offer a significantly improved fit and so this method was abandoned.

Conclusion

It is clear from the experiment that pyrolysis has occurred but that it does not produce the anticipated species. It is impossible to know if the sample of Meldrum's acid is decomposing on initial vaporisation, or if the FVP conditions

Figure 6.10: Experimental and difference (experimental – theoretical) radial-distribution curves, $P(r)/r$, for the decomposition products of Meldrum's acid. The ratio of Meldrum's acid to the decomposition products was fixed to the stoichiometry of the reaction. Before Fourier inversion the data were multiplied by $s.\exp(-0.00002s^2)/(Z_C - f_C)(Z_O - f_O)$.

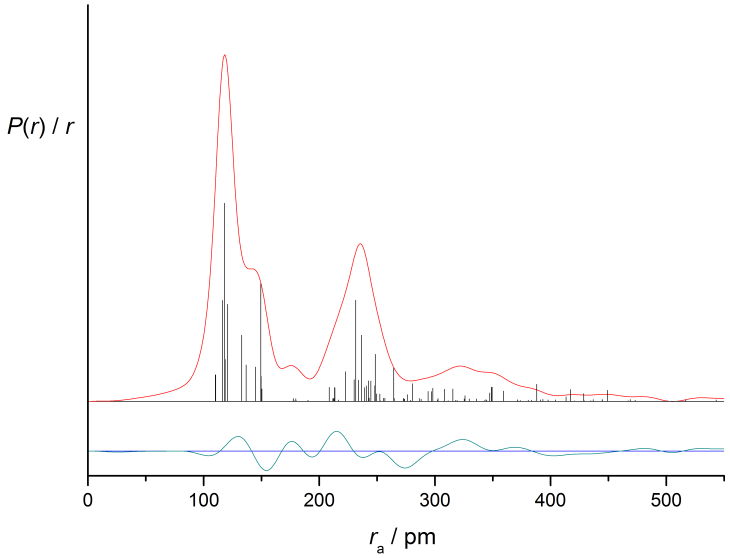

present in the oven lead to a different decomposition route. What is clear is that the sensitivity of the pyrolysis of Meldrum's acid, along with an inability to calibrate the nozzle-to-camera distance using this particular VHT nozzle configuration, make the study of ketene using Meldrum's acid unattractive. The study of larger, substituted ketenes generated from derivatives of Meldrum's acid is probably beyond the scope of the current experimental set-up present in Edinburgh. Possible enhancements to rectify this will be discussed in the final chapter.

6.3.4 Pyrolysis of acetic anhydride

Having studied Meldrum's acid and found the data impossible to analyse it was obvious that for such an experiment be successful a system with a simpler, cleaner decomposition route was required. Further discussion with Prof. McNab led to the study of acetic anhydride, which is expected to pyrolyse to form acetic acid and ketene in a good yield.[42] Two previous studies suggest the decomposition mechanism to be an intramolecular rearrangement,[43,44] with the most obvious route involving one of the methyl H atoms moving to the central O and subsequent breaking of the C–O bond.

Experimental

Acetic anhydride (>99 %) was obtained from Sigma Aldrich and was pyrolysed using the VHT nozzle described earlier in this chapter. The sample was attached to the room-temperature inlet and passed into the VHT oven (Scheme B, Figure 6.1). It was during this experiment that the drop in vapour pressure with increasing VHT oven temperature was first encountered (see Section 6.2.5). Acetic anhydride has a vapour pressure of 1 mmHg at 272 K,[45] sufficient for study by GED, but with a pyrolysis temperature of 823 K the amount of scattering was much smaller than expected, although data were still obtained using a long exposure time. During subsequent tests it was found that the scattering intensity dropped roughly linearly with the temperature. A second dataset, with stronger scattering, was collected at a lower pyrolysis temperature of 673 K. When these data were analysed the refinement suggested that around 20% of the resultant stream was unreacted acetic anhydride. Whilst a refinement could be conducted using these data the films collected at 823 K proved suitable for data analysis, and so the analysis presented uses these data. Information about the data used (including the nozzle-to-camera distance, correlation parameters, *etc.*) are given in the Appendix in Table A6.14. Calibration of the nozzle-to-camera distance using benzene was performed for this experiment.

Results

***Ab initio* calculations** The key structural parameters obtained for acetic acid and ketene are given in the Discussion in Table 6.5 with full results in the Appendix in Tables A6.12 and A6.13 along with the atomic numbering scheme (Figure A6.4).

Gas electron diffraction refinement Due to the lower vapour pressure at the higher temperature the films obtained were fainter, but when data were extracted they still offered reasonable quality MICs. A trial refinement with the model including the two conformers of acetic anhydride, acetic acid and ketene gave the best R factor when only 2(5)% of the vapour was acetic anhydride (see Figure A6.5) and so in the final refinement the small amount of acetic anhydride was ignored and the refinement proceeded using a model containing only acetic acid and ketene, reducing the number of parameters required to 13. As this dataset offers one of the best examples of FVP–GED, the refinement is presented in full.

The final model contained only ketene (C_{2v} symmetry) and acetic acid (C_s symmetry). The C–C, C=C, C–O and C=O bonds in acetic acid and ketene combine to form a single peak in the bonded region of the RDC, and so the average and four differences were required to describe the heavy-atom bonded distances. They were defined as r_{av} = (rC=C_{ket} + rC=O_{ket} + rC–C_{AcOH} + rC–O_{AcOH} + rC=O_{AcOH}) / 5 (p_1), r_{dif1} = rC–C_{AcOH} - rC–O_{AcOH} (p_2), r_{dif2} = rC–C_{AcOH} - rC=O_{AcOH} (p_3), r_{dif3} = rC–C_{AcOH} - rC=C_{ket} (p_4) and r_{dif4} = rC–C_{AcOH} - rC=O_{ket} (p_5). The other bond lengths used were a single value of rC–H (p_6) for both molecules and rO–H (p_7) for acetic acid. To complete the structure of acetic acid five bond angles were used. The methyl group was modelled as having local C_s symmetry and so ∠C–C–H (p_8) and ∠H–C–H (p_9) were used. The acetyl fragment was completed by using ∠C–C=O (p_{10}) to place the oxygen. The hydroxyl group was placed using ∠C–C–O (p_{11}) and ∠C–O–H (p_{12}). In accordance with the *ab initio* calculations a planar conformation of the hydroxyl group was assumed. Ketene required only one further parameter, ∠H–C–H (p_{13}). The abundance of each species was fixed at 0.5.

Table 6.4: Refined and calculated geometric parameters for the pyrolysis products of acetic anhydride (acetic acid and ketene) (distances in pm and angles in °) from the GED refinement.[a,b]

	Parameter	MP2/ 6-311++G**	SARACEN (r_{h1})	Restraint
Independent parameters				
p_1	rC–O/C–C_{av}	131.3	129.7(1)	—
p_2	rC–O/C–C_{dif1}	14.5	14.3(7)	14.5(8)
p_3	rC–O/C–C_{dif2}	29.4	31.0(20)	—
p_4	rC–O/C–C_{dif3}	18.2	17.8(7)	18.2(8)
p_5	rC–O/C–C_{dif4}	34.4	34.4(5)	34.4(5)
p_6	rC–H	108.0	108.4(7)	—
p_7	rO–H	96.8	97.0(9)	96.8(10)
p_8	∠H–C–C_{AcOH}	109.2	109.4(9)	109.2(10)
p_9	∠H–C–H_{AcOH}	109.4	109.5(10)	109.4(10)
p_{10}	∠C–C=O_{AcOH}	126.3	126.1(6)	—
p_{11}	∠C–C–O_{AcOH}	111.0	111.2(7)	—
p_{12}	∠C–O–H_{AcOH}	106.0	105.9(10)	106.0(10)
p_{13}	∠H–C–H_{Ket}	121.8	122.1(10)	121.8(10)
Dependent parameters				
dp_1	rC=C_{Ket}	132.2	131.3(11)	—
dp_2	rC=O_{Ket}	116.8	114.8(10)	—
dp_3	rC–C_{AcOH}	150.4	149.2(9)	—
dp_4	rC–O_{AcOH}	135.9	134.9(6)	—
dp_5	rC=O_{AcOH}	121.0	118.1(12)	—
dp_6	p_{10} - p_{11}	15.3	14.9(10)	15.3(10)

[a] Figures in parentheses are the estimated standard deviation of the last digits.
[b] See text for parameter definitions.

Results *Ab initio* calculations were also undertaken for ketene and acetic acid, with key parameters listed in Table 6.5 and full details in the Appendix in Tables A6.12 and A6.13.

The starting parameters for the r_{h1} refinement[33] were taken from the theoretical geometry optimised at the MP2/6-311++G** level. A theoretical Cartesian force field was obtained at this level and converted into a force field described by a set of symmetry coordinates using the SHRINK program,[33] which generated both the amplitudes of vibration (u_{h1}) and the corrections (k_{h1}). All thirteen geometric parameters and six groups of vibrational amplitudes were then refined. Flexible

Figure 6.11: Experimental and difference (experimental – theoretical) radial-distribution curves, $P(r)/r$, for the decomposition products of acetic anhydride. Before Fourier inversion the data were multiplied by $s.\exp(-0.00002s^2)/(Z_C - f_C)(Z_O - f_O)$.

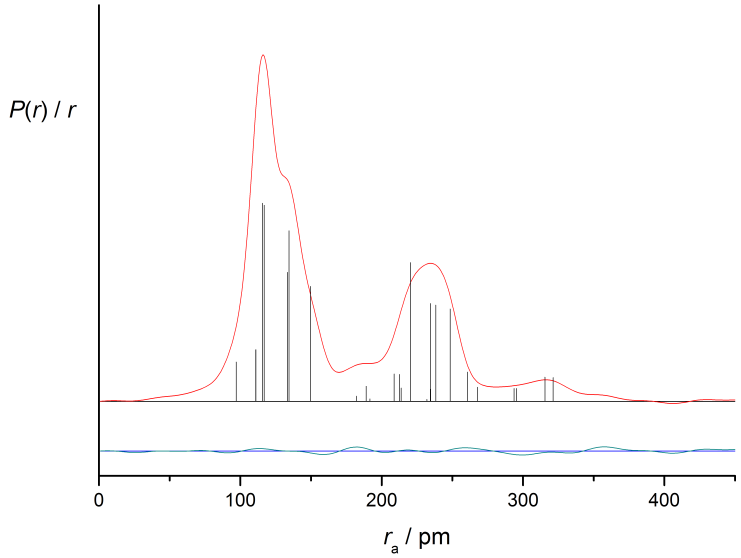

restraints were employed during the refinement using the SARACEN method.[35–37] Altogether, nine geometric restraints (Table 6.4) and five amplitude restraints (Table A6.15) were employed. The success of the final refinement, for which $R_G = 0.087$ ($R_D = 0.048$), can be assessed on the basis of the radial-distribution curve (Figure 6.11) and the molecular-scattering intensity curves (Figure A6.6). Final refined parameters are listed in Table 6.4. Appendix 6 contains the interatomic distances and the corresponding amplitudes of vibration (Table A6.15), with the least-squares correlation matrix (Table A6.16) and the experimental coordinates from the GED analysis (Table A6.17).

Discussion A selection of parameters from this GED study, previous studies[9,46–48] and *ab initio* calculations is shown in Table 6.5.

For the refinement to be valid it is important that the refined structures of both ketene and acetic acid are consistent with those found previously. In general this is the case, but, the e.s.d.s on the bond lengths are understandably quite large

Table 6.5: Selected structural parameters for lowest energy structures of ketene and acetic acid[a]

Parameter	MP2/6-311++G**	Prev. GED[9,46]	Prev. MW[47,48]	This study
Ketene				
rC=C	132.2	130.0(20)	131.4[b]	131.3(11)
rC=O	116.8	116.0(20)	116.1[b]	114.8(10)
rC–H	108.0	107.0(20)[c]	108.3[b]	108.4(7)
∠H–C–H	121.8	117.5(125)[c]	122.4[b]	122.1(10)
Acetic acid				
rC–C	150.4	152.0(5)	149.4(10)	149.2(9)
rC–H_{av}	109.1	110.2(10)	110.2(12)	108.4(7)
rC–O	135.9	136.4(3)	135.7(5)	134.9(6)
rC=O	121.0	121.4(3)	120.9(6)	118.1(12)
rO–H	96.8	97.0[c]	97.0(3)	97.0(9)
∠C–C=O	126.3	126.6(6)	126.2(7)	126.1(6)
∠C–C–O	111.0	110.6(6)	112.0(6)	111.2(7)
∠C–O–H	106.0	107.0[c]	105.9(5)	105.9(10)

[a] Bond distances in pm and angles in °.
[b] No e.s.d.s were quoted.
[c] This parameter was assumed.

owing to the increased amount of peak overlap in the RDC.

The structure of ketene obtained entirely from the GED experiment is effectively limited to rC=C and rC=O; even a pure sample would probably require restraints on rC–H and ∠H–C–H. The structural parameters obtained for these two distances are consistent with the previous GED experiment, although rC=O of 114.8(10) pm is probably too short, being 2 pm (and 2σ) shorter than the MP2 calculations suggest. The bond length rC=C, at 131.3(11) pm, is consistent with the value obtained from MW spectroscopy and that calculated at the MP2/6-311++G** level. The other two parameters, rC–H and ∠H–C–H, were directly restrained and were therefore close to the values obtained at the MP2/6-311++G** level.

The parameters obtained for acetic anhydride show a similar level of agreement. The distance rC–C is found to be 149.2(9) pm, which is just over 1σ shorter than the MP2/6-311++G** level suggests, but consistent with the previous MW study. rC–O and rC=O are found to be shorter by around 2σ than the other methods suggest.

The two heavy-atom bond angles, ∠C–C=O and ∠C–C–O, in acetic acid were both refined independently whilst the difference between them was restrained to the difference found at the MP2/6-311++G** level. The resulting values lie very close to the values found by calculations.

It is clear from the comparison with the structure obtained using other methods that the precision, and probably the accuracy, is reduced compared to a standard GED experiment. There are many potential reasons for this. Whilst the analysis of the data collected indicated only a very small amount of acetic anhydride, it does not rule out the presence of other species in the vapour. The reasonably good fit shown in the RDC (Figure 6.11) and the general level of agreement of the structural parameters appear to rule out major impurities, but not the presence of minor impurities, which could affect the structural parameters obtained. Without an independent analysis of the make-up of the pyrolysed vapour, such as that offered by a mass spectrometer, drawing conclusions is difficult.

All the heavy-atom bond lengths are found to be a little shorter than would be expected. As the nozzle-to-camera distance was calibrated it is unlikely that this is the cause of the problem, and so this result could suggest a systematic error. Without further study it is difficult to narrow down the possible sources of error, with possible explanations including the presence of an unknown impurity with shorter bond lengths or some problem with the vibrational corrections used owing to the high temperatures.

It is therefore not clear if the parameters obtained represent a limitation of the technique, insomuch that it will always be difficult to study multiple species with similar distances, or if optimising the pyrolysis conditions could result in a purer vapour and therefore better agreement. However, if the problem were simply due to peak overlap it would be anticipated that the three parameters relating to the bonded distance differences, which are restrained, would refine to a value much closer to the applied restraint.

Conclusion

The data collected suggest almost complete dissociation of acetic anhydride to acetic acid and ketene. The refinement of the data is successful, although the parameters obtained are generally less accurate than would be anticipated from a standard GED experiment.

6.3.5 Pyrolysis of acetone

The decomposition of acetone to form ketene and methane is a process used in industry and is widely reported in the literature.[49] Although it was not anticipated to offer as high a yield of ketene as acetic anhydride it was felt worthwhile to investigate another possible route to ketene. It is unclear from the literature if the mechanism of decomposition is *via* intramolecular rearrangement or a radical mechanism. Two early studies offered differing views[50,51] but a more recent study concluded that the process was consistent with a Rice-Herzfeld free radical mechanism.[52]

Experimental

Acetone (obtained from Sigma Aldrich, >99%) was studied using the same experimental set-up as acetic anhydride, with a VHT oven temperature of 820 K. A model was created containing acetone, methane and ketene, using a total of nine parameters.

Results

A reasonable fit to the data was achieved. However, only a small amount of the material had undergone pyrolysis, with the refinement indicating that the mole fraction of acetone in the vapour was 0.63(2). The RDC is shown in Figure 6.12 for which $R_{\mathrm{G}} = 0.123$ ($R_{\mathrm{D}} = 0.050$). Key structural parameters obtained are listed in Table 6.6, with further details presented in Appendix 6 [theoretical structural parameters for acetone (Table A6.18), atomic labelling for acetone (Figure A6.7), nozzle-to-plate distances, weighting functions, *etc.* (Table A6.19), refined parameters (Table A6.20), interatomic distances and amplitudes of vibration (Table A6.21), correlation matrix (Table A6.22), experimental GED coordinates (Table A6.23), molecular intensity curve (Figure A6.8) and plot of R factor *vs* decomposition (Figure A6.9)].

Figure 6.12: Experimental and difference (experimental – theoretical) radial-distribution curves, $P(r)/r$, for the decomposition products of acetone. Before Fourier inversion the data were multiplied by $s.\exp(-0.00002s^2)/(Z_C - f_C)(Z_O - f_O)$.

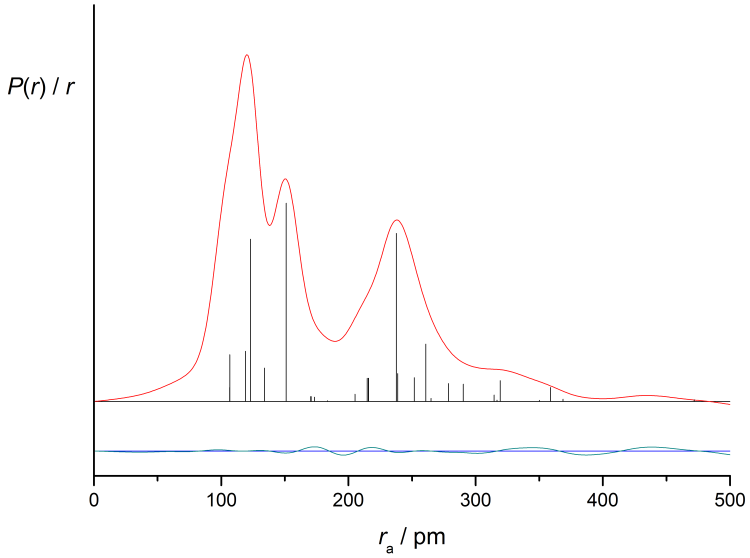

Discussion

The key results from this study, a previous GED study,[53] and a previous MW study[54] are given in Table 6.6.

Table 6.6: Selected structural parameters for lowest energy structures of ketene and acetone.[a]

Parameter	MP2/6-311++G**	Prev. GED[9,53]	Prev. MW[47,54]	This study
Ketene				
rC=C	132.2	130.0(20)	131.4[b]	134.1(7)
rC=O	116.8	116.0(20)	116.1[b]	119.1(9)
rC–H	108.0	107.0(20)[c]	108.3[b]	106.9(5)
∠H–C–H	121.8	117.5(125)[c]	122.4[b]	121.8(10)
Acetone				
rC–C	151.6	151.6(4)	150.7[b]	151.3(3)
rC=O	122.0	121.1(4)	122.2[b]	123.0(4)
∠C–C=O	122.0	—[d]	121.4[b]	120.2(3)

[a] Bond distances in pm and angles in °.
[b] No e.s.d.s were quoted.
[c] This parameter was assumed.
[d] This parameter was not reported.

It can be seen that, with the exception of ∠C–C=O, the parameters derived for acetone are consistent with those found previously. The parameters obtained for ketene are less accurate, with the two key bond lengths being longer than those predicted at the MP2/6-311++G** level by 2-3σ. Given that the refinement suggests the mole fraction of ketene in the vapour is only 0.19, it is unsurprising that the structural parameters are not more accurate.

6.4 Conclusion

A new VHT nozzle, designed to allow FVP experiments in conjunction with GED, has been developed for use in Edinburgh. Initial calibration and testing found that light emitted by the very hot pyrolysis oven caused fogging of the photographic film. Initial work was also limited by the inability to calibrate the nozzle-to-camera distance accurately and, although upgrades were made to overcome this, they came too late to help with the study of the generation of ketene, which was undertaken as an initial test project.

Three pyrolysis routes were chosen, which all generated ketene along with other by-products. The three routes were the pyrolysis of Meldrum's acid to form ketene, acetone and carbon dioxide, the pyrolysis of acetic anhydride to form ketene and acetic acid, and the pyrolysis of acetone to form methane and ketene.

The structure of Meldrum's acid had not been studied before using GED and so this molecule was analysed using the standard GED equipment. The resulting structure is generally comparable to those obtained using theoretical calculations but comparison to a previous crystal structure reveals differences between the gas phase and solid state. Acetic anhydride had been studied previously but the refinement used a dynamic model which is too complex for use in a multi-species pyrolysis refinement. The original data were therefore re-analysed using a static model with the SARACEN method and offered comparable results.

The new VHT nozzle was used to collect data for the pyrolysis products of the three systems. It was immediately apparent from data analysis of all three pyrolysed systems that pyrolysis has occurred. In the case of the pyrolysis of Meldrum's acid it was impossible to fit the resultant data, as decomposition either occurred by an unexpected route, or on initial vaporisation of the compound. For the other two systems the fit to the expected decomposition products was much better and a structure of ketene could be extracted.

In the case of the pyrolysis of acetic anhydride the refinement suggested that total decomposition had occurred and the data were fitted to a model containing only the pyrolysis products (acetic acid and ketene). Whilst the resultant refinement

produced less accurate structures than would be expected for a standard GED experiment, there was no evidence of significant impurities, and it was concluded that pyrolysis had occurred relatively cleanly.

For the pyrolysis of acetone, ketene made up only around 12% of the pyrolysed vapour, and the resultant structure was less accurate.

This work represents some of the first focussed work conducted to extend the GED technique to the study of short-lived molecules generated *in situ*. It is clear that pyrolysis occurs and, if the system is chosen carefully, the data can be analysed using GED alone. However, data analysis of a vapour containing a mixture of species is necessarily more complicated than for standard GED experiments and as more, larger, species are present in the vapour an increasing amount of computed information is required in order to refine the data. Whilst it is routine to use *ab initio* data to supplement GED data, it is always important to consider the amount of information that is truly experimental in nature. If larger systems are to be studied it would be advantageous to increase the amount of experimental information available.

The use of mass spectrometry in conjunction with GED is one way this can be achieved, and this will be discussed in the final chapter. The use of previously determined experimental structures and/or rotational constants is also of interest. In this work it was decided that only the GED structures of compounds studied recently in Edinburgh would be used in the refinement of the pyrolysis data, with the intention of avoiding problems with inconsistent data. However, with the exception of the pyrolysis of Meldrum's acid, which failed for other reasons, this approach was not applicable to these studies, as the acetic anhydride pyrolysed fully and the structure of acetone was not studied. To the best of the authors' knowledge the GED structure of a molecule has never been used to restrain its structure in a mixed vapour using the SARACEN method, so testing of this route would be required before it is used further.

The best structures of unstable molecules will be determined when the amount of experimental data is maximised. The potential exists to study all the additional species in the stream by GED, to obtain or use previously published

rotational constants in the refinement and to determine the make-up of the vapour independently using mass spectrometry. Further work, both in terms of experimental set-up and data analysis, will be required to investigate these possibilities and to decide upon the optimal strategy.

6.5 References

[1] J. C. Williamson, M. Dantus, S. B. Kim and A. H. Zewail, *Chem. Phys. Lett.*, 1992, **196**, 529.

[2] C.-Y. Ruan, V. A. Lobastov, R. Srinivasan, B. M. Goodson, H. Ihee and A. H. Zewail, *Proc. Nat. Acad. Sci.*, 2001, **98**, 7117.

[3] A. H. Zewail, *J. Phys. Chem.*, 1993, **97**, 12427.

[4] N. I. Giricheva, G. V. Girichev, N. P. Kuzmina, Y. S. Medvedeva and A. Y. Rogachev, *J. Struct. Chem.*, 2009, **50**, 52.

[5] T. Iijima, W. Suzuki and Y. F. Yano, *Jpn. J. Appl. Phys.*, 1998, **37**, 5064.

[6] S. L. Hinchley, H. E. Robertson, K. B. Borisenko, A. R. Turner, B. F. Johnston, D. W. H. Rankin, M. Ahmadian, J. N. Jones and A. H. Cowley, *Dalton Trans.*, 2004, 2469.

[7] F. Chick and T. M. Wilsmore, *J. Chem. Soc., Trans.*, 1908, 946.

[8] J. Y. Beach and D. P. Stevenson, *J. Chem. Phys.*, 1938, **6**, 75.

[9] T. T. Broun and R. L. Livingston, *J. Am. Chem. Soc.*, 1952, **74**, 6084.

[10] J. Bregman and S. H. Bauer, *J. Am. Chem. Soc.*, 1955, **77**, 1955.

[11] B. Rozsondai and I. Hargittai, *J. Mol. Struct.*, 1973, **17**, 53.

[12] M. Korn, H.-G. Mack, H.-W. Praas, C. O. Della Vedova and H. Oberhammer, *J. Mol. Struct.*, 1995, **352**, 145.

[13] B. Rozsondai, J. Tremmel, I. Hargittai, V. N. Khabashesku, N. D. Kagramanov and O. M. Nefedov, *J. Am. Chem. Soc.*, 1989, **111**, 2845.

[14] A. N. Meldum, *J. Chem. Soc., Trans.*, 1908, **93**, 598.

[15] D. Davidson and S. A. Bernhard, *J. Am. Chem. Soc.*, 1948, **70**, 3426.

[16] I. Lee, I. S. Han, C. K. Kim and H. W. Lee, *Bull. Korean Chem. Soc.*, 2003, **24**, 1141.

[17] C. E. Pfluger and P. D. Boyle, *J. Chem. Soc. Perkin Trans. 2*, 1985, 1547.

[18] A. S. Ivanov, *Chem. Soc. Rev.*, 2008, **37**, 789.

[19] Y. Hu, P. Wei, H. Huang, Z.-G. Le and Z.-C. Chen, *Synth. Comm.*, 2005, **35**, 2955.

[20] W. J. Hehre, R. Ditchfield and J. A. Pople, *J. Chem. Phys.*, 1972, **56**, 2257.

[21] P. C. Hariharan and J. A. Pople, *Theo. Chim. Acta.*, 1972, **56**, 2257.

[22] M. S. Gordon, *Chem. Phys. Lett.*, 1980, **76**, 163.

[23] A. D. McLean and G. S. Chandler, *J. Chem. Phys.*, 1980, **72**, 5639.

[24] R. Krishnan, J. S. Binkley, R. Seeger and J. A. Pople, *J. Chem. Phys.*, 1980, **72**, 650.

[25] D. E. Woon and T. H. Dunning Jr., *J. Chem. Phys.*, 1993, **98**, 1358.

[26] R. A. Kendall, T. H. Dunning Jr. and R. J. Harrison, *J. Chem. Phys.*, 1992, **96**, 6796.

[27] T. H. Dunning Jr., *J. Chem. Phys.*, 1989, **90**, 1007.

[28] K. A. Peterson, D. E. Woon and T. H. Dunning Jr., *J. Chem. Phys.*, 1994, **100**, 7410.

[29] A. Wilson, T. van Mourik and T. H. Dunning Jr., *THEOCHEM*, 1996, **388**, 339.

[30] C. M. Huntley, G. S. Laurenson and D. W. H. Rankin, *J. Chem. Soc., Dalton Trans.*, 1980, 954.

[31] H. Fleischer, D. A. Wann, S. L. Hinchley, K. B. Borisenko, J. R. Lewis, R. J. Mawhorter, H. E. Robertson and D. W. H. Rankin, *Dalton Trans.*, 2005, 2469.

[32] A. W. Ross, M. Fink and R. Hilderbrandt, *International Tables for Crystallography*, Kluwer Academic Publishers, Dordrecht, Netherlands, 1992, p. 245.

[33] V. A. Sipachev, *THEOCHEM*, 1985, **121**, 143.

[34] P. D. McCaffrey, R. J. Mawhorter, A. R. Turner, P. T. Brain and D. W. H. Rankin, *J. Phys. Chem. A.*, 2007, **111**, 6103.

[35] A. J. Blake, P. T. Brain, H. McNab, J. Miller, C. A. Morrison, S. Parsons, D. W. H. Rankin, H. Robertson and B. A. Smart, *J. Phys. Chem. A*, 1996, **100**, 12280.

[36] P. T. Brain, C. A. Morrison, S. Parsons and D. W. H. Rankin, *J. Chem. Soc., Dalton Trans.*, 1996, 4589.

[37] N. W. Mitzel and D. W. H. Rankin, *Dalton Trans.*, 2003, 3650.

[38] G. Wu, C. Van Alsenoy, H. J. Geise, E. Sluyts, B. J. Van der Veken, I. F. Shishkov and L. V. Khristenko, *J. Phys. Chem. A.*, 2000, **104**, 1567.

[39] A. E.-A. M. Gaber, *Synthesis*, 2001, **14**, 2059.

[40] H. McNab, *Aldrichimica Acta*, 2004, **37**, 19.

[41] C. Wentrup, G. Gross, H.-M. Berstermann and P. Lorencak, *J. Org. Chem.*, 1985, **50**, 2877.

[42] G. J. Fisher, A. F. MacLean and A. W. Schnizer, *J. Org. Chem.*, 1953, **18**, 1055.

[43] P. G. Blake and A. Speis, *Phys. Org.*, 1990, **3**, 279.

[44] I. Lee, O. J. Cha and B.-S. Lee, *J. Phys. Org. Chem.*, 2004, **3**, 279.

[45] "Vapor Pressure", *in CRC Handbook of Chemistry and Physics, 89th Edition (Internet Version 2009)*, David R. Lide, ed., CRC Press/Taylor and Francis, Boca Raton, FL.

[46] J. L. Derissen, *J. Mol. Struct.*, 1971, **7**, 67.

[47] A. P. Cox, L. F. Thomas and J. Sheridan, *Spectrochim. Acta.*, 1959, 542.

[48] B. P. Van Eijck, J. Van Opheusden, M. M. M. Van Schaik and E. Van Zoeren, *J. Mol. Spec.*, 1981, **86**, 465.

[49] G. Froment, H. Pijcke and G. Goethals, *Chem. Eng. Sci.*, 1961, **13**, 173.

[50] L. A. Wall and W. J. Moore, *J. Phys. Chem.*, 1951, **55**, 965.

[51] J. R. McNesby, T. W. Davis and A. S. Gordon, *J. Chem. Phys.*, 1953, **21**, 956.

[52] S. H. Mousavipour and P. Pacey, *J. Phys. Chem.*, 1996, **100**, 3573.

[53] C. Kato, S. Konaka, T. Iijima and M. Kimura, *Bull. Chem. Soc. Jap.*, 1969, **42**, 2148.

[54] R. Nelson and L. Pierce, *J. Mol. Spect.*, 1965, **18**, 344.

Chapter 7

The molecular structures of dibenzylsulfone and the benzyl radical

7.1 Introduction

The previous chapter details the FVP–GED apparatus used in Edinburgh and the results of a preliminary study of the generation of ketene. From this work it was clear that in order to have the best chance of success the system studied should be chosen carefully. Data analysis is obviously more complex when a number of species are present in the vapour and so the molecules present must be as simple as possible or should possess high symmetry. Ideally pyrolysis should occur in a high yield and produce few or no by-products. To facilitate easy repeatability an air- and moisture-stable precursor is also desirable; whilst it is feasible to study reactive starting materials it is more difficult to do so. Finally, the target molecule itself must also be of interest.

A literature search found a number of potential systems, which finally led to the choice of dibenzylsulfone (DBS) as the precursor to the benzyl radical. Dibenzylsulfone (Ph–CH_2–SO_2–CH_2–Ph) has been shown to pyrolyse to form dibenzyl in high yield.[1] The proposed reaction mechanism is the cleavage of DBS to produce the benzyl radical and SO_2, so it is anticipated that the pyrolysis of DBS will offer a source of the benzyl radical. The original study observed dibenzyl as the final product but this almost certainly occurred *via* the formation of the benzyl radical rather than internal rearrangement. The experiment was conducted over the course of 1 hour during which time the DBS was slowly pyrolysed and subsequently trapped on a cold finger cooled with an acetone/dry ice slush.[1] In the FVP-GED apparatus the interaction zone of the gas and electron beam is itself the pyrolysis zone and so the radicals have a greatly reduced time in which to recombine. This hypothesis can be tested by allowing for the presence of dibenzyl in the final refinement of the benzyl radical.

It was therefore decided that DBS would be an ideal second candidate for study using the FVP–GED system.

The conditions reported by the previous study were a pyrolysis temperature of 923 K at a pressure of 0.1 Torr. These compare with the limits of the FVP–GED apparatus which are around 900 K and 1 Torr. It is feasible that the yield under

these conditions will be lower than the previous study reports and that a mixture of DBS and the benzyl radical will be obtained. It is therefore important to determine the structure of DBS using standard GED to aid analysis of data from the pyrolysed system.

This chapter presents the structure of DBS and the results of the pyrolysis experiment.

7.2 Dibenzylsulfone

Other than for use as a synthetic building block there is little literature relating to DBS and no previous structural studies have been conducted either in the gas-phase or the solid state. A number of compound with a similar SO_2 moiety have been studied, including a recent study of $CF_3SO_2CF_3$ by the Edinburgh GED group.[2] From this study it was found that the geometry around the S atom determined *ab initio* was sensitive to the basis set used and that the best results were obtained when additional polarisation functions were included. Similar behaviour can be expected for this system, and so it is both important to be aware of this potential problem, and interesting to compare how well different theoretical methods agree with the experimental structure.

7.2.1 Experimental

DBS (99%) was purchased from Sigma-Aldrich and used without further purification.

Theoretical methods

The calculations for dibenzylsulfone were performed using a Silicon Graphics Altix 4700 and the Gaussian 03 program.[3] All MP2 methods were frozen core (fc). The M05–2X calculations using the 6-311G(2*pd*,2*df*) basis set were performed by Ragnar Bjornsson (St. Andrews).

Geometry optimisations DBS has four dihedral angles around which rotation can occur; the two C–C–C–S and two C–C–S–O dihedrals. A comprehensive scan covering the entire conformational space of the molecule is prohibitively expensive as scanning 180° around ϕC–C–C–S and 360° around ϕC–C–S–O in 15° steps would require ∼83,000 geometry optimisations, or at an average of 30 minutes for a HF/3–21G* optimisation, 4.7 CPU years. Instead a series of one-dimensional scans were conducted in which one of the four dihedral angles was varied whilst the others were fixed. This method initially led to two conformers being found (**A** and **B** in Figure 7.1) but a trial refinement gave a poor fit to the experimental data and a more thorough search revealed a third conformer (**C** in Figure 7.1).

Further geometry optimisations were conducted for all conformers at the HF,[4] MP2,[5] B3LYP[6–8] and M05–2X[9,10] levels of theory using Pople-type basis sets.[11–15] The M05–2X functional was chosen because it claims to offer a good description of long-range forces and provide accurate energy differences between conformers. It would have been interesting to use different basis sets and compare the results, but the large size of DBS meant further calculations were prohibitively expensive.

The optimised structures of the three conformers of DBS along with the atomic number scheme are shown in Figure 7.1. For the sake of clarity only key heavy atoms are labelled in **B** and **C**.

Frequency calculations Analytic second derivatives[16,17] of the energies with respect to nuclear coordinates calculated at various levels of theory served both to confirm the nature of the minima found by the optimisation and to provide vibrational information for use in the SARACEN refinement.[18–20]

Electron diffraction

Data were collected for dibenzylsulfone using the Edinburgh gas diffraction apparatus.[21] An accelerating voltage of *ca.* 40 kV (electron wavelength *ca.* 6.0 pm) was used. Sample and nozzle temperatures were maintained at 493 K and 513 K respectively. Scattering intensities were recorded on Kodak Electron

Figure 7.1: Molecular structure of the three conformers of dibenzylsulfone.

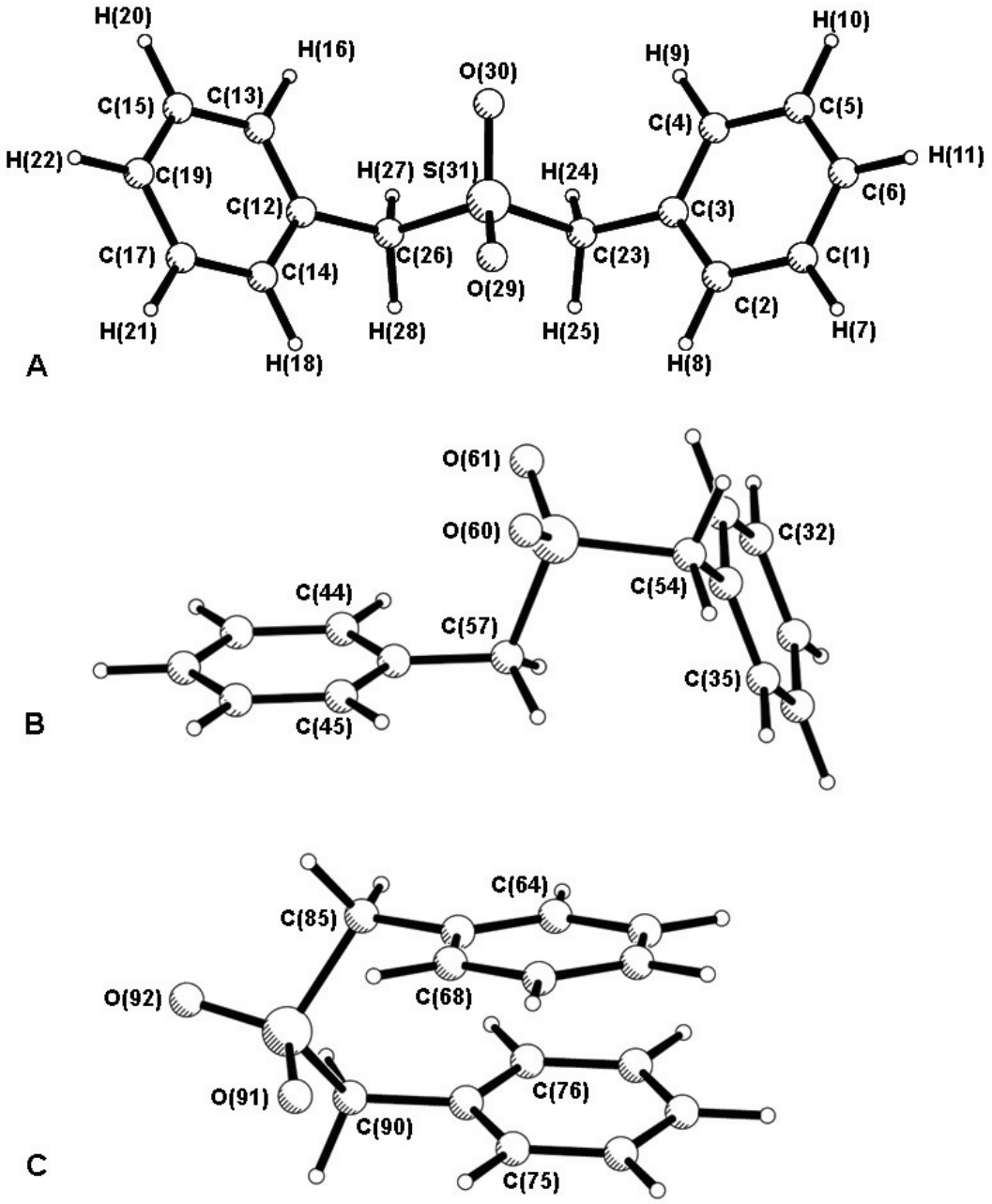

Image films at nozzle-to-plate distances of 249.8 and 90.4 mm. The weighting points for the off-diagonal weight matrices, correlation parameters and scale factors for the two camera distances for each molecule are given in the Appendix (Table A7.2), together with electron wavelengths, which were determined from the scattering patterns of benzene vapour, recorded immediately after the

compound patterns and analysed in exactly the same way to minimise systematic errors in wavelengths and camera distances. The scattering intensities were measured using an Epson Expression 1680 Pro flatbed scanner and converted to optical densities as a function of the scattering variable, s, using an established program.[22] Data reduction and least-squares refinements were carried out using the ed@ed v3.0 program,[23] employing the scattering factors of Ross *et al.*[24]

7.2.2 Results

Theoretical calculations

Three potential-energy minima of DBS have been identified. The three conformers (**A**, **B** and **C**) are shown in Figure 7.1. **A** possesses C_{2v} symmetry whilst both **B** and **C** have C_1 symmetry. **B** can be considered as being similar to **A** with one benzyl group rotated out of the plane of symmetry. The left-hand side of **B** in Figure 7.1 is close to having local C_s symmetry through the Ph–CH_2-SO_2 section but the right hand side is twisted such that the CH_2–Ph section has no symmetry. **C** is very different to the other two conformations with the two rings arranged in such a way that they partially eclipse one another. **C** is presumably stabilised by favourable H...C contacts between the two rings. Such a moiety is unusual in an isolated molecule, but a search for similar packing features in the Cambridge structural database (CSD) found a number of compounds with similar intra-molecular arrangements of benzene rings[25,26] including a similar arrangement in $S(CH_2–Ph)_2$, albeit with a 2–coordinate sulfur atom.[27]

Table 7.1 shows the number of imaginary frequencies found for each calculation conducted. It is clear that the nature of the stationary point for each conformer is dependent on the level of theory and basis set used. It is likely that long-range interactions between the ring systems are important and therefore the calculations will be sensitive both to the method used, due to the different ways MP2 and DFT handle long range interactions, and to the size of the basis set used, due to basis set superposition error (BSSE).

The key parameters for each conformer are shown in Table 7.1. A comprehensive

list of computed structural parameters is given in Appendix 7 in Table A7.1.

From Table 7.1 it is clear that, as expected, the parameters are strongly dependent on the method used. For example rS=O in **A** varied from 143.8 pm to 147.2 pm in the calculations shown in Table 7.1, and rS–C from 179.6 pm to 185.1 pm. When extra polarisation functions were added, in the form of the 6-311G(2*dp*,2*df*) basis set, both rS=O and rS–C shortened by around 1.5 pm. The changes in bond angles found around S tended to vary less considerably. ∠C–C–S varies by around 2° across the calculations, with the angles being wider when HF or B3LYP is used and narrower when MP2 and the M05-2X functional is used. ∠C–S=O, ∠C–S–C and ∠O=S=O were all more consistent, varying by a maximum of 1°.

Table 7.1: Selected structural parameters, and nature of minima found, for the three conformers of dibenzylsulfone calculated using the HF, MP2, B3LYP and M05-2X methods.[a]

Parameter	HF 6-31G*	MP2 6-31G*	MP2 6-311++G**	B3LYP 6-31G*	B3LYP 6-311++G**	M05-2X 6-31G*	M05-2X 6-311++G**	M05-2X 6-311G(2*pd*,2*df*)
Conformer **A**								
rS=O	143.8	147.1	146.1	147.2	146.8	146.5	146.1	144.4
rS–C	179.6	181.0	181.4	184.7	185.1	181.1	181.1	179.8
rC–C	151.0	149.9	149.9	150.3	150.0	150.1	149.9	149.7
∠C–C–S	111.8	109.1	109.2	111.1	111.5	109.3	109.5	109.0
∠C–S=O	108.1	107.7	107.9	108.0	108.2	107.8	108.0	108.1
∠C–S–C	102.7	103.2	102.8	102.3	102.1	102.7	102.7	102.9
∠O=S=O	120.4	121.4	120.9	121.0	120.5	121.2	120.7	120.4
No. imag. freq.	1	2	–[b]	0	0	2	1	0
Conformer **B**								
rS=O(60)	143.9	147.2	146.2	147.3	149.9	146.5	146.1	144.4
rS=O(61)	143.9	147.2	146.3	147.3	149.9	146.6	146.2	144.5
rS–C(54)	179.5	180.9	181.3	184.4	184.7	181.0	181.0	179.7
rS–C(57)	179.3	180.6	181.0	184.4	184.7	180.8	180.9	179.5
rC(34)–C(54)	150.9	149.9	150.0	150.4	150.1	150.2	149.9	149.7
rC(43)–C(57)	151.0	149.9	149.9	150.3	150.1	150.1	149.9	149.7
∠C(43)–C(57)–S	111.6	109.0	109.5	111.0	111.4	108.9	109.1	108.7
∠C(34)–C(54)–S	116.0	113.3	112.4	115.4	115.4	113.4	112.9	113.2
∠C(54)–S(62)=O(60)	106.1	107.2	107.8	106.4	108.5	106.8	107.2	107.0
∠C(54)–S(62)=O(61)	108.2	107.8	108.5	108.0	108.0	107.9	107.8	108.1
∠C–S–C	104.8	103.6	103.1	104.0	104.2	104.0	104.1	104.0
∠O=S=O	119.8	120.9	120.6	120.5	120.1	120.4	120.1	119.9
ϕC(33)–C(34)–C(54)–S(62)	70.1	69.7	71.1	69.6	70.9	68.8	69.6	69.0

ϕC(34)-C(54)-S(62)-C(57)	58.3	54.2	51.0	59.0	57.9	53.9	52.3	54.1
ϕC(54)-S(62)-C(57)-C(43)	179.1	-179.1	-177.8	-178.8	-179.2	179.0	178.9	179.3
ϕS(62)-C(57)-C(43)-C(44)	91.2	89.4	92.7	91.9	90.8	89.1	90.6	88.8
ΔG^c	–3.8	–5.7	–11.3	–2.3	–2.5	–13.3	–7.7	–6.1
No. imag. freq.	0	2	–[b]	0	0	0	0	0
Conformer **C**								
rS=O(91)	143.9	147.4	146.4	147.4	147.0	146.7	146.3	144.6
rS=O(92)	144.1	147.3	146.3	147.4	147.1	146.7	146.3	144.5
rS–C(85)	179.9	181.1	181.2	185.1	185.2	181.4	181.3	180.0
rS–C(26)	179.4	180.6	180.6	184.2	184.3	180.7	180.6	179.4
rC(65)–C(85)	150.9	150.1	150.3	150.3	150.1	150.3	150.1	149.9
rC(74)–C(88)	151.0	150.2	150.3	150.5	150.3	150.3	150.1	149.9
$\angle$C(74)–C(88)–S	118.3	115.0	114.9	117.3	117.7	114.9	114.8	114.9
$\angle$C(65)–C(85)–S	117.2	116.2	116.2	117.2	117.4	116.3	116.2	116.4
$\angle$C(85)–S(93)=O(91)	109.2	108.5	108.3	109.2	109.0	109.1	108.9	109.1
$\angle$C(85)–S(93)=O(92)	105.4	106.2	106.5	105.6	105.5	106.5	106.0	106.1
$\angle$C–S–C	108.7	106.2	106.1	107.4	108.1	106.8	107.3	106.8
$\angle$O=S=O	119.3	120.5	120.4	120.1	119.9	119.9	119.7	119.5
ϕC(64)-C(65)-C(85)-S(93)	116.3	118.4	118.6	114.2	113.9	118.2	117.9	117.9
ϕC(65)-C(85)-S(93)-C(88)	-78.8	-74.6	-73.0	-83.9	-83.0	-78.7	-77.6	-78.8
ϕC(85)-S(93)-C(88)-C(74)	60.9	49.1	47.4	58.2	60.0	49.4	48.9	49.7
ϕS(93)-C(88)-C(74)-C(75)	61.3	59.5	59.8	62.0	63.0	59.6	60.1	59.4
ΔG^c	7.6	–14.8	–	7.9	8.0	–7.2	–2.6	–1.0
No. imag. freq.	0	0	–[b]	0	0	0	0	0

[a] All distances in pm and angles in °. See Figure 7.1 for atom numbering.

[b] Frequency calculations were not conducted.

[c] Relative to **A** in kJ mol^{-1}.

Gas electron diffraction refinements

The theoretical calculations suggested the existence of three conformers, although not all conformers were PES minima at all levels of theory. The calculations also varied greatly in their estimations of the relative energies of the conformers and so it was decided to include all three conformers in the GED model even though the predicted proportion of **A** was, in many calculations, too small to be detected. Fully modelling three conformers, two of which possess C_1 symmetry, would require a large number of parameters and so simplifications were required. It was therefore decided that the model would be based on the more symmetric **A** and that the slight deviations in bond lengths found in **B** and **C** would not be modelled. The differences in the key bond lengths between **A**, **B** and **C** are small, with the largest differences at the M05-2X/6-311G(2*df*,2*dp*) level being 0.3 pm between the rS–C distances. However, the differences in bond angles around the S atom are more pronounced and so additional parameters were included to allow these to vary in **B** and **C** as were the required unique dihedral angles.

The benzyl ring was modelled as having C_s symmetry and so three ring C–C distances are required. These three distances, along with rC(3)–C(23) and rS=O, all lie under a single peak and so were modelled using the average (p_1) and four differences (p_2–p_5), defined such that $p_1 = \frac{1}{5}$ [rC(1)–C(6) + rC(1)–C(2) + rC(2)–C(3) + rC(3)–C(23) + rS(31)=O(29)], p_2 = [rC(3)–C(23) - rC(1)–C(6)], p_3 = [rC(3)–C(23) - rC(1)–C(2)], p_4 = [rC(3)–C(23) - rC(2)–C(3)] and p_5 = [rC(3)–C(23) - rS(31)=O(29)]. The other bond lengths used were rC–H (p_6) and rC–S (p_9).

As well as the three bond lengths an additional two angles were required to describe the geometry of the ring. The two angles used were ∠C(2)–C(3)–C(4) (p_7) and ∠C(1)–C(6)–C(5) (p_8). The other angles used to describe the heavy atoms were ∠C(3)–C(23)–S(31) (p_{14}), ∠C(23)–S(31)–C(26) (p_{10}) and ∠O(29)=S(31)=O(30) (p_{11}). The H atoms around the ring were placed using ∠C(3)–C(2)–H(8) (p_{12}) and ∠C(6)–C(1)–H(7) (p_{13}). The two H atoms bonded to C(23) were placed using ∠C(3)–C(23)–H (p_{15}) and the beta angle, ∠H(24)–

C(23)–H(25) (p_{16}). These parameters, along with forced C_{2v} symmetry, were sufficient to describe **A**.

B was modelled using three extra parameters. The dihedral angle ϕC(34)–C(54)–S(62)–C(57) (p_{17}) was used to describe the position of the second -CH_2- fragment and ϕC(33)–C(34)–C(54)–S(62) (p_{18}) allowed the phenyl ring to rotate. A difference of around 4.5° between the two ∠C–C–S angles was predicted by the *ab initio* calculations and, considering that this angle has a large effect on many non-bonded parameters between the two ring systems, it was felt essential to include this deviation. As ∠C(43)–C(57)–S was consistently close to the value found in **A**, it was modelled using the same parameter as in **A** (p_{14}), but an extra parameter (p_{25}) was included to describe ∠C(34)–C(54)–S. The differences in other angles between **A** and **B** are all much smaller and so were not included.

In **C** the two ∠C–C–S angles were different to both one another and to the angles found in **A** and **B**, so ∠C(65)–C(85)–S(93) (p_{19}) and ∠C(74)–C(88)–S(93) (p_{26}) were included as separate parameters. The angle ∠C(85)–S(93)–C(88) (p_{20}) was also included as a separate parameter for **C**. A total of four dihedral angles were required to describe the rotation of the the two benzyl fragments in **C**, these being ϕC(64)–C(65)–C(85)–S(93) (p_{21}), ϕC(65)–C(85)–S(93)–C(88) (p_{22}), ϕC(85)–S(93)–C(88)–C(74) (p_{23}) and ϕS(93)–C(88)–C(74)–C(75) (p_{24}).

Two additional parameters were used to allow the proportion of **A** (p_{27}) and **B** (p_{28}) to vary, with the proportion of **C** given by 1 - p_{27} - p_{28}.

The starting parameters for the r_{h1} refinement[28] were taken from the theoretical geometry optimised at the M05–2X/6–311G(2*df*,2*pd*) level. A theoretical Cartesian force field was obtained at this level and converted into a force field described by a set of symmetry coordinates using the SHRINK program,[28] which generated both the amplitudes of vibration (u_{h1}) and the curvilinear corrections (k_{h1}). All 26 geometric parameters and 8 groups of vibrational amplitudes were then refined. Flexible restraints were employed during the refinement using the SARACEN method.[18–20] Altogether, 17 geometric restraints (Table 7.2) and two amplitude restraints (Appendix 7, Table A7.3) were employed. The success of the final refinement, for which $R_G = 0.058$ ($R_D = 0.023$), can be assessed on the basis

of the radial-distribution curve (Figure 7.2) and the molecular-scattering intensity curves (Appendix 7, Figure A7.1). Final refined parameters are listed in Table 7.2. The Appendix contains the interatomic distances and the corresponding amplitudes of vibration (Table A7.3), with the least-squares correlation matrix (Table A7.4) and the experimental coordinates from the GED analysis (Table A7.5).

Figure 7.2: Experimental and difference (experimental – theoretical) radial-distribution curves, $P(r)/r$, for dibenzylsulfone. Before Fourier inversion the data were multiplied by $s.\exp(-0.00002s^2)/(Z_S - f_S)(Z_C - f_C)$.

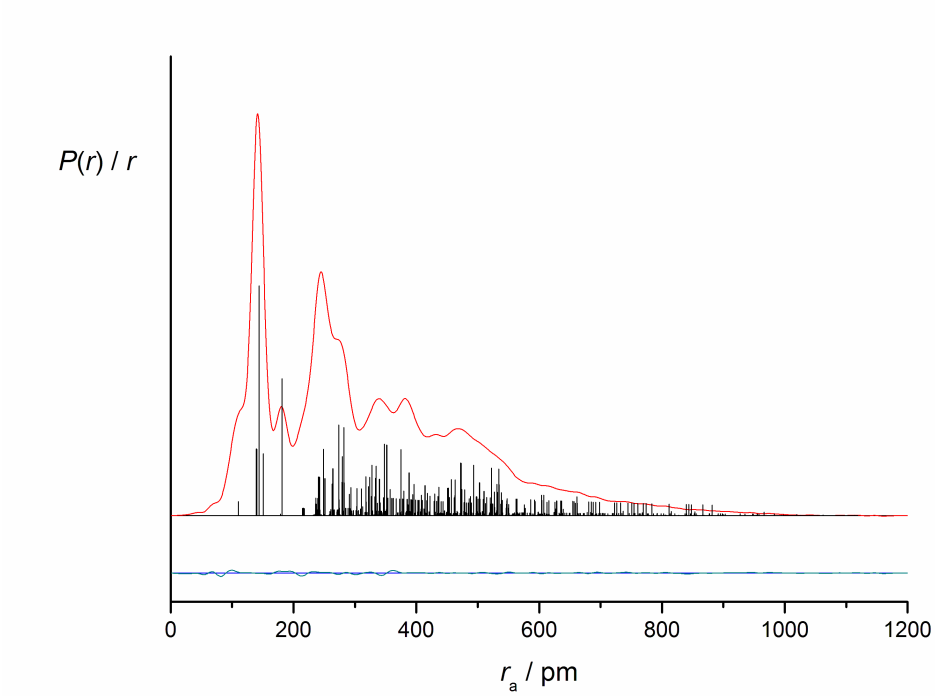

Table 7.2: Refined and calculated geometric parameters for dibenzylsulfone (distances in pm and angles in °) from the GED study.[a,b]

	Parameter	M05-2X/ 6-311G(2*df*,2*pd*)	SARACEN (r_{h1})	Restraint
Independent parameters				
p_1	rS=O/C–C av	142.0	142.9(1)	—
p_2	rS=O/C–C dif1	11.1	10.3(5)	11.1(5)
p_3	rS=O/C–C dif2	11.3	11.0(5)	11.3(5)
p_4	rS=O/C–C dif3	10.9	11.2(5)	10.9(5)
p_5	rS=O/C–C dif4	5.3	6.6(3)	5.3(12)
p_6	rC–H	108.0	110.0(3)	108.0(6)
p_7	∠C(1)–C(6)–C(5)	119.3	119.3(4)	—
p_8	∠C(2)–C(3)–C(4)	119.7	119.6(4)	—
p_9	rC–S	179.6	181.2(2)	—
p_{10}	∠C–S–C	102.9	102.8(9)	102.9(10)
p_{11}	∠O=S=O	120.4	119.6(11)	—
p_{12}	∠C(3)–C(2)–H(8)	120.0	120.5(10)	120.0(10)
p_{13}	∠C(6)–C(1)–H(7)	120.0	119.2(10)	120.0(10)
p_{14}	∠C–C–S	108.7	112.0(6)	—
p_{15}	∠C–C–H(24)	111.3	109.8(8)	111.3(10)
p_{16}	∠H–C–H	108.9	108.4(10)	108.9(10)
p_{17}	**B** ϕC(34)–C(54)–S(62)–C(57)	55.0	54.5(20)	55.0(20)
p_{18}	**B** ϕC(33)–C(34)–C(54)–S(62)	20.0	16.9(17)	20.0(20)
p_{19}	**C** ∠C(65)–C(85)–S(93)	116.4	117.4(7)	—
p_{20}	**C** ∠C–S–C	106.8	106.8(10)	106.8(10)
p_{21}	**C** ϕC(64)–C(65)–C(85)–S(93)	27.0	25.6(18)	27.0(20)
p_{22}	**C** ϕC(65)–C(85)–S(93)–C(88)	-78.0	-81.0(34)	—
p_{23}	**C** ϕC(85)–S(93)–C(88)–C(74)	49.7	49.7(27)	—
p_{24}	**C** ϕS(93)–C(88)–C(74)–C(75)	30.0	37.4(40)	—
p_{25}	**B** C(34)–C(54)–S(62)	113.2	116.7(6)	—
p_{26}	**C** C(74)–C(88)–S(93))	114.9	115.7(7)	—
p_{27}	Proportion **A**	0.04	0.05	—
p_{28}	Proportion **B**	0.73	0.60(5)	—
Dependent parameters				
dp_1	p_7 - p_8	0.5	0.3(3)	0.5(2)
dp_2	rS=O	144.4	144.1(2)	—
dp_3	rC(1)–C(2)	138.4	139.7(4)	—
dp_4	rC(2)–C(3)	138.8	139.6(4)	—
dp_5	rC(1)–C(6)	138.6	140.4(4)	—
dp_6	rC(2)–C(23)	149.7	150.7(3)	—
dp_7	p_{25} - p_{14}	4.5	4.7(5)	4.5(5)
dp_8	p_{26} - p_{19}	-1.5	-1.7(5)	1.5(5)

[a] Figures in parentheses are the estimated standard deviation of the last digits.
[b] See text for parameter definitions.

7.2.3 Discussion

The molecular structures of the three conformers of dibenzylsulfone have been investigated in the gas phase by GED supplemented using the SARACEN method.[18–20] An independent theoretical investigation of the structures was also undertaken.

For the most part the experimental structures of the three conformers of DBS agree well with the calculated structures, and where theory did not offer a precise result the experimental results can offer guidance. As would be expected for such complex system a large number of restraints were required, with the extent of peak overlap in the RDC apparent in Figure 7.2 as an almost continuous series of non-bonded distances from r_a = 2 – 10 pm. As such, the amount of information available from GED data alone is always going to be limited but a number of conclusions can be drawn, especially with regard to the relative stability of different conformers, which is often predicted poorly by theory.[29]

The distance rS–C lies under a unique peak in the RDC and the experimental distance was found to be 181.2(2) pm. This result agrees well with the MP2 and MO5-2X calculations using the 6-311++G** basis set, which for **A** found the distance to be 181.4 pm and 181.1 pm respectively. However, this bond length was found to shorten significantly when the 6-311G(2*df*,2*pd*) basis set was used, with the M05-2X functional returning a value of 179.8 pm for **A**. This suggests that obtaining reliable results from *ab initio* calculations is not as simple as using larger polarisation functions. The B3LYP calculations appear to overestimate this bond length by 3–4 pm. Counter to this, the rS=O distance, found to be 144.1(2) pm by experiment, agrees most closely with the calculation using the 6-311G(2*df*,2*pd*) basis set, which offers a result of 144.4 pm for **A**. All other basis sets, independent of the level of theory used, overestimate this distance by around 2 pm.

The four unique C–C distances in the molecule were all found by experiment to be slightly longer than calculations suggest, tending to be around 2σ longer than calculations using the 6-311++G** basis set.

Many of the bond angles required the use of a restraint and so match the calculated values closely. It was possible to refine both ∠O=S=O and one of the two ∠C–C–S for both **B** and **C** without using a restraint, although the differences between the two unique ∠C–C–S for **B** and **C** were restrained. The experimental ∠O=S=O was 119.6(11)° which is consistent with calculated values. For **B** ∠C(34)–C(54)–S(62) was found to be 116.7(6)° and ∠C(43)–C(59)–S(62) 112.0(6)°, whilst the theoretical values range from 112.4 – 116.0° for ∠C(43)–C(59)–S(62) and 108.7 – 111.6° for ∠C(43)–C(59)–S(62). The B3LYP and HF calculations yield the widest bond angles and are closest to the experimental results, whilst the calculations at the MP2 and M05-2X levels are further from the experimental values. This is in direct contrast to the trend found for bond lengths, where the MP2 and M05-2X methods were closest to the experimental values. For **C** the experimental bond angles ∠C(65)—C(85)–S(93) and ∠C(74)–C(88)–S(93) are 117.4(7) and 115.8(7), respectively, which compare well with the calculated values, which for **C** differ much less as a function of computational method than for **B**.

The experimental dihedral angles for **B** and **C** all lie close to the theoretical values. For **C** it was possible to refine three of the four dihedral angles without the need for a restraint.

The abundances of the three conformers determined experimentally were 5% of **A**, 60(5)% of **B** and 35(5)% of **C**. The abundance of **A** was varied to give the best R factor but no e.s.d. was determined. When converted to energy differences (accounting for the multiplicities of each species) **B** is the most stable, with **A** 4.6 kJ mol^{-1} higher in energy than **B** and **C** 2.2 kJ mol^{-1} higher than **B**. Without an e.s.d. on the abundance of **A** it is difficult to produce comparable e.s.d.s for the energy difference, but a crude estimation based on the e.s.d. of 5% for **B** offers a standard deviation of around 0.4 kJ mol^{-1} for **B** and **C**, whilst it is likely the error on the energy of **A** is much larger. It is difficult to obtain a consistent picture from the *ab initio* calculations, with the global minimum switching between **B** and **C** when different levels of theory and basis sets are used. The calculations do suggest that it is important to consider ΔG as opposed to ΔE, as including

entropy often changes the results significantly and in some cases even changes which conformer is predicted to be the global minimum. The M05-2X functional is parametrised to offer accurate energies and does offer the closest agreement to that determined experimentally. When only ΔE is considered the M05-2X/6-311G(2df,2pd) level suggests **B** and **C** are approximately equal in energy with **A** 7.8 kJ mol^{-1} higher in energy. Including ΔG changes the picture dramatically, with **B** becoming the most stable conformation with **A** 5.9 kJ mol^{-1} higher in energy relative to **B** and **C** 5.0 kJ mol^{-1} higher relative to **B**.

7.2.4 Conclusion

The structure of dibenzylsulfone (DBS) has been determined by GED using the SARACEN method and an independent theoretical investigation has been conducted. DBS was found to exist as a mixture of 3 conformers. The results obtained from *ab initio* calculations tended to be dependent on the level of theory and basis set used, especially for parameters related to the sulphur atom, and no clear convergence was found. Whilst the experimental parameters obtained are generally consistent with the range of values obtained from *ab initio* calculations it is not the case that one level of theory and/or basis set produced the best results. Instead some experimental parameters agree closely with those obtained using one theoretical method, and other experimental parameters with another.

7.3 The benzyl radical

7.3.1 Introduction

The benzyl radical is one of the simplest aromatic radicals and has been the subject of much work.[30–35] It is thought to play an important role in the combustion of hydrocarbons, including in the phenomenon of *"knock"* in petrol engines.[30,31] Despite its importance a full experimental structure has never been determined although the molecule has been studied extensively using a variety of techniques, for example, theoretical methods,[32,33] EPR,[34] and IR spectroscopy.[35]

The benzyl radical has been found to possess greater stability than other simple radicals. This is attributed to its high resonance energy,[36] which in turn can be explained by the four possible resonance structures shown in Figure 7.3. The unpaired electron is therefore predicted to be delocalised over a number of positions in the molecule, with the results of previous EPR[34] and theoretical studies[32] supporting this.

Figure 7.3: The resonance forms of the benzyl radical

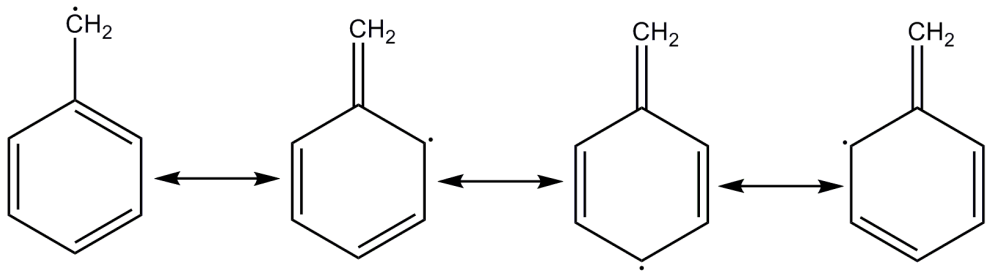

It is not immediately obvious how much information is available *via* GED alone, as the four bonded C–C distances will lie under a single peak in the RDC, as will a number of C...C non-bonded distances. To complicate matters further the chosen precursor (DBS) pyrolyses to produce SO_2 in addition to the benzyl radical, and the S=O distance is close in length to bonded C–C distances. However, despite these concerns electron diffraction is probably the only technique by which a complete structure of the benzyl radical can be obtained. It is anticipated that with the use of other structural information *via* the SARACEN method[18–20] a quality refinement can be achieved.

7.3.2 Experimental

The benzyl radical was generated *in situ* by the pyrolysis of DBS using the VHT nozzle described in the previous chapter.

Theoretical methods

Other than by using unrestricted methods[37] calculations for the benzyl radical were conducted in the same manner as for DBS. The optimised structure of the benzyl radical along with the atomic numbering scheme is shown in Figure 7.4.

Figure 7.4: Molecular structure of the benzyl radical

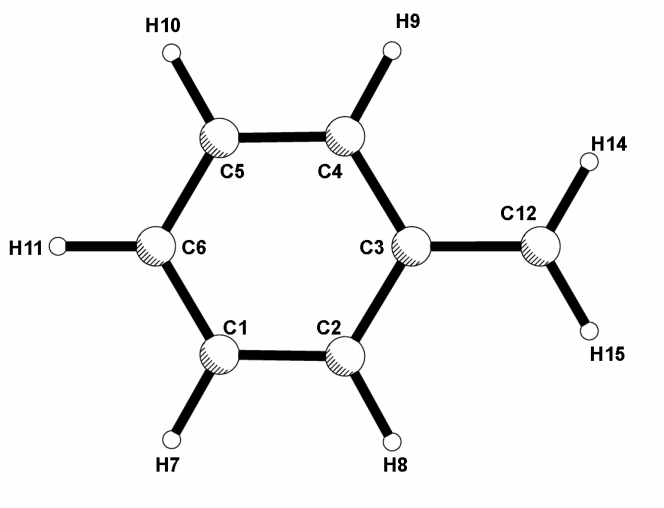

Electron diffraction

Data were collected for the benzyl radical using the Edinburgh gas diffraction apparatus in conjunction with the VHT nozzle described in the previous chapter.[21] An accelerating voltage of *ca.* 40 kV (electron wavelength *ca.* 6.0 pm) was used. A sample of DBS was vaporised at 450 K in the medium temperature internal oven and was passed through the VHT oven, maintained at 900 K, where pyrolysis occured. Scattering intensities were recorded on Kodak Electron Image films with an assumed nozzle-to-plate distance of 213.2 mm. The weighting points

for the off-diagonal weight matrices, correlation parameters and scale factors are given in Appendix 7 (Table 7.6). The scattering intensities were measured using an Epson Expression 1680 Pro flatbed scanner and converted to optical densities as a function of the scattering variable, s, using an established program.[22] Data reduction and least-squares refinements were carried out using the ed@ed v3.0 program,[23] employing the scattering factors of Ross *et al.*[24]

7.3.3 Results

Theoretical calculations

The results from the geometry optimisations conducted for SO_2 and the benzyl radical are given in Tables 7.3 and 7.4 respectively. For the benzyl radical no large deviations are found as the size of the basis set is increased. The calculations for SO_2 vary more considerably. Such behaviour is expected for calculations involving sulfur, with a more detailed discussion of the difficulties in calculating such parameters offered in a previous study.[38]

Table 7.3: Structural parameters for SO_2.[a]

	HF		MP2			
Parameter	3-21G*	6-31G*	6-31G*	6-311G*	6-311+G*	6-311++G**
rS–O	141.9	141.4	147.8	146.5	146.9	146.9
∠O–S–O	118.7	118.8	119.8	119.5	119.3	119.3

[a] All distances in pm and angles in °.

Table 7.4: Selected structural parameters for the benzyl radical.[a]

	HF		MP2			
Parameter	3-21G*	6-31G*	6-31G*	6-311G*	6-311+G*	6-311++G**
rC(1)–C(2)	138.9	139.0	136.6	136.7	136.9	136.8
rC(1)–C(6)	140.3	140.5	138.7	138.8	138.9	138.9
rC(1)–H(7)	107.2	107.6	108.7	108.6	108.7	108.6
rC(2)–C(3)	142.7	142.8	140.9	141.0	141.0	141.0
rC(2)–C(8)	107.3	107.6	108.8	108.7	108.7	108.7
rC(3)–C(12)	140.4	140.5	141.0	141.2	141.4	141.4
rC(6)–H(11)	107.2	107.5	108.6	108.5	108.6	108.5
rC(12)–H(13)	107.3	107.5	108.3	108.3	108.3	108.3
∠C(2)–C(1)–C(6)	120.5	120.4	120.5	120.5	120.5	120.5
∠C(2)–C(1)–H(7)	119.8	119.8	119.7	119.7	119.7	119.7
∠C(1)–C(2)–C(3)	120.9	121.0	121.0	121.0	121.0	120.9
∠C(1)–C(2)–H(8)	120.2	120.0	120.2	120.1	120.1	120.2
∠C(2)–C(3)–C(4)	117.5	117.4	117.5	117.5	117.5	117.6
∠C(2)–C(3)–C(12)	121.2	121.3	121.2	121.2	121.2	121.2
∠C(4)–C(5)–C(6)	120.4	120.4	120.5	120.5	120.5	120.5
∠C(1)–C(6)–C(5)	119.7	119.7	119.5	119.5	119.4	119.5
∠C(1)–C(6)–H(11)	120.2	120.2	120.3	120.3	120.3	120.3
∠C(3)–C(1)–H(13)	121.1	121.2	121.2	121.1	121.1	120.8
∠H(13)–C(12)–H(14)	117.7	117.6	117.6	117.9	117.9	118.4
Energy[b]	-267.6412	-269.1404	-269.9515	-270.0397	-270.0476	-270.0993
Gibbs Free Energy[b]	-267.5498	-269.0498	-269.8635	-269.9533	–	–

[a] All distances in pm and angles in °. See Figure 7.4 for atom numbering.

[b] Energy in Hartrees.

Gas electron diffraction refinements

Initially it was necessary to conduct a number of test refinements to ascertain the nature of the vapour as the potential exists for there to be a mixture of the benzyl radical, SO_2, dibenzyl and/or DBS. To test for the the possibility of incomplete decomposition a model was created containing a mixture of DBS, SO_2 and the benzyl radical, while a second model containing a mixture of the benzyl radical, SO_2 and dibenzyl was used to test for recombination of the radicals.

The results of the refinement containing various mixtures of DBS and the benzyl radical are plotted in Figure 7.5. The refinement was carried out with the structures of three conformers of DBS fixed to the experimental structures obtained in Section 7.2. The ratios of the conformers were also fixed to those previously obtained, corrected for the higher temperature, and the ratio of SO_2 to benzyl radical was fixed to 1:2. It can be seen from Table 7.5 that the lowest R factor is obtained when there is no DBS present. The 95% confidence limit for this plot (R_G / $R_{Gmin} = 1.016$) is not shown because it would be very close to the point at R_G / $R_{Gmin} = 1.0$. Any attempt to refine the key bond lengths in DBS resulted in unreasonable values. Of particular importance is that if the rS–C distance were refined the value obtained was around 150.0 pm, as opposed to the expected value close to 180.0 pm. The main difference between the GED pattern of DBS and the decomposition products is the presence of an S–C bond and it appears from this refinement that such a bond is not present. This, combined with the results shown in Figure 7.5, provides strong evidence for full decomposition.

A similar process was conducted for the model containing the benzyl radical, SO_2 and the possible recombination product, dibenzyl. The R factor is plotted against the mole fraction of dibenzyl in Figure 7.6. The solid horizontal line represents the 95% confidence limit. In the refinement the main heavy atom parameters for both molecules were refined, with restraints applied as required. Total decomposition of the starting material (DBS) was assumed. The mole fraction of SO_2 present is determined from the stoichiometry of the pyrolysis process and so the the mole fraction of all three species is determined solely by the level of recombination. The

Figure 7.5: A plot showing the R factor variation as a function of the amount of decomposition of DBS. 1.0 on the x axis denotes complete decomposition.

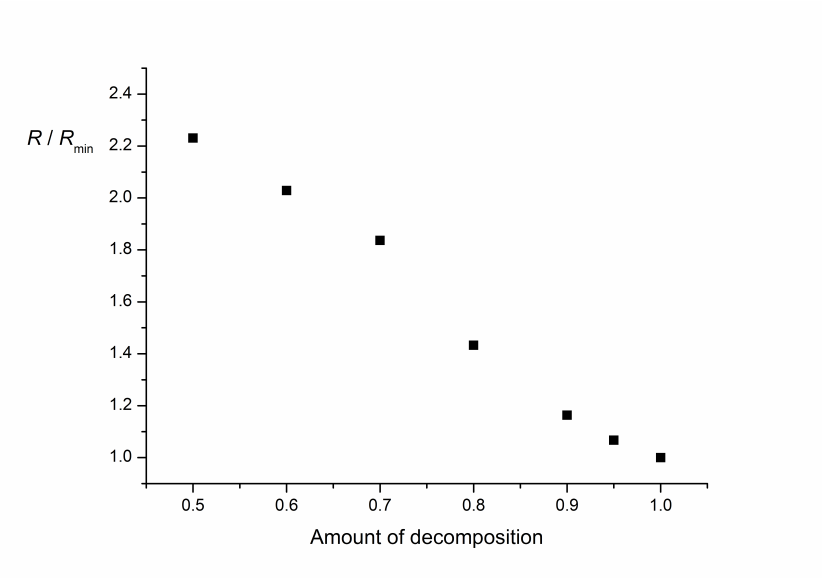

Figure 7.6: A plot showing the R-factor variation against the mole fraction of dibenzyl present in the pyrolysed gas flow. The solid line denotes the 95% confidence level.[39]

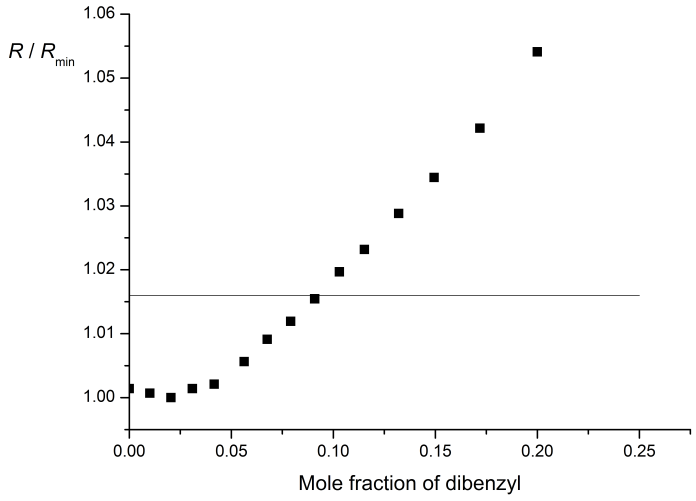

differences between the scattering pattern obtained for dibenzyl and the benzyl radical are subtle and this is reflected in the smaller deviations in R factor than was found for the previous model containing DBS and decomposition products. The lowest R factor was obtained when the proportion mole fraction of dibenzyl is set to roughly 0.02 with the plot suggesting that the uncertainty is around 0.05, and so the fraction of dibenzyl radicals present can be estimated at 0.02(5). As

this value is small it was decided that the final refinement could be conducted using a model containing only the benzyl radical and SO_2. The presence of a small amount of dibenzyl is not expected to introduce a significant systematic error in to the final refinement.

The final refinement was conducted using a model containing the benzyl radical and SO_2. Both molecules were modelled as having C_{2v} symmetry. All the key bond lengths in this molecule lie under the same peak centred around 143 pm. rC(1)–C(6), rC(1)–C(2), rC(2)–C(3), rC(3)–C(12) and rS=O were therefore modelled using the average (p_1) and four differences (p_2 – p_5), such that $p_1 = \frac{1}{5}$ [rC(1)–C(6) + rC(1)–C(2) + rC(2)–C(3) + rC(3)–C(12) + rS=O] and rS=O = $p_1 + p_2$, rC(3)–C(12) = $p_1 + p_3$, rC(2)–C(3) = $p_1 + p_4$, rC(1)–C(2) = $p_1 + p_5$ and rC(1)–C(6) = p_1 - ($p_2 + p_3 + p_4 + p_5$). An single value of rC–H was used (p_2). The ring was constructed using the two angles ∠C(1)–C(6)–C(5) (p_9) and ∠C(2)–C(3)–C(4) (p_{10}). The angle ∠H(13)–C(12)–H(14) (p_{10}) was used to place H(13) and H(14). An additional parameter (p_4) was used to define ∠O=S=O in SO_2.

The starting parameters for the r_{h1} refinement[28] were taken from the theoretical geometry optimised at the UMP2/6–311++G** level, with the exception that rS–O was instead taken from a previously reported value.[38] This was due to the difficulty in calculating accurate parameters for SO_2 as detailed in this previous study. A theoretical Cartesian force field was obtained at this level and converted into a force field described by a set of symmetry coordinates using the SHRINK program,[28] which generated both the amplitudes of vibration (u_{h1}) and the curvilinear corrections (k_{h1}). All 10 geometric parameters and 8 groups of vibrational amplitudes were then refined. Flexible restraints were employed during the refinement using the SARACEN method.[18–20] Altogether, 8 geometric restraints (Table 7.2) and five amplitude restraints (Appendix 7, Table A7.7) were employed. The success of the final refinement, for which $R_G = 0.063$ (R_D = 0.037), can be assessed on the basis of the radial-distribution curve (Figure 7.7) and the molecular-scattering intensity curves (Appendix 7, Figure A7.2). Final refined parameters are listed in Table 7.5. The Appendix contains the interatomic

distances and the corresponding amplitudes of vibration (Table A7.7), with the least-squares correlation matrix (Table A7.8) and the experimental coordinates from the GED analysis (Table A7.9).

The fraction of SO_2 in the vapour must stoichiometrically be $\frac{1}{3}$. At the end of the refinement this ratio was varied, and it was found that the minimum R factor did occur at the value of 0.33. Figure 7.8 shows the variation of the R factor with this ratio.

Table 7.5: Refined and calculated geometric parameters for the benzyl radical (distances in pm and angles in °) from the GED study.[a,b]

	Parameter	MP2/ 6-311++G**	SARACEN (r_{h1})	Restraint
Independent parameters				
p_1	rC–C/S=O av	140.2	143.0(1)	—
p_2	rC–H	108.0	110.1(6)	—
p_3	rS=O/C–C dif1	2.8	3.1(6)	2.8(3)
p_4	∠O=S=O	119.3	119.0(11)	119.3(10)
p_5	rS=O/C–C dif2	1.2	1.4(3)	1.2(3)
p_6	rS=O/C–C dif3	0.7	0.7(3)	0.7(3)
p_7	rS=O/C–C dif4	-3.4	-3.2(3)	-3.4(3)
p_8	∠H–C–H	118.4	118.4(11)	118.4(10)
p_9	∠C(1)–C(6)–C(5)	117.6	116.6(6)	—
p_{10}	∠C(2)–C(3)–C(4)	119.5	118.6(5)	119.5(5)
Dependent parameters				
dp_1	rS=O	143.0[c]	146.2(4)	—
dp_2	rC(1)–C(6)	138.9	141.0(6)	—
dp_3	rC(1)–C(2)	136.8	139.8(4)	—
dp_4	rC(2)–C(3)	141.0	143.7(4)	—
dp_5	rC(3)–C(12)	141.4	144.5(4)	—
dp_6	$p_9 - p_{10}$	-1.9	-2.1(4)	-1.9(4)
dp_7	∠C(1)–C(2)–C(3)	120.9	121.3(5)	—
dp_8	∠C(2)–C(1)–C(6)	120.5	121.1(4)	—

[a] Figures in parentheses are the estimated standard deviations of the last digits.
[b] See text for parameter definitions.
[c] See reference 38.

Figure 7.7: Experimental and difference (experimental – theoretical) radial-distribution curves, $P(r)/r$, for the benzyl radical and SO_2. Before Fourier inversion the data were multiplied by $s.\exp(-0.00002s^2)/(Z_S - f_S)(Z_C - f_C)$.

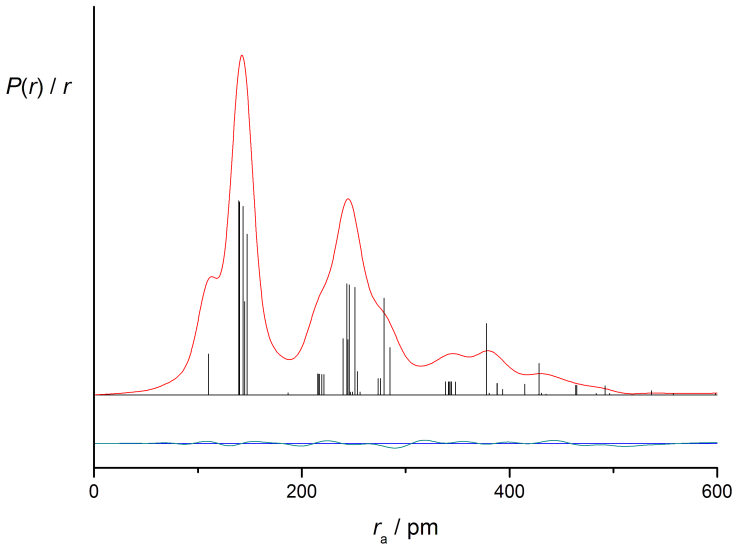

Figure 7.8: A plot showing the R-factor variation as a function of the amount of the SO_2 in the refinement of the benzyl radical. The solid line denotes the 95% confidence level.[39]

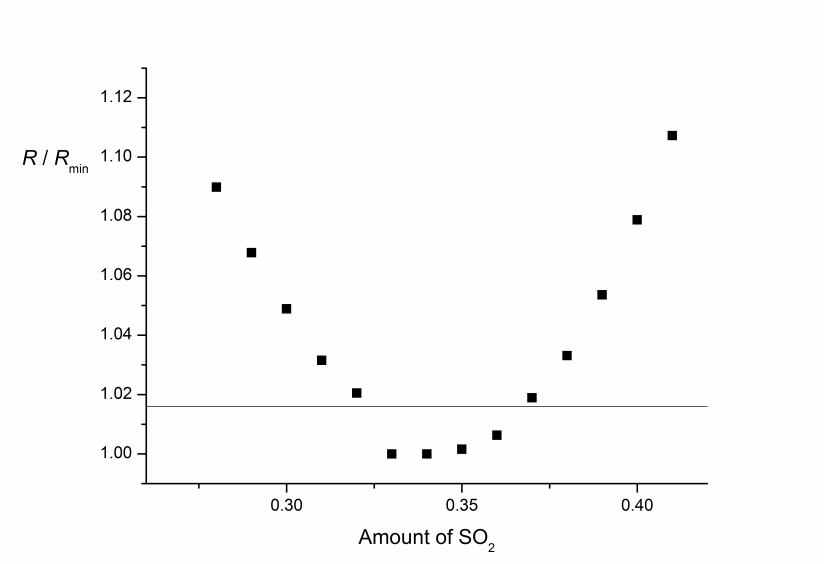

7.3.4 Discussion

Once the refinement was complete it was clear that there were systematic errors in the experimental bond lengths. The average C–C/S=O distance was refined and the distance differences were refined with restraints. The RDC shows a good fit in this area, but the mean bond length is too long, leading to values for all bond lengths that are too long. Due to the construction of the VHT nozzle it was not possible to run a benzene calibration immediately after a sample and therefore data were extracted using an assumed nozzle-to-camera distance from a previous benzene calibration of the nozzle. It was initially assumed that the nozzle was quite rigid and that this distance would not change dramatically from run to run but, as detailed in Chapter 6, this was later found not to be the case, and therefore it is likely that the nozzle-to-camera distance used to extract the data for the benzyl radical was incorrect. It was decided that in this case the experimental rS=O distance would be used to calibrate the other distances. The experimental value of rS=O has previously been determined to be 143.076(13) pm, compared to the distance found for this experiment of 146.8(6) pm. To correct the experimental distances bond lengths were scaled by a factor of 0.9746 (= 143.076 / 146.8). The resultant scaled bond lengths are given in Table 7.6.

Table 7.6: Scaled bond lengths for the benzyl radical.[a]

Parameter	Theory	Unscaled	Scaled
rC(1)–C(6)	138.9	141.0(6)	138.0(6)
rC(1)–C(2)	136.8	139.8(4)	136.8(4)
rC(2)–C(3)	141.0	143.7(4)	140.6(4)
rC(3)–C(12)	141.4	144.5(4)	141.4(4)
rC–H	108.5	110.1(6)	107.7(6)

[a] All distances in pm. See Figure 7.4 for atom numbering.

An attempt was made to modify the VHT nozzle to allow for benzene calibration, with some of this work detailed in Chapter 6. Whilst it should now be possible to collect benzene calibration data at the same time as pyrolysis data an unrelated problem with the VHT nozzle meant that, even though the required modifications were complete, additional data could not be collected in time for inclusion in this

thesis.

Scaling the bond lengths is not an ideal solution, although there is a strong argument for doing so and the scaled parameters are consistently more accurate, including rC–H, which was not subjected to a restraint. However, a large number of restraints were required in the refinement and once the bond lengths are scaled the amount of experimental information extracted is limited. It is likely that the large number of restraints are inevitable for this type of molecule due to the large degree of peak overlap. That the refinement strongly suggests that no DBS is present, that there is only a small mole fraction of dibenzyl and that the mole fraction of SO_2 is 0.33 are all reassuring, but do not preclude the presence of other species. Other than by judging the quality of fit the current experimental set-up offers no independent verification of the make-up of the vapour. With the exception of nozzle-to-camera distance calibration the largest improvement to analysis of such data would be the ability to couple a mass spectrometer to the GED apparatus. More discussion of the benefits of a mass spectrometer is offered in Chapter 8.

Concentrating on the experimental structure obtained, it can be seen that most parameters agree reasonably closely with those calculated *ab initio*. The bond lengths, once scaled, are all within 1–2σ of those calculated at the UMP2/6-311++G** level of theory, with the tendency being for the experimental bond length to be a little shorter. Although the distance differences in the refinement are restrained to those predicted *ab initio* the fit in this area of the RDC is good. The bond angles also show a similar level of agreement, with the two refined $\angle$C–C–C being 1–2σ narrower than the highest level of theory suggests.

7.3.5 Conclusion

Dibenzylsulfone was pyrolysed at 900 K to form the benzyl radical. Refinements were performed which included the presence of starting material and recombination products. These refinements indicated that no starting material remained and that only a small amount of recombination had occurred, and so the final refinement was conducted with a model of only the main decomposition products, these being the benzyl radical and SO_2. The experimental data show a good fit to the parametrised model but a large number of restraints were needed and the bond lengths had to be scaled due to an inability to determine the nozzle-to-camera distance experimentally. The refined structure is close to that calculated using the UMP2 method, with bond lengths and bond angles agreeing to within 1–2σ. This work represents a step forward in the determination of the structures of short-lived molecules in Edinburgh.

7.4 References

[1] E. C. Leonard Jr, *J. Org. Chem.*, 1962, **27**, 1921.

[2] M. E. Tuttolomondo, P. E. Argaaraz, E. L. Varetti, S. A. Hayes, D. A. Wann, H. E. Robertson, D. W. H. Rankin and A. B. Altabef, *Eur. J. Inorg. Chem.*, 2007, 1381.

[3] M. J. Frisch, G. W. Trucks, H. B. Schlegel, G. E. Scuseria, M. A. Robb, J. R. Cheeseman, J. A. Montgomery, Jr., T. Vreven, K. N. Kudin, J. C. Burant, J. M. Millam, S. S. Iyengar, J. Tomasi, V. Barone, B. Mennucci, M. Cossi, G. Scalmani, N. Rega, G. A. Petersson, H. Nakatsuji, M. Hada, M. Ehara, K. Toyota, R. Fukuda, J. Hasegawa, M. Ishida, T. Nakajima, Y. Honda, O. Kitao, H. Nakai, M. Klene, X. Li, J. E. Knox, H. P. Hratchian, J. B. Cross, V. Bakken, C. Adamo, J. Jaramillo, R. Gomperts, R. E. Stratmann, O. Yazyev, A. J. Austin, R. Cammi, C. Pomelli, J. W. Ochterski, P. Y. Ayala, K. Morokuma, G. A. Voth, P. Salvador, J. J. Dannenberg, V. G. Zakrzewski, S. Dapprich, A. D. Daniels, M. C. Strain, O. Farkas, D. K. Malick, A. D. Rabuck, K. Raghavachari, J. B. Foresman, J. V. Ortiz, Q. Cui, A. G. Baboul, S. Clifford, J. Cioslowski, B. B. Stefanov, G. Liu, A. Liashenko, P. Piskorz, I. Komaromi, R. L. Martin, D. J. Fox, T. Keith, M. A. Al-Laham, C. Y. Peng, A. Nanayakkara, M. Challacombe, P. M. W. Gill, B. Johnson, W. Chen, M. W. Wong, C. Gonzalez and J. A. Pople, *Gaussian 03, Revision C.02*, Gaussian, Inc., Wallingford, CT, 2004.

[4] C. C. J. Roothaan, *Rev. Mod. Phys.*, 1951, **23**, 69.

[5] C. Møller and M. S. Plesset, *Phys. Rev.*, 1934, **46**, 618.

[6] A. D. Becke, *J. Chem. Phys.*, 1993, **98**, 5648.

[7] C. Lee, W. Yang and R. G. Parr, *Phys. Rev. B: Condens. Matter*, 1992, **37**, 785.

[8] B. Miehlich, A. Savin, H. Stoll and H. Preuss, *Chem. Phys. Lett.*, 1989, **157**, 200.

[9] Y. Zhao, N. E. Schultz and D. G. Truhlar, *J. Chem. Th. Comput.*, 2006, **2**, 364.

[10] Y. Zhao and D. G. Truhlar, *Acc. Chem. Res.*, 2008, **41**, 157.

[11] W. J. Hehre, R. Ditchfield and J. A. Pople, *J. Chem. Phys.*, 1972, **56**, 2257.

[12] P. C. Hariharan and J. A. Pople, *Theo. Chim. Acta.*, 1972, **56**, 2257.

[13] M. S. Gordon, *Chem. Phys. Lett.*, 1980, **76**, 163.

[14] A. D. McLean and G. S. Chandler, *J. Chem. Phys.*, 1980, **72**, 5639.

[15] R. Krishnan, J. S. Binkley, R. Seeger and J. A. Pople, *J. Chem. Phys.*, 1980, **72**, 650.

[16] M. J. Frisch, M. Head-Gordon and J. A. Pople, *Chem. Phys. Lett.*, 1990, **166**, 275.

[17] M. J. Frisch, M. Head-Gordon and J. A. Pople, *Chem. Phys. Lett.*, 1990, **166**, 281.

[18] A. J. Blake, P. T. Brain, H. Mc Nab, J. Miller, C. A. Morrison, S. Parsons, D. W. H. Rankin, H. Robertson and B. A. Smart, *J. Phys. Chem. A*, 1996, **100**, 12280.

[19] P. T. Brain, C. A. Morrison, S. Parsons and D. W. H. Rankin, *J. Chem. Soc., Dalton Trans.*, 1996, 4589.

[20] N. W. Mitzel and D. W. H. Rankin, *Dalton Trans.*, 2003, 3650.

[21] C. M. Huntley, G. S. Laurenson and D. W. H. Rankin, *J. Chem. Soc., Dalton Trans.*, 1980, 954.

[22] H. Fleischer, D. A. Wann, S. L. Hinchley, K. B. Borisenko, J. R. Lewis, R. J. Mawhorter, H. E. Robertson and D. W. H. Rankin, *Dalton Trans.*, 2005, 2469.

[23] S. L. Hinchley, H. E. Robertson, K. B. Borisenko, A. R. Turner, B. F. Johnston, D. W. H. Rankin, M. Ahmadian, J. N. Jones and A. H. Cowley, *Dalton Trans.*, 2004, 2469.

[24] A. W. Ross, M. Fink and R. Hilderbrandt, *International Tables for Crystallography*, Kluwer Academic Publishers, Dordrecht, Netherlands, 1992, p. 245.

[25] J. Pauls, E. Iravani, P. Kohl and B. Neumuller, *Z. Anorg. Allg. Chem.*, 2004, **630**, 876.

[26] J. Concellon, P. Bernad, V. del Solar, J. R. Suarez, S. Garcia-Granda and M. R. Diaz, *J. Org. Chem.*, 2006, **71**, 6420.

[27] K. Pramanik, P. Ghosh and A. Chakravorty, *Inorg. Chem.*, 1998, **37**, 5678.

[28] V. A. Sipachev, *THEOCHEM*, 1985, **121**, 143.

[29] T. van Mourik, P. G. Karamertzanis and S. L. Price, *J. Phys. Chem. A.*, 2005, **110**, 8.

[30] W. M. Davis, S. M. Heck and H. O. Pritchard, *J. Chem. Soc., Faraday Trans.*, 1998, **94**, 2725.

[31] F. F. Fenter, B. Nozire, F. Caralp and R. Lesclaux, *Int. J. Chem. Kinetics*, 2004, **26**, 171.

[32] H. F. Hameka, *J. Org. Chem.*, 1987, **52**, 5025.

[33] J. Pacansky, B. Liu and D. DeFrees, *J. Am. Chem. Soc.*, 1986, **51**, 3720.

[34] R. V. Lloyd and D. E. Wood, *J. Am. Chem. Soc.*, 1974, **96**, 659.

[35] E. G. Baskir, A. K. Maltsev, V. A. Korolev, V. N. Khabashesku and O. M. Nefedov, *Russ. Chem. Bull.*, 1993, **42**, 1438.

[36] M. Szwarc, *Discuss. Faraday Soc.*, 1947, **2**, 39.

[37] J. A. Pople and R. K. Nesbet, *J. Chem. Phys.*, 1954, **22**, 571.

[38] J. M. L. Martin, *J. Chem. Phys.*, 1998, **108**, 2791.

[39] W. C. Hamilton, *Acta. Cryst.*, 1965, **18**, 502.

Chapter 8

Conclusions and future work

8.1 Primary derivatives of Group 15 elements and beyond.....

The first part of this thesis was concerned with small, primary derivatives of phosphine and arsine. Chapters 2, 3 and 4 focussed on the structures of a series of primary phosphines and their adducts with borane while Chapter 5 detailed the studies of vinylarsine and vinyldichloroarsine.

8.1.1 Primary phosphines

As detailed in Chapters 2 and 3, the study of the phosphines was a success and, with the structures of a total of nine primary phosphines determined, represents one of the most complete structural studies on such compounds. The study focussed on unsaturated derivatives because they offer the most interesting possibilities for use as ligands or in further synthesis, but saturated and aryl derivatives were also studied to offer a more complete picture of the bonding trends. Whilst there are a limited number of other small phosphines that could be studied, the work could be made more complete with by the determination of the structure of ethylphosphine,[1] propylphosphine[2] and cylcopropylphosphine[3] by GED, meaning that the gas-phase molecular structures of all accessible systems with up to three C atoms would be known.

8.1.2 Phosphine-borane adducts

The main motivation for the study of these phosphines was their interesting structural properties and conformational behaviour. Primary phosphines have potential applications throughout chemistry but their use is generally avoided due to their high reactivity and toxicity. Tertiary phosphines are naturally less prone to oxidation, and to infer more stability are routinely protected *via* complexation, for example with borane. It is thought that a similar process could make primary phosphines more user-friendly.[4] The aim of the second part of this project was to study the series of primary phosphines as an adduct with borane. As part

of a wider series of studies by J.-C. Guillemin, such as measurement of the gas-phase acidity[5] and photoelectron spectra,[6] it was hoped that knowledge of the structures would allow a deeper understanding of the nature of the stability inferred, as well as to help understand trends within the series of compounds.

The work studying the phosphine-borane adducts began well, with the structure of methylphosphine-borane reported in Chapter 2. However, as detailed in Chapter 4, the unsaturated phosphine-boranes suffered from decomposition upon vaporisation and even the more stable saturated and aryl phosphine-boranes dissociated to the free phosphine and diborane. Decomposition of the unsaturated systems is understandable, and fits with the previous observation that such systems have lower kinetic stability than the free phosphine. The phenomena of dissociation, confirmed in the laboratory by the Guillemin group, has no obvious explanation.

Whilst it is obvious that there are synthetic advantages to using phosphine-borane adducts,[4] given the difficulty when storing and handling the future potential of such compounds is questionable.

8.1.3 Primary arsines

When it became clear that further study of the phosphine-borane adducts would be impossible it was decided to study primary arsines. Even less work is reported in the literature for primary arsines, with the GED structure of vinylarsine in Chapter 5 offering the first complete molecular structures of a primary arsine. However, it was realised that the decreased stability of the arsines compared to the analogous phosphines could make further investigations difficult, and so the study of vinyldichloroarsine was also undertaken with a view to studying the dichloroarsines as more stable analogues. Synthesis of these highly toxic and unstable molecules could only be conducted by an experienced worker during collaborative visits to Edinburgh, therefore the future of this work is at present unclear.

8.1.4 Future avenues

If the arsines prove too unstable there exists numerous other candidates for which little experimental information is known. In particular the study of analogous compounds with heavier heteroatoms would be of significant computational interest to benchmark basis sets and theoretical methods. Remaining in Group 15 the study of antimony or bismuth derivatives would offer a computational challenge, but no primary derivatives of these elements are found in the literature. Moving to Group 14 or 16 offers interesting choices, with potential molecules that have already been synthesised including selenols,[7] tellurols,[8] stannanes[9] and germanes.[10] for all of which only sporadic structural studies are present in the literature.

Chapters 3 and 5 compare the structures of the phosphines and arsines to that of the nitrogen analogues. Despite being well known many of the amines have not been investigated structurally. Study of these molecules would be interesting to fill in the gaps in the literature. Some, such as vinylamine, are difficult to generate, and so techniques such as FVP-GED will be useful, as will general reductions in the vapour pressure requirements of the GED apparatus.

In general the study of this class of compounds is not significantly more difficult than conducting an experiment on a stable molecule. The main difficulties lie with obtaining a pure sample, which requires the molecules to be synthesised in Edinburgh, and the inability to store such compounds for more than a few days. The rate of success has been lower than for more stable compounds, with experiments often being repeated because samples decomposed or contained impurities.

There remains many compounds for which the only barrier to structural determination is the desire and funding to study them. Whilst it may be argued that it would be cheaper to simply calculate the structure of simpler molecules *ab initio* it is noted throughout this thesis that while experiment and theory generally predict similar structures the two often disagree about the relative stability of different conformers. In addition, for molecules containing heavy

atoms for which gas-phase structures are rare, it is difficult to have faith in the computed structures without experimental verification.

8.2 FVP-GED and other short-lived molecules

Chapters 6 and 7 present the first efforts in Edinburgh to study the structures of short-lived molecules using a combination of FVP and GED. The routine generation of new and interesting species is an exciting prospect and would greatly extend the number of species that could be studied by GED. However, as the work in Chapters 6 and 7 proved, such a goal is not easy to achieve. However, it is opinion of this author that such an outcome is close, and that with further modifications to the techniques such work could become routine.

GED is the only technique that could offer experimental determination of such molecules routinely, so the driving force behind this work is clear. The main difficulty in this work is analysing the GED data obtained when multiple species are present. GED data, as a 1-dimensional representation of 3-dimensional molecules, is already limited in its scope to determine complete structures. This becomes much more difficult as more species are present in the vapour.

There are, simplistically, two possible solutions – obtain more data or reduce the number of species. The later is difficult, as whilst it may be possible to remove some species from a vapour (*e.g.* scrubbing CO_2), it is unlikely that it could be achieved in every case. Some molecules can be generated cleanly, such as the dissociation of a dimer. However, it will not always be possible to optimise FVP conditions to achieve total decomposition of the precursor. Regardless of whether the problem is leftover precursor or by-products, it seems inconceivable that a clean vapour could be generated in all but the most favourable of cases.

It seems obvious, therefore, that attention must be focussed on obtaining additional data. It is already routine to use additional data *via* the SARACEN method,[11–13] evidenced throughout this thesis in the form of restraints based on computed structures, and in the case of methylphosphine, methylphosphine-

borane and vinylarsine, by the use of published rotational constants. All modern GED data analysis relies on additional data to produce more reliable structures, and the study of molecules generated *in situ* is no different. Theoretical structures of all the molecules studied in Chapters 6 and 7 were calculated and restraints were applied when required. However, in order to routinely study vapours which consist of a mixture of species more experimental data is required, otherwise too many parameters will require restraints, and it becomes difficult to assess how "experimental" the GED structure is.

The additional sources that have been identified are mass spectrometry, microwave spectroscopy and previous GED structures.

The use of MW spectroscopy in GED refinements is relatively routine. It is obvious that the best refinement of any mixed vapour will include as much MW data as can be obtained, and it may be the case, depending on the systems studied, that it is worthwhile working in collaboration with a MW spectroscopist to obtain data for new molecules.

Where one of the by-products of an FVP reaction is easily studied by GED, doing so would provide experimental restraints for use with the SARACEN method. Such an approach has not been used before, so further testing would be required, but it is expected that it would maximise the information obtained about the target molecule. However, it is anticipated that the addition of a mass spectrometer to the GED apparatus would offer the largest advantage and so it will be discussed in more detail.

8.2.1 The benefits of mass spectrometry coupled GED (MS-GED)

Standard electron diffraction is routinely conducted without a mass spectrometer coupled to the apparatus, so why should one be used to study species generated *in situ*?

A GED refinement is considered to be correct if the R factor is low, the difference curve is flat and the structure is chemically reasonable. It is important to

to remember that this does not guarantee that the refined structure is the actual structure. Whilst modern *ab initio* calculations make incorrect structural determination unlikely for stable molecules, it is of fundamental importance to know the exact composition of the vapour entering the diffraction zone. For a standard GED experiment, samples are routinely checked for purity before being run, and, if necessary, further work can be conducted to probe the behaviour of the sample. For example, calorimetry can offer an insight in to decomposition at raised temperatures.

However, when molecules are generated *in situ* the composition of the vapour will be unknown. The work conducted for this thesis uses the results of previous studies to assess the likely decomposition routes but relies on the GED data alone to calculate the actual proportion of each species in the vapour. Using GED data in this way is far from ideal – a larger number of parameters will normally be required to model a mixed vapour, with similar distances correlated to one another. A parameter or parameters to describe the mole fraction of each species will also be required. For example, in the gas-phase study of CsCl it was impossible to confidently extract the 3 bond lengths present in a mixed vapour of CsCl monomer and dimer,[14] or to accurately determine the fraction of each, and in this case there are only two distances under each of the two peaks. It is obvious that more complex vapours with numerous similar distances will rely heavily on other sources of data. Mass spectrometry offers a way to fix the ratios of all species in the GED refinement – effectively increasing the amount of experimental data and reducing the number of correlated parameters.

However, an arguably larger benefit of coupling mass spectrometry with GED is that the exact composition of the vapour, in terms of the species present, can be determined. The current experimental set-up relies on GED refinements to work out the % of decomposition but this does not offer any insight in to other, unexpected species that could be present. The study of Meldrum's acid is a good example of this – decomposition obviously occurred, but the data could not be analysed. Searching for potential mixtures using GED data alone is not viable. Even in the cases of the pyrolysis of acetic anhydride and the benzyl radical it is

impossible to know if (albeit) small deviations from the theoretical structures indicate a deficiency with the *ab initio* calculations, the GED technique, or indicate the presence of a small amount of other species.

To have confidence in the results of FVP-GED experiments the coupling of a mass spectrometer is key and it is likely that such a set-up will be required to make significant progress in this area of work.

8.2.2 Developments to VHT data collection

The work presented in Chapters 6 and 7 shows that data can be collected using the experimental set-up present in Edinburgh, but as is natural during the course of any work, a number of possible enhancements to the experimental procedure have been identified.

The use of a mass spectrometer has been detailed already, as has the use of image plates. Image plates would allow data collection at higher temperatures using the current nozzle, but would not necessarily be required if a new nozzle was designed. It may be possible for the nozzle tip to be at a lower temperature having pyrolysis occurring prior to reaching it. It may also be possible to improve shielding or to vary the nozzle-to-camera distance, the electron wavelength, or detector size to ensure that the nozzle tip can be position further from the detector. If the light problems can be resolved then the photographic film could be replaced by a CCD instead, allowing much more data to be collected in a single experiment, and as such, allowing a greater range of FVP conditions (temperature, flow rate, *etc*) to be varied in a single run. Combined with a mass spectrometer, this would allow the data collection conditions to be optimized to a far greater level than is possible at the moment. If the glowing of the nozzle tip cannot be solved it may be possible to coat the CCD with a thin layer of aluminium to block light from reaching the detector.

Improving the detector technology could increase the amount of data collected in a given time and allow access to higher temperatures, but neither of these things are useful if the desired pyrolysed vapour cannot be generated. The pyrolysis

nozzle design is therefore of primary importance.

The nozzle designed by the Ivanovo group is similar to a design they use routinely to study molecules at high temperature. However, other than for a few cases, they do not use the nozzle to conduct pyrolysis experiments. The enclosed nozzle design is perfect for the study of involatile, stable compounds that are being studied using the conventional GED technique. However, such a system has proven difficult to use for FVP experiments. With no valves and with everything internal to the GED machine, it is difficult to have an accurate picture of what is occurring inside the apparatus. Using the MT oven to vaporise a sample is a difficult proposition as the only ways to gauge the flow rate through the system are either *via* a pressure gauge located on the other side of the machine (with a cold traps between the gauge and the nozzle) or to use the observed scattering intensity as a guide. The time available to collect data is also a limiting factor, as with no valves or fine temperature control, a sample in the MT oven often vaporises and travels through the system very rapidly.

To take this work forward the best strategy would be to leave behind the enclosed nozzle and to conduct pyrolysis external to the GED apparatus. The ovens and glassware to do this are widely available and so tube diameter and the length of pyrolysis zone used can effectively be considered as variables to be optimized. The difficult engineering problem is then to design a nozzle that can be used with this apparatus. Ideally a nozzle that is capable of reaching the same temperature as the pyrolysis zone would be built to allow maximal flexibility (and also to be the pyrolysis zone if desired), but such a design could be difficult. In most cases it should be possible to transport the pyrolysis products through the system at a lower temperature, and a so a nozzle capable of heating to around 800 K would be sufficient in many cases, and such temperature should be achievable using a system of in-line heaters and compressed air.

8.2.3 Future compounds

Current work is hampered by the problems detailed in this chapter, and as such, whilst there are numerous systems that could be studied, most require further modifications to the experimental set-up.

There exist many ketenes which can be accessed by the FVP technique for which no structure is known,[15] including asymmetrically substituted ketenes. However, it is anticipated that having a mass spectrometer is prerequisite to conducting this work as the pyrolysis conditions would have to be optimized.

The benzyl radical could also be generated by other precursors. The study of the pyrolysis of dibenzyloxalate to form the benzyl radical and CO_2 was planned but could not be completed within the timescale of this thesis due to a fault with the pyrolysis oven. Dibenzyloxalate is anticipated to be a better precursor because CO_2 has a bond length close to 120 pm, distinct from the C–C distances in the benzyl ring.

If this avenue of work proves successful it would be interesting to study a range of substituted benzyl radicals. It is presumed that adding functional groups or halogens to the benzyl rings would have little effect on the decomposition but this would need to be confirmed. Such compounds are not commercially available so synthesis could be the largest barrier to their study, however, with structures of substituted benzyl radicals supported by *ab initio* calculations it would be possible to see the effect of substituents on the nature and location of the unpaired electron.

The remaining literature on FVP is vast and it is likely that further improvements to the FVP-GED technique could make it possible to study a large number of short-lived species. One such possible target molecule is the cyclopentadienyl radical generated by the pyrolysis of nickelocene.[16] A previous study found that the radical could be generated in an 85% yield at 1200 K. At the lower temperatures available with the current FVP-GED equipment in Edinburgh the previous study reported a mixture of species, and so was not studied.

8.3 References

[1] P. Groner, R. D. Johnson and J. R. Durig, *J. Chem. Phys.*, 1988, **88**, 3456.

[2] J. R. Durig, T. K. Gounev, M. S. Lee and T. S. Little, *J. Mol. Struct.*, 1994, **327**, 23.

[3] L. A. Dinsmore, C. O. Britt and J. E. Boggs, *J. Chem. Phys.*, 1971, **54**, 915.

[4] K. Bourumeau, A.-C. Gaumont and J.-M. Denis, *J. Organomet. Chem.*, 1997, **529**, 205.

[5] M. Hurtado, M. Yánez, R. Herrero, A. Guerrero, J. Dávalos, M. A. José-Luis, B. Khater and J.-C. Guillemin, *Chem.-Eur. J.*, 2009, **15**, 4622.

[6] B. Németh, B. Khater, T. Veszprémi and J.-C. Guillemin, *Dalton Trans.*, 2009, **18**, 3526.

[7] H. Møllendal, A. Konovalov and J.-C. Guillemin, *J. Phys. Chem. A.*, 2009, **113**, 6342.

[8] B. Khater, J.-C. Guillemin, G. Bajor and T. Veszprémi, *Inorg. Chem.*, 2008, **47**, 1502.

[9] J.-C. Guillemin, S. Legoupy, S. Batten and A. Legon, *Phys. Chem. Chem. Phys.*, 2006, **8**, 2145.

[10] A. Horn, H. Møllendal, J. Demaison, D. Petiprez, J. R. A. Moreno, A. Benidar and J.-C. Guillemin, *J. Phys. Chem. A.*, 2005, **109**, 3822.

[11] A. J. Blake, P. T. Brain, H. Mc Nab, J. Miller, C. A. Morrison, S. Parsons, D. W. H. Rankin, H. Robertson and B. A. Smart, *J. Phys. Chem. A*, 1996, **100**, 12280.

[12] P. T. Brain, C. A. Morrison, S. Parsons and D. W. H. Rankin, *J. Chem. Soc., Dalton Trans.*, 1996, 4589.

[13] N. W. Mitzel and D. W. H. Rankin, *Dalton Trans.*, 2003, 3650.

[14] R. J. Mawhorter, M. Fink and J. G. Hartley, *J. Chem. Phys.*, 1985, **83**, 4418.

[15] H. McNab, *Aldrichimica Acta*, 2004, **37**, 19.

[16] P. Schissel, D. J. McAdoo, E. Hedaya and D. W. McNeil, *J. Chem. Phys.*, 1968, **49**, 5061.

Appendix